Dynamic Covalent Assembly of Abiotic, Information-bearing Oligomers

by

Tao Wei

A dissertation submitted in partial fulfillment
of the requirements for the degree of
Doctor of Philosophy
(Chemical Engineering)
in The University of Michigan
2017

Doctoral Committee:

Assistant Professor Timothy F. Scott, Chair
Professor Mark A. Barteau
Professor Joerg Lahann
Professor Anne McNeil

Tao Wei

taowei@umich.edu

ORCID ID: 0000-0001-8923-293X

DEDICATION

This dissertation is dedicated to

Liang

Mom and Dad

Suying and Xuexian

For their love and endless support

ACKNOWLEDGEMENTS

I would like to thank my PhD advisor Prof. Timothy F. Scott for his support, guidance, patience, encouragement, and wisdom throughout my doctoral studies at the University of Michigan. I would also like to express my gratitude to my dissertation committee members, Professor Mark Barteau, Professor Joerg Lahann and Professor Anne McNeil for their constructive discussions and advice.

I am fortunate to have met many talented and fun individuals throughout my PhD. Some of these amazing people include Jin Ge, Ray Seo, Wenjun Huang, Molly Kozminsky, Jeff Lowe, Eric and Jai Holt, Lynn Secondo, Xiaozhou Sheng and Ziyong Lin; I am grateful for our fun times. I cannot thank these individuals enough for their support and friendship.

I must emphasize how lucky I am to have extremely supportive and encouraging lab mates including Dr. Scott Zavada, Dr. Joseph Furgal, Dowon Ahn, Megan Dunn, Harry van der Laan, Max Ma, Samuel Leguizamon, Abdulla Alqubati, Austin Bingham, Dr. Jae Hwan Jung, Dr. Jungting Li, Sameer Sathe, and Dan Li. I want to thank them for building the family atmosphere of Polymer Dojo and I really appreciate their friendship. Especially, I want to thank Scott, Dowon, and Megan for their invaluable help in building the lab in early years. I want to mention Scott, who's always been a great friend and a mentor, for his kind advice on research and life. I want to thank Megan and Sam for their

support and I really enjoyed our discussions over Pokémon and doing raid battles together. I am also fortunate enough to have worked with Joe and Jae Hwan on various projects, from whom I learned a lot. In addition, I want to acknowledge Harry for his effort on maintaining a safe lab environment.

I am also very grateful to Professor Greg Thurber at U-M and Thurber lab members for their help on instrumentation such as high performance liquid chromatography (HPLC). Especially, I want to thank Liang Zhang and Submit Bhatnagar for their great effort on the daily maintenance of HPLC and their help on HPLC trouble shooting. Special thanks are in order to James Windak of the Chemistry Department Mass Spec Services Lab for his help with determining molecule compositions. Gratitude is also given to the U-M Chemical Engineering faculty and staff, especially Susan Hamlin, Kelly Raickovich, Barbara Perry and Shelley Fellers for their assistance.

I would also like to acknowledge the funding that supported my graduate studies. This includes the U.S. Department of Energy, the National Science Foundation, and the National Institutes of Health.

I am eternally thankful for the love and support of my parents, my husband Liang, my parents-in-law Suying and Xuexian, and the rest of my family. I especially want to mention my 'partner in crime' Liang, who's also a chemical engineering graduate student at U-M, for being a constant source of motivation and support, and I look forward to starting our next chapter in Boston. I want to express my gratitude to my parents for always believing in me, respecting and supporting every decision I made. I'd also like to acknowledge my parents in law for their endless support and making me always feel at home. I want to thank my cousin in law Yun Li and her husband Jun Zhao for letting us

crash at their place and treating us to delicious Chinese food every time we visit Seattle. Last but not the least, I want to thank cat Meme for bringing joy and laughter to our life.

TABLE OF CONTENTS

DEDICATION ii

ACKNOWLEDGEMENTS iii

LIST OF FIGURES x

LIST OF SCHEMES xviii

LIST OF TABLES xx

ABSTRACT xxii

Chapter 1 Introduction 1

1.1 Background and Research Overview 1

1.2 Sequence-controlled Polymers 2

1.2.1 Synthetic Approaches to Sequence-controlled Polymerization 4

1.2.2 Nucleic Acids as Biological Sequence-controlled Polymers and DNA Nanotechnology 10

1.2.3 Sequence-specific Peptoids 14

1.3 Dynamic Covalent Chemistry 28

1.4 Dynamic Imine Chemistry and Its Emerging Applications 32

1.5 Covalent Self-assembly 40

1.6 Overview of Subsequent Chapters 42

1.7 References 43

Chapter 2 Dynamic Covalent Assembly of Peptoid-Based Molecular Ladders 55

2.1 Original Publication Information 55

2.2 Abstract 55

2.3 Introduction 56

2.4 Experimental 58
2.4.1 General Experimental Procedure 58
2.4.2 Monomer Synthesis 59
2.4.3 Synthesis of Peptoids Bearing Dynamic Covalent Functionalities 69
2.4.4 Cleavage and Side-chain Deprotection 70
2.4.5 Purification of Oligopeptoids by Preparative RP-HPLC 71
2.4.6 Characterization of Peptoids Bearing Dynamic Covalent Functionalities 74
2.4.7 General Procedure for Self-assembly of Molecular Ladders of Length *n* 83
2.5 Results and Discussion 84
2.5.1 Formation of Short Peptoid-based *n*-Rung Ladders (*n* = 3~6) 87
2.5.2 Formation of Long Peptoid-based *n*-Rung Ladders (*n* = 8~16) 90
2.6 Conclusions 94
2.7 References 95

Chapter 3 Reaction Kinetics and Registry Mechanism of n-Rung Molecular Ladder Formation 99

3.1 Original Publication Information 99
3.2 Abstract 99
3.3 Introduction 100
3.4 Experimental 101
3.4.1 General Experimental Procedures 101
3.4.2 Experimental Procedures for Kinetics of Molecular Ladder Formation 103
3.4.3 Synthesis and Characterization of DABCYL-EN for Subsequent Solid-phase Peptoid Synthesis 104
3.4.4 Synthesis and Characterization of Oligopeptoids for FRET Study 106
3.4.5 Photoluminescence Spectroscopy 112
3.5 Results and Discussion 113
3.5.1 Kinetics of Molecular Ladder Formation with *n* Rungs 113
3.5.2 Registry Mechanism of *n* × *n* Molecular Ladder Formation by Förster Resonance Energy Transfer (FRET) 121
3.6 Conclusions 127
3.7 References 129

Chapter 4 Long, Self-assembled Molecular Ladders by Vernier Templating 131
4.1 Original Publication Information 131
4.2 Abstract 131
4.3 Introduction 132
4.4 Experimental 134
4.4.1 General Experimental Procedure 134
4.4.2 Monomer Synthesis 135
4.4.3 Synthesis and Characterization of Peptoids for Vernier Templating and Molecular Ladder Scrambling 138
4.4.4 General Procedure for Vernier-templated Self-assembly of Molecular Ladders of Length $m \times n$ 141
4.4.5 Procedure for Dynamic Covalent Assembly of Ladder ME^3A-Im_4 142
4.4.6 Procedure for Molecular Ladder Scrambling by Strand Exchange 143
4.5 Results and Discussion 144
4.5.1 Vernier-templated Assembly of Complementary $m \times n$ Oligopeptoids 144
4.5.2 Molecular Ladder Scrambling by Strand Exchange 151
4.6 Conclusion 156
4.7 References 157

Chapter 5 In Situ Deprotection and Dynamic Covalent Assembly Using a Dual Role Catalyst 158
5.1 Original Publication Information 158
5.2 Abstract 158
5.3 Introduction 159
5.4 Experimental 161
5.4.1 General Experimental Procedure 161
5.4.2 Monomer Synthesis 161
5.4.3. Solid-phase Synthesis of Oligo(peptoid)s 172
5.4.4 Amine Protecting Groups and Deprotection 179
5.4.5 Deprotection of Acetal Group by Lewis Acids 182
5.5 Results and Discussion 183
5.5.1 Orthogonal Protecting Groups for Amines and Aldehydes 183

5.5.2 Optimization of Acetal Deprotection by Sc(III) 188
5.5.3 Sc(III) as a Dual Role Catalyst 195
5.5.4 Information-bearing Peptoids and Self-assembly of Complex Structures..... 199
5.6 Conclusion 207
5.7 References 208
Chapter 6 Concluding Remarks and Future Directions 211
6.1 Summary of Research 211
6.2 Future Work 217
6.3 References 221

LIST OF FIGURES

Figure 1.1. The range of characteristics for synthetic and biological polymers reveals a gap that is strategically filled by sequence-defined polymers such as peptoid-based materials. 2
Figure 1.2. Transcription of a DNA-template (orange) into a sequence-defined mRNA chain (green), catalyzed by an RNA polymerase (blue). 4
Figure 1.3. Solid-phase approach: sequentially attaching monomers one by one. 5
Figure 1.4. Soluble polymer supporter for azide-alkene click reaction. 6
Figure 1.5. Sequence controlled living radical polymerization utilizing iterative single-monomer addition with allyl alcohol. 6
Figure 1.6. Positioning control in living radical polymerization of styrene. 7
Figure 1.7. Step-growth polymerization for the synthesis of sequence-controlled polymers: (a) metal-catalyzed radical polymerization; (b) regio-selective ROMP of asymmetric substituted clycloоctene. 8
Figure 1.8. Sequence-controlled radical polymerization by templated synthesis..... 9
Figure 1.9. The advent of DNA nanotechnology. (A) Sticky end hybridization. (B) The sticky end-mediated assembly of a branched nucleic acid junction into a square lattice. 12
Figure 1.10. Schematic of DNA origami. (A) Synthesized oligomeric DNA strands are designed to hybridize with one long DNA strand such that it raster-fills a predetermined shape. (B) Through careful consideration of the oligomeric DNA sequences, this approach can be used to assemble arbitrary, complex shapes (e.g., a butterfly) in a single step. 13
Figure 1.11. Peptide versus peptoid structures. Example tetramers are shown of each. .. 15
Figure 1.12. β-peptoid and γ-peptoid structures and synthesis techniques. 22

Figure 1.13. Branching peptoid-based structures. Various side chains were incorporated into the podand, and first, second and third generation dendrimers were synthesized using the structure on the right. 24
Figure 1.14. Peptoids as antifouling coatings. 27
Figure 1.15. pH-Mediated dynamic covalent condensation chemistries: (a) the condensation of boronic acids with diols produces boronate esters; (b) the addition of amines to aldehydes yields imines, whereas (c) the reaction of hydrazides with aldehydes affords acylhydrazones. 30
Figure 1.16. The photoreversible thiol/oNQM Michael addition. 31
Figure 1.17. Schematic representation of reversible component redistribution (phase separation) upon external stimuli (i.e. thermal or salt) of charged and uncharged aldehyde and amine monomers. 34
Figure 1.18. The controlled formation of micellar aggregates from (1) the aromatic aldehyde polar head group reversibly reacting with various amines to form an amphiphilic surfactant that can self-assemble into micelles. 35
Figure 1.19. Schematic showing the formation of imine bonds from difunctionalized aldehydes and aliphatic amines to form macrocycles and oligomers leading to the vesicles, vesicle clusters, and finally vesicle networks capable of forming pH-reversible hydrogels. 36
Figure 1.20. Schematic representation of dynamic covalently cross-linked polymeric gel synthesis from PIB-b-P(NH2-Leu-HEMA) and HOC-PIBCHO in 1,4-dioxane at room temperature and responsiveness toward pH. 37
Figure 1.21. Schematic showing the dynamics of imine bonds. 38
Figure 1.22. Reversible humidity-responsive color changing COF/aramid fabrics. 39
Figure 1.23. Schematic representation of dynamic nucleic acid analogues. Reversible covalent bond formation between (A) bifunctional hetero- or homotopic nucleobase derivatives, or (B) side-chain-functionalised polymers with monofunctionalised nucleobase derivatives, affords dynamic main-chain or dynamic side-chain polymers, respectively. 41
Figure 2.1. ^{1}H NMR spectrum of 4-(2-aminoethyl)-N-(*tert*-butoxycarbonyl) phenylamine 61

Figure 2.2. ^{13}C NMR spectrum of 4-(2-aminoethyl)-N-(*tert*-butoxycarbonyl) phenylamine 61
Figure 2.3. ^{11}H NMR spectrum of 4-(1,3-Dioxacyclopent-2-yl)benzonitrile. 63
Figure 2.4. ^{13}C NMR spectrum of 4-(1,3-Dioxacyclopent-2-yl)benzonitrile. 63
Figure 2.5. ^{1}H NMR spectrum of 4-(1,3-Dioxacyclopent-2-yl)benzylamine. 64
Figure 2.6. ^{13}C NMR spectrum of 4-(1,3-Dioxacyclopent-2-yl)benzylamine. 65
Figure 2.7. ^{1}H NMR spectrum of 2-(2-Ethoxyethoxy)ethyl tosylate..... 66
Figure 2.8. ^{1}H NMR spectrum of 2-(2-Ethoxyethoxy)ethyl azide..... 67
Figure 2.9. ^{1}H NMR spectrum of 2-(2-Ethoxyethoxy)ethyl amine..... 68
Figure 2.10. Chemical structures of amine– and aldehyde– functionalized peptoids 69
Figure 2.11. Analytical HPLC traces of aldehyde–functionalized oligopeptoids. 73
Figure 2.12. Analytical HPLC traces of amine–functionalized oligopeptoids. 73
Figure 2.13. ESI mass spectra of aldehyde– and amine–functionalized oligopeptoids purified by preparative RP-HPLC. (*a*) E^3A-Al_3; (*b*) E^3A-Am_3; (*c*) E^3A-Al_4; (*d*) E^3A-Am_4; (*e*) E^3A-Al_6 & (*f*) E^3A-Am_6. 74
Figure 2.14. MALDI mass spectra of aldehyde–functionalized oligopeptoids purified by preparative RP-HPLC. 75
Figure 2.15. MALDI mass spectra of amine–functionalized oligopeptoids purified by preparative RP-HPLC. 75
Figure 2.16. ^{1}H NMR spectrum (700 mHz, $CDCl_3$) of E^3A–Al_3. 77
Figure 2.17. ^{1}H NMR spectrum (700 mHz, $CDCl_3$) of E^3A–Al_4. 78
Figure 2.18. ^{1}H NMR spectrum (700 mHz, $CDCl_3$) of E^3A–Al_6. 78
Figure 2.19. ^{1}H NMR spectrum (700 mHz, $CDCl_3$) of E^3A–Am_3. 79
Figure 2.20. ^{1}H NMR spectrum (700 MHz, $CDCl_3$) of E^3A–Am_4..... 80
Figure 2.21. ^{1}H NMR spectrum (700 MHz, $CDCl_3$) of E^3A–Am_6..... 80
Figure 2.22. Analytical GPC of aldehyde–functionalized oligopeptoids. 81
Figure 2.23. Analytical GPC of amine–functionalized oligopeptoids. 81
Figure 2.24. Influence of $Sc(OTf)_3$ on the rate of molecular ladder formation. 86
Figure 2.25. Characterization of peptoid-based molecular ladders (n = 3 ~ 6). 88
Figure 2.26. MALDI mass spectra of reduced molecular ladders (n = 3~6). 90
Figure 2.27. Characterizations of peptoid-based molecular ladders (n = 8 ~ 16)..... 90

Figure 2.28. Deconvoluted GPC traces of peptoid-based ladders (n = 3 ~ 16). 92
Figure 3.1. Characterizations of the E^3A_21 internal standard employed in kinetics experiments: (a) chemical structure, (b) MALDI mass spectrum and (c) analytical HPLC trace of E^3A_21 purified preparative RP-HPLC. 104
Figure 3.2. Chemical Structure of peptoid sequences subjected to FRET study. 107
Figure 3.3. Analytical HPLC traces of oligopeptoids comprised of FRET pairs. 109
Figure 3.4. Deconvoluted ESI-MS spectra of oligopeptoids containing FRET pairs purified by preparative RP-HPLC: (a) Al_12–EDANS; (b) Am_12–DABCYL; (c) Bz_12–EDANS; (d) Al–Bz_11–EDANS; (e) Am–Bz_11–DABCYL; (f) Bz_11–Am–DABCYL. 110
Figure 3.5. UV absorption and emission of peptoids containing either EDANS or DABCYL subjected to FRET study: (a) Al_12–EDANS, 99.3%; (b) Bz_12–EDANS; (c) Al–Bz_11–EDANS; (d) Am_12–DABCYL; (e) Am–Bz_11–DABCYL; (f) Bz_11–Am–DABCYL. 111
Figure 3.6.Analytical GPC of (a) Am_12-DABCYL and (b) Al_12-EDANS. 112
Figure 3.7. Kinetics of the formation of molecular ladder with n = 12 rungs (Im_12) over the course of 13 days. (a) MALDI-TOF mass spectra of the crude reaction mixture at increasing time intervals, and (b) concentration of the desired molecular ladder Im_12 and its out-of-registry intermediates versus time during the self-assembly process. 113
Figure 3.8. Concentration evolution of desired molecular ladders with n rungs (n =4, 8, 10, and 12). 115
Figure 3.9. Kinetics of the formation of molecular ladder with n = 8 rungs over the course of 7 days. (a) MALDI-TOF mass spectra of the crude reaction mixture at increasing time intervals; (b) Concentration of the desired molecular ladder Im_8 and its out of registry molecular ladders versus time during the molecular ladder assembly process. 116
Figure 3.10. Kinetics of the formation of molecular ladder with n = 10 rungs over the course of 13 days. (a) MALDI-TOF mass spectra of the crude reaction mixture at increasing time intervals; (b) Concentration of the desired molecular ladder Im_10 and its out of registry molecular ladders versus time during the molecular ladder assembly process..... 117

Figure 3.11. Kinetics of the formation of molecular ladder with n = 4 rungs over the course of 2 days. (a) MALDI-TOF mass spectra of the crude reaction mixture at increasing time intervals; (b) Concentration of the desired molecular ladder Im_4 and its out of registry molecular ladders versus time during the molecular ladder assembly process..... 117
Figure 3.12. (a) Structures of chromophore-labeled peptoid sequences. A dodec-aldehyde strand was affixed with a fluorescence donor EDANS (Al_12–EDANS) whereas its complementary dodecamine sequence was affixed with a quencher DABCYL (Am_12–DABCYL). As the fluorescence donor and quencher come in close proximity once the molecular ladder forms, radiationless energy transfer between the moieties quenches the donor fluorescence. (b) The absorption and fluorescence spectra of Al_12–EDANS, and the absorption spectrum of Am_12–DABCYL. 122
Figure 3.13. Examining dynamic covalent peptoid hybridization by Förster resonance energy transfer (FRET). The relative fluorescence intensity of chloroform solutions containing 25 μM donor- and acceptor-functionalized peptoids. 124
Figure 3.14. Circular dichroism (CD) spectra of Al_12 and Am_12. 126
Figure 4.1. 1H NMR spectrum of 2-(2-(2-Methoxyethoxy)ethoxy)ethylamine (ME^3A). 138
Figure 4.2. ESI mass spectra of aldehyde- and amine-functionalized oligopeptoids incorporating ME^3A spacer purified by preparative RP-HPLC: (a) ME^3A-Al_4 & (b) ME^3A-Am_4. 139
Figure 4.3. ^1H NMR spectrum (700 MHz, $CDCl_3$) of ME^3A-Al_4..... 140
Figure 4.4. ^1H NMR spectrum (700 MHz, $CDCl_3$) of ME^3A-Am_4..... 140
Figure 4.5. Analytical HPLC traces of aldehyde- and amine-functionalized oligopeptoids incorporating ME^3A spacer: (a) ME^3A-Al_4 (purity 98%) & (b) ME^3A-Am_4 (purity 97%). 141
Figure 4.6. MALDI mass spectrum of molecular ladder formed by dynamic covalent dimerization of oligopeptoids incorporating ME^3A spacer. 142
Figure 4.7. MALDI Mass spectra of Vernier-templated 12-rung molecular ladders. 145
Figure 4.8. MALDI mass spectra of reduced, Vernier-templated 12-rung ladders. 146
Figure 4.9. GPC traces of Vernier-templated 12-rung molecular ladders. 147

Figure 4.10. Deconvoluted GPC traces of peptoid-based, Vernier-templated 12-rung molecular ladders (a) VA_Al×Am_3×4, (b) VA_Al×Am_4×3, (c) VA_Al×Am_4×6, and (d) VA_Al×Am_6×4 (straight reaction mixtures). 148
Figure 4.11. MALDI mass spectra of scrambling *via* transimination between E^3A-Am_4 and ME^3A-HB_4 at different time points. 153
Figure 4.12. MALDI mass spectra of scrambling *via* imine metathesis between Im_4 and ME^3A-Im_4 at different time points. 154
Figure 4.13. Concentration of scrambled molecular ladders versus time during strand exchange *via* transimination or imine metathesis. 155
Figure 5.1. ^{1}H NMR spectrum of compound 1. 163
Figure 5.2. ^{13}C NMR spectrum of compound 1. 163
Figure 5.3. ^{1}H NMR spectrum of compound 2. 165
Figure 5.4. ^{1}H NMR spectrum of compound 3. 166
Figure 5.5. ^{1}H NMR spectrum of compound 4. 167
Figure 5.6. ^{1}H NMR spectrum of compound 5. 168
Figure 5.7. ^{1}H NMR spectrum of compound 6. 169
Figure 5.8. ^{1}H NMR spectrum of compound 7. 170
Figure 5.9. ^{1}H NMR spectrum of compound 8. 172
Figure 5.10. Chemical structure of oligopeptoid NPPOC-Am_3. 174
Figure 5.11. Chemical structures of oligopeptoids (a) Act-Al_2-Boc-Am_2, (b) Teoc-Am_4 and (c) Act-Al_4. 175
Figure 5.12. ESI spectra of oligo(peptoid)s purified by preparative HPLC. 178
Figure 5.13. Photodeprotection of NPPOC..... 179
Figure 5.14. Erbium(III)-mediated deprotection of Teoc. 180
Figure 5.15. Analytical HPLC traces of oligo(peptoid) Teoc-Am_4 before and after treatment with 1 M TBAF..... 181
Figure 5.16. Deprotection of Alloc by Pd(0) in the presence of phenylsilane..... 182
Figure 5.17. Deprotection of acetal group by Lewis acids. 185
Figure 5.18. Influence of solvent on acetal deprotection by Sc(III). 188
Figure 5.19. Influence of water content on acetal deprotection at 50°C. 190

Figure 5.20. Influence of Sc(III) concentration on the equilibrium of peptoid-based 8-rung ladder (Im_8) formation. 191
Figure 5.21. Influence of Sc(III) concentration on acetal deprotection characterized by MALDI mass spectrometry..... 192
Figure 5.22. Influence of water content on acetal deprotection at 70°C. 193
Figure 5.23. Effect of Sc(III) on acetal deprotection at 70°C. 194
Figure 5.24. Influence of water content on acetal deprotection and subsequent self-assembly of 4-rung peptoid ladders characterized by MALDI mass spectrometry. 195
Figure 5.25. Influence of Sc(III) concentration on acetal deprotection and subsequent self-assembly of 4-rung peptoid ladders (Im_4) characterized by MALDI mass spectrometry..... 196
Figure 5.26. *In situ* deprotection and self-assembly of a 8-rung peptoid ladder (Im_8) by using Sc(III) as a dual role catalyst. 197
Figure 5.27. Kinetics of *in situ* deprotection and molecular ladder formation for Act-Al_4–Am-4, treated with 0.20 equivalents Sc(III) in 2 v/v% water/MeCN at 70°C. MALDI mass spectra of the crude reaction mixture are shown at increasing time intervals. 198
Figure 5.28. ESI spectra of information-bearing complementary peptoid strands (a) ME3A-1001001 and (b) ME3A-0110110 purified by preparative HPLC. 200
Figure 5.29. Self-assembly of information-bearing complementary peptoids ME^3A-1001001 (strand I) and ME^3A-0110110 (strand II) into a 7-rung ladder (Im_7) characterized by MALDI mass spectrometry. 201
Figure 5.30. Facilitating handshake line shuffling to achieve in-registry molecular ladders with the addition of aniline or acetic acid. 203
Figure 5.31. Characterization of peptomer Leu-Am_2-ActAl_2: (a) chemical structures; (b) ESI spectra of purified peptoids; (c) circular dichroism (CD) spectrum. 205
Figure 5.32. *In situ* deprotection and self-assembly of peptoid-peptide hybrids Leu-Am_2-ActAl_2 into a 4-rung molecular ladder (Im_4). 206
Figure 5.33. Illustration of Σ('sigma')-strand structure. 207
Figure 6.1. Dynamic covalent assembly of peptoid-based grids. 217

Figure 6.2. ESI mass spectra of base strand (a) and building strand (b) purified by preparative HPLC. 218
Figure 6.3. MALDI mass spectra of Ladder-I and Ladder-II. 219

LIST OF SCHEMES

Scheme 1.1. Schematic diagram of the solid-phase peptoid synthetic procedure. 17
Scheme 1.2. Solution polymerization using N-substituted NCAs and NTAs for peptoid polymer synthesis.[21] 19
Scheme 1.3. The three types of imine reactions (a) imine condensation, (b) exchange, and (c) metathesis. 33
Scheme 2.1. Synthesis of 4-(2-aminoethyl)-N-(*tert*-butoxycarbonyl) phenylamine (1). Reagents and conditions: di-*tert*-butyl dicarbonate, 10% acetic acid in water, 1,4-dioxane, r.t. overnight.[40] 60
Scheme 2.2. Synthesis of 4-(1,3-dioxacylclopent-2-yl) (3). Reagents and conditions: (a) ethylene glycol, toluene-p-sulfonic acid, toluene, reflux; (b) $LiAlH_4$, Et_2O, 0°C for 4 h then r.t. for 12 h.[41] 62
Scheme 2.3. Synthesis of 2-(2-ethoxyethoxy)ethylamine (E^3A) (6). Reagents and conditions: (a) tosyl chloride, THF, 0°C, (b) NaN_3, DMF, 60°C, 36 h, and (c) TPP, water.[42] 65
Scheme 2.4. Dimerization of peptoid-based molecular ladders (*m* = *n*)..... 83
Scheme 2.5. Dynamic covalent assembly of *n*–rung peptoid-based molecular ladders initially by imine condensation reactions and followed by imine exchange reactions..... 84
Scheme 3.1. Synthesis of DABCYL-EN for subsequent use as a primary amine-bearing submonomer in solid-phase peptoid synthesis..... 105
Scheme 4.1. Vernier templates for macromolecular synthesis. 133
Scheme 4.2. 2-(2-(2-Methoxyethoxy)ethoxy)ethylamine (ME^3A) (3). Reagents and conditions: (a) tosyl chloride, THF, 0°C, (b) NaN_3, DMF, 60°C, 36 h, and (c) TPP, water.[10] 135

Scheme 4.3. Dynamic covalent assembly of peptoid-based ladders by Vernier-Templating. (a) Structures of linear oligopeptoids bearing pendant amine (E^3A-Am_*n*) and aldehyde (E^3A-Al_*m*) functional groups. (b) Vernier-templated assembly of complementary oligopeptoids with non-commensurate functionalities into molecular ladders with *m* × *n* rungs (VA_Al×Am_*m*×*n*, where VA is 'Vernier assembly'). 144
Scheme 4.4. Scrambling between a tetra-amine peptoid strand and a peptoid-based, 4-rung molecular ladder. 151
Scheme 4.5. Scrambling between two different 4-rung peptoid-based ladders. 152
Scheme 5.1. Synthesis of 4-(2-aminoethyl)-N-(2-(2-nitrophenyl) propylcarbonyloxy) phenylamine (1). Reagents and conditions: 2-(2-nitrophenyl)propyl chloroformate (NPPOC chloride), 10% aq. acetic acid, 1,4-dioxane, r.t. overnight. 162
Scheme 5.2. Synthesis of 4-(2-aminoethyl)-N-(2-(trimethyl)ethoxycarbonyloxy) phenylamine (7). Reagents and conditions: (a) di-tert-butyl dicarbonate, THF, r.t., overnight; (b) tosyl chloride, THF, 6 M NaOH, 0°C; (c) NaN_3, DMF, 60°C; (d) TFA, DCM, r.t., 30 min; (e) N-[2-(trimethylsilyl) ethoxycarbonyloxy] succinimide, DMF, 60°C, overnight; (f) TPP, THF, DI water. 164
Scheme 5.3. Synthesis of 4-(2-aminoethyl)-N-(allylcarbonyloxy)phenylamine. Conditions: allyl chloroformate, 10% aq. acetic acid, 1,4-dioxane, r.t. overnight. 171
Scheme 5.4. Synthetic procedure for oligo(peptoid)s Act-Al_2–Am_2 and Act-Al_4–Am_4..... 176
Scheme 5.5. Structures of the oligo(peptoid) pendant groups used in this study. 183
Scheme 5.6. Acetal-aldehyde and Boc-amine bearing peptoid oligomers are treated with TFA to effect *in situ* acetal and Boc deprotection and oligomer self-assembly. 184
Scheme 5.7. Upon Pd(0)-catalyzed Alloc deprotection, amine- and acetal-bearing oligomers generated by solid phase peptoid synthesis are photocleaved from resin, purified, and treated with $Sc(OTf)_3$ to effect *in situ* acetal deprotection and oligomer self-assembly..... 187
Scheme 5.8. Incorporation of sequence information into peptoid strands and subsequent self-assembly of complementary strands into peptoid-based ladders. 199

LIST OF TABLES

Table 2.1. Structural information of aldehyde–functionalized oligopeptoid sequences subjected to MALDI mass spectrometry, HPLC and GPC analysis. 82
Table 2.2. Structural information of amine–functionalized oligopeptoid sequences subjected to MALDI mass spectrometry, HPLC and GPC analysis. 82
Table 2.3. GPC analysis of peptoid-based, dimerized molecular ladders 92
Table 3.1. Structural information of peptoid sequences subjected to FRET study. 108
Table 3.2. Molecular weight of the desired molecular ladder with n = 12 rungs and its out of registry ladders subjected to MALDI analysis. 115
Table 3.3. Molecular weight of the desired molecular ladder with n = 4 rungs and its out of registry ladders subjected to MALDI analysis. 118
Table 3.4. Molecular weight of the desired molecular ladder with n = 8 rungs and its out of registry ladders subjected to MALDI analysis. 119
Table 3.5. Molecular weight of the desired molecular ladder with n = 10 rungs and its out of registry ladders subjected to MALDI analysis. 119
Table 4.1. Deconvoluted peak analysis of VA_Al×Am_3×4. 149
Table 4.2. Deconvoluted peak analysis of VA_Al×Am_4×3. 150
Table 4.3. Deconvoluted peak analysis of VA_Al×Am_4×6. 150
Table 4.4. Deconvoluted peak analysis of VA_Al×Am_6×4. 150
Table 5.1. Yields of acetal deprotection by 0.2 eq. Sc(III) at 50°C in different solvents. 189
Table 5.2. Yields of acetal deprotection by 0.2 eq. Sc(III) at 50°C with different water contents. 189
Table 5.3. Yields of acetal deprotection in 2 v/v% water/MeCN at 50°C with different equivalents of Sc(III). 192

Table 5.4. Yields of acetal deprotection by 0.2 eq. Sc(III) at 70°C with different water contents. 193
Table 5.5. Yields of acetal deprotection in 2 v/v% water/MeCN at 70°C with different equivalents of Sc(III). 194

ABSTRACT

A long-standing challenge in the field of self-assembly is creating nanostructures that rival the complexity of their biological counterparts. One example is the DNA double helix, which has been used to construct complex, multi-dimensional structures triggered by the self-assembly instructions encoded in DNA sequences. However, due to the weakness of hydrogen bonding in the DNA structures, these assemblies are fragile and susceptible to thermal and mechanical degradation. To address these deficiencies, dynamic covalent self-assembly of sequence-specific peptoids is used to create chemically and thermomechanically robust nanostructures. In particular, the dynamic covalent assembly used relies on the reversible amine/aldehyde reaction to generate imine linkages.

This dissertation details the design and synthesis of sequence-specific peptoids that contain dynamic covalent functional groups (amines and aldehydes) that self-assemble into molecular ladders through imine condensation and exchange reactions catalyzed by scandium(III) triflate. Furthermore, three potential mechanisms of ladder formation are proposed here, including a 'molecular zipper', a 'molecular hand-shake line' and 'toehold displacement'. MALDI mass spectrometry and distance measurements using Förster resonance energy transfer (FRET) were employed to determine the hybridization mechanism, indicating that two complementary strands initially interact and bind by

rapidly ‘zipping-up’ at any point generating molecular ladders with an arbitrary number of rungs, followed by slowly shuffling through a ‘molecular hand-shake line’ until these ladders come into registry.

In addition, small precursor peptoids of mismatched numbers of complementary functional groups are used to self-assemble into large structures through Vernier-templating. Strand exchange experiments based on transimination and imine metathesis are designed to determine the rate-limiting step for Vernier-templated assembly.

Finally, this dissertation discusses the development of an elegant approach for the dynamic covalent assembly of oliogmeric species bearing both amine and aldehyde functional groups by employing scandium(III) triflate as a dual role catalyst, effecting both *in situ* ethylene acetal deprotection and imine exchange reactions.

Combined, these findings open up possibilities to design and construct robust, complex nanostructures based on the self-assembly of sequence-specific, dynamic covalent oligomers with potential applications from information storage to high precision nano-filtration membrane to smart matrix grids for energy harvesting.

Chapter 1
Introduction

1.1 Background and Research Overview

The term 'self-assembly' describes processes in which pre-existing components spontaneously aggregate to form ordered structures or patterns owing to the local interactions amongst the components themselves.[1-2] Many important examples of self-assembly can be found throughout chemistry, materials science, and biology, such as the formation of molecular crystals,[3] phase-separated polymers,[4] self-assembled monolayers,[5] lipid bilayers,[6] polypeptide folding,[7] and nucleic acid hybridization.[8] Self-assembly mechanisms necessarily utilize kinetically labile molecular interactions, where a rapid equilibrium exists between the initial reactants and the potential products.[2] This characteristic affords a mechanism for error correction during the assembly process, allowing for the formation of the most thermodynamically stable product by minimization of the Gibbs energy. Thus, these self-assembly reactions effect the arrangement of components into the final desired structure *via* an iterative, 'trial-and-error' exploration of the potential alternative configurations.

Self-assembly processes are often based upon weak intermolecular interactions such as hydrogen bonding, π stacking, or van der Waals interactions.[9] One consequence of the relative weakness of these transient interactions is that the assembled structures are often fragile and susceptible to mechanical degradation. Covalent bonds typically exhibit bond

energies that are over an order of magnitude higher than those for hydrogen bonds[10] and could conceivably provide a route for the fabrication of far more mechanically robust assemblies. However, the creation of exquisite nanostructures by self-assembly and the toughness imparted by covalent bonds are generally perceived as mutually exclusive owing to the prevalent irreversibility of covalent bond-generating reactions. Fortunately, several covalent interactions are known to be reversible under particular reaction conditions,[11-12] enabling the error correction mechanism that is essential for the selective fabrication of supramolecular structures. As a result of the enormously greater strength and directionality offered by covalent bonds in comparison to the weaker interactions observed in biology, these 'dynamic' covalent chemistries offer an elegant approach to nanostructure assembly that combines complexity and toughness.

Nucleic acids (also known as polynucleotides) present the most versatile class of materials for producing nanostructures to date and, through careful consideration of their residue sequence, can be designed to self-assemble *via* the hybridization of complementary strands into arbitrary structures with nanometer precision.[13-15] Unfortunately, the versatility of nucleic acid assemblies is tempered by their thermal and mechanical instability,[16] attributable to the weakness of the hydrogen bonds that hold the strands together. The substitution of the canonical nucleic acid base pairs with dynamic covalent base pairs would preclude this instability and yield a unique and powerful nanofabrication strategy wherein the complex, information-driven assembly of nucleic acids is combined with the strength of covalent bonds.

This thesis details an exploration of the hypothesis that the assembly of complementary, sequence-specific oligomeric peptoids can be mediated by reversible,

dynamic covalent bonds, enabling the fabrication of arbitrary, robust, multi-dimensional nanostructures unattainable using conventional self-assembly interactions.

1.2 Sequence-controlled Polymers

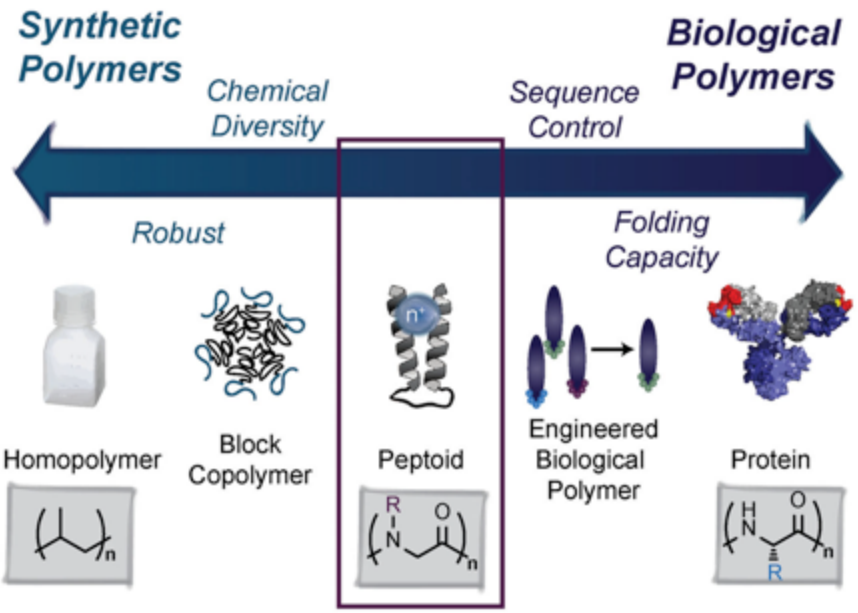

Figure 1.1. The range of characteristics for synthetic and biological polymers reveals a gap that is strategically filled by sequence-defined polymers such as peptoid-based materials.[17]

Sequence-controlled polymers are macromolecules that comprise well-ordered sequences of different monomer constituents (Figure 1.1). The ability to precisely control monomer sequence in synthetic polymer chains is of great importance and could find utility in many areas. For instance, precisely controlled sequences in synthetic polymers have great potential as data storage devices as each functional pendant groups could be considered as an inforamtion "bit".[18] Moreover, the ability to manipulate monomer sequence could offer fine structural control of synthetic polymer chains, therefore affecting structure-property relation and macroscopic properties of polymers as it

influences polymer-polymer interaction, folding, crystallization, or self-assembly. However, in common synthetic copolymer, the distribution of monomer units is generally poorly controlled, and therefore the compositions vary from chain to chain.[18-21] Alternating, block or graft copolymers represent the simplest level of sequence-controlled polymers and they lack the structural sophistication achieved by natural biopolymers (see Figure 1.1). Nature has developed a range of sequence-controlled polymers, which represent the highest level of sequence control and has afforded a plethora of sophisticated functions from carrying the genetic code to catalyzing chemical reactions.[17-21] These functions are enabled by the precise control of molecular interactions on the ångström scale – the length scale of individual bonds.[17] For example, nucleic acids such as DNA are based on the ordered sequences of A-T, G-C base pairs and the genetic information encoded in these sequences could instruct the synthesis of sequence-defined mRNA and peptides through transcription and translation process (Figure 1.2).[18-19] The application of DNA goes well beyond biotechnology to areas of nanotechnology and materials science.[17, 22-23] More recently, the sequence-specific binding properties of DNA have been employed to direct the self-assembly of materials at the nanoscale.[22-23]

Most recently, polymer chemists have sought to improve synthetic strategies to imitate nature's degree of sequence control in order to close the gap between synthetic polymers and naturally occurring polymers.[17-21] There are various synthetic methods reported to develop sequence-controlled polymers such as templating, kinetic control, orthogonal reactivities, and the linking of structures after polymerization, [17-21] allowing for the advancement of synthetic polymers.[24-26]

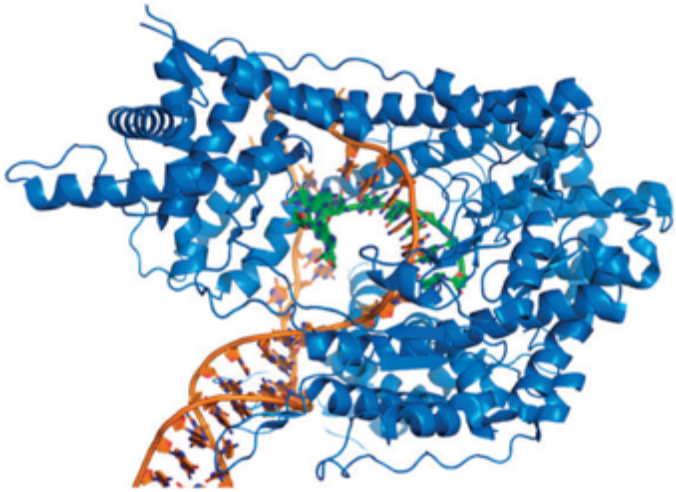

Figure 1.2. Transcription of a DNA-template (orange) into a sequence-defined mRNA chain (green), catalyzed by an RNA polymerase (blue).[19]

1.2.1 Synthetic Approaches to Sequence-controlled Polymerization

Sequence-controlled polymers could be synthesized by either chemical or biotechnological approaches. The latter method, dependent on highly evolved biological mechanisms, is very efficient. The enzymes of living organisms can be re-programmed to prepare sequence-specific polymers[18] and such examples include the polymerase chain reaction[27] (PCR) and protein engineering[28]. These biological pathways are limited mostly to naturally occurring polymers, whereas synthetic chemistry could provide sequence-specific polymers with much more chemical diversity.[18] In addition, compared to biological methods, synthetic chemistry techniques could afford larger-scale production of sequence-controlled polymers at a reduced cost. One prominent strategy to control monomer sequences relies on the step-wise, iterative synthesis to sequentially attach monomer units on insoluble solid supports (i.e., cross-linked resins), with washing of unreacted reagents, and deprotection of the reactive site, followed by cleavage of product from the support (see Figure 1.3). Merrifield et al.[29] pioneered this solid-phase synthesis

strategy primarily for the preparation of peptides in late 1940s, and this strategy, which remains as one of the best synthetic methods for sequence control,[17] has quickly expanded to the synthesis of DNA, RNA, peptidomimetic polymers and a wide range of resin-bound organic compounds and building blocks.[30] Nonetheless, one limitation of solid-phase synthesis is to prepare sequence-defined artificial polymers of significant main chain lengths as near quantitative yields are required for each monomer coupling reactions in order to achieve longer polymer chains with high yields. Furthermore, monomer-coupling efficiency is affected by the limited accessibility of reactive sites on the solid-support resin. This problem could be solved by the utilization of individual soluble polymer chain as supports (Figure 1.4). Thus, linear polystyrene soluble supports, containing optimized end-groups for step-wise iterative synthesis, has been developed to and synthesized by living polymerization.[31] This strategy could be applied to the synthesis of various non-natural sequence-specific polymers.

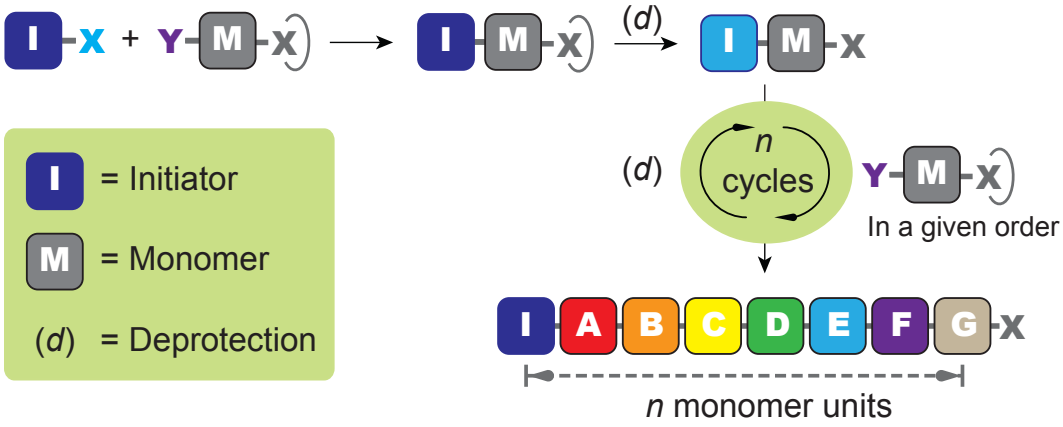

Figure 1.3. Solid-phase approach: sequentially attaching monomers one by one.[18]

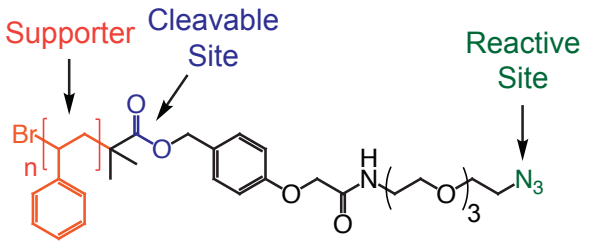

Figure 1.4. Soluble polymer supporter for azide-alkene click reaction.

Several other mechanisms for sequence-controlled polymerization have also been developed in 'traditional' polymerization processes, including ionic polymerization[32-34], controlled radical polymerization[21, 35-36], and ring-opening metathesis polymerization[37], etc. A tremendous progress has been made in the field of controlled polymerization chemistry and opens up avenues to precision synthesis of polymers with controlled molecular weight and complex architectures in ways that were unimaginable a few decades ago.[34] The obtained molecular architectures are not limited to multiblock copolymers.

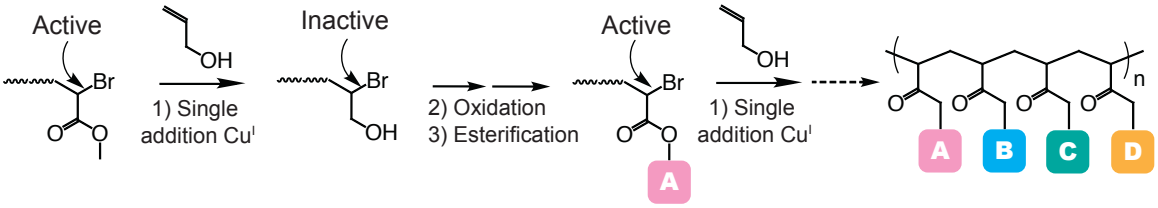

Figure 1.5. Sequence controlled living radical polymerization utilizing iterative single-monomer addition with allyl alcohol.[38]

For instance, Tong et al. described an atom-transfer radical addition (ATRA) based strategy to synthesize vinyl copolymers with monomer level sequence control.[38] At the beginning of each cycle of this approach (Figure 1.5), an ally alcohol monomer of low-activity is added at the vinyl chain end *via* ATRA, which was first developed by

Matyjaszewski and colleagues.[39-40] The resulting halogen chain end is inactive for radical generation or further propagation, even in the presence of a metal catalyst. However, this halogen terminal becomes active for another allyl alcohol single-monomer addition once the hydroxylmethyl residue is oxidized into a carboxylic acid, which could be further functionalized through esterification to introduce specific side groups and to reactivate the new chain end for the next ATRA reaction.[38]

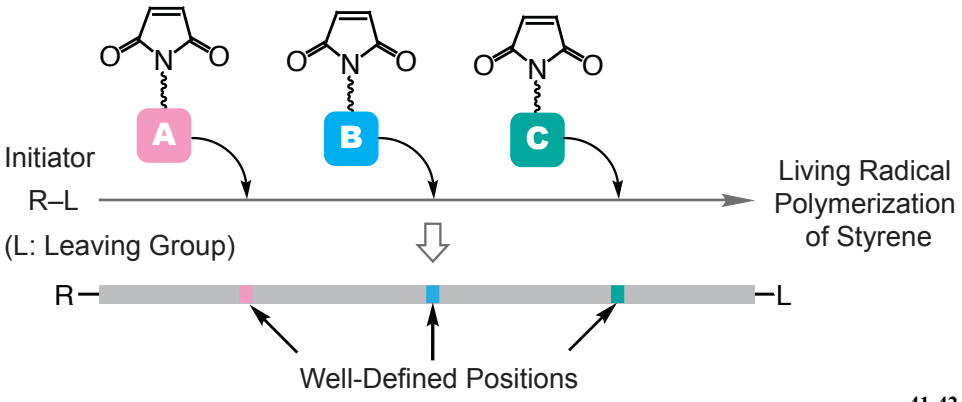

Figure 1.6. Positioning control in living radical polymerization of styrene.[41-42]

By utilization of specific comonomer pairs such as the combinations of an-electron donor and an acceptor monomer that favor cross-propagation over homopropagation, monomer sequence control could also be achieved in chain-growth polymerization. For instance, maleic anhydride and *N*-substituted maleimide monomers demonstrate a very low tendency for homopolymerization but they are prone to cross-propagate with styrene instead.[41-42] Therefore, these monomers are rapidly consumed in the presence of styrene.[41] Lutz et al. utilized the concept of sequential atom transfer radical copolymerization of styrene donor monomers and various *N*-substituted maleimide acceptor comonomers to introduce the location functionalization to polymer chains

(Figure 1.6).[41-42] The acceptor comonomers could be introduced into narrow regions of the growing polymer chains as a result of the preferred donor-acceptor cross-propagation, thereby allowing for the precise control of the polymer backbone. However, this strategy is limited by the chain-to-chain deviations in length, composition, and sequence during chain growth.[18]

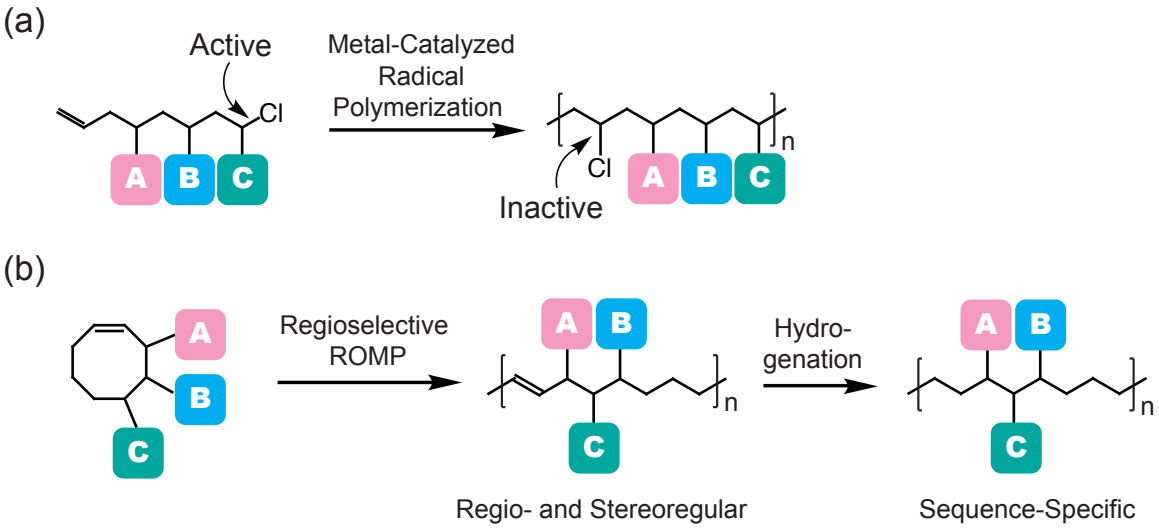

Figure 1.7. Step-growth polymerization for the synthesis of sequence-controlled polymers: (a) metal-catalyzed radical polymerization;[43-44] (b) regio-selective ROMP of asymmetric substituted cyclooctene.[45]

Sequence-controlled oligomers comprised of reactive chain ends can be polymerized by step growth, making step-growth polymerizations also suitable for the synthesis of sequence-defined polymers. For instance, Satoh and colleagues reported the synthesis of sequence-regulated vinyl copolymers consisting of styrene, acrylate and vinyl chloride units by step-growth radical polymerization.[43-44] This process utilizes a metal-catalyzed radical addition reaction between a reactive C-Cl bond and a non-conjugated C = C double bond. Copper catalyst can activate the C-Cl bond to form a carbon radical species,

which will add to the C = C double bond to generate a C-C backbone with an inactive C-Cl pendant group (Figure 1.7 (a)).[43-44] Furthermore, Hillmyer and coworkers demonstrated the synthesis of sequence-specific vinyl copolymers by regioselective ring-opening metathesis polymerization (ROMP) of various multisubstituted cyclooctenes using the Grubbs catalysts and subsequent hydrogenation.[45]

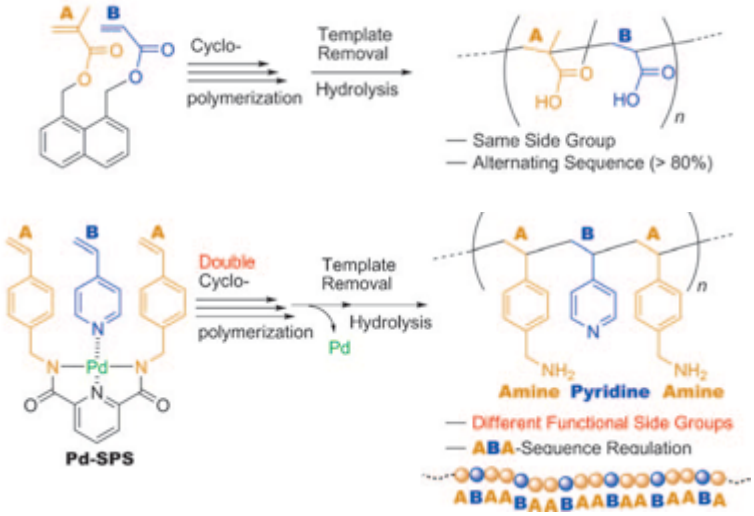

Figure 1.8. Sequence-controlled radical polymerization by templated synthesis.[46-47]

Finally, template-based synthesis is commonly observed in nature and plays an essential role to control monomer sequences of biopolymers including RNA and proteins. Therefore, template synthesis, in conjunction with living polymerization, has also been extensively explored for the synthesis of sequence-defined artificial polymers. For example, Ouchi and Sawamoto utilized a naphthalene framework as a template that attaches monomer units such as methacrylate and acrylate adjacent to each other through a cleavable ester linkage (see the top figure of Figure 1.8). Hence, well-defined polymers bearing AB-alternating between methyl methacrylate and acrylate sequences were prepared *via* a metal-catalyzed living radical polymerization of an AB-templated divinyl

monomer.[46-47] They further developed metal-complex frameworks that could attach multiple vinyl monomers bearing different functional groups through readily cleavable coordination interactions (see the bottom figure of Figure 1.8), thus allowing for an ABA, ABC, and other triple-unit alternating sequences.[46-47] However, the structures of sequence-defined polymers prepared from this template synthesis strategy are limited to simple periodic patterns.

1.2.2 Nucleic Acids as Biological Sequence-controlled Polymers and DNA Nanotechnology

Nucleic acids (e.g., DNA and RNA) are macromolecules that serve as the ubiquitous information-bearing molecules throughout biology. For DNA, information is encoded in the sequence of nucleobase residues affixed to a single deoxyribophosphate strand. These nucleobases dimerize *via* hydrogen bonding, where adenine base pairs with thymine and cytosine base pairs with guanine, such that DNA itself consists of a double helix of complementary strands, a structure that was first described in 1953 by Watson and Crick[48] and by Wilkins et al.[49] Thus, DNA can be considered a ladder polymer whose information is borne by its rungs.

The promise of nucleic acids as a nanostructure construction material is a consequence of their remarkable hybridization selectivity, their long persistence length,[50] and their high information density. These characteristics are attributable to several structural features. Upon the hybridization of two complementary single DNA strands, the base stacking of adjacent nucleobases, in conjunction with the chirality of the

deoxyribophosphate backbone, causes the double stranded DNA to twist into a helix.[51] The DNA strands in this double helix are anti-parallel, where the strands have opposite 5′ → 3′ polarity.[51] Moreover, the nucleobases dimerize such that a purine (adenine or guanine) pairs with a pyrimidine (thymine or cytosine); owing to the size difference between the purine and pyrimidine nucleobases, a mismatched base pair can yield a thermodynamically unfavorable distortion in the polymer backbone,[52] thus hybridization with the ideal complementary strand is strongly favored. Finally, as DNA is composed of four nucleobases, information can be considered as encoded in base-4 (i.e., DNA is a quaternary numeral system); consequently, for a DNA sequence with n bases, there are 4^n unique sequence compositions.[50]

In 1982, Seeman advanced the concept that nucleic acids could self-assemble into non-linear structures such as branched junctions and lattices,[53] thus heralding the field of nucleic acid nanotechnology. By annealing oligonucleotide sequences that lack the sequence symmetry typically found in their biological counterparts, the maximization of Watson-Crick base pairing (equivalent to the minimization of Gibbs energy, a thermodynamic stability criterion) affords junctions from which multiple double helices may emanate. Furthermore, by utilizing 'sticky end' overhangs where oligomeric tails remain temporarily unhybridized, each junction may be linked together directly (see Figure 1.9 (a)), or with linear DNA fragments interspersed between them. It was thus theorized that it should be possible to assemble periodic, multi-dimensional nucleic acid networks (Figure 1.9 (b)).[53] In a nanotechnological tour de force, Seeman employed the self-assembly of asymmetric oligonucleotide strands to fabricate a cubic molecule composed exclusively of DNA.[54] The capacity of nucleic acids to generate complex

nanostructures was also applied to the fabrication of ordered organic/inorganic hybrid materials. For example, the assembly of DNA strands affixed to the surface of metallic and semiconductor nanoparticles was shown to effect the aggregation of particles into well-defined, three-dimensional arrays,[55-56] structures potentially useful for biodetection[57] and photonic device[58] applications.

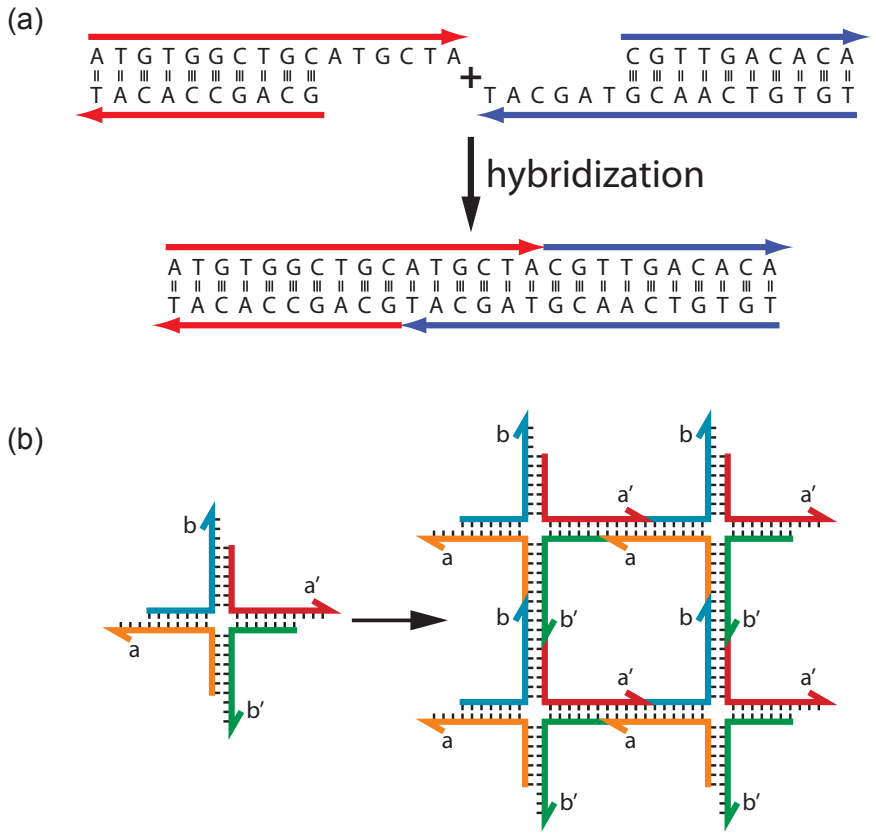

Figure 1.9. The advent of DNA nanotechnology. (A) Sticky end hybridization. (B) The sticky end-mediated assembly of a branched nucleic acid junction into a square lattice.[52]

A tremendous increase in interest in nucleic acid nanotechnology was precipitated by the development of 'DNA origami',[14] a fabrication technique whereby two-dimensional shapes are made by raster-filling with a long, single-stranded DNA scaffold held in place

by hundreds of short oligonucleotide 'staple strands'. Once synthesized and mixed, the staple and scaffold strands self-assemble in a single step to yield arbitrary nanostructures with a spatial resolution of ~6 nm (see Figure 1.10 (a)). By considering the nucleic acid sequence of the single long strand, information can be encoded in the hundreds of complementary short strands such that, upon assembly, arbitrary structures of unprecedented sophistication can be generated from the bottom up (Figure 1.10 (b)). The flexibility of this technique has since been demonstrated repeatedly to fabricate a variety of structures such as 'nano-breadboards'[59-60] and molecular containers.[61-62]

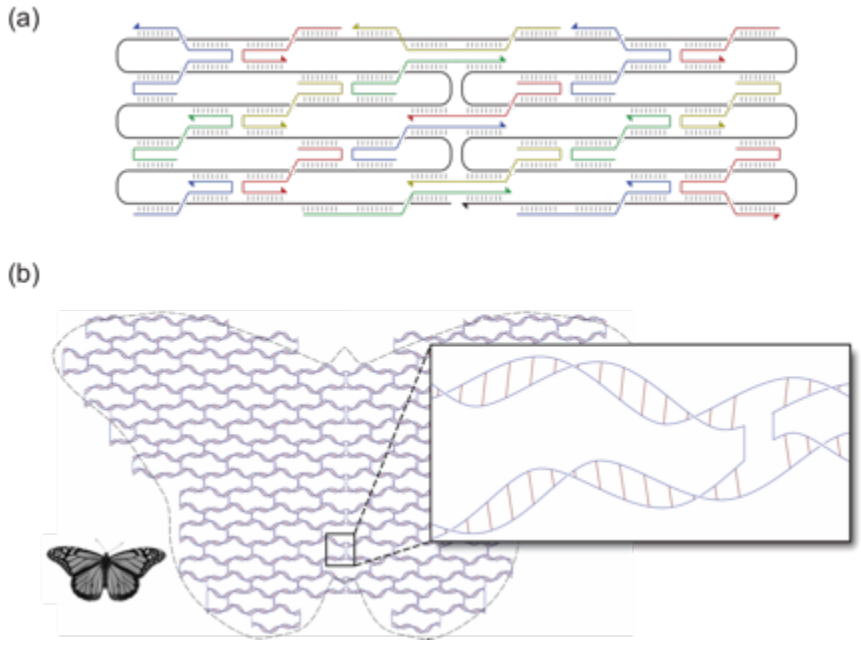

Figure 1.10. Schematic of DNA origami. (A) Synthesized oligomeric DNA strands are designed to hybridize with one long DNA strand such that it raster-fills a predetermined shape. (B) Through careful consideration of the oligomeric DNA sequences, this approach can be used to assemble arbitrary, complex shapes (e.g., a butterfly) in a single step.

Despite these impressive advances in nucleic acid nanotechnology, there still exist limitations with respect to the mechanical and thermal stability of assembled structures

that are held together with hydrogen bonds utilized by the canonical Watson-Crick base pairs. Notably, even non-canonical, synthetic base pairs employ weak intermolecular forces to effect dimerization, such as hydrophobic interactions,[63] thus their incorporation in nucleic acid-based nanostructures would not significantly raise the structural thermomechanical stability. Force-induced melting, where applying opposite forces to the strands of double stranded DNA perpendicular to its axis unzips and separates the double helix into two single strands, is necessary for DNA transcription and replication as enzyme complexes break the hydrogen bonds between complementary nucleotides.[64] Although this phenomenon is indispensible in biology, it is disadvantageous when constructing nanostructures and machines where the integrity of the structure must be maintained under load. Whereas DNA can be mechanically unzipped under a load of ~15 pN,[65-66] covalent bonds typically rupture at forces greater than 1 nN, approximately two orders of magnitude higher.[67] Thus, it can be anticipated that this hundred-fold difference in mechanical strength would be reflected in the robustness of nanostructures generated using dynamic covalent base pairs when compared with their DNA-based counterparts.

1.2.3 Sequence-specific Peptoids

Peptoids, comprised of *N*-substituted glycine units, represent a new class of non-natural, sequence-defined polymers that can fold into higher order nanostructures (Figure 1.11).[17, 68-69] Structurally similar to peptides, the side chains of peptoids are attached to the nitrogen instead of α-carbon. Their biomimetic and sequence-specific structures open up brand new avenues for the development of sequence programmable, folded polymers

with the robustness typical of synthetic materials.[17] Therefore, peptoid polymers are of great potential to bridge the gap between synthetic polymers and biological materials (see Figure 1.1).

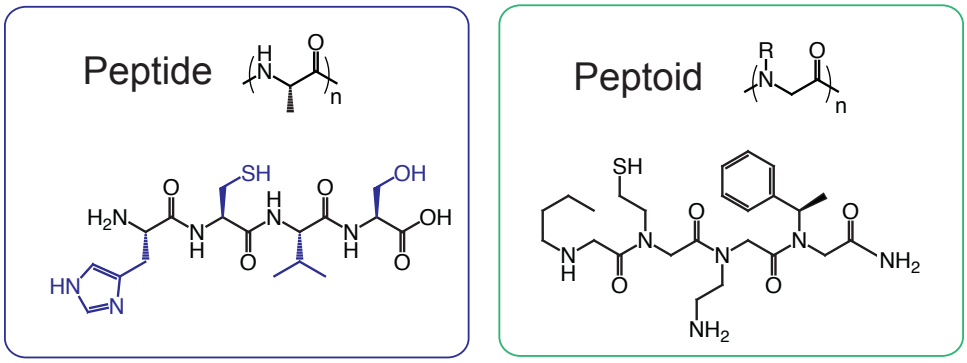

Figure 1.11. Peptide versus peptoid structures. Example tetramers are shown of each.[17]

Since the development of the 'submonomer' approach to solid-phase synthesis of peptoids by Zuckermann in 1992[68], they find utility in a plethora of fields. Given each monomer is individually tunable, this synthetic procedure affords for almost infinite combinations of peptoid sequences, thereby offering opportunities to screen for specific sequences with unique properties using combinatorial chemistry.[17,70] In addition, compared to polypeptides and polynucleotides, peptoids are more robust and versatile as they exhibit increased chemical diversity and are more resistant to enzymatic and environmental degradations at a reduced synthetic cost.[17] Lastly, the step-wise solid-phase approach would yield nearly uniform peptoids with polydispersity index (PDI) approaching 1, therefore allowing for precise structural regulation in synthetic polymers.[17] Their ease of synthesis and structural diversity allows testing of basic design principles for creating new biologically active and nanostructured materials. Thus, peptoids are proposed for the investigation of informational polymers that are able to

self-assemble into nanostructures through dynamic covalent interactions for our study. Herein, this section mainly reviews the synthetic methods and distinct applications of peptoids as modular and tunable structures that could potentially straddle the boundary between biopolymers and synthetic polymers.

1.2.3.1 Synthesis

Two main synthetic approaches are developed to synthesize peptoids in the past. The first approach employs an iterative step-wise technique, typically performed on a solid support resin, that allows for sequential addition of monomers and offers precise sequence control (Scheme 1.1). The alternative polymerization strategy is usually implemented in solution and is able to generate higher molecular weight polymers (Scheme 1.2). In addition, methods relying on biosynthetic pathyways to prepare sequence-defined polymers are also reported.[21]

(1) 'Submonomer' Approach to Solid-phase Synthesis

The step-wise submonomer approach to solid-phase synthesis begins by introducing individual monomers in the growing peptoid chain sequentially *via* a two-step addition: acylation and nucleophilic displacement (Scheme 1.1).[68, 71] First, acylation occurs, where a carbodiimide-activated bromoacetic acid acrylates a resin-bound amine. Subsequently, a primary amine displaces the bromide to introduce the side chain. The cycle can then be repeated to achieve a desired chain sequence. This simple procedure, which could be performed either manually or using an automated synthesizer, is capable of synthesizing sequence-specific oligomers of up to fifty repeat units long in high yield.

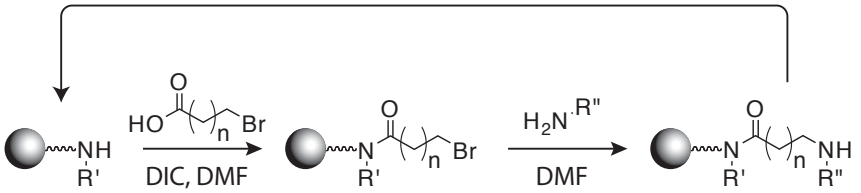

Scheme 1.1. Schematic diagram of the solid-phase peptoid synthetic procedure.
* The sequential addition of bromoalkyl carboxylic acids and primary amines yields sequence-specific oligomers without a deprotection step. Here, DIC is N,N'-diisopropyl-carbodiimide and DMF is dimethylformamide.

Altough this iterative approach seems tedious and time consuming in comparison, the step-wise modular synthesis is necessary for the precise monomer sequence control of peptoid polymers. Synthesis on a solid-support simplifies purification process for each cycle as excess reagents and unwanted side products could be easily washed away. The automation of coupling reactions assisted by microwave also allows for rapid and facile synthesis.[72] Moreover, very pure peptoid materials with high yield could be obtained as a result of almost quantitative yields of the two-step synthesis. The nature of this synthesis also enables the incorporation of various functional groups as side chains, affording an unlimited library of functions groups. A plethora of monomers with aliphatic, aromatic, heterocyclic, and ionic moieties are reported to be introduced as side chains into peptoids.[73] Side chains with reactive functional groups such as amines, aldehydes require protection, but many heterocycles can be used directly with no protection.[17, 74] As reported in the literature, functional groups introduced as the side chains range from small aliphatic groups, to amino acid-like side chains, to large moieties (such as carbohydrate, dyes, etc).[17, 74] These individual side groups also notably influences polymer properties and functions. For instance, Kirshenbaum et al[75] reported photo-

responsive peptoids bearing azobenzene side groups and Zuckermann et al.[76] demonstrated the incorporation of chiral moieties led entropic constraints and facilitated the formation of secondary structures. In addition, reactive functional groups such as ketones, aldehydes and thiols are introduced to peptoids as chemoselective coupling sites for conjugation of peptoids to biomolecules or to substrates.[77] Furthermore, Kirshenbaum et al. functionalized peptoid oligomers as substrates for azide-alkyene [3+2] cycloaddition conjugation reactions.[78]

(2) Ring-opening Polymerization (ROP) in Solution Phase

While step-wise submonomer synthesis is necessary for sequence control of polymers, the limitation lies in the length of polymers that can be synthesized.[17] Techniques using traditional living polymerization have thus been developed to overcome this limitation. The ring-opening polymerization (ROP) of *N*-substituted α-amino acid-*N*-carboxyanhydrides (*N*-substituted NCAs) to form polysarcosine was initially developed in 1926.[79] More recently, by using ROP of *N*-substituted NCAs, the Luxenhofer group reported the synthesis of well-defined homopolypeptoids and multiblock copolypeptoids (Scheme 1.2). The *N*-substitution could suppress irreversible chain termination, resulting in high monomer conversion and polymers with molecular weights of approximately 1–10 kg/mol and low polydispersity index (PDI) values (<1.1).[80-82] Different side groups could also be introduced to peptoids by varying the *N*-substitution. For instance, a variety of aliphatic side chains ranging from one to four carbons were incorporated into peptoids. While polymers with shorter side-chains were demonstrated to be water-soluble, those with longer chains were not soluble in water,

allowing for the design of amphiphilic block compolymers.[17] Matrix-assisted laser desorption/ionization time of flight mass spectrometry (MALDI-TOF MS), NMR, and GPC were used to characterize these polymers. The kinetics of polymerization followed a pseudo first-order with respect to the initiator, affording predictable molecular weights.[17, 80-82]

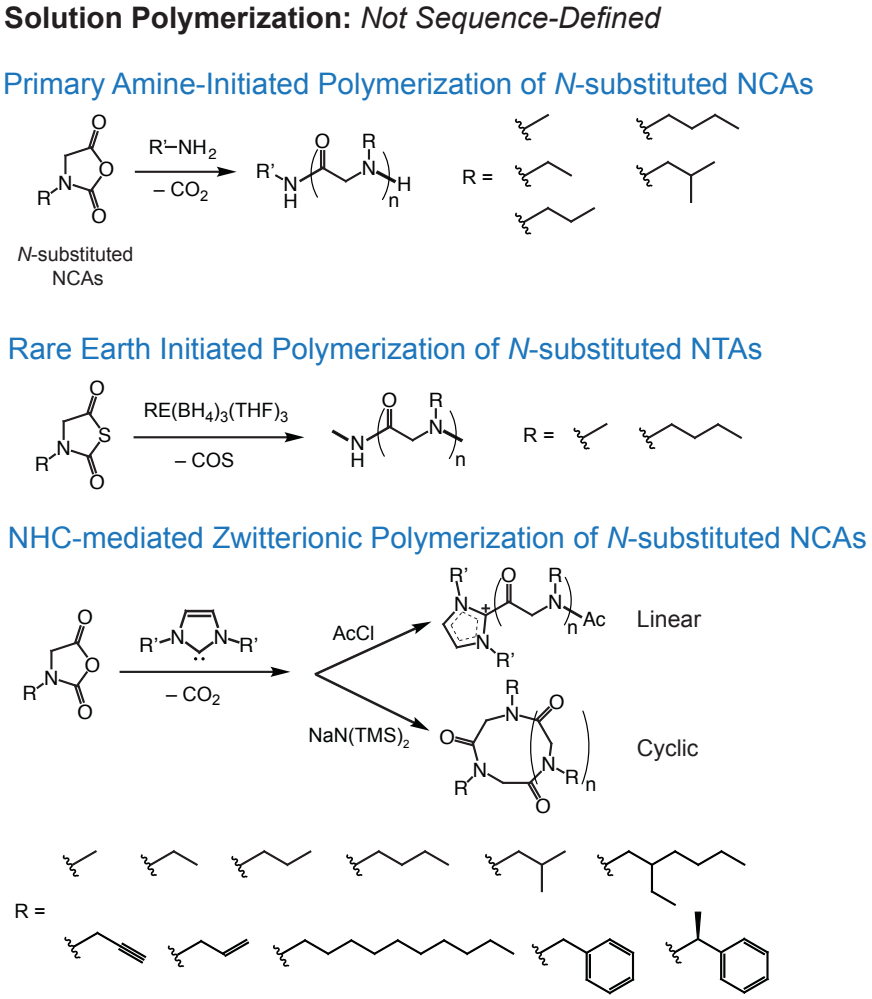

Scheme 1.2. Solution polymerization using N-substituted NCAs and NTAs for peptoid polymer synthesis.[21]

***** For $RE(BH_4)_3(THF)_3$, the rare earth (RE) can be Sc, Y, La, Nd, Dy, or Lu.

Several derivatives of the ring opening polymerization of *N*-substituted NCAs have also been reported. Zhang et al. utilized *N*-heterocyclic carbene (NHC) to mediate ROP polymerization of *N*-substituted NCAs and interestingly discovered that this synthetic approach could generate either liner or cyclic polymers (see Scheme 1.2).[83] Solvents and NHC structures significantly influence the molecular weight and polymerization rate. Kinetics studies revealed the polymerization of cyclic poly(*N*-decylglycine) peptoids followed pseudo-first order and resulted in high monomer conversions with narrow PDIs (1.03 – 1.05) and molecular weights ranging from 4.8 – 31 kg/mol.[84] The synthesis of block-copolymers with poly(*N*-methylglycine) with same degree of monomer conversion was achieved and these block copolymers assembled into spherical micelles that gradually transitioned into tubular micelles. Amino acid *N*-thiocarboxyanhydride (NTA), the thio-analogue of *N*-substituted NCAs, is much more stable than NCA against moisture and heat (see Scheme 1.2).[85-86] Therefore, Ling and coworker used NTAs to prepare hydrophilic polymers with sarcosine monomers,[85] hydrophobic polymers with butyl side-chains, and block copolymers that are thermoresponsive.[86] Polymerization of NTAs necessitates higher temperature as a result of its low reactivity; nonetheless, the yields, molecular weights, and polydispersities of the synthesized polymers are equivalent to those polymerized from *N*-substituted NCAs.[17]

(3) Biological Polymerization Process

While chemical synthetic approach enable rapid and facile synthesis of peptoid polymer, techniques based on biosynthetic pathways could facilitate the synthesis of longer sequence-defined peptoids and increase the ease of synthesis.[17] Although the

current methods based on biological machinery could only lead to small peptoids, these strategies open up great opportunities for enzyme-based synthesis of peptoids. Suga et al.[87] demonstrated a ribosomal synthesis of peptoids and peptide-peptoid hybrids. They exploited a cell-free translation system in conjuction with flexizymes – artificial aminoacyl-tRNA ribozymes to incorporate *N*-substituted glycines.[87] Various functional groups were incorporated such as alkyls, esters, azides, alkenes, and alkynes. However, linear peptoids of only up to six monomer units were generated in low yields.[87] The synthesis of cyclic peptoid-peptide hybrids linked by thioether was also described. Baldessari and coworker utilized an enzymatic procedure involving a lipase to synthesize poly(*N*-(2-hydroxyethyl)-β-propylamide oligomers, which was characterized by MALDI-TOF MS, showing low molecular weight and low dispersity.[88]

1.2.3.2 Modification of Primary Structure

The introduction of backbone-variants of the conventional *N*-substituted glycine peptoids (α-peptoids) provides additional conformations, expands the available ensemble of peptidomimetic foldamer scaffolds, and opens avenues to design nanoarchitectures with more tunability and stability. The most common variant is the β-peptoid, or *N*-alkyl-β-alanine oligomer.[89] Compared to α-peptoids, an additional methylene unit is added in the backbone of β-peptoids (Figure 1.12).

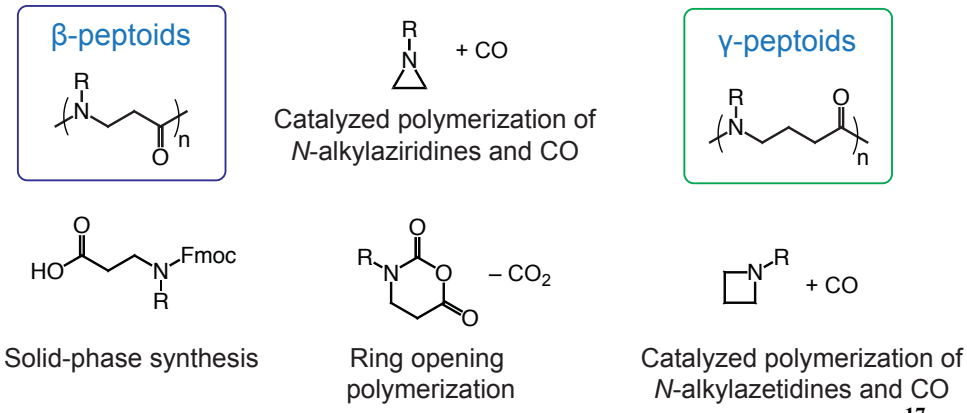

Figure 1.12. β-peptoid and γ-peptoid structures and synthesis techniques.[17]

Hanton et al.[90] described the first catalytic synthesis of poly-β-peptoids by the copolymerization of N-alkylaziridines and carbon monoxide with quantitative yields. The resultant poly-β-peptoids were characterized by ^{1}H and ^{13}C-NMR in addition to IR and MALDI-TOF MS, and were demonstrated to show controlled molecular weights (2 – 11 kg/mol with PDI from 1.11 – 1.64). $BnCOCo(CO)_4$ is utilized to catalyze the polymerization and is readily synthesized and purified with an extraction before polymerization. To achieve a comprehensive understanding of the reaction mechanism, *in situ* infrared spectroscopy was employed to monitor chain growth over time by applying various catalysts.[91] Several side-products including a lactam and polyamines can form instead of the amine based-polymer using the above-mentioned technique. The cobalt catalyst, $CH_3C(O)Co(CO)_3P(o\text{-tolyl})_3$, afforded rapid dissociation of the $P(o\text{-tolyl})_3$ ligand, the residual cobalt complex efficiently catalyzed the polymerization without forming lactam side-products.[17] The resultant β-peptoids prepared by cobalt-based catalysts were subjected to NMR and MALDI-TOF MS analysis, and then immobilized on gold serving as an anti-fouling material.[92]

Similarly, γ-peptoids, with an extra methylene in the backbone in comparison to β-peptoids (Figure 1.12), could be synthesized using cobalt-catalyzed polymerization of *N*-alkylazetidine and carbon monoxide.[93-94] However, the synthetic approach to prepare γ-peptoids is moderately successful as it only yields short sequences with low yield, therefore limiting the applications of γ-peptoids.

Step-wise modular synthesis is also employed for the synthesis of sequence-defined β-peptoids (Figure 1.12). Hamper and coworker reported a two-step monomer addition cycle including initial acylation with an acrylic acid followed by a Michael addition with a primary amine.[95] Arvidsson et al. continued this work by optimizing the synthesis and investigating Lewis acid as catalyst.[96] The highest yield was achieved by utilizing a Tentagel S PHB as a solid-support in the presence of water and tetrahydrofuran (THF).[96] However, the nucleophilic substitution for the step-wise synthesis of β-peptoids was demonstrated to be less efficient than that of α-peptoids. Olsen et al. further employed Fmoc-protected monomers (Figure 1.12) to synthesize β-peptoids unfortunately with poor yields.[97] Birkofer et al. utilized ring-opening polymerization of *N*-*p*-tolyl-*β*-alanine-N-carboxyanhydride for the synthesis of β-peptoids.[98] More recently, researchers found that this reaction exhibits a living polymerization character based on its kinetic analysis, and therefore has been utilized to create block copolymer.[99] However, this approach is limited as molecular weights of final products cannot be reliably predetermined, thus requiring further characterization.

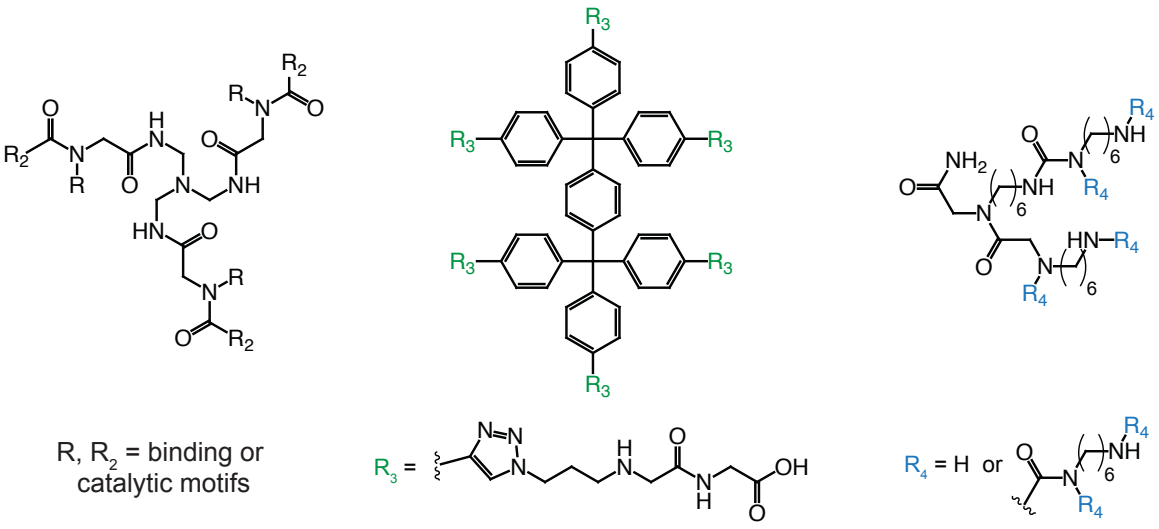

Figure 1.13. Branching peptoid-based structures. Various side chains were incorporated into the podand, and first, second and third generation dendrimers were synthesized using the structure on the right.[17]

Peptoid-based dendrimers have also been explored (Figure 1.13). Bradley et al. utilized *N*-(6-aminohexyl)glycine as the monomer unit of their dendrimer, which was assembled on a solid-support resin.[100] The coupling reactions of the aminohexylglycine were accelerated with microwave irradiation.[100] Thus, dendrimers of three generations were prepared. Double coupling were required in preparation of the second and third generation structures allowing for high yield. The final 3rd generation dendrimeric products were characterized by mass-spectrometry and HPLC, indicating an 85% yield. These dendrimeric structures were further utilized as transfection agents and demonstrated to be non-toxic and capable of transfecting HEK293T cells.[100] Moreover, Peschko et al. demonstrated peptoid dendrimers assembled on a hexaphenylxylylene (HPX) and tetraphenyl-methane (TPM) core using azide/alkyne click chemistry (Figure 1.13).[101] Peptoid arms were prepared with an *N*-terminal azide- or alkyne-bearing monomer and aryl or methoxyethyl side chains *via* solid-phase synthesis whereas rigid

cores were functionalized with alkyne or azide moieties. Copper catalyzed azide-alkyne cycloaddition was used to assemble the dendrimers that was subsequently washed with ethylenediaminem netetraacetic acid. While dendrimers with the HPX core were insoluble in organic solvents, dendrimers with TPM core were proven to be soluble in polar solvents such as acetonitrile, ensuing HPLC purification. The resultant peptoid dendrimers were analyzed by electrospray ionization (ESI) MS and NMR diffusion-ordered spectroscopy (DOSY) was used to calculate the hydrodynamic radii of the compounds.

1.2.3.3 Applications

A major application of sequence-defined polymers is to prepare functional coatings on materials. Recently, an emphasis of ongoing research aims to maintain the surface integrity from complicated medical devices to surfaces as large as a ship's hull.[17, 102] It becomes increasingly important to prohibit the adhesion of proteins, bacteria, and marine microbes in order to preserve the lifetime of materials.[17, 102] Therefore, the Messersmith group explored the potential of polypeptoids as antifouling materials.[103-105] Antifouling peptoids comprised of two blocks were designed. The first block contains 5-unit of *N*-(2-methoxyethyl) glycine monomer, which was specifically selected to bolster the anti-fouling behavior. The second block comprised L-3,4-dihydroxyphenylalanine (DOPA) alternating with primary amines and was designed to emulate mussel adhesion peptides (Figure 1.14 (a)). Subsequently, these peptoids were exploited to modify titanium surfaces, which exhibited resistance of cell adsorption after five months monitored by fluorescence microscopy (Figure 1.14 (b)). [84]

Peptoids have also been applied to separate enantiomers of natural products and synthetic drugs.[106] Liang and coworker reported a series of silica modified peptoid structures for chiral separations.[107] They designed peptoids bearing *N*-(S)-1-phenylethyl) glycine monomers from three to seven units in length, which were further used to separate enantiomers of twelve different BINOL (1,1'-bi-2-naph-thol) derivatives.[107] The ability to separate BINOL improved with the increase in peptoid chain length. However, the increase in separation reached a limit at 6 units in peptoid length and after that the separation ability no longer increased with length but started to decline instead.[107] Methylation of hydroxyl groups and the placement of bulky groups near hydroxyl groups hindered the formation of hydrogen bonding between the substrates and the solid-phase, therefore reducing the separation ability. This also confirms that hydrogen-bonding interaction plays a key role in chiral separation. Further studies were systematically performed to evaluate other contributing factors for chiral separations. Wu et al. synthesized a series of (*R*-)-*N*-(1-phenylethyl)glycine-based trimer peptoids by varying the N-terminus moieties.[108] The effect of linear and branched alkyl chains, as well as cyclic chiral and aromatic monomers on chiral separation was also explored. The chromatographic supports with achiral monomers at the N-terminus were demonstrated to show better separation than peptoids based on (*R*-)-*N*-(1-phenylethyl)glycine monomers of the same length.[108] This is likely attributable to the elimination of unwanted π-π stacking with the aromatic analytes.[108]

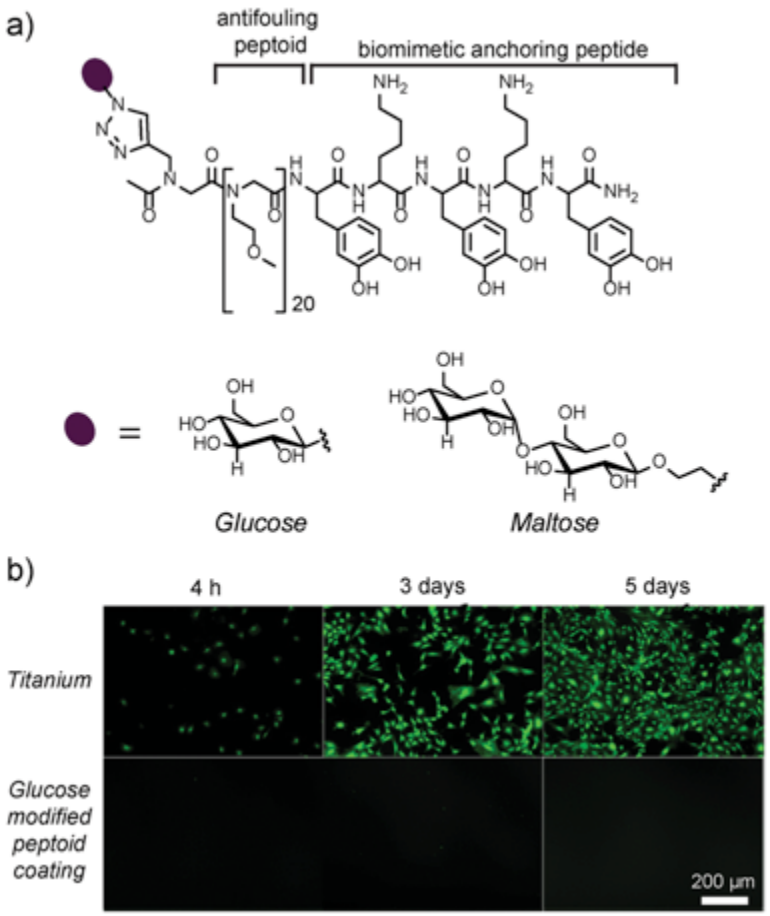

Figure 1.14. Peptoids as antifouling coatings.[84]

In nature, native biopolymers play an essential role in precisely controlling the crystallinity of biomaterials such as bone and abalone nacre.[109] One major focus of this area is to emulate the same degree of morphological control with inexpensive, well-defined synthetic materials, such as peptoids. Recently, peptoids have been rationally designed to simulate mineralization proteins in order to regulate the crystallization of calcite ($CaCO_3$).[110] Influence of changes in peptoid sequence on the crystallization rate of calcite and the final morphology has also been systematically studied.[110] Peptoids are also demonstrated to mimic natural biological constructs such as lipitoids and surfactants. Peptoids in conjunction with traditional components, including surfaces, cofactors, nanoparticles, polymers and biomolecules, offer more opportunities. As a result, these

complex hybrid materials exhibit advanced programmable functions. Examples include the detection of diagnostic analytes, gene delivery, and controlled macromolecular phase morphologies.[17] The aforementioned applications showcase the utility of peptoids as sequence-defined polymers in engineering advanced materials with desired structural and functional properties and demonstrate the great potential of peptoids to gap between natural and synthetic polymers.

1.3 Dynamic Covalent Chemistry

Dynamic covalent chemistry refers to a class of covalent bond-forming reactions whose addition products can be reverted back to the constituent reactants under particular reaction conditions. The equilibrium of the hydrogen bond-mediated base pairing observed in DNA shifts towards the reactants (i.e., the unpaired bases) at raised temperatures; thus, a dynamic covalent analogue of DNA might similarly employ thermally reversible reactions to mediate its self-assembly. Although all bimolecular addition reactions are, to some extent, reversible as dictated by the temperature dependence of the equilibrium constant, most reactions can essentially be considered irreversible as there are several temperature constraints that exclude the majority of these reactions from being thermally reversible dynamic covalent building blocks, including consideration of a practical temperature range, high temperature induced side reactions, and chemical decomposition temperatures. The Diels–Alder reaction, a [4+2] cycloaddition between a conjugated diene and a substituted alkene (i.e., a dienophile) that is reversible at raised temperatures, is perhaps the best known thermally reversible covalent reaction and a conspicuous option for use as a dynamic covalent base pair.

Unfortunately, many diene and dienophile pairs require excessive heating to undergo the retro-Diels–Alder reaction, which can trigger irreversible side reactions.[111] Moreover, as this cycloaddition affords a mixture of non-planar endo- and exo-isomers, base pair stacking and dimerization between adjacent Diels–Alder base pairs on a double-stranded dynamic covalent DNA analogue would be sterically disrupted, adversely affecting the hybridization selectivity.

Temperature is not the only stimulus that can be employed to reversibly affect the equilibrium of a chemical reaction. For example, pH-sensitive, reversible condensation reactions have been used extensively as dynamic covalent chemistries.[112-116] Diols are well known to participate in pH-reversible condensation reactions with boronic acids to yield boronate esters (Figure 1.15 (a)); indeed, hindered vicinal diols, such as pinacol and pinanediol, are commonly utilized as boronic acid protecting groups that can be removed under acidic conditions.[117] This reversible boronate esterification has proven invaluable in materials chemistry, finding utility in applications including targeted drug delivery nanocarriers that release their payload at low pH,[113-114] dynamic covalent macromolecular architectures,[115] and crystal engineering.[116]

Several alternative pH-reversible condensation reactions have also been extensively investigated. In particular, the condensation reactions of aldehydes with amines and hydrazides to afford Schiff base imines (Figure 1.15 (b)) and acylhydrazones (Figure 1.15 (c)) respectively, have proven popular for the creation of dynamic combinatorial libraries. These pH-sensitive, reversible condensation reactions are attractive dynamic covalent base pair candidates and will be used in this project for several reasons. Their synthetic accessibility enables the facile incorporation in sequence-specific polymer strands.

Moreover, their conjugation products are sufficiently small to enable the hybridization of complementary strands without disrupting base stacking. Finally, chemical orthogonality between the reversible boronic acid/diol and amine/aldehyde reactions, forming boron–oxygen and imine bonds, respectively, has been reported,[118-121] enabling the information incorporated on oligomeric strands to be encoded in base-4 rather than base-2 as would occur for a single dynamic covalent base pair system, thus significantly increasing the information density.

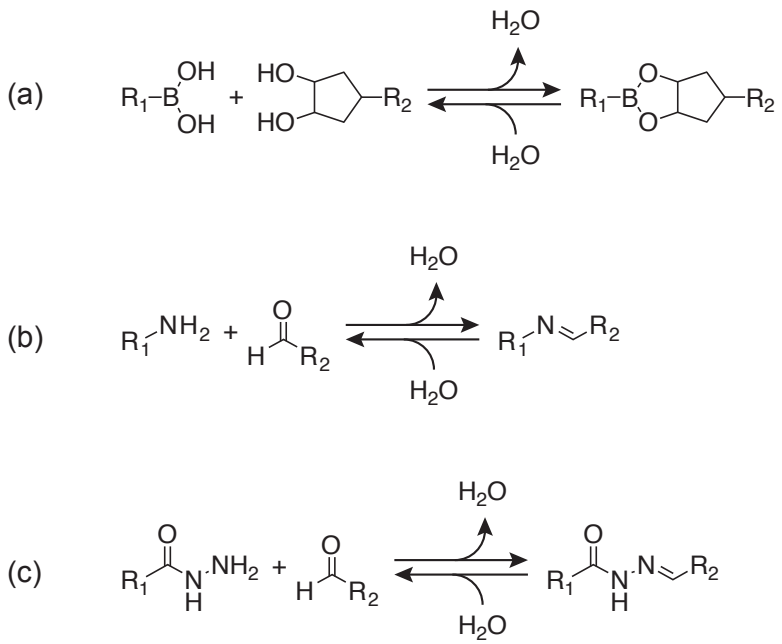

Figure 1.15. pH-Mediated dynamic covalent condensation chemistries: (a) the condensation of boronic acids with diols produces boronate esters; (b) the addition of amines to aldehydes yields imines, whereas (c) the reaction of hydrazides with aldehydes affords acylhydrazones.
*Equilibration for each of these reactions requires acidic conditions.

In addition to thermo- and pH-reversible dynamic covalent chemistries, photochemically triggered dynamic covalent reactions have also been developed. These

processes, which utilize light to reversibly break and re-form bonds, include photoinduced cyclization reactions and the photoreversible thiol/*o*NQM Michael addition. Unlike thermoreversible chemistries, photoreversible reactions only undergo bond cleavage and rearrangement upon irradiation, otherwise exhibiting little to no reaction in the absence of irradiation. Photochemical approaches have the clear advantage of enabling the 3D spatial control of the reversion as well as the ability to remotely trigger a process on and off. Photoinduced cyclization reactions, hereafter referred to as photodimerizations, occur when two functionalities incorporating carbon-carbon double bonds undergo a photo-induced cycloaddition reaction. The corresponding photo-scission reaction is achieved simply by exposure of the sample to a different irradiating wavelength; however, akin to Diels–Alder cycloadditions, photodimerizations yield multiple, non-planar isomers and thus are similarly ill-suited for dynamic covalent base pairs. Conversely, the thiol/*o*NQM Michael addition[122-123] (Figure 1.16) would serve as an ideal mechanism for an efficient photo-mediated dynamic covalent base pair. Here, the incident irradiation intensity controls the rate of the reverse reaction and determines the equilibrium extent of reaction, analogous to the temperature control that is exerted over Diels–Alder and other thermo-reversible systems such as Watson-Crick base pairs.

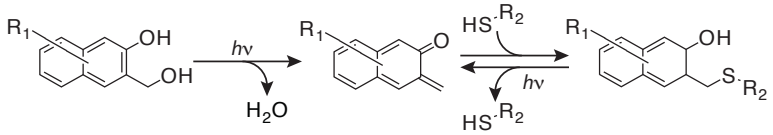

Figure 1.16. The photoreversible thiol/oNQM Michael addition.
*Irradiation of 3-(hydroxymethyl)-2-naphthol (left) effects photo-induced dehydration to generate the *o*NQM reactive species (center) which, in the presence of a thiol, participates in a Michael addition reaction.[124-125] Further irradiation of the thioether adduct (right) reverses this reaction, cleaving the C-S bond and restoring the thiol and *o*NQM functional groups.

1.4 Dynamic Imine Chemistry and Its Emerging Applications

Imine bond formation from an amine and an aldehyde is one example of dynamic covalent chemistry, which has been extensively utilized in the construction of complex, symmetrical structures as its inherent reversibility affords for 'proof-reading' and 'error-checking'.[126] The fast and efficient reversibility of imine in water and organic solvents provides great opportunities for the development of dynamic combinatorial chemistry.[127] Amines and aldehydes could also find utility as dynamic covalent base pairs in our study. Herein, this section details imine reactions and its emerging applications.

The reversible condensation between amines and aldehydes, also known as "Schiff base", was discovered by the German chemist Hugo Schiff in 1864 and was named after him.[126] Imine formation involves an amino and carbonyl groups that react to form a C=N bond either intra- or intermolecularly with the removal of a water molecule. Several factors affect the equilibrium of imine, including solvent, concentration, pH, temperature, as well as steric and electronic factors. The reversible nature of imine enables us to drive the reaction direction forward or backward. For instance, the removal of water molecule drives the equilibrium forward whereas the addition of water or hydrolysis leads to the backward reaction. Water molecules could be removed by either azeotropic distillation using a Dean-Stark apparatus or by adding drying agents to the reaction mixture. Three different types of equilibrium-controlled reactions, that imines can participate in, allow the exchange of the amino fragment of the C=N units (Scheme 1.3):[126-127]

(i) Formation/Hydrolysis – the imine reverts back to the precursor amine and aldehyde-containing material(s) upon adding water, which can subsequently undergo reaction with another component present in the reaction mixture.

(ii) Transimination – upon introduction of a second amine, the original imine may undergo transimination, contributing to the exchange of R groups.

(iii) Metathesis – upon introduction of a second imine, the two imines can undergo metathesis reaction resulting in the exchange of two R groups.

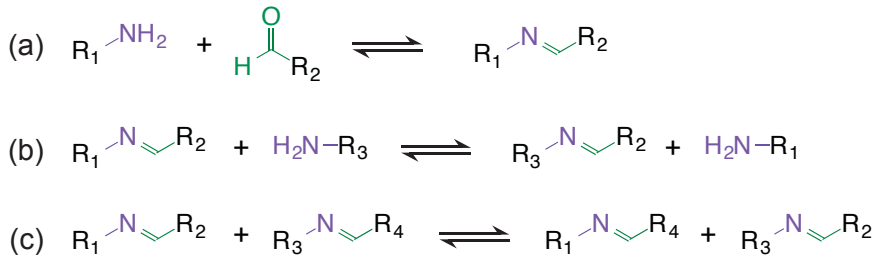

Scheme 1.3. The three types of imine reactions (a) imine condensation, (b) exchange, and (c) metathesis.

The reversible nature and fast exchange of imine enables 'proof-reading' and 'error-checking', thus allowing for the formation of the most thermodynamically stable products. Lehn and colleagues systematically studied the rate of the transimination reactions in the presence of lanthanide ions as catalyst.[128] They discovered that the exchange rates increased linearly with a decrease in ionic radius, with scandium (III) being the most efficient catalyst.[128] They further investigated the scandium(III)-catalyzed exchange in Schiff bases and demonstrated scandium(III) triflate can efficiently catalyze imine exchange reaction with turnover frequencies up to 3600 h^{-1} and rate accelerations up to 6×10^5.[127] Imines can also be permanently 'fixed' through reductive amination–the reduction of the C=N bond to a secondary amine by reducing reagents such sodium

cyanoborohydride or sodium triacetoxyborohydride (STAB), subsequently trapping the products achieved under thermodynamic control. However, reductive amination also removes the reversibility of imine.

Dynamic imine bonds have been extensively applied to the construction of molecular receptors, self-sorting, configurational rotary switches, molecular walker that mimic biological process, complex structures, and responsive materials with unique properties. For example, Lehn et al. have developed a stimuli responsive imine based dynamic covalent system,[129] which undergoes reversible phase separation upon heating or chemical stimulus when dissolved in acetonitrile/water mixtures (Figure 1.17). The amine/aldehyde-based reaction relies on charged and uncharged monomers which allow for the system to be soluble in a mixed aqueous solution. When the system is heated, or a salt such as NaCl is added the system undergoes reorganization to form a biphasic system, where the charged aldehyde and amine couple together and the uncharged monomers couple together. The process is reversible upon cooling or salt removal.

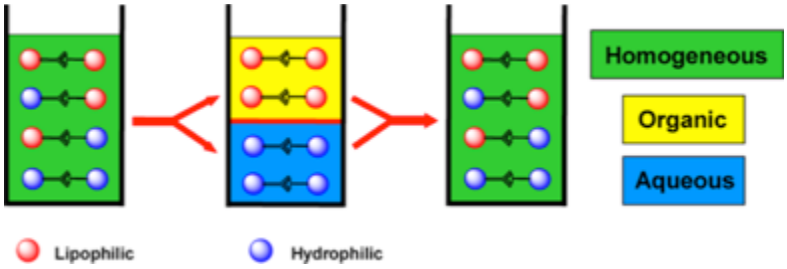

Figure 1.17. Schematic representation of reversible component redistribution (phase separation) upon external stimuli (i.e. thermal or salt) of charged and uncharged aldehyde and amine monomers.[129]

Dynamic covalent chemistry has been introduced to both surfactant and polymeric micelles as a method of mediating the assembly. Minkenberg et al.[130] converted a non-

amphiphilic surfactant comprised of a polar head group with an aromatic aldehyde into an amphiphile by exposing the surfactant to an aliphatic amine that upon reversible imine bond formation between the aldehyde and amine left an apolar tail that could self-assemble into pH-controlled micelles as shown in Figure 1.18. This allowed them to control the micelle formation by switching between the assembled amphiphilic structure to the disassembled non-amphiphilic state by means of reversible imine formation controlled by manipulating the pH. They also showed the potential utility of this technology to be used in drug delivery systems by controlling the uptake and release of Nile Red, a hydrophobic organic dye.

Figure 1.18. The controlled formation of micellar aggregates from (1) the aromatic aldehyde polar head group reversibly reacting with various amines to form an amphiphilic surfactant that can self-assemble into micelles.[130]

Minkenberg et al.[131] further built on this work by combining two water soluble dynamic covalent surfactants containing either aldehyde or amine functional groups to generate vesicles composed of reversible imine bonds. These vesicles cluster to form vesicle networks that lead to pH-reversible gels shown in Figure 1.19, which potentially could be used as self-healing materials or as vesicles for drug delivery systems. Self-assembling hydrogels also serve as promising mimics for biological agents such as the cytoskeleton and extracellular matrix.

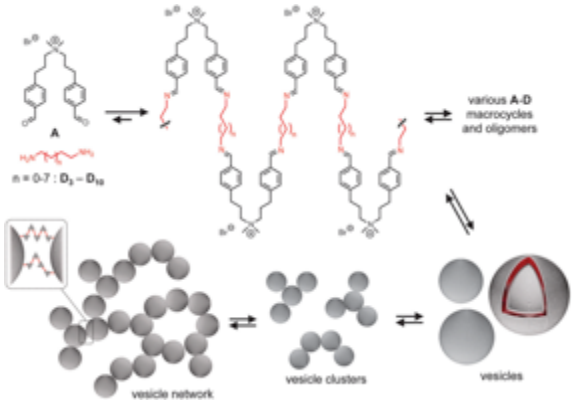

Figure 1.19. Schematic showing the formation of imine bonds from difunctionalized aldehydes and aliphatic amines to form macrocycles and oligomers leading to the vesicles, vesicle clusters, and finally vesicle networks capable of forming pH-reversible hydrogels.[131]

Minkenberg and colleagues[132] continued this work by fabricating gemini surfactants by utilizing the same amine/aldehyde reaction then used those surfactants to make wormlike micelles. Gemini surfactants are characterized by having multiple amphiphilic functional groups on each short strand. This is the first evidence of a reversible aggregation of Gemini surfactants to form wormlike micelles; these so-called Gemini surfactants have shown great potential in both biological applications such as gene transfection and industrial applications as viscoelastic additives for cosmetics. They formed the surfactants from aliphatic amines of various lengths and a bis-aldehyde-functionalized quaternary ammonium head group.

Haldar et al.[133] demonstrated the construction of self-healing gels from side-chain primary amine leucine pendant diblock copolymers of polyisobutylene (PIB) ((P(H_2N-Leu-HEMA)-*b*-PIB)) in the presence of PIB based dialdehyde functionalized cross-linker (HOC-PIB-CHO) through imine (–HC=N–) bond formation without the help of any external stimuli (Figure 1.20). These hydrogels were prepared by varying wt% of gelator concentration, [H_2N]/[CHO] ratios and molecular weight of the block segments in 1,4-

dioxane at ambient temperature. The mechanical properties of gels were characterized by rheological measurements. Higher value of storage modulus (*G*') than the loss modulus (*G*'') was detected within the linearity limits of deformation, demonstrating the rheological behavior in the gel is dominated by an elastic behavior rather than a viscous behavior. The *G*' values show a significant dependence on the cross-linking density in the gel network. Rheology analysis through step-strain measurements (strain = 0.1 to 200%) was performed at 25 °C to examine the self-healing property of the gels. The polymeric gel network exhibits reversible sol-gel transition for several cycles by adjusting the pH of the medium upon exposure to hydrochloric acid (HCl) and triethyamine (Et_3N) triggers. FT-IR spectroscopy indicated the formation of imine bonds in the gel network. Poor swelling ability of the gels implied highly inter connected networks formed during gelation, which was further confirmed by field emission-scanning electron microscopy (FE-SEM). Such pH-responsive dynamical covalently cross-linked gels with reasonable mechanical stability provide avenues to develop smart soft materials for organ repair and pH triggered delivery of biologically relevant materials.

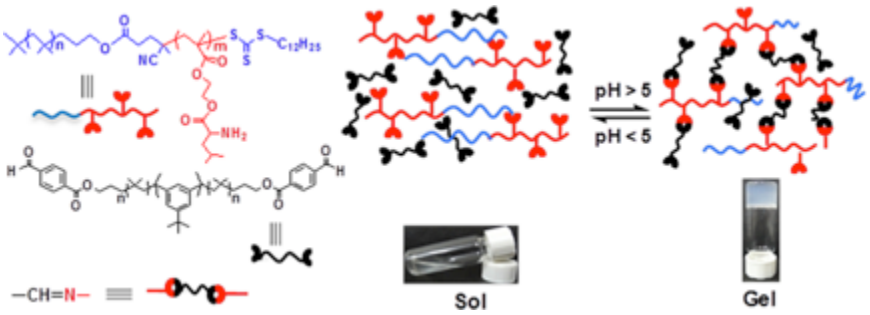

Figure 1.20. Schematic representation of dynamic covalently cross-linked polymeric gel synthesis from PIB-b-P(NH2-Leu-HEMA) and HOC-PIBCHO in 1,4-dioxane at room temperature and responsiveness toward pH.[133]

Kovaricek et al.[134] showed the advantages of salicylaldehyde (SALAL) in the reversible formation of imines with different amine compounds (Figure 1.21). They also showed motional covalent dynamics with SALAL and aliphatic diamines meaning the initial monoimines formed undergo this interchange reaction that elicits a motion that can be described as "stepping-in-place" or "single-step." They were able to control the rate of motion by changing the reaction conditions and the length of the diamines. This technology would be useful in the formation of molecular electronics.

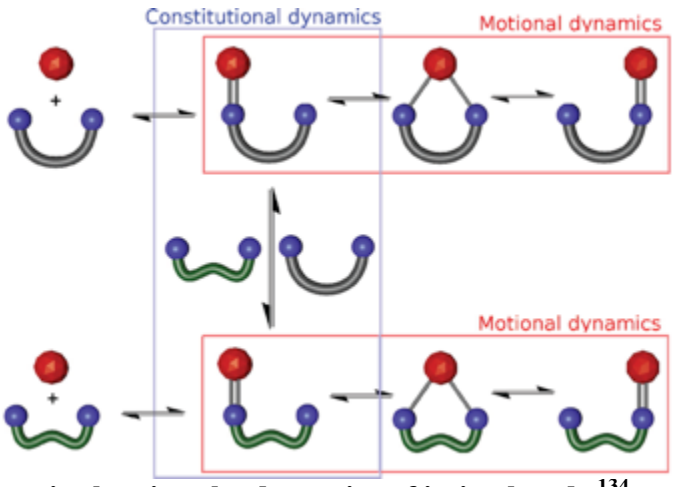

Figure 1.21. Schematic showing the dynamics of imine bonds.[134]

A series of 2D mesoporous COF materials based on imine Schiff base formation for high pressure gas storage has been developed by El-Kaderi et al.[135] These materials while having lower performance than the 3D materials developed by Yaghi et al, have reasonable surface areas and gas uptakes compared to other 2D based materials. Their methodology uses the co-condenstion of 1,3,6,8-tetrakis(p-formylphenyl)pyrene and p-phenylenediamine to form a 2D network with hydrogen uptake at 35 Bar at up to 24 mmol/g, 29 mmol/g for CO_2 and 10 mmol/g for methane. Building off the work of Yaghi and El-Kaderi et al, Zeng and colleagues developed a COF system using two different

types of dynamic covalent chemistries through an orthogonal reaction approach (boronic acid/catechol and Schiff base imine) to synthesize high porosity materials with high H_2 adsorption capacity.[136] Using 4-formylphenylboronic acid (FPBA), 1,3,5-tris(4-aminophenyl)-benzene (TAPB) and 2,3,6,7,10,11-hexadydroxytriphenylene (HHTP) they were able to control the condensation procedure to favor the reaction sequence to get different shapes and sizes of 2D COF materials. One material NTU-COF-2 achieved a surface area of 1619 m^2/g with a pore volume of 0.86 cm^3/g. Gas storage uptake measurements on this material 1.55 wt% or 174 cm^3/g at 1 bar and 77 K for hydrogen and 10.2 wt% (51.8 cm^3/g) of CO_2 at 273 K and 1 bar.

Nanofabric COF materials are another intriguing area of imine-based applications. Huang et al. used a mixture of 2,6-Dihydroxynaphthalene-1,5- dicarbaldehyde (DHNDA) and 2,4,6-tris(4-aminophenyl)-pyridine (TAPP) to develop a self tautomerizing COF through solvothermal synthesis.[137] They observed the material to undergo a morphological transformation from microspheres to nanofibers by implementing a unique dissolution-recrystallization mechanism, possible due to the reversible nature of the dynamic imine bonds. The nanofibers were capable of growing on an aramid fiber surfaces to make nanofiber composites and offered reversible colorimetric humidity-responsive behavior (Figure 1.22). These types of materials offer applications as sensors and catalyst surfaces.

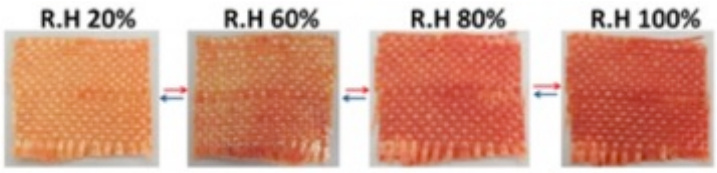

Figure 1.22. Reversible humidity-responsive color changing COF/aramid fabrics.[137]

1.5 Covalent Self-assembly

As noted earlier, the error correction mechanism that enables self-assembly necessitates transient, reversible inter-component interactions. Although weak intermolecular bonds such as hydrogen bonding or van der Waals interactions are typically employed to accomplish this error correction, dynamic covalent bonds are also capable of effecting the molecular rearrangement required to achieve thermodynamic equilibrium.[11] The idea of utilizing dynamic covalent bonds to mediate self-assembly is not new; however, relative to more conventional self-assembly approaches, the concept is still in its infancy. Reversible condensation reactions have found particular utility in dynamic covalent self-assembly. The boronic acid/diol condensation was used by Yaghi et al. for the assembly of covalent organic frameworks (COFs).[116] As the generated crystal structures were held together exclusively by strong, covalent bonds between B, C, and O atoms, the rigid architectures exhibited high thermal stability and permanent porosity.[116] Similarly, Tanoue et al. employed the amine/aldehyde condensation to fabricate one- and two-dimensional molecular crystals,[138] and the Severin group utilized concurrent, chemically orthogonal boronic acid/diol and amine/aldehyde condensations to mediate the assembly of macrocycles, molecular cages, and dendritic nanostructures.[119-120]

Dynamic covalent self-assembly has also been explored to effect the reconfiguration of information-bearing oligomeric sequences. Jean-Marie Lehn (Nobel prize in Chemistry, 1987) has been a significant proponent of exploiting dynamic covalent bonds for the constitutional rearrangement of dynamic, reversible nucleic acid analogues or 'DyNAs'.[124, 139] Lehn identified that polymers incorporating either main-chain- and side-

chain-reversible functionalities (see Figure 1.23 (a) and (b), respectively) were capable of undergoing this sequence adaptation, and utilized the hydrazide/aldehyde condensation (Figure 1.15 (c)) to yield nucleobase-appended polymers that undergo constitutional exchange with monomers in solution.[124] The Ghaderi group similarly demonstrated the dynamic sequence modification of oligomers using side-chain-reversible functional groups.[125] Here, the sequence of nucleobases affixed to an oligomeric backbone was rearranged *via* transthioesterification reactions in response to changing nucleic acid templates.

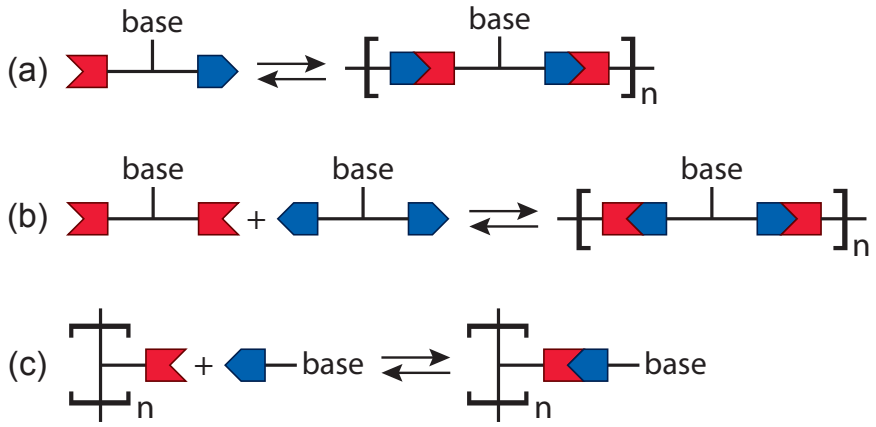

Figure 1.23. Schematic representation of dynamic nucleic acid analogues. Reversible covalent bond formation between (A) bifunctional hetero- or homotopic nucleobase derivatives, or (B) side-chain-functionalised polymers with monofunctionalised nucleobase derivatives, affords dynamic main-chain or dynamic side-chain polymers, respectively.

Despite their ingenious approaches to rearranging the sequence of oligomeric nucleic acid analogues, neither Lehn nor Ghadiri utilized dynamic covalent reactions specifically for the inter-strand base pairing interactions between complementary oligomeric strands. Preliminary attempts at exploiting dynamic covalent reactions for base pairing have only been reported by the Moore group. Moore et al. employed scandium(III)-catalyzed imine metathesis for the dynamic covalent self-assembly of complementary *m*-phenylene

ethynylene oligomers into *n*-rung molecular ladders.[140-141] Unfortunately, this approach proved only moderately successful as the ladder formation became kinetically trapped at four or more rungs.[141] Consequently, ladders containing five or more rungs were unable to be synthesized in high yield under the conditions used owing to the inadequate capacity for error-correction of misaligned, out-of-register byproducts.[141] This result highlights the necessity for considering the reaction kinetics to allow for bond rearrangement on an appropriate time scale. Thus, both thermodynamic and kinetic elements of a given dynamic covalent reaction will be taken into account throughout this project such that the oligomeric strands are able to hybridize selectively.

1.6 Overview of Subsequent Chapters

The remaining chapters of this dissertation are organized as follows:

Chapter 2 details the design and synthesis of sequence-specific oligomeric peptoids that contain dynamic functional amine and aldehyde groups and the utilization of complementary peptoids with commensurate length for the self-assembly of molecular ladders through scandium (III)-catalyzed imine reactions. Chapter 2 also explains the advantages of sequence-specific peptoids as building blocks for self-assembly.

Chapter 3 discusses the kinetics and potential hybridization mechanism of molecular ladder formation. We proposed three potential mechanisms including 'zipper', molecular handshake line and 'toehold displacement' in this chapter and utilized MALDI kinetics as well as Förster resonance energy transfer (FRET) measurements to determine the actual mechanism for ladder formation. We also examined the rate-limiting mechanism for the formation of peptoid-based ladder.

Chapter 4 examines the utilization of dynamic covalent chemistry, in conjunction with template-directed assembly to enable the fabrication of extended nanostructures that are both precise and tough. This chapter details the dynamic covalent assembly of peptoid-based molecular ladders up to 12 rungs through scandium (III)-catalyzed imine metathesis by employing the concept of Vernier templating, where small precursor units with mismatched numbers of complementary function groups are coreacted to yield larger structures with sizes pre-determined by the respective precursor functionalities.

Chapter 5 describes the dynamic covalent assembly of oligomeric species bearing both amine and aldehyde functional groups by employing scandium(III) triflate as a dual role catalyst, effecting both *in situ* ethylene acetal deprotection and imine exchange reactions. This chapter also details the optimization of reaction conditions to use Sc(III) as a dual role catalyst.

Chapter 6 gives the overall summary and conclusions of this work followed by a discussion of future work.

1.7 References

1. Whitesides, G. M.; Mathias, J. P.; Seto, C. T., Molecular Self-Assembly and Nanochemistry: A Chemical Strategy for the Synthesis of Nanostructures. *Science* **1991,** *254* (5036), 1312-1319.

2. Whitesides, G. M.; Boncheva, M., Beyond molecules: Self-assembly of mesoscopic and macroscopic components. *Proc. Natl. Acad. Sci. U. S. A.* **2002,** *99* (8), 4769-4774.

3. Blake, A. J.; Champness, N. R.; Hubberstey, P.; Li, W. S.; Withersby, M. A.; Schroder, M., Inorganic crystal engineering using self-assembly of tailored building-blocks. *Coord. Chem. Rev.* **1999,** *183*, 117-138.

4. Thomas, E. L., Materials science - The ABCs of self-assembly. *Science* **1999,** *286* (5443), 1307-1307.

5. Ulman, A., Formation and structure of self-assembled monolayers. *Chem. Rev.* **1996,** *96* (4), 1533-1554.

6. Schnur, J. M., Lipid Tubules: A Paradigm for Molecularly Engineered Structures. *Science* **1993,** *262* (5140), 1669-1676.

7. Gething, M. J.; Sambrook, J., Protein folding in the cell. *Nature* **1992,** *355* (6355), 33-45.

8. Zuker, M., Mfold web server for nucleic acid folding and hybridization prediction. *Nucleic Acids Res.* **2003,** *31* (13), 3406-3415.

9. Zhang, S. G., Fabrication of novel biomaterials through molecular self-assembly. *Nat. Biotechnol.* **2003,** *21* (10), 1171-1178.

10. Smith, M. B.; March, J., *March's Advanced Organic Chemistry - Reactions, Mechanisms, and Structure (6th Edition)*. John Wiley & Sons: Hoboken, New Jersey, 2007.

11. Rowan, S. J.; Cantrill, S. J.; Cousins, G. R. L.; Sanders, J. K. M.; Stoddart, J. F., Dynamic covalent chemistry. *Angew. Chem. Int. Ed.* **2002,** *41* (6), 898-952.

12. Kloxin, C. J.; Scott, T. F.; Adzima, B. J.; Bowman, C. N., Covalent Adaptable Networks (CANS): A Unique Paradigm in Cross-Linked Polymers. *Macromolecules* **2010,** *43* (6), 2643-2653.

13. Winfree, E.; Liu, F. R.; Wenzler, L. A.; Seeman, N. C., Design and self-assembly of two-dimensional DNA crystals. *Nature* **1998,** *394* (6693), 539-544.

14. Rothemund, P. W. K., Folding DNA to create nanoscale shapes and patterns. *Nature* **2006,** *440* (7082), 297-302.

15. Wei, B.; Dai, M. J.; Yin, P., Complex shapes self-assembled from single-stranded DNA tiles. *Nature* **2012,** *485* (7400), 623-626.

16. Clausen-Schaumann, H.; Rief, M.; Tolksdorf, C.; Gaub, H. E., Mechanical stability of single DNA molecules. *Biophys. J.* **2000,** *78* (4), 1997-2007.

17. Knight, A. S.; Zhou, E. Y.; Francis, M. B.; Zuckermann, R. N., Sequence Programmable Peptoid Polymers for Diverse Materials Applications. *Adv. Mater.* **2015,** *27* (38), 5665-5691.

18. Lutz, J. F.; Ouchi, M.; Liu, D. R.; Sawamoto, M., Sequence-Controlled Polymers. *Science* **2013,** *341* (6146), 628-636.

19. Badi, N.; Lutz, J.-F., Sequence control in polymer synthesis. *Chem. Soc. Rev.* **2009,** *38* (12), 3383-3390.

20. Jenkins, A. D.; Jones, R. G.; Moad, G., Terminology for reversible-deactivation radical polymerization previously called" controlled" radical or" living" radical polymerization (IUPAC Recommendations 2010). *Pure Appl. Chem.* **2009,** *82* (2), 483-491.

21. Matyjaszewski, K., Atom transfer radical polymerization (ATRP): current status and future perspectives. *Macromolecules* **2012,** *45* (10), 4015-4039.

22. Aldaye, F. A.; Palmer, A. L.; Sleiman, H. F., Assembling materials with DNA as the guide. *Science* **2008,** *321* (5897), 1795-1799.

23. Jones, M. R.; Seeman, N. C.; Mirkin, C. A., Programmable materials and the nature of the DNA bond. *Science* **2015,** *347* (6224).

24. Hawker, C. J.; Wooley, K. L., The convergence of synthetic organic and polymer chemistries. *Science* **2005,** *309* (5738), 1200-1205.

25. Poelma, J. E.; Fors, B. P.; Meyers, G. F.; Kramer, J. W.; Hawker, C. J., Fabrication of complex three‐dimensional polymer brush nanostructures through light‐mediated living radical polymerization. *Angewandte Chemie* **2013,** *125* (27), 6982-6986.

26. Leibfarth, F. A.; Mattson, K. M.; Fors, B. P.; Collins, H. A.; Hawker, C. J., External regulation of controlled polymerizations. *Angewandte Chemie International Edition* **2013,** *52* (1), 199-210.

27. Saiki, R. K.; Gelfand, D. H.; Stoffel, S.; Scharf, S. J.; Higuchi, R.; Horn, G. T.; Mullis, K. B.; Erlich, H. A., Primer-directed enzymatic amplification of DNA with a thermostable DNA polymerase. *Science* **1988,** *239* (4839), 487-491.

28. McGrath, K. P.; Fournier, M. J.; Mason, T. L.; Tirrell, D. A., Genetically directed syntheses of new polymeric materials. Expression of artificial genes encoding proteins with repeating-(AlaGly) 3ProGluGly-elements. *J. Am. Chem. Soc.* **1992,** *114* (2), 727-733.

29. Merrifield, R. B., Solid phase peptide synthesis. I. The synthesis of a tetrapeptide. *J. Am. Chem. Soc.* **1963,** *85* (14), 2149-2154.

30. Cherkupally, P.; Ramesh, S.; de la Torre, B. G.; Govender, T.; Kruger, H. G.; Albericio, F., Immobilized coupling reagents: Synthesis of amides/peptides. *ACS combinatorial science* **2014,** *16* (11), 579-601.

31. Pfeifer, S.; Zarafshani, Z.; Badi, N.; Lutz, J.-F., Liquid-phase synthesis of block copolymers containing sequence-ordered segments. *J. Am. Chem. Soc.* **2009,** *131* (26), 9195-9197.

32. Szwarc, M., 'Living'polymers. *Nature* **1956,** *178*, 1168-1169.

33. Ouchi, M.; Sawamoto, M., 50th Anniversary Perspective: Metal-Catalyzed Living Radical Polymerization: Discovery and Perspective. *Macromolecules* **2017,** *50* (7), 2603-2614.

34. Bates, F. S.; Hillmyer, M. A.; Lodge, T. P.; Bates, C. M.; Delaney, K. T.; Fredrickson, G. H., Multiblock polymers: panacea or pandora's box? *Science* **2012,** *336* (6080), 434-440.

35. Patten, T. E.; Xia, J.; Abernathy, T.; Matyjaszewski, K., Polymers with very low polydispersities from atom transfer radical polymerization. *Science* **1996,** *272* (5263), 866.

36. Ouchi, M.; Terashima, T.; Sawamoto, M., Transition metal-catalyzed living radical polymerization: toward perfection in catalysis and precision polymer synthesis. *Chem. Rev* **2009,** *109* (11), 4963-5050.

37. Bielawski, C. W.; Grubbs, R. H., Living ring-opening metathesis polymerization. *Progress in Polymer Science* **2007,** *32* (1), 1-29.

38. Tong, X.; Guo, B.-h.; Huang, Y., Toward the synthesis of sequence-controlled vinyl copolymers. *Chem. Commun.* **2011,** *47* (5), 1455-1457.

39. Coessens, V.; Matyjaszewski, K., Synthesis of polymers with hydroxyl end groups by atom transfer radical polymerization. *Macromolecular rapid communications* **1999,** *20* (3), 127-134.

40. Coessens, V.; Pyun, J.; Miller, P. J.; Gaynor, S. G.; Matyjaszewski, K., Functionalization of polymers prepared by ATRP using radical addition reactions. *Macromolecular rapid communications* **2000,** *21* (2), 103-109.

41. Pfeifer, S.; Lutz, J.-F., A facile procedure for controlling monomer sequence distribution in radical chain polymerizations. *J. Am. Chem. Soc.* **2007,** *129* (31), 9542-9543.

42. Lutz, J. F.; Schmidt, B. V.; Pfeifer, S., Tailored Polymer Microstructures Prepared by Atom Transfer Radical Copolymerization of Styrene and N‐substituted Maleimides. *Macromolecular rapid communications* **2011,** *32* (2), 127-135.

43. Satoh, K.; Mizutani, M.; Kamigaito, M., Metal-catalyzed radical polyaddition as a novel polymer synthetic route. *Chem. Commun.* **2007,** (12), 1260-1262.

44. Satoh, K.; Ozawa, S.; Mizutani, M.; Nagai, K.; Kamigaito, M., Sequence-regulated vinyl copolymers by metal-catalysed step-growth radical polymerization. *Nature communications* **2010,** *1*, 6.

45. Zhang, J.; Matta, M. E.; Hillmyer, M. A., Synthesis of sequence-specific vinyl copolymers by regioselective ROMP of multiply substituted cyclooctenes. *ACS Macro Letters* **2012,** *1* (12), 1383-1387.

46. Hibi, Y.; Ouchi, M.; Sawamoto, M., Sequence‐Regulated Radical Polymerization with a Metal‐Templated Monomer: Repetitive ABA Sequence by Double Cyclopolymerization. *Angewandte Chemie* **2011,** *123* (32), 7572-7575.

47. Hibi, Y.; Tokuoka, S.; Terashima, T.; Ouchi, M.; Sawamoto, M., Design of AB divinyl "template monomers" toward alternating sequence control in metal-catalyzed living radical polymerization. *Polymer Chemistry* **2011,** *2* (2), 341-347.

48. Watson, J. D.; Crick, F. H. C., Molecular Structure of Nucleic Acids: A Structure for Deoxyribose Nucleic Acid. *Nature* **1953,** *171* (4356), 737-738.

49. Wilkins, M. H. F.; Stokes, A. R.; Wilson, H. R., Molecular Structure of Deoxypentose Nucleic Acids. *Nature* **1953,** *171* (4356), 738-740.

50. Yan, H.; Liu, Y., DNA Nanotechnolgy: An Evolving Field. In *Nanotechnology: Science and Computation*, Chan, J.; Jonoska, N.; Rozenberg, G., Eds. Springer-Verlag: Berlin, Germany, 2006; pp 35-53.

51. Lu, X. J.; Olson, W. K., 3DNA: a software package for the analysis, rebuilding and visualization of three-dimensional nucleic acid structures. *Nucleic Acids Res.* **2003,** *31* (17), 5108-5121.

52. Modrich, P., DNA Mismatch Correction. *Annu. Rev. Biochem.* **1987,** *56*, 435-466.

53. Seeman, N. C., Nucleic Acid Junctions and Lattices. *J. Theor. Biol.* **1982,** *99* (2), 237-247.

54. Chen, J. H.; Seeman, N. C., Synthesis from DNA of a molecule with the connectivity of a cube. *Nature* **1991,** *350* (6319), 631-633.

55. Mirkin, C. A.; Letsinger, R. L.; Mucic, R. C.; Storhoff, J. J., A DNA-based method for rationally assembling nanoparticles into macroscopic materials. *Nature* **1996,** *382* (6592), 607-609.

56. Alivisatos, A. P.; Johnsson, K. P.; Peng, X. G.; Wilson, T. E.; Loweth, C. J.; Bruchez, M. P.; Schultz, P. G., Organization of 'nanocrystal molecules' using DNA. *Nature* **1996,** *382* (6592), 609-611.

57. Elghanian, R.; Storhoff, J. J.; Mucic, R. C.; Letsinger, R. L.; Mirkin, C. A., Selective colorimetric detection of polynucleotides based on the distance-dependent optical properties of gold nanoparticles. *Science* **1997,** *277* (5329), 1078-1081.

58. Hung, A. M.; Micheel, C. M.; Bozano, L. D.; Osterbur, L. W.; Wallraff, G. M.; Cha, J. N., Large-area spatially ordered arrays of gold nanoparticles directed by lithographically confined DNA origami. *Nature Nanotechnology* **2010,** *5* (2), 121-126.

59. Acuna, G. P.; Bucher, M.; Stein, I. H.; Steinhauer, C.; Kuzyk, A.; Holzmeister, P.; Schreiber, R.; Moroz, A.; Stefani, F. D.; Liedl, T.; Simmel, F. C.; Tinnefeld, P., Distance

Dependence of Single-Fluorophore Quenching by Gold Nanoparticles Studied on DNA Origami. *ACS Nano* **2012,** *6* (4), 3189-3195.

60. Maune, H. T.; Han, S. P.; Barish, R. D.; Bockrath, M.; Goddard, W. A.; Rothemund, P. W. K.; Winfree, E., Self-assembly of carbon nanotubes into two-dimensional geometries using DNA origami templates. *Nature Nanotechnology* **2010,** *5* (1), 61-66.

61. Ke, Y. G.; Sharma, J.; Liu, M. H.; Jahn, K.; Liu, Y.; Yan, H., Scaffolded DNA Origami of a DNA Tetrahedron Molecular Container. *Nano Letters* **2009,** *9* (6), 2445-2447.

62. Andersen, E. S.; Dong, M.; Nielsen, M. M.; Jahn, K.; Subramani, R.; Mamdouh, W.; Golas, M. M.; Sander, B.; Stark, H.; Oliveira, C. L. P.; Pedersen, J. S.; Birkedal, V.; Besenbacher, F.; Gothelf, K. V.; Kjems, J., Self-assembly of a nanoscale DNA box with a controllable lid. *Nature* **2009,** *459* (7243), 73-76.

63. Ogawa, A. K.; Wu, Y. Q.; McMinn, D. L.; Liu, J. Q.; Schultz, P. G.; Romesberg, F. E., Efforts toward the expansion of the genetic alphabet: Information storage and replication with unnatural hydrophobic base pairs. *J. Am. Chem. Soc.* **2000,** *122* (14), 3274-3287.

64. Santosh, M.; Maiti, P. K., Force induced DNA melting. *Journal of Physics-Condensed Matter* **2009,** *21* (3).

65. Bockelmann, U.; EssevazRoulet, B.; Heslot, F., Molecular stick-slip motion revealed by opening DNA with piconewton forces. *Phys. Rev. Lett.* **1997,** *79* (22), 4489-4492.

66. Bockelmann, U.; Thomen, P.; Essevaz-Roulet, B.; Viasnoff, V.; Heslot, F., Unzipping DNA with optical tweezers: high sequence sensitivity and force flips. *Biophys. J.* **2002,** *82* (3), 1537-1553.

67. Beyer, M. K.; Clausen-Schaumann, H., Mechanochemistry: The mechanical activation of covalent bonds. *Chem. Rev.* **2005,** *105* (8), 2921-2948.

68. Zuckermann, R. N.; Kerr, J. M.; Kent, S. B. H.; Moos, W. H., Efficient Method for the Preparation of Peptoids [Oligo(N-substituted glycines)] by Submonomer Solid-Phase Synthesis. *J. Am. Chem. Soc.* **1992,** *114* (26), 10646-10647.

69. Sun, J.; Zuckermann, R. N., Peptoid Polymers: A Highly Designable Bioinspired Material. *Acs Nano* **2013,** *7* (6), 4715-4732.

70. Potyrailo, R.; Rajan, K.; Stoewe, K.; Takeuchi, I.; Chisholm, B.; Lam, H., Combinatorial and high-throughput screening of materials libraries: review of state of the art. *ACS combinatorial science* **2011,** *13* (6), 579-633.

71. Simon, R. J.; Kania, R. S.; Zuckermann, R. N.; Huebner, V. D.; Jewell, D. A.; Banville, S.; Ng, S.; Wang, L.; Rosenberg, S.; Marlowe, C. K.; Spellmeyer, D. C.; Tan,

R. Y.; Frankel, A. D.; Santi, D. V.; Cohen, F. E.; Bartlett, P. A., Peptoids: A modular approach to drug discovery. *Proc. Natl. Acad. Sci. U. S. A.* **1992,** *89* (20), 9367-9371.

72. Olivos, H. J.; Alluri, P. G.; Reddy, M. M.; Salony, D.; Kodadek, T., Microwave-assisted solid-phase synthesis of peptoids. *Org Lett* **2002,** *4* (23), 4057-4059.

73. Culf, A. S.; Ouellette, R. J., Solid-Phase Synthesis of N-Substituted Glycine Oligomers (α-Peptoids) and Derivatives. *Molecules* **2010,** *15* (8), 5282-5335.

74. Burkoth, T. S.; Fafarman, A. T.; Charych, D. H.; Connolly, M. D.; Zuckermann, R. N., Incorporation of Unprotected Heterocyclic Side Chains into Peptoid Oligomers via Solid-Phase Submonomer Synthesis. *J. Am. Chem. Soc.* **2003,** *125* (29), 8841-8845.

75. Shah, N. H.; Kirshenbaum, K., Photoresponsive peptoid oligomers bearing azobenzene side chains. *Org. Biomol. Chem.* **2008,** *6* (14), 2516-2521.

76. Wu, C. W.; Sanborn, T. J.; Huang, K.; Zuckermann, R. N.; Barron, A. E., Peptoid oligomers with α-chiral, aromatic side chains: sequence requirements for the formation of stable peptoid helices. *J. Am. Chem. Soc.* **2001,** *123* (28), 6778-6784.

77. Horn, T.; Lee, B.-C.; Dill, K. A.; Zuckermann, R. N., Incorporation of chemoselective functionalities into peptoids via solid-phase submonomer synthesis. *Bioconjug. Chem.* **2004,** *15* (2), 428-435.

78. Holub, J. M.; Jang, H.; Kirshenbaum, K., Clickity-click: highly functionalized peptoid oligomers generated by sequential conjugation reactions on solid-phase support. *Org. Biomol. Chem.* **2006,** *4* (8), 1497-1502.

79. Sigmund, F.; Wessely, F., Untersuchungen über α-Amino-N-Carbonsäureanhydride. II. *HS Z. Physiol. Chem* **1926,** *157*, 91-105.

80. Fetsch, C.; Grossmann, A.; Holz, L.; Nawroth, J. F.; Luxenhofer, R., Polypeptoids from N-substituted glycine N-carboxyanhydrides: hydrophilic, hydrophobic, and amphiphilic polymers with poisson distribution. *Macromolecules* **2011,** *44* (17), 6746-6758.

81. Fetsch, C.; Luxenhofer, R., Highly Defined Multiblock Copolypeptoids: Pushing the Limits of Living Nucleophilic Ring‐Opening Polymerization. *Macromolecular rapid communications* **2012,** *33* (19), 1708-1713.

82. Gangloff, N.; Fetsch, C.; Luxenhofer, R., Polypeptoids by Living Ring‐Opening Polymerization of N‐Substituted N‐Carboxyanhydrides from Solid Supports. *Macromolecular rapid communications* **2013,** *34* (12), 997-1001.

83. Guo, L.; Lahasky, S. H.; Ghale, K.; Zhang, D., N-Heterocyclic carbene-mediated zwitterionic polymerization of N-substituted N-carboxyanhydrides toward poly (α-

peptoid) s: kinetic, mechanism, and architectural control. *J. Am. Chem. Soc.* **2012,** *134* (22), 9163-9171.

84. Lee, C.-U.; Smart, T. P.; Guo, L.; Epps III, T. H.; Zhang, D., Synthesis and characterization of amphiphilic cyclic diblock copolypeptoids from N-heterocyclic carbene-mediated zwitterionic polymerization of N-substituted N-carboxyanhydride. *Macromolecules* **2011,** *44* (24), 9574-9585.

85. Tao, X.; Deng, C.; Ling, J., PEG‐Amine‐Initiated Polymerization of Sarcosine N‐Thiocarboxyanhydrides Toward Novel Double‐Hydrophilic PEG‐b‐Polysarcosine Diblock Copolymers. *Macromolecular rapid communications* **2014,** *35* (9), 875-881.

86. Tao, X.; Deng, Y.; Shen, Z.; Ling, J., Controlled polymerization of N-substituted glycine N-thiocarboxyanhydrides initiated by rare earth borohydrides toward hydrophilic and hydrophobic polypeptoids. *Macromolecules* **2014,** *47* (18), 6173-6180.

87. Goto, Y.; Katoh, T.; Suga, H., Flexizymes for genetic code reprogramming. *Nat. Protoc.* **2011,** *6* (6), 779.

88. Monsalve, L. N.; Petroselli, G.; Erra‐Ballsells, R.; Vázquez, A.; Baldessari, A., Chemoenzymatic synthesis of novel N‐(2‐hydroxyethyl)‐β‐peptoid oligomer derivatives and application to porous polycaprolactone films. *Polymer International* **2014,** *63* (8), 1523-1530.

89. Olsen, C. A., β‐peptoid "Foldamers"−Why the additional methylene unit? *Peptide Science* **2011,** *96* (5), 561-566.

90. Jia, L.; Sun, H.; Shay, J. T.; Allgeier, A. M.; Hanton, S. D., Living alternating copolymerization of N-alkylaziridines and carbon monoxide as a route for synthesis of poly-β-peptoids. *J. Am. Chem. Soc.* **2002,** *124* (25), 7282-7283.

91. Darensbourg, D. J.; Phelps, A. L.; Gall, N. L.; Jia, L., Mechanistic studies of the copolymerization reaction of aziridines and carbon monoxide to produce poly-β-peptoids. *J. Am. Chem. Soc.* **2004,** *126* (42), 13808-13815.

92. Wang, L.; Wang, G. T.; Zhao, X.; Jiang, X. K.; Li, Z. T., Hydrogen Bonding-Directed Quantitative Self-Assembly of Cyclotriveratrylene Capsules and Their Encapsulation of C-60 and C-70. *J. Org. Chem.* **2011,** *76* (9), 3531-3535.

93. Liu, G.; Jia, L., Cobalt‐Catalyzed Carbonylative Copolymerization of N‐Alkylazetidines and Tetrahydrofuran. *Angewandte Chemie International Edition* **2006,** *45* (1), 129-131.

94. Chai, J.; Liu, G.; Chaicharoen, K.; Wesdemiotis, C.; Jia, L., Cobalt-catalyzed carbonylative polymerization of azetidines. *Macromolecules* **2008,** *41* (23), 8980-8985.

95. Hamper, B. C.; Kolodziej, S. A.; Scates, A. M.; Smith, R. G.; Cortez, E., Solid phase synthesis of β-peptoids: N-substituted β-aminopropionic acid oligomers. *The Journal of organic chemistry* **1998,** *63* (3), 708-718.

96. Norgren, A. S.; Zhang, S.; Arvidsson, P. I., Synthesis and circular dichroism spectroscopic investigations of oligomeric β-peptoids with α-chiral side chains. *Org Lett* **2006,** *8* (20), 4533-4536.

97. Olsen, C. A.; Lambert, M.; Witt, M.; Franzyk, H.; Jaroszewski, J. W., Solid-phase peptide synthesis and circular dichroism study of chiral β-peptoid homooligomers. *Amino Acids* **2008,** *34* (3), 465-471.

98. Birkofer, L.; Kachel, H., Synthese eines N-Carboxy-β-aminosäureanhydrids. *Naturwissenschaften* **1954,** *41* (24), 576-576.

99. Grossmann, A.; Luxenhofer, R., Living Polymerization of N‐Substituted β‐Alanine N‐Carboxyanhydrides: Kinetic Investigations and Preparation of an Amphiphilic Block Copoly‐β‐Peptoid. *Macromolecular rapid communications* **2012,** *33* (19), 1714-1719.

100. Diaz-Mochon, J. J.; Fara, M. A.; Sanchez-Martin, R. M.; Bradley, M., Peptoid dendrimers—microwave-assisted solid-phase synthesis and transfection agent evaluation. *Tetrahedron Lett.* **2008,** *49* (5), 923-926.

101. Peschko, K.; Schade, A.; Vollrath, S. B.; Schwarz, U.; Luy, B.; Muhle‐Goll, C.; Weis, P.; Bräse, S., Dendrimer‐Type Peptoid‐Decorated Hexaphenylxylenes and Tetraphenylmethanes: Synthesis and Structure in Solution and in the Gas Phase. *Chemistry-A European Journal* **2014,** *20* (49), 16273-16278.

102. Banerjee, I.; Pangule, R. C.; Kane, R. S., Antifouling coatings: recent developments in the design of surfaces that prevent fouling by proteins, bacteria, and marine organisms. *Advanced Materials* **2011,** *23* (6), 690-718.

103. Lee, H.; Dellatore, S. M.; Miller, W. M.; Messersmith, P. B., Mussel-inspired surface chemistry for multifunctional coatings. *Science* **2007,** *318* (5849), 426-430.

104. Statz, A. R.; Meagher, R. J.; Barron, A. E.; Messersmith, P. B., New peptidomimetic polymers for antifouling surfaces. *J. Am. Chem. Soc.* **2005,** *127* (22), 7972-7973.

105. Ham, H. O.; Park, S. H.; Kurutz, J. W.; Szleifer, I. G.; Messersmith, P. B., Antifouling glycocalyx-mimetic peptoids. *J. Am. Chem. Soc.* **2013,** *135* (35), 13015-13022.

106. Ward, T. J.; Ward, K. D., Chiral separations: a review of current topics and trends. *Anal. Chem.* **2011,** *84* (2), 626-635.

107. Wu, H.; Liang, T.; Yin, C.; Jin, Y.; Ke, Y.; Liang, X., Enantiorecognition ability of peptoids with α-chiral, aromatic side chains. *Analyst* **2011,** *136* (21), 4409-4411.

108. Wu, H.; Li, K.; Yu, H.; Ke, Y.; Liang, X., Investigation of peptoid chiral stationary phases varied in absolute configuration. *J. Chromatogr. A* **2013,** *1281*, 155-159.

109. Meldrum, F. C.; Cölfen, H., Controlling mineral morphologies and structures in biological and synthetic systems. *Chem. Rev.* **2008,** *108* (11), 4332-4432.

110. Chen, C.-L.; Qi, J.; Zuckermann, R. N.; DeYoreo, J. J., Engineered biomimetic polymers as tunable agents for controlling CaCO3 mineralization. *J. Am. Chem. Soc.* **2011,** *133* (14), 5214-5217.

111. Adzima, B. J.; Aguirre, H. A.; Kloxin, C. J.; Scott, T. F.; Bowman, C. N., Rheological and Chemical Analysis of Reverse Gelation in a Covalently Cross-Linked Diels-Alder Polymer Network. *Macromolecules* **2008,** *41* (23), 9112-9117.

112. Nishiyabu, R.; Kubo, Y.; James, T. D.; Fossey, J. S., Boronic acid building blocks: tools for self assembly. *Chem. Commun.* **2011,** *47* (4), 1124-1150.

113. Li, Y. P.; Xiao, W. W.; Xiao, K.; Berti, L.; Luo, J. T.; Tseng, H. P.; Fung, G.; Lam, K. S., Well-Defined, Reversible Boronate Crosslinked Nanocarriers for Targeted Drug Delivery in Response to Acidic pH Values and cis-Diols. *Angew. Chem. Int. Ed.* **2012,** *51* (12), 2864-2869.

114. Chen, W. X.; Cheng, Y. F.; Wang, B. H., Dual-Responsive Boronate Crosslinked Micelles for Targeted Drug Delivery. *Angew. Chem. Int. Ed.* **2012,** *51* (22), 5293-5295.

115. Bapat, A. P.; Roy, D.; Ray, J. G.; Savin, D. A.; Sumerlin, B. S., Dynamic-Covalent Macromolecular Stars with Boronic Ester Linkages. *J. Am. Chem. Soc.* **2011,** *133* (49), 19832-19838.

116. Cote, A. P.; Benin, A. I.; Ockwig, N. W.; O'Keeffe, M.; Matzger, A. J.; Yaghi, O. M., Porous, crystalline, covalent organic frameworks. *Science* **2005,** *310* (5751), 1166-1170.

117. Yang, W.; Gao, X.; Wang, B., Biological and Medicinal Applications of Boronic Acids. In *Boronic Acids*, Hall, D. G., Ed. Wiley-VCH: Weinheim, Germany, 2005; pp 481-512.

118. Kelly, A. M.; Perez-Fuertes, Y.; Arimori, S.; Bull, S. D.; James, T. D., Simple protocol for NMR analysis of the enantiomeric purity of diols. *Org Lett* **2006,** *8* (10), 1971-1974.

119. Christinat, N.; Scopelliti, R.; Severin, K., Multicomponent assembly of boron-based dendritic nanostructures. *J. Org. Chem.* **2007,** *72* (6), 2192-2200.

120. Christinat, N.; Scopelliti, R.; Severin, K., Multicomponent assembly of boronic acid based macrocycles and cages. *Angew. Chem. Int. Ed.* **2008,** *47* (10), 1848-1852.

121. Hutin, M.; Bernardinelli, G.; Nitschke, J. R., An iminoboronate construction set for subcomponent self-assembly. *Chemistry-a European Journal* **2008,** *14* (15), 4585-4593.

122. Arumugam, S.; Popik, V. V., Light-Induced Hetero-Diels-Alder Cycloaddition: A Facile and Selective Photoclick Reaction. *J. Am. Chem. Soc.* **2011,** *133* (14), 5573-5579.

123. Arumugam, S.; Popik, V. V., Attach, Remove, or Replace: Reversible Surface Functionalization Using Thiol-Quinone Methide Photoclick Chemistry. *J. Am. Chem. Soc.* **2012,** *134* (20), 8408-8411.

124. Hickman, D. T.; Sreenivasachary, N.; Lehn, J. M., Synthesis of components for the generation of constitutional dynamic analogues of nucleic acids. *Helv. Chim. Acta* **2008,** *91* (1), 1-20.

125. Ura, Y.; Beierle, J. M.; Leman, L. J.; Orgel, L. E.; Ghadiri, M. R., Self-Assembling Sequence-Adaptive Peptide Nucleic Acids. *Science* **2009,** *325* (5936), 73-77.

126. Belowich, M. E.; Stoddart, J. F., Dynamic imine chemistry. *Chem. Soc. Rev.* **2012,** *41* (6), 2003-2024.

127. Giuseppone, N.; Schmitt, J. L.; Schwartz, E.; Lehn, J. M., Scandium(III) catalysis of transimination reactions. Independent and constitutionally coupled reversible processes. *J. Am. Chem. Soc.* **2005,** *127* (15), 5528-5539.

128. Giuseppone, N.; Schmitt, J. L.; Lehn, J. M., Generation of dynamic constitutional diversity and driven evolution in helical molecular strands under Lewis acid catalyzed component exchange. *Angewandte Chemie International Edition* **2004,** *43* (37), 4902-4906.

129. Hafezi, N.; Lehn, J. M., Adaptation of dynamic covalent systems of imine constituents to medium change by component redistribution under reversible phase separation. *Journal of the American Chemical Society* **2012,** *134*, 12861-12868.

130. Minkenberg, C. B.; Florusse, L.; Eelkema, R.; Koper, G. J. M.; van Esch, J. H., Triggered Self-Assembly of Simple Dynamic Covalent Surfactants. *J. Am. Chem. Soc.* **2009,** *131* (32), 11274-11275.

131. Minkenberg, C. B.; Hendriksen, W. E.; Li, F.; Mendes, E.; Eelkema, R.; van Esch, J. H., Dynamic covalent assembly of stimuli responsive vesicle gels. *Chem. Commun.* **2012,** *48* (79), 9837-9839.

132. Minkenberg, C. B.; Homan, B.; Boekhoven, J.; Norder, B.; Koper, G. J. M.; Eelkema, R.; van Esch, J. H., Responsive Wormlike Micelles from Dynamic Covalent Surfactants. *Langmuir* **2012,** *28* (38), 13570-13576.

133. Haldar, U.; Bauri, K.; Li, R.; Faust, R.; De, P., Polyisobutylene-Based pH-Responsive Self-Healing Polymeric Gels. *Acs Appl Mater Inter* **2015,** *7* (16), 8779-8788.

134. Kovaricek, P.; Lehn, J. M., Merging Constitutional and Motional Covalent Dynamics in Reversible Imine Formation and Exchange Processes. *J. Am. Chem. Soc.* **2012,** *134* (22), 9446-9455.

135. Rabbani, M. G.; Sekizkardes, A. K.; Kahveci, Z.; Reich, T. E.; Ding, R.; El-Kaderi, H. M., A 2D mesoporous imine-linked covalent organic framework for high pressure gas storage applications. *Chemistry - A European Journal* **2013,** *19*, 3324-3328.

136. Zeng, Y.; Zou, R.; Luo, Z.; Zhang, H.; Yao, X.; Ma, X.; Zou, R.; Zhao, Y., Covalent Organic Frameworks Formed with Two Types of Covalent Bonds Based on Orthogonal Reactions. *Journal of the American Chemical Society* **2015,** *137*, 1020-1023.

137. Huang, W.; Jiang, Y.; Li, X.; Li, X.; Wang, J.; Wu, Q.; Liu, X., Solvothermal Synthesis of Microporous, Crystalline Covalent Organic Framework Nanofibers and Their Colorimetric Nanohybrid Structures. *ACS Applied Materials & Interfaces* **2013,** *5* (18), 8845-8849.

138. Tanoue, R.; Higuchi, R.; Enoki, N.; Miyasato, Y.; Uemura, S.; Kimizuka, N.; Stieg, A. Z.; Gimzewski, J. K.; Kunitake, M., Thermodynamically Controlled Self-Assembly of Covalent Nanoarchitectures in Aqueous Solution. *ACS Nano* **2011,** *5* (5), 3923-3929.

139. Sreenivasachary, N.; Hickman, D. T.; Sarazin, D.; Lehn, J. M., DyNAs: Constitutional dynamic nucleic acid analogues. *Chemistry-a European Journal* **2006,** *12* (33), 8581-8588.

140. Hartley, C. S.; Elliott, E. L.; Moore, J. S., Covalent assembly of molecular ladders. *J. Am. Chem. Soc.* **2007,** *129* (15), 4512-4513.

141. Elliott, E. L.; Hartley, C. S.; Moore, J. S., Covalent ladder formation becomes kinetically trapped beyond four rungs. *Chem. Commun.* **2011,** *47* (17), 5028-5030.

Chapter 2

Dynamic Covalent Assembly of Peptoid-Based Molecular Ladders

2.1 Original Publication Information

Wei, T.; Jung, J. H.; Scott, T. F., Dynamic Covalent Assembly of Peptoid-Based Ladder Oligomers by Vernier Templating. *J. Am. Chem. Soc.* **2015,** *137* (51), 16196-16202.

Wei, T.; Furgal, J. C.; Jung, J. H.; Scott, T. F., Long, self-assembled molecular ladders by cooperative dynamic covalent reactions. *Polym. Chem.* **2017,** *8* (3), 520-527.

Modifications have been made to the original document in order to adapt the content to the proper format.

2.2 Abstract

Dynamic covalent chemistry (DCC), based on reversible or rearrangeable covalent interactions, provides avenues for the selective fabrication of intricate nanostructures that retain the robustness of covalent bonds. Here, we demonstrated the dynamic covalent assembly of complementary $n \times n$ oligopeptoid precursors into n–rung molecular ladders *via* scandium (III)-catalyzed imine metathesis through dimerization. Owing to their monomer diversity and synthetic accessibility, sequence-specific oligopeptoids bearing dynamic covalent functionalities were employed as precursors for molecular ladder fabrication. The generated ladder structures were characterized using matrix-assisted laser desorption/ionization (MALDI) mass spectrometry and gel permeation

chromatography (GPC), confirming successful fabrication of molecular ladders with up to 16 rungs, longest molecular ladder generated by dynamic covalent assembly to date.

2.3 Introduction

A long-term goal in materials science has been the creation of synthetic nanostructures that rival the structural sophistication and complexity of biological structures, with exacting spatial control on the molecular level.[1-5] A variety of naturally–occurring supramolecular assemblies arise from weak, non-covalent interactions such as van der Waals forces, pi stacking, dipole interactions, hydrogen bonding, ion pairing, or coordinative metal complexation.[4, 6-9] One such assembly is the DNA double helix, which has been further utilized for the formation of complex, asymmetric, multi-dimensional structures triggered by the self-assembly instruction encoded in DNA sequences.[10-13] However, owing to the typical weakness of non-covalent interactions, these supramolecular assemblies are often fragile and susceptible to thermal and mechanical degradation.[14-15] In contrast, dynamic covalent chemistry (DCC), based on reversible or rearrangeable covalent interactions, provides an alternative avenue for the selective fabrication of intricate nanostructures while retaining the robustness of covalent bonds.[4, 16-19] In DCC, the reaction mixture components should be able to undergo continuous exchange through reversible formation and breakage of covalent bonds, thereby affording for an error-correction mechanism and achieving equilibrium at the most thermodynamically stable products. Particularly, the reversible reaction between amine and aldehyde functional groups to form imine bonds operates under thermodynamic control such that by constantly replacing the kinetically competitive intermediate species, the most thermodynamically stable products are generated. Therefore, the rearrangement

of imine bonds has been extensively applied to the construction of exotic molecules and sophisticated structures as a result of the inherent 'error-checking' and 'proof-reading' associated with their reversibility.[5, 14-16, 19-23] Additionally, Lewis acids have been found to efficiently catalyse imine metathesis, such that the subsequent rapid bond rearrangement allows equilibrium to be attained on appropriate time scales.[24] Finally, the directionality of the imine bond precludes homodimerization, enabling its utilization in the fabrication of complex, asymmetric constructs.[5]

Nevertheless, kinetic trapping inevitably occurs when some components of the reaction mixture cannot exchange freely with others in order to reach thermodynamic equilibrium.[4, 17, 25] Previously, preliminary attempts at exploiting dynamic covalent reactions for base pairing have, to the best of knowledge, only been reported by the Moore group. Moore et al. employed Sc(III)-catalyzed imine metathesis for the dynamic covalent self-assembly of complementary m-phenylene ethynylene oligomers into *n*–rung molecular ladders. Unfortunately, this approach proved only moderately successful as the ladder formation became kinetically trapped at four or more rungs.[5, 26] Consequently, a thorough design of building blocks is usually required to curtail kinetic trapping and ensure the free exchange between each component of the reaction mixture.

Peptoids are a class of sequence-defined, peptidomimetic oligomers composed of repeating N-substituted glycine monomer units that are readily fabricated with near uniformity and in excellent yield via a solid-phase, 'submonomer' synthesis approach.[27-32] Since the pendant group on each monomeric residue can be individually selected, this synthetic strategy enables chemically–diverse sequence information to be encoded into peptoid chains. Compared to their biological counterparts such as polypeptides and

polynucleotides, peptoids offer increased chemical diversity, improved resistance to enzymatic and environmental degradation, and a reduced synthetic cost.[32-35] Moreover, due to the existence of tertiary amide bonds, peptoid backbones are normally considered to be flexible. [33, 36-38] It is also reported previously that peptoids adopt an alternating zig-zag pattern resulting from the ability of adjacent backbone monomers to adopt opposed rotational states, thereby allowing the backbone to remain linear and untwisted.[39] All these attributes of peptoids would potentially provide cooperative binding of dynamic covalent functionalities and thus promote hybridization selectivity and formation of the desired products.[14-15]

Therefore, in conjunction with dynamic covalent chemistry, the utilization of peptoids as nanoconstruction media provides a promising route towards the fabrication of exquisite molecular architectures with exacting structural control and robustness. Here we demonstrate the dynamic covalent assembly of complementary $n \times n$ oligopeptoids into molecular ladders with n rungs *via* scandium (III)-catalysed imine metathesis through dimerization.

2.4 Experimental

2.4.1 General Experimental Procedure

All chemicals and reagents, unless specified, were purchased from commercial sources and used as received without any further purification. ^{1}H and ^{13}C NMR spectra were collected using Varian MR400 and Varian VNMRS 700 spectrometers. Chemical shifts were measured in δ (ppm) relative to residual solvent signals as internal standards ($CDCl_3$: 7.24 for ^{1}H, 77.23 for ^{13}C; CD_3OD: 4.78 and 3.31 for ^{1}H, 49.15 for ^{13}C). Matrix-

assisted laser desorption/ionization (MALDI) mass spectra were recorded using a Bruker Autoflex mass spectrometer, whereas electrospray ionization (ESI) mass spectra were recorded using an Agilent Q-TOF 1200 series spectrometer. All MALDI analyses, excluding Im_**16**, were performed in reflectron positive ion mode using 2-(4-hydroxyphenylazo)benzoic acid (HABA) as the matrix, where 3 μL of a solution of the sample in chloroform (1.5 mM) was mixed with 10 μL of a mixture of 6 mg matrix in 300 μL acetonitrile, spotted on a MALDI sample plate (Bruker), and allowed to air dry. MALDI analysis for Im_**16** was performed in linear positive ion mode. Reverse phase high performance liquid chromatography (RP-HPLC) was performed using a Shimadzu LC-6AD HPLC pump, equipped with a Shimadzu FRC 70A fraction collector, using analytical and preparative reversed phase Phenomenex Luna C18(2) columns with a linear gradient of water and acetonitrile as the eluent at 30°C, and monitored with a Shimadzu Prominence UV/vis detector at 214 nm. Analytical gel permeation chromatography (GPC) was similarly performed using a Shimadzu LC-6AD HPLC pump, equipped with a series of three Phenogel GPC/SEC columns (length 300 mm × diameter 7.8 mm, pore sizes of 500, 100, and 50 Å) with 94:4:2 (v/v/v) $CHCl_3$:MeOH:Et_3N as the eluent at 30°C, and monitored with a Shimadzu Prominence UV/vis detector at 313 nm. The analytical GPC was calibrated utilizing low dispersity polystyrene standards (Polystyrene Standard (Low Molecular) Readycal Set, Fluka).

2.4.2 Monomer Synthesis

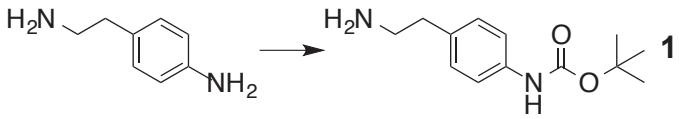

Scheme 2.1. Synthesis of 4-(2-aminoethyl)-N-(*tert*-butoxycarbonyl) phenylamine (1). Reagents and conditions: di-*tert*-butyl dicarbonate, 10% acetic acid in water, 1,4-dioxane, r.t. overnight.[40]

4-(2-Aminoethyl)-*N*-(*tert*-butoxycarbonyl)phenylamine (1). The method to synthesize compound **1** was adapted from a published approach.[40] Di-*tert*-butyl dicarbonate (10 g, 45.8 mmol) in 200 mL 1,4-dioxane was added into to a solution of 4-(2-aminoethyl)aniline (6 g, 44.1 mmol) in 200 mL 10% aq. acetic acid. The reaction mixture was stirred at room temperature overnight and then diluted with 600 mL deionized (DI) water and washed with Et_2O (300 mL) three times. The aqueous phase was adjusted to pH 14 by addition of 2 M NaOH (aq) and was extracted with Et_2O (150 mL) three times. The combined organic layer was washed with DI water three times, dried over Na_2SO_4, filtered, and evaporated to dryness to yield **1** as a light yellow solid (7.0 g, 67%).

^{1}H NMR (400 MHz, CD_3OD) δ: 7.32 (d, J = 8.4, 2H, Ar), 7.11 (d, J = 8.4, 2H, Ar), 2.81-2.85 (m, 2H, -CH_2-NH_2), 2.69 (t, J = 7.2, 2H, -CH_2-Ar), 1.51 (s, 9H, (-CH_3)$_3$).

^{13}C NMR (100 MHz, CD_3OD) δ: 155.41 (1C, -C=O), 138.72 (1C, Ar), 135.22 (1C, Ar), 130.04 (2C, Ar), 120.13 (2C, Ar), 80.72 (1C, -C(CH_3)$_3$), 44.27 (1C, -CH_2-NH_2), 39.48 (1C, -$C$$H_2$-Ar), 28.72 (3C, (-$CH_3$)$_3$).

MS (ESI+): calcd for $C_{13}H_{20}N_2O_2$: $[M+H]^+$ = 237.1598 $[M+Na]^+$ = 259.1417, found: m/z = 237.1595 $[M+H]^+$, m/z = 259.1415 $[M+Na]^+$.

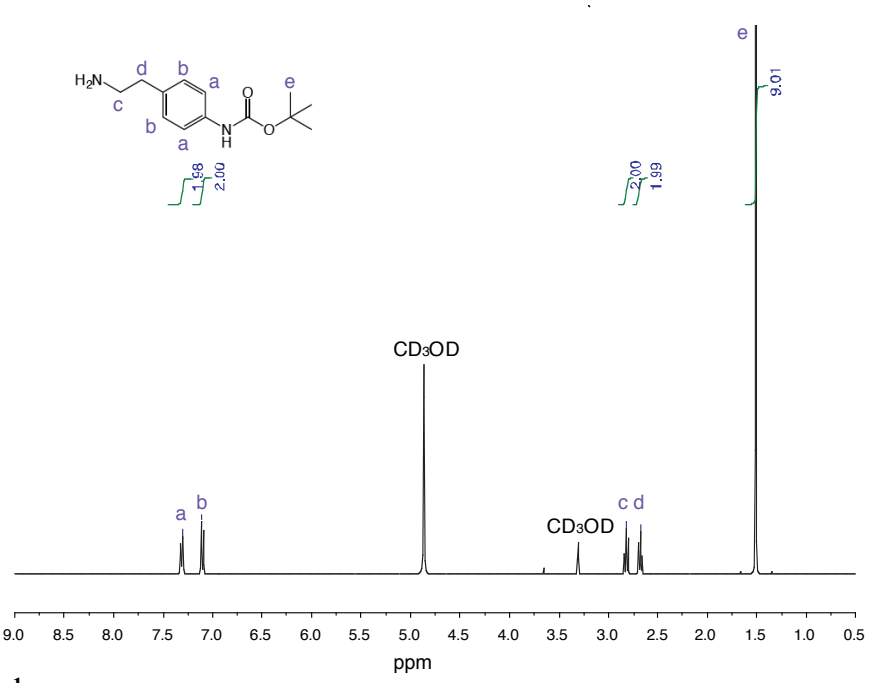

Figure 2.1. ^{1}H NMR spectrum of 4-(2-aminoethyl)-N-(*tert*-butoxycarbonyl) phenylamine

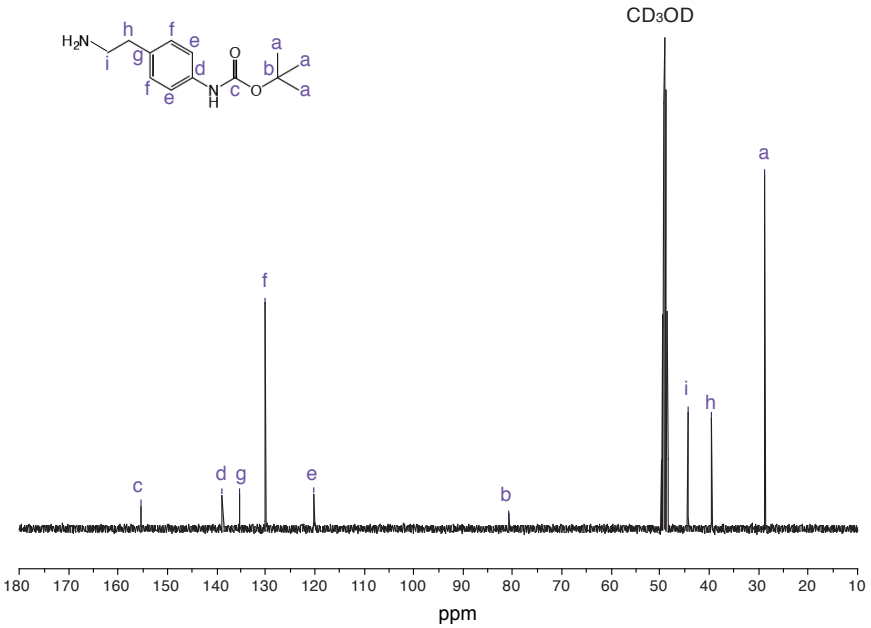

Figure 2.2. ^{13}C NMR spectrum of 4-(2-aminoethyl)-N-(*tert*-butoxycarbonyl) phenylamine

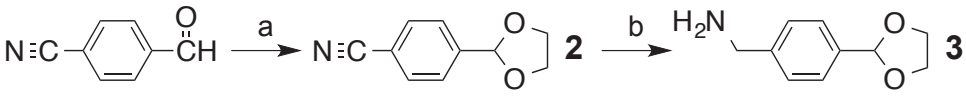

Scheme 2.2. Synthesis of 4-(1,3-dioxacylclopent-2-yl) (3). Reagents and conditions: (a) ethylene glycol, toluene-p-sulfonic acid, toluene, reflux; (b) $LiAlH_4$, Et_2O, 0°C for 4 h then r.t. for 12 h.[41]

4-(1,3-Dioxacyclopent-2-yl)benzonitrile (2). The method to synthesize compound **2** was adapted from a published approach.[41] Ethylene glycol (42.2 mL, 0.768 mol) and toluene-*p*-sulfonic acid (0.02 g, 0.10 mmol) were added into a solution of 4-cyanobenzaldehyde (25 g, 0.190 mol) in 200 mL of toluene. The reaction mixture was stirred and refluxed overnight. Azeotropic distillation with a Dean-Stark trap was used to remove water generated during the reaction. The reaction mixture was then cooled to room temperature and 40 mL of a 5% $NaHCO_3$ aqueous solution was added. The organic layer was extracted, washed with DI water three times, and dried over Na_2SO_4. The solvent was subsequently evaporated to dryness under reduced pressure to yield **2** as a white crystalline solid (28.75 g, 86.4%).

^{1}H NMR (400 MHz, $CDCl_3$) δ: 7.67 (d, J = 8.0, 2H, Ar), 7.59 (d, J = 8.4, 2H, Ar), 5.84 (s, 1H, CH), 4.12 - 4.03 (AA′BB′, 4H, $(CH_2O)_2$).

^{13}C NMR (100 MHz, $CDCl_3$) δ: 143.20 (1C, Ar), 132.34 (2C, Ar), 127.30 (2C, Ar), 118.72 (1C, CN), 113.02 (1C, Ar), 102.56 (1C, CH), 65.57 (2C, -CH_2O-).

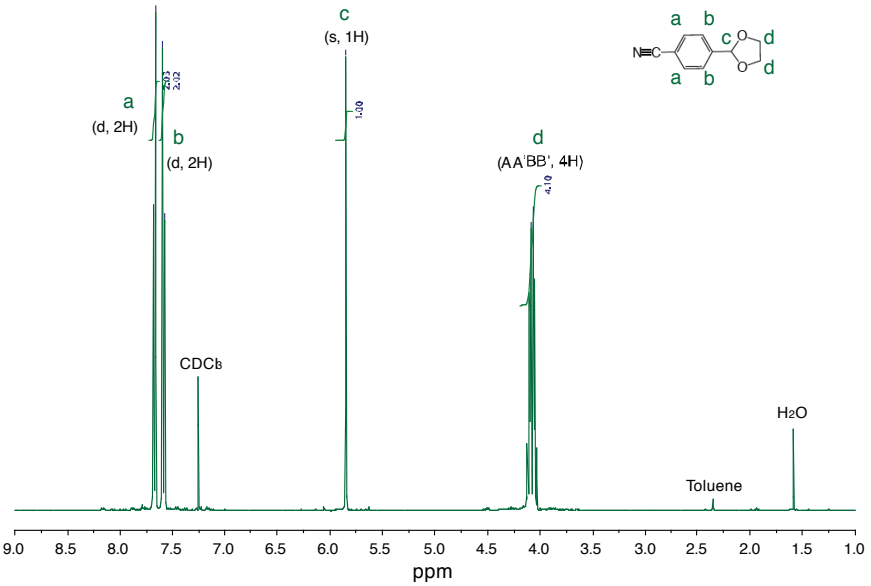

Figure 2.3. ^{11}H NMR spectrum of 4-(1,3-Dioxacyclopent-2-yl)benzonitrile.

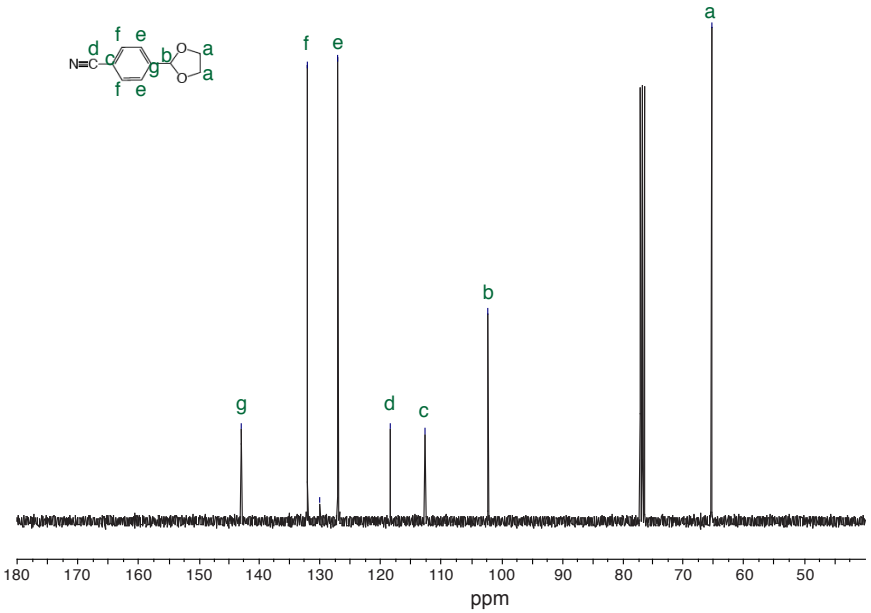

Figure 2.4. ^{13}C NMR spectrum of 4-(1,3-Dioxacyclopent-2-yl)benzonitrile.

4-(1,3-Dioxacyclopent-2-yl)benzylamine (3). The method to synthesize compound **3** was adapted from a published approach.[41] A solution of compound **2** (10 g, 0.057 mol) in 100 mL of dry Et_2O was added dropwise into a well-mixed suspension of $LiAlH_4$ (4.33 g, 0.114 mol) in 100 mL of dry Et_2O at 0°C under nitrogen. The reaction mixture was

stirred for 4 h at 0°C and 12 h at room temperature, then quenched by 95% ethanol (30 mL), and further quenched with 50% ethanol in water (20 mL). The ether supernatant was separated, evaporated to dryness under reduced pressure and the product redissolved in ether. The solvent was then washed twice with DI water, dried over sodium sulfate, and removed to afford yellow oil. The oil was purified on a silica gel column, initially flushed with ethyl acetate and subsequently eluted with a 90:10 to 70:30 ethyl acetate:methanol gradient. Solvent removal yielded compound **3** as a light yellow oil (7.20 g, 70.4%).

^{1}H NMR (400 MHz, $CDCl_3$) δ: 7.44 (d, J = 8.0, 2H, Ar), 7.32 (d, J = 8.0, 2H, Ar), 5.80 (s, 1H, CH), 4.14 - 4.0 (AA′BB′, 4H, $(CH_2O)_2$), 3.87 (s, 2H, -CH_2-NH_2).

^{13}C NMR (100 MHz, $CDCl_3$) δ: 144.53 (1C, Ar), 136.53 (1C, Ar), 127.16 (2C, Ar), 126.77 (2C, Ar), 103.72 (1C, CH), 65.39 (2C, -CH_2O-), 46.35 (1C, -CH_2-NH_2).

MS (ESI+): calcd for $C_{10}H_{13}NO_2$: $[M+H]^+$ = 180.1019, found: m/z = 180.1016 $[M+H]^+$.

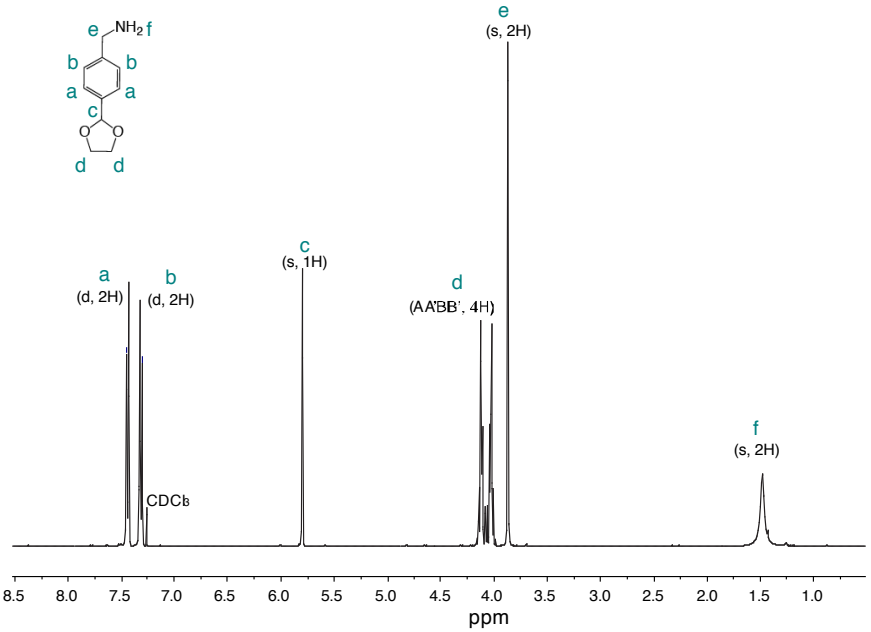

Figure 2.5. ^{1}H NMR spectrum of 4-(1,3-Dioxacyclopent-2-yl)benzylamine.

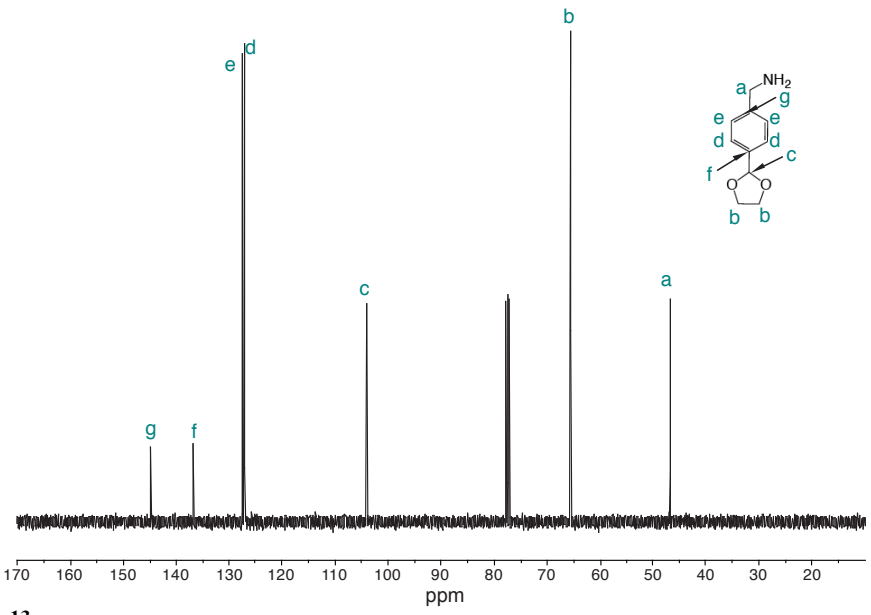

Figure 2.6. ^{13}C NMR spectrum of 4-(1,3-Dioxacyclopent-2-yl)benzylamine.

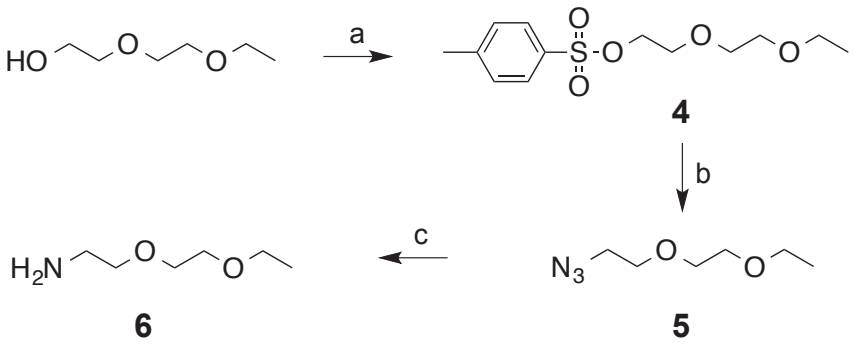

Scheme 2.3. **Synthesis of 2-(2-ethoxyethoxy)ethylamine (E^{3}A)** (6). Reagents and conditions: (a) tosyl chloride, THF, 0°C, (b) NaN_3, DMF, 60°C, 36 h, and (c) TPP, water.[42]

2-(2-Ethoxyethoxy)ethyl tosylate (**4**). The method to synthesize compound **4** was adapted from a published approach.[42] Diethylene glycol monoethyl ether (20 g, 0.15 mol) and 50 ml of THF were charged to a 500 mL round bottom flask with a magnetic stirrer. This reaction mixture was cooled to 0°C and 50 ml of 6 M NaOH was added, followed by dropwise addition of tosyl chloride (54 g, 0.28 mol) in 80 ml THF under N_2. After stirring for 1 h at 0°C, the reaction mixture was allowed to reach room temperature and

stirred for another 1 h. The resulting mixture was extracted with Et_2O (400 ml) and the organic layer was washed with 1 M NaOH and water. After drying over $MgSO_4$, the solution was evaporated under vacuum to yield **4** as a colorless liquid (42 g, 98%).

^{1}H NMR (400 MHz, $CDCl_3$) δ: 7.78 (d, J = 8.0, 2H, -S-C=CH-C*H*), 7.33 (d, J = 8.5, 2H, -S-C=CH-C*H*), 4.15 (t, J = 5.0, 2H, -CH_2-CH_2-O-Ts), 3.68 (t, J = 5.0, 2H, CH_2-CH_2-O-Ts), 3.60-3.42 (m, 6H, O-CH_2-CH_2-O-CH_2-CH_3), 2.43 (s, 3H, C-CH_3), 1.17 (t, J = 7.0, 3H, O-CH_2-CH_3).

^{13}C NMR (100 MHz, $CDCl_3$) δ: 144.79 (1C, -S-C_q-Ar), 132.95 (1C, C_p-Ar), 130.26 (1C, C_m-Ar), 129.80 (1C, C_m-Ar), 127.90 (1C, C_o-Ar), 126.95 (1C, C_o-Ar), 70.75 (1C, O-*C*H_2-CH_2-O-CH_2-CH_3), 69.68 (1C, O-CH_2-*C*H_2-O-CH_2-CH_3), 69.29 (1C, -*C*H_2-CH_2-O-Ts), 68.61 (1C, -CH_2-*C*H_2-O-Ts), 66.57 (1C, O-*C*H_2-CH_3), 21.56 (1C, C-*C*H_3) , 15.11 (1C, O-CH_2-*C*H_3).

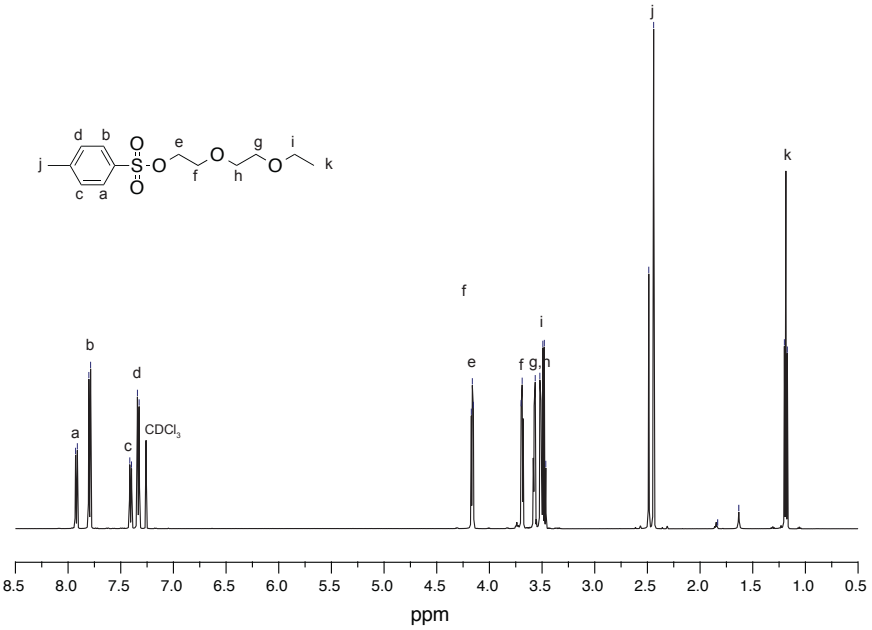

Figure 2.7. ^{1}H NMR spectrum of 2-(2-Ethoxyethoxy)ethyl tosylate.

2-(2-Ethoxyethoxy)ethyl azide (**5**). The method to synthesize compound **5** was adapted from a published approach.[42] A 500 mL round bottom flask was charged with compound **4** (40 g, 0.14 mol) and DMF (250 ml) under N_2. To this mixture, NaN_3 (31.5 g, 3.5 eq, 0.49 mol) was added. The reaction mixture was heated at 60°C for 36 h and then cooled to room temperature. The reaction mixture was diluted with a large amount of water and extracted with Et_2O. The organic layer was washed with water and dried over $MgSO_4$, and evaporated under vacuum to afford compound **5** as a yellow liquid (19 g, 85%).

^{1}H NMR (400 MHz, $CDCl_3$) δ: 3.64 (m, 4H, O-C*H*$_2$-C*H*$_2$-O), 3.58 (m, 2H, N_3-CH_2-C*H*$_2$-O), 3.51 (q, J = 7.5, 2H, O-C*H*$_2$-CH_3), 3.38 (t, J = 5.0, 2H, N_3-C*H*$_2$-CH_2-O), 1.19 (t, J = 7.5, 3H, O-CH_2-C*H*$_3$).

^{13}C NMR (100 MHz, $CDCl_3$) δ: 70.70 (1C, N_3-CH_2-*C*H_2-O), 69.97 (1C, O-*C*H_2-CH_2-O-CH_2-CH_3), 69.80 (1C, O-CH_2-*C*H_2-O-CH_2-CH_3), 66.63 (1C, O-*C*H_2-CH_3), 50.60 (1C, N_3-*C*H_2-CH_2-O), 15.08 (1C, O-CH_2-*C*H_3).

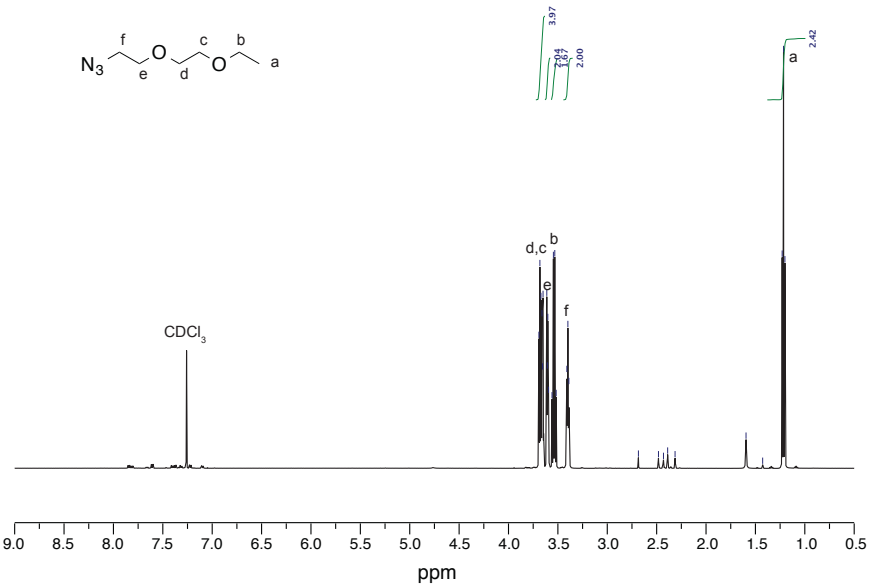

Figure 2.8. ^{1}H NMR spectrum of 2-(2-Ethoxyethoxy)ethyl azide.

2-(2-Ethoxyethoxy)ethylamine (E^3A) (**6**). The method to synthesize compound **6** was adapted from a published approach.[42] A 250 mL three necked round bottom flask equipped with magnetic stirrer was charged with compound **5** (20 g, 0.13 mmol) and THF (160 ml). Triphenylphosphine (TPP) (40 g, 0.15 mol, 1.1 eq) was then added and stirred overnight at room temperature under N_2. The reaction mixture was quenched with water (220 mL), and allowed to stir for another day. The resulting solution was washed with toluene and DCM, and evaporated under vacuum to yield compound **6** as a yellow liquid (10 g, 58%).

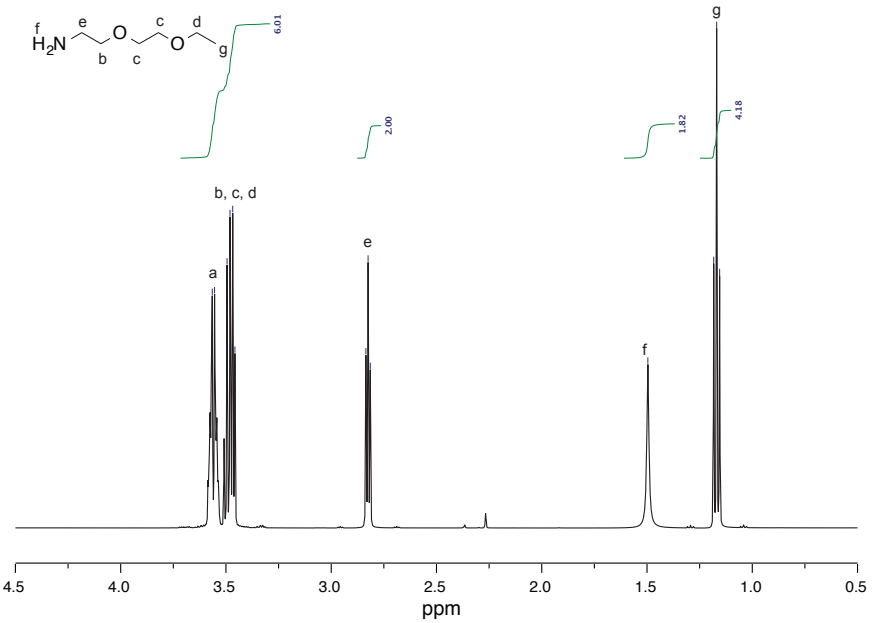

Figure 2.9. ^{1}H NMR spectrum of 2-(2-Ethoxyethoxy)ethyl amine.

^{1}H NMR (400 MHz, $CDCl_3$) δ: 3.62-3.42 (m, 8H, NH_2-CH_2-CH_2-O-CH_2-CH_2-O-CH_2-CH_3), 2.82 (m, 2H, NH_2-CH_2-CH_2-O), 1.48 (s, 2H, NH_2), 1.16 (t, J = 7.5, 3H, O-CH_2-CH_3).

^{13}C NMR (100 MHz, $CDCl_3$) δ: 73.14 (1C, NH_2-CH_2-*C*H_2-O), 70.72 (1C, O-*C*H_2-CH_2-O-CH_2-CH_3), 69.64 (1C, O-CH_2-*C*H_2-O-CH_2-CH_3), 66.45 (1C, O-*C*H_2-CH_3), 41.35 (1C, NH_2-*C*H_2-CH_2-O), 15.00 (1C, O-CH_2-*C*H_3).

MS (ESI+) (m/z): calcd for $C_6H_{16}NO_3^+$: $[M+H]^+$ = 134.1176, found: *m*/*z* = 134.1179 $[M+H]^+$.

2.4.3 Synthesis of Peptoids Bearing Dynamic Covalent Functionalities

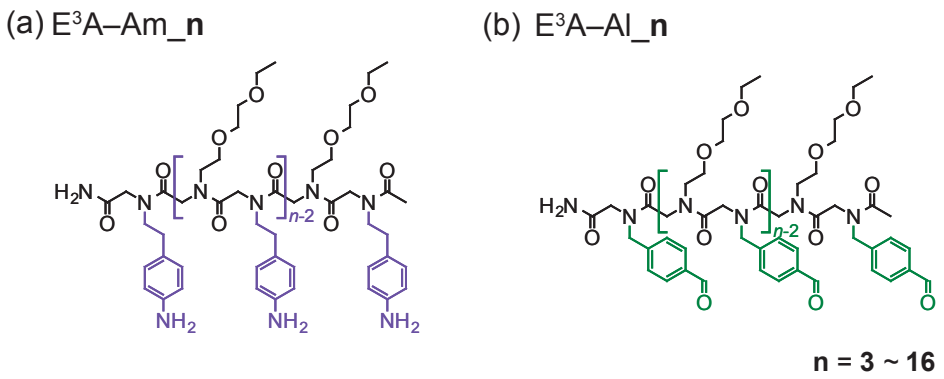

Figure 2.10. Chemical structures of amine– and aldehyde– functionalized peptoids

The synthesis of oligopeptoids was carried out on 222 mg of Rink amide resin (0.1 mmol scale, 100-200 mesh, 1% DVB, ChemPrep Inc.) using an automated microwave peptide synthesizer (Liberty Blue, CEM Corporation). Three primary amine monomers 4-(2-aminoethyl)-*N*-(*tert*-butoxycarbonyl)phenylamine, 4-(1,3-dioxacyclopent-2-yl) benzyl-amine, and 2-(2-Ethoxyethoxy)ethylamine were synthesized as described above. All other monomers, reagents, and solvents were purchased from commercial sources and directly used without further purification. The oligomer synthetic procedure was adapted from the submonomer approach to solid-phase peptoid synthesis.[27-28] The resin was

deprotected with 20% 4-methylpiperidine in DMF (v/v) for 30 s at 75°C and then 90 s at 90°C, followed by bromoacetylation for 5 min at 75°C with simultaneous addition of 1.5 mL of 1.0 M bromoacetic acid in DMF and 1.5 mL of 1.0 M DIC in DMF. Subsequently, halide displacement was performed by addition of 3 mL of 1.0 M primary amine monomer in NMP followed by an incubation of 5 min at 75°C. These bromoacetylation and displacement reactions were alternated until the desired peptoid sequence was achieved. All synthesized peptoids were acetylated by treatment with acetic anhydride to cap the secondary amine end groups.

2.4.4 Cleavage and Side-chain Deprotection

After solid-phase synthesis, the resultant dried Rink-amide resin was transferred to a 25 mL solid-phase peptide synthesis vessel (CG-1866, Chemglass) and treated with 4 mL of TFA cleavage cocktail for 10 ~ 25 min while bubbling with nitrogen at room temperature. The TFA cleavage solution was collected by filtering through the fritted glass into a 25 mL round bottom flask. The remaining resin was further rinsed twice with 2mL of fresh TFA cleavage cocktail to collect any residual peptoid. The cleavage solution was combined and evaporated by blowing a gentle stream of nitrogen to yield crude peptoid, the structures of which are illustrated in Figure 2.10. The crude product was reconstituted in HPLC grade MeCN/water (v/v, the least amount of MeCN to dissolve the crude peptoid oil) and further purified by preparative HPLC.

To note, TFA cleavage cocktail and cleavage time are dependent on the number and variety of protecting groups used. 95% aq.[43] TFA was used to deprotect acetal-protected aldehyde-functionalized peptoids, whereas 95% TFA in DCM was used to deprotect Boc-

protected amine-functionalized peptoids. Additionally, the crude amine-functionalized peptoids were subjected to 1 M $NaHCO_3$ to adjust the pH to ~7.6 prior to HPLC purification.[14]

2.4.5 Purification of Oligopeptoids by Preparative RP-HPLC

All deprotected peptoids were purified by preparative RP-HPLC using a linear gradient of H_2O (A) and MeCN (B) at a flow rate of 12 mL/min. The purified fractions were combined, concentrated, reconstituted in 50% MeCN/H_2O (v/v), frozen with liquid nitrogen, and lyophilized to afford fluffy white powder.

Preparative HPLC method for aldehyde functionalized oligopeptoids:

A) E^3A–Al_**3** and E^3A–Al_**4**: (1) 30% B, 0.1 – 4.1 min; (2) 30% – 70% B, 4.1 – 19.1 min; (3) 70% – 30% B, 19.1 – 21.1 min

B) E^3A-Al_**6**: (1) 30% B, 0.1 – 4.1 min; (2) 30% – 70% B, 4.1 – 19.1 min; (3) 70% B, 19.1 – 22.1 min; (4) 70% – 30% B, 22.1 – 24.1 min

C) E^3A–Al_**8**: (1) 30% B, 0.1 – 4.1 min; (2) 30% – 80% B, 4.1 – 24.1 min; (3) 80% – 30% B, 24.1 – 27.1 min

D) E^3A–Al_**10**: (1) 30% B, 0.1 – 4.1 min; (2) 30% – 85% B, 4.1 – 26.1 min; (3) 85% – 30% B, 26.1 – 29.1 min

E) E^3A–Al_**12**: (1) 30% B, 0.1 – 4.1 min; (2) 30% – 85% B, 4.1 – 26.1 min; (3) 85% B, 26.1 – 27.1 min; (4) 85% – 30% B, 27.1 – 30.1 min

F) E^3A–Al_**16**: (1) 30% B, 0.1 – 4.1 min; (2) 30% – 60% B, 4.1 – 12.1 min; (3) 60% – 80% B, 12.1 – 28.1 min; (4) 80% – 30% B, 28.1 – 31.1 min

Preparative HPLC method for amine functionalized oligopeptoids:

A) E^3A–Am_**3**, E^3A–Am_**4**, and E^3A–Am_**6**: (1) 20% B, 0.1 – 4.1 min; (2) 20% – 65% B, 4.1 – 30.1 min; (3) 65% – 20% B, 30.1 – 32.1 min

B) E^3A–Am_**8** & E^3A–Am_**10**: (1) 20% B, 0.1 – 4.1 min; (2) 20% – 65% B, 4.1 – 30.1 min; (3) 65% – 20% B, 30.1 – 32.1 min

C) E^3A–Am_**12**: (1) 25% B, 0.1 – 4.1 min; (2) 25% – 65% B, 4.1 – 36.1 min; (3) 65% – 25% B, 36.1 – 38.1 min

D) E^3A–Am_**16**: (1) 35% B, 0.1 – 4.1 min; (2) 35% – 55% B, 4.1 – 12.1 min; (3) 55% – 70% B, 12.1 – 25.1 min; (4) 70% – 35% B, 25.1 – 28.1 min

The purity of the collected, aldehyde- and amine-functionalized peptoids was further examined by analytical RP-HPLC at a flow rate of 1mL/min.

Analytical HPLC method for E^3A-Al_**3** ~ E^3A-Al_**6** and E^3A-Am_**3** ~ E^3A-Am_**6**:

A: H_2O, B: MeCN; 30% – 70% B 0 – 15 min, 70% – 30% B 15 – 18 min.

Analytical HPLC method for E^3A-Al_**8** ~ E^3A-Al_**16** and E^3A-Am_**8** ~ E^3A-Am_**16**:

A: H_2O, B: MeCN; 20% – 90% B 0 – 20 min, 90% – 20% B 20 – 23 min.

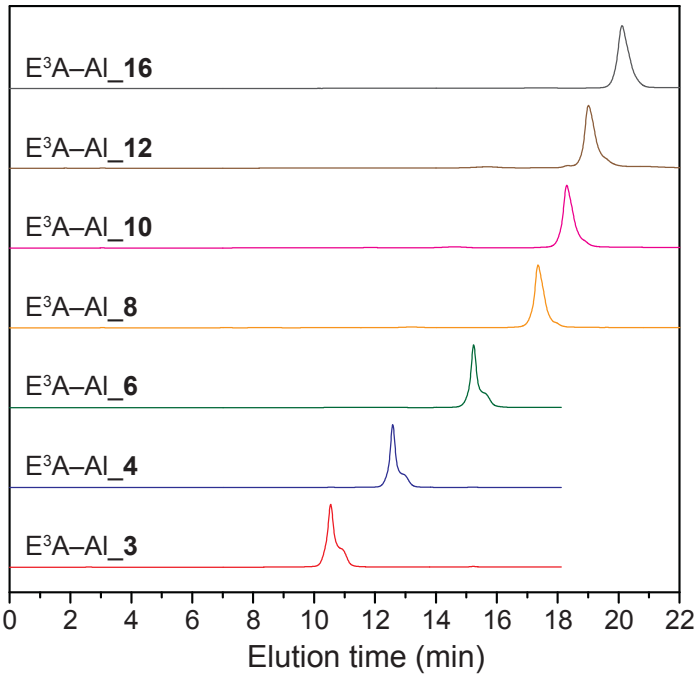

Figure 2.11. **Analytical HPLC traces of aldehyde–functionalized oligopeptoids.** *Purity: E^3A-Al_3, 98%; E^3A-Al_4, purity 99%; E^3A-Al_6, 98%; E^3A–Al_8, 97.5%; E^3A–Al_10, 96.1%; E^3A–Al_12, 95.4%; E^3A–Al_16, 99.3%.

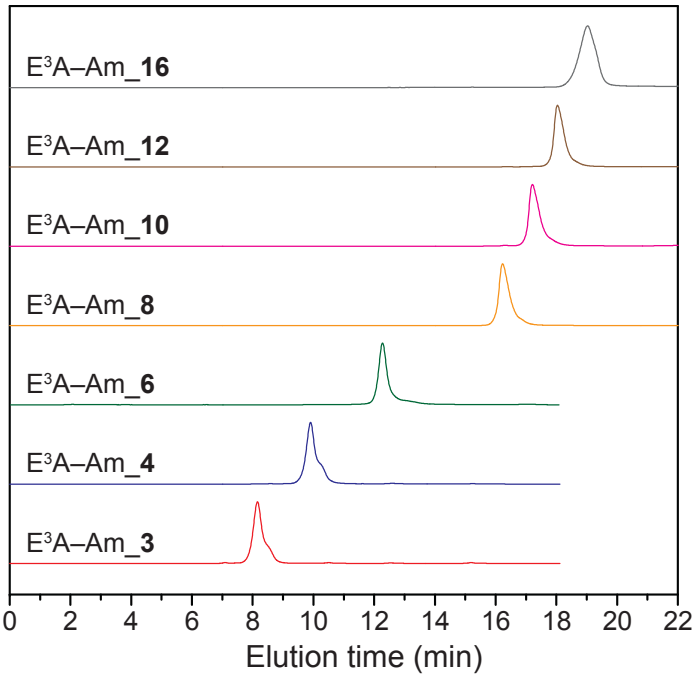

Figure 2.12. **Analytical HPLC traces of amine–functionalized oligopeptoids.** *Purity: E^3A–Am_3, purity 98%; E^3A–Am_4, purity 98%; E^3A–Am_6, purity 99%; E^3A–Am_8, 99.8%; E^3A–Am_10, 96.9%; E^3A–Am_12, 98.8%; E^3A–Am_16, 98.9%.

2.4.6 Characterization of Peptoids Bearing Dynamic Covalent Functionalities

2.4.6.1 Mass spectra of Purified, Aldehyde- and Amine-Functionalized Peptoids

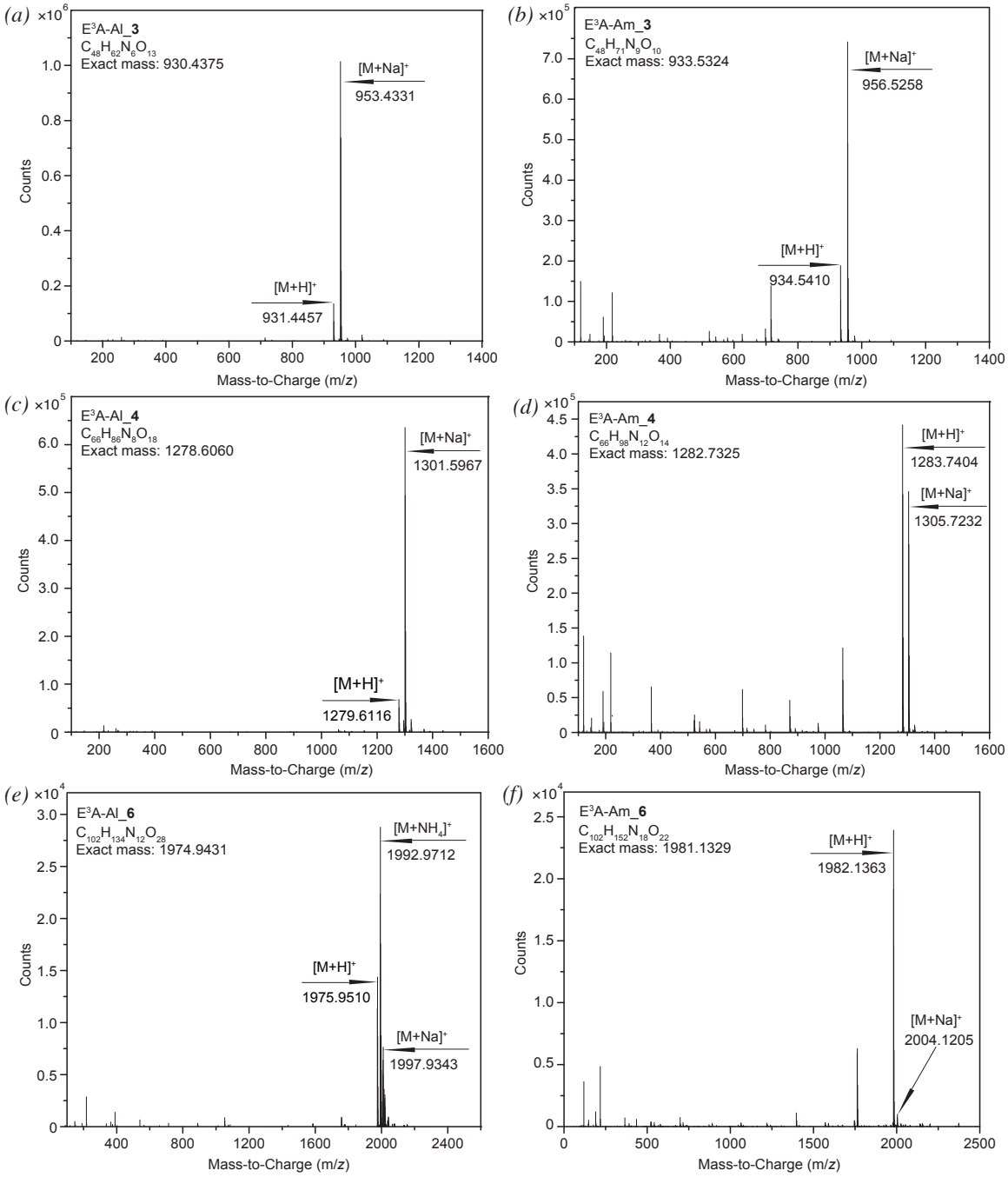

Figure 2.13. **ESI mass spectra of aldehyde– and amine–functionalized oligopeptoids purified by preparative RP-HPLC.** (*a*) E^3A-Al_3; (*b*) E^3A-Am_3; (*c*) E^3A-Al_4; (*d*) E^3A-Am_4; (*e*) E^3A-Al_6 & (*f*) E^3A-Am_6.

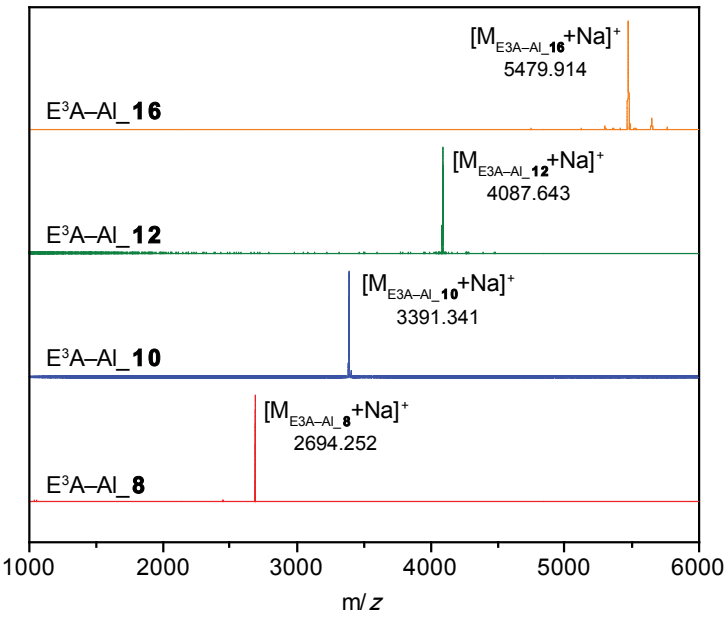

Figure 2.14. **MALDI mass spectra of aldehyde–functionalized oligopeptoids purified by preparative RP-HPLC.**
*Expected exact mass: $[M_{E^3A–Al\_8}+Na]^+$ = 2694.269; $[M_{E^3A–Al\_10}+Na]^+$ = 3390.606; $[M_{E^3A–Al\_12}+Na]^+$ = 4086.943; $[M_{E^3A–Al\_16}+Na]^+$ = 5479.618.

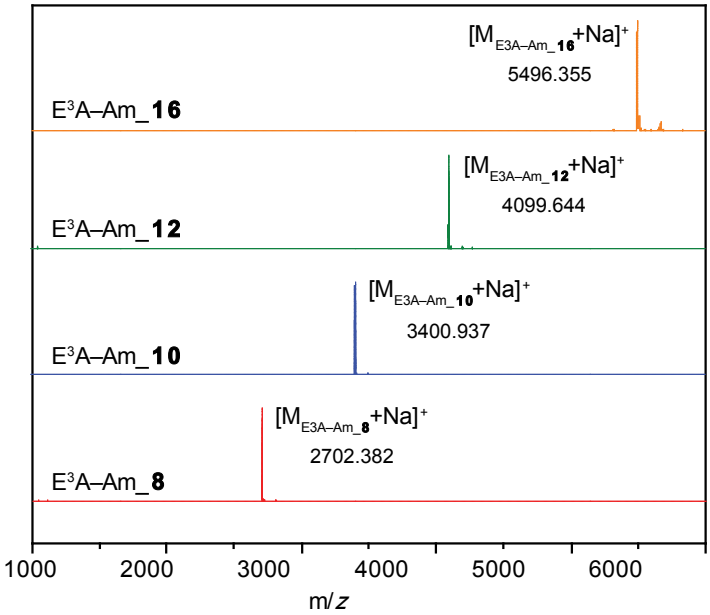

Figure 2.15. **MALDI mass spectra of amine–functionalized oligopeptoids purified by preparative RP-HPLC.**
*Expected exact mass: $[M_{E^3A–Am\_8}+Na]^+$ = 2702.522; $[M_{E^3A–Am\_10}+Na]^+$ = 3400.923; $[M_{E^3A–Am\_12}+Na]^+$ = 4099.323; $[M_{E^3A–Am\_16}+Na]^+$ = 5496.124.

MS (ESI+):

E^3A-Al_**3**: calcd for $C_{48}H_{62}N_6O_{13}$: $[M+H]^+$ = 931.4448, $[M+Na]^+$ = 953.4267, found: *m*/*z* = 931.4457 $[M+H]^+$, *m*/*z* = 953.4331 $[M+Na]^+$

E^3A-Am_**3**: calcd for $C_{48}H_{71}N_9O_{10}$: $[M+H]^+$ = 934.5397, $[M+Na]^+$ = 956.5216, found: *m*/*z* = 934.5410 $[M+H]^+$, *m*/*z* = 956.5258 $[M+Na]^+$

E^3A-Al_**4**: calcd for $C_{66}H_{86}N_8O_{18}$: $[M+H]^+$ = 1279.6133, $[M+Na]^+$ = 1301.5952, found: *m*/*z* = 1279.6116 $[M+H]^+$, *m*/*z* = 1301.5967 $[M+Na]^+$

E^3A-Am_**4**: calcd for $C_{66}H_{98}N_{12}O_{14}$: $[M+H]^+$ = 1283.7398, $[M+Na]^+$ = 1305.7217, found: *m*/*z* = 1283.7404 $[M+H]^+$, *m*/*z* = 1305.7232 $[M+Na]^+$

E^3A-Al_**6**: calcd for $C_{102}H_{134}N_{12}O_{28}$: $[M+H]^+$ = 1975.9504, $[M+NH_4]^+$ = 1992.9769, $[M+Na]^+$ = 1997.9323, found: *m*/*z* = 1975.9510 $[M+H]^+$, *m*/*z* = 1992.9712 $[M+NH_4]^+$, *m*/*z* = 1997.9343 $[M+Na]^+$

E^3A-Am_**6**: calcd for $C_{102}H_{152}N_{18}O_{22}$: $[M+H]^+$ = 1982.1402, $[M+Na]^+$ = 2004.1221, found: *m*/*z* = 1982.1363 $[M+H]^+$, *m*/*z* = 2004.1205 $[M+Na]^+$

2.4.6.2 NMR Spectra of Purified, Aldehyde- and Amine-Functionalized Peptoids

E^3A-Al_**3**

^{1}H NMR (700 MHz, $CDCl_3$) δ: 9.96-10.01 (m, Ar-C*H*O), 7.72-7.92 (m, Ar), 7.36-7.48 (m, Ar), 4.64-4.87 (m, Ar-CH_2-N-), 3.88-4.34 (m, -N-CH_2-CH_2-O-, -N-CH_2-CO-), 3.34-3.63 (m, -O-CH_2-CH_2-O-, -O-CH_2-CH_3, -N-CH_2-CH_2-O-), 2.06-2.18 (m, -CO-CH_3), 1.05-1.17 (m, -O-CH_2-CH_3)

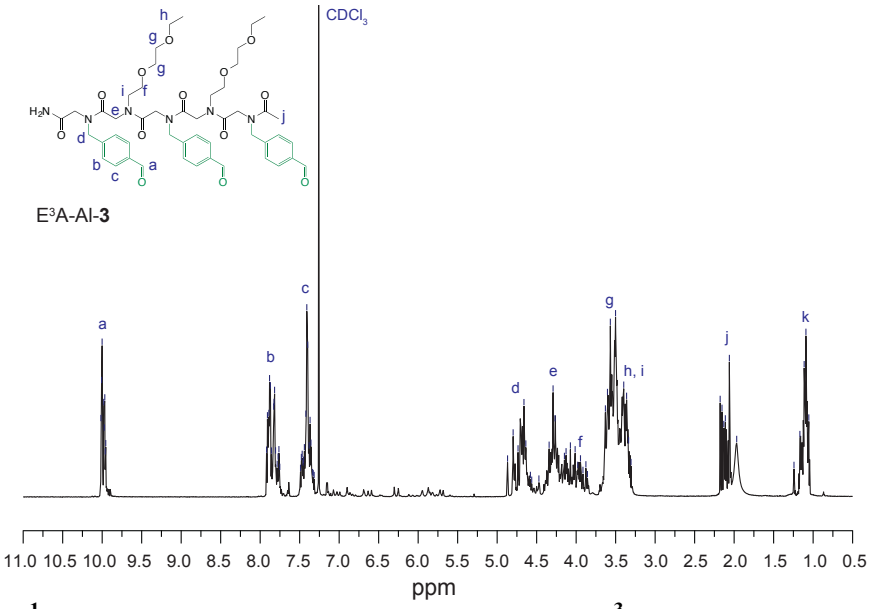

Figure 2.16. ^{1}H NMR spectrum (700 mHz, $CDCl_3$) of E^3A–Al_3.

E^3A-Al_**4**

^{1}H NMR (700 MHz, $CDCl_3$) δ: 9.95-10.01 (m, Ar-C*H*O), 7.75-7.90 (m, Ar), 7.35-7.51 (m, Ar), 4.56-4.74 (m, Ar-CH_2-N-), 4.00-4.33 (m, -N-CH_2-CH_2-O-, -N-CH_2-CO-), 3.34-3.62 (m, -O-CH_2-CH_2-O-, -O-CH_2-CH_3, -N-CH_2-CH_2-O-), 1.95-2.12 (m, -CO-CH_3), 1.04-1.16 (m, -O-CH_2-CH_3)

E^3A-Al_**6**

^{1}H NMR (700 MHz, $CDCl_3$) δ: 9.95-10.00 (br, Ar-C*H*O), 7.72-7.89 (br, Ar), 7.33-7.49 (br, Ar), 4.35-4.63 (br, Ar-CH_2-N-), 4.03-4.29 (br, -N-CH_2-CH_2-O-, -N-CH_2-CO-), 3.32-3.48 (br, -O-CH_2-CH_2-O-, -O-CH_2-CH_3, -N-CH_2-CH_2-O-), 2.00-2.12 (br, -CO-CH_3), 1.05-1.10 (br, -O-CH_2-CH_3)

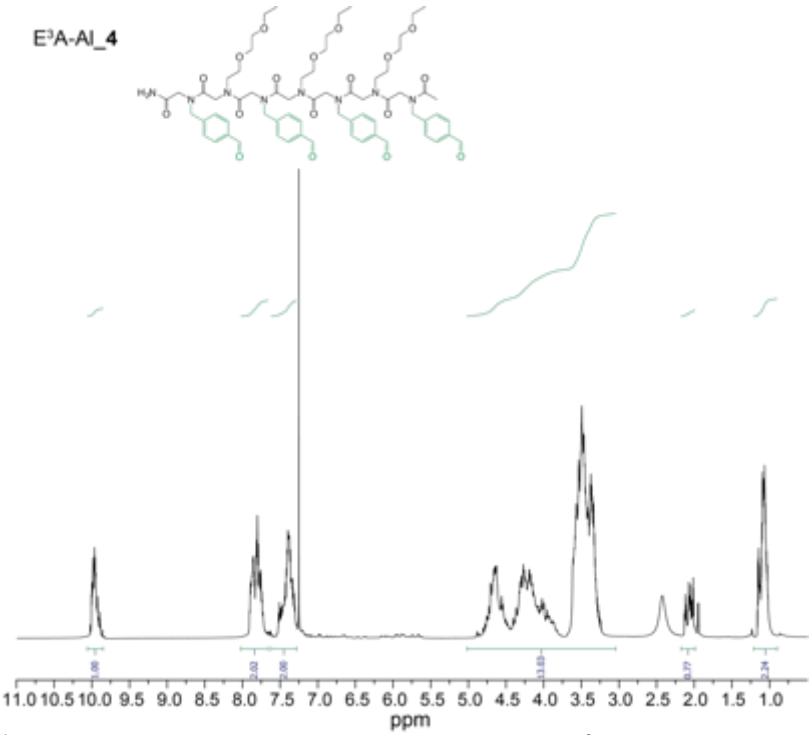

Figure 2.17. **^{1}H NMR spectrum (700 mHz, $CDCl_3$) of E^3A–Al_4.**

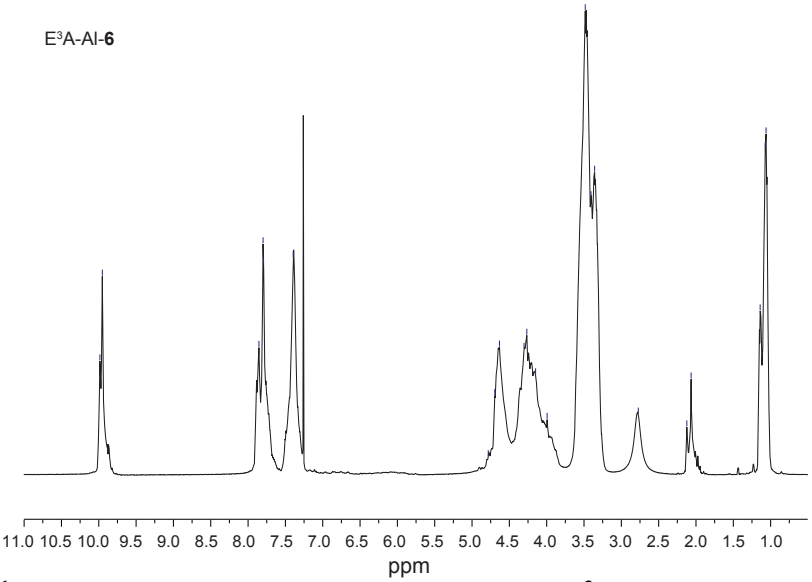

Figure 2.18. ^{1}H NMR spectrum (700 mHz, $CDCl_3$) of E^3A–Al_6.

E^3A-Am_**3**

^{1}H NMR (700 MHz, $CDCl_3$) δ: 6.78-6.94 (m, Ar), 6.56-6.60 (m, Ar), 3.73-4.27 (m, -N-CH_2-CO-, -N-CH_2-CH_2-O-), 3.26-3.57 (m, -O-CH_2-CH_2-O-,-O-CH_2-CH_3, Ar-CH_2-CH_2-

N-, -N-CH_2-CH_2-O-), 2.60-2.73 (m, -Ar-CH_2-CH_2-N-), 1.80-1.97 (m, -CO-CH_3), 1.17-1.21 (m, -O-CH_2-CH_3)

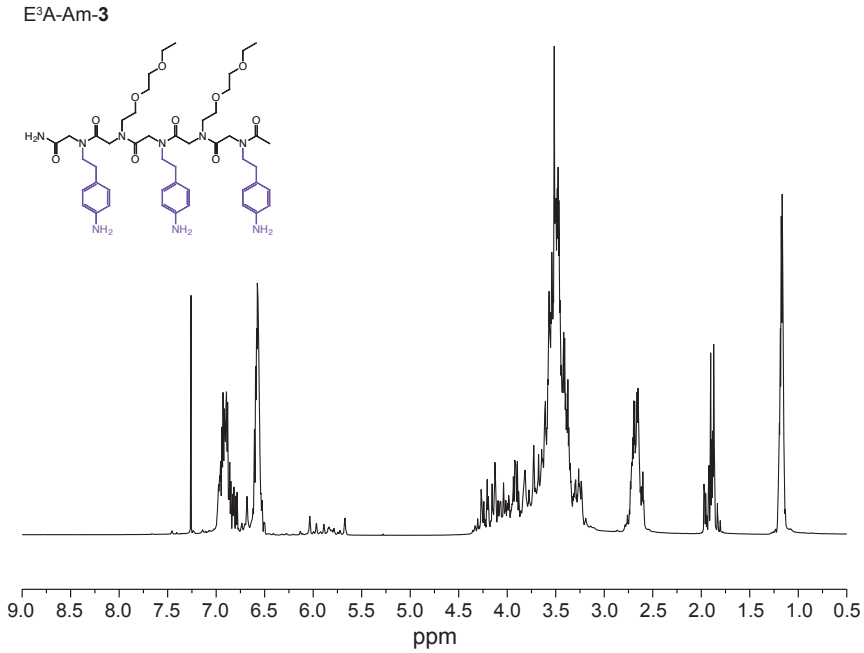

Figure 2.19. ^{1}H NMR spectrum (700 mHz, $CDCl_3$) of E^3A–Am_3.

E^3A-Am_**4**

^{1}H NMR (700 MHz, $CDCl_3$) δ: 6.83-6.97 (m, Ar), 6.54-6.60 (m, Ar), 3.75-4.31 (m, -N-CH_2-CO-, -N-CH_2-CH_2-O-), 3.20-3.55 (m, -O-CH_2-CH_2-O-,-O-CH_2-CH_3, Ar-CH_2-CH_2-N-, -N-CH_2-CH_2-O-), 2.60-2.71 (m, -Ar-CH_2-CH_2-N-), 1.85-1.98 (m, -CO-CH_3), 1.17-1.20 (m, -O-CH_2-CH_3)

E^3A-Am_**6**

^{1}H NMR (700 MHz, $CDCl_3$) δ: 6.91-6.98 (br, Ar), 6.60 (br, Ar), 3.89-4.37 (br, -N-CH_2-CO-, -N-CH_2-CH_2-O-), 3.22-3.60 (br, -O-CH_2-CH_2-O-,-O-CH_2-CH_3, Ar-CH_2-CH_2-N-, -N-CH_2-CH_2-O-), 2.67-2.70 (br, -Ar-CH_2-CH_2-N-), 1.87-1.99 (br, -CO-CH_3), 1.17-1.20 (br, -O-CH_2-CH_3)

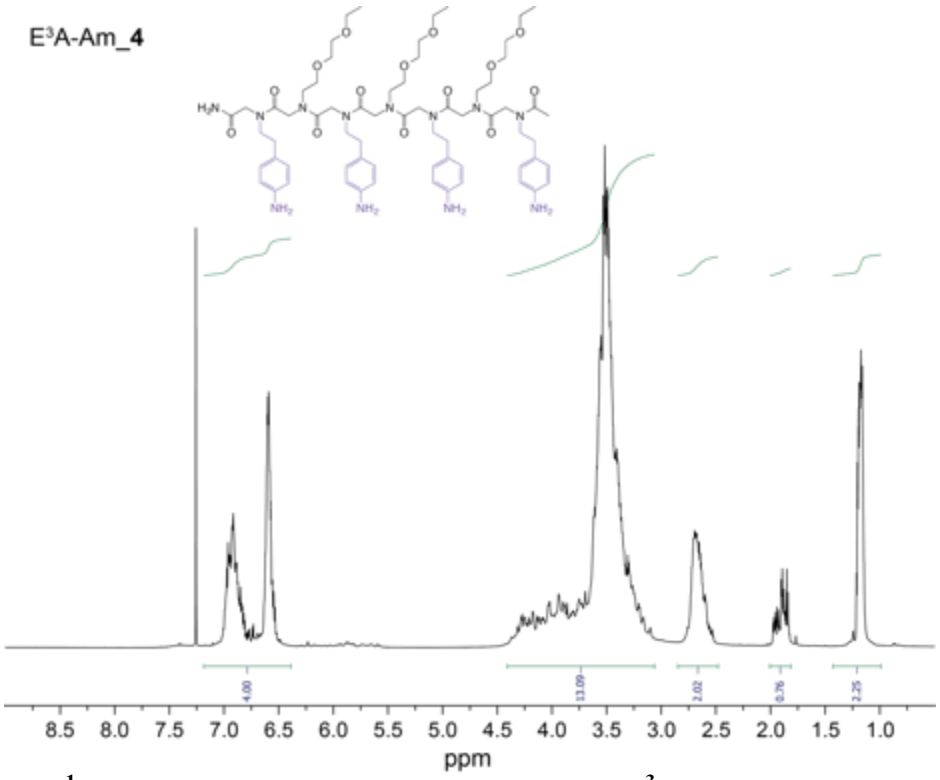

Figure 2.20. ^{1}H NMR spectrum (700 MHz, $CDCl_3$) of E^3A–Am_4.

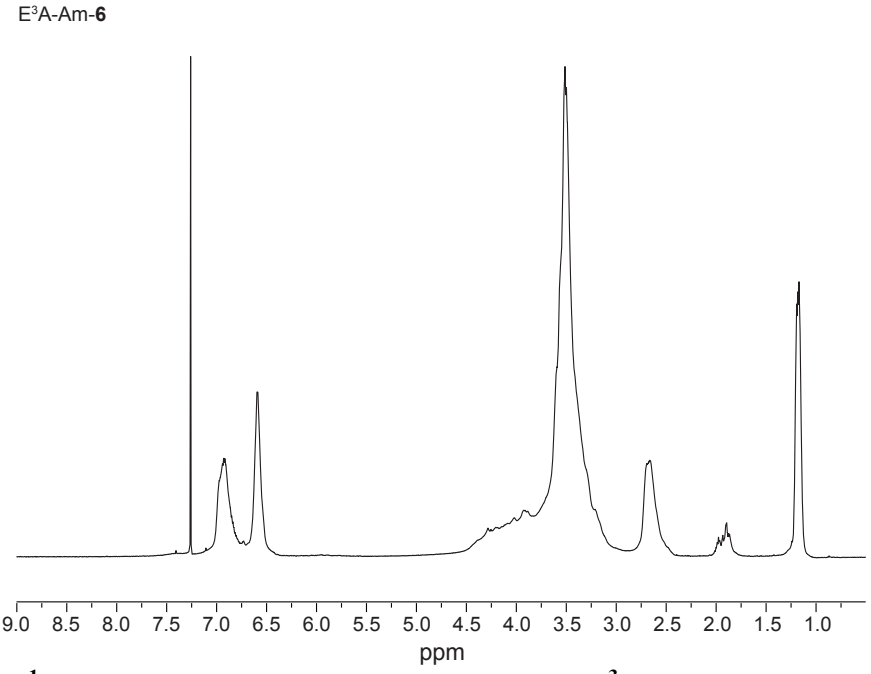

Figure 2.21. ^{1}H NMR spectrum (700 MHz, $CDCl_3$) of E^3A–Am_6.

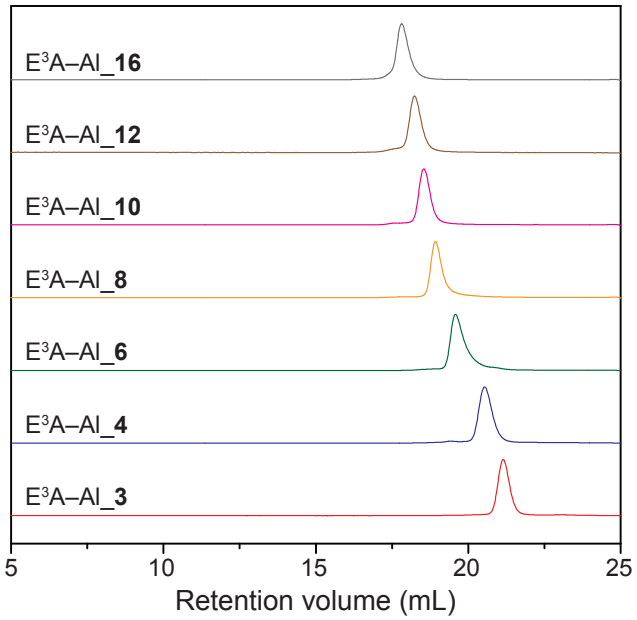

Figure 2.22. **Analytical GPC of aldehyde–functionalized oligopeptoids.**
*Analytical GPC method: isocratic flow rate at 1 mL/min; eluent: $CHCl_3/CH_3OH/Et_3N$ (94/4/2, v/v/v). E^3A–Al_3, V_r = 21.14 mL, M_n = 1240 g/mol; E^3A–Al_4, V_r = 20.53 mL, M_n = 1624 g/mol; E^3A–Al_6, V_r = 19.58 mL, M_n = 2574 g/mol; E^3A–Al_8, V_r = 18.92 mL, M_n = 3667 g/mol; E^3A–Al_10, V_r = 18.54 mL, M_n = 4571 g/mol; E^3A–Al_12, V_r = 18.24 mL, M_n = 5502 g/mol; E^3A–Al_16, V_r = 17.81 mL, M_n = 7245 g/mol.

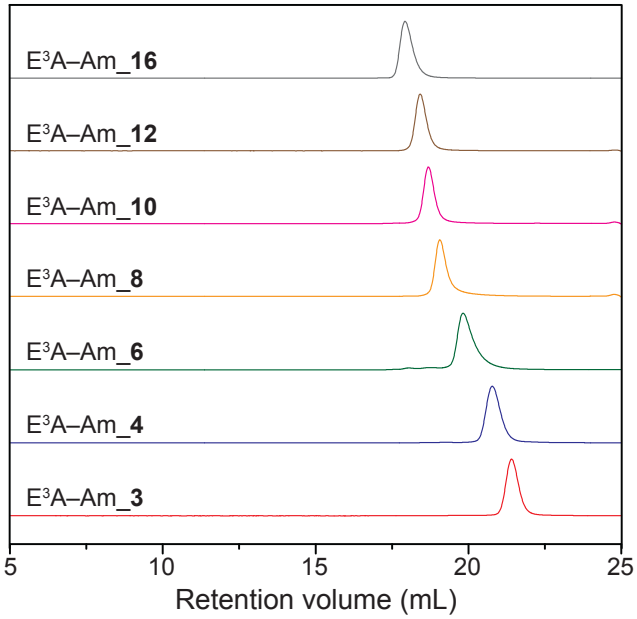

Figure 2.23. **Analytical GPC of amine–functionalized oligopeptoids.**
*Analytical GPC method: isocratic flow rate at 1 mL/min; eluent: $CHCl_3/CH_3OH/Et_3N$ (94/4/2, v/v/v). E^3A–Am_3, V_r = 21.41 mL, M_n = 934 g/mol; E^3A–Am_4, V_r = 20.78 mL, M_n = 1283 g/mol; E^3A–Am_6, V_r = 19.82 mL, M_n = 1981 g/mol; E^3A–Am_8, V_r = 19.10 mL, M_n = 3390 g/mol; E^3A–Am_10, V_r = 18.68 mL, M_n = 4194 g/mol; E^3A–Am_12, V_r = 18.42 mL, M_n = 4923 g/mol; E^3A–Am_16, V_r = 17.92 mL, M_n = 6750 g/mol.

Table 2.1. **Structural information of aldehyde–functionalized oligopeptoid sequences subjected to MALDI mass spectrometry, HPLC and GPC analysis.**

Code	Formula	Exact mass M (g/mol)	Molecular weight (g/mol)
E^3A–Al_**3**	$C_{48}H_{62}N_6O_{13}$	930.4375	931.0530
E^3A–Al_**4**	$C_{66}H_{86}N_8O_{18}$	1278.6060	1278.6060
E^3A–Al_**6**	$C_{102}H_{134}N_{12}O_{28}$	1974.9431	1976.2500
E^3A–Al_**8**	$C_{138}H_{182}N_{16}O_{38}$	2671.280	2673.048
E^3A–Al_**10**	$C_{174}H_{230}N_{20}O_{48}$	3367.617	3369.846
E^3A–Al_**12**	$C_{210}H_{278}N_{24}O_{58}$	4063.954	4066.644
E^3A–Al_**16**	$C_{282}H_{374}N_{32}O_{78}$	5456.628	5460.240

Table 2.2. **Structural information of amine–functionalized oligopeptoid sequences subjected to MALDI mass spectrometry, HPLC and GPC analysis.**

Code	Formula	Exact mass M (g/mol)	Molecular weight (g/mol)
E^3A–Am_**3**	$C_{48}H_{71}N_9O_{10}$	933.5324	934.1490
E^3A–Am_**4**	$C_{66}H_{98}N_{12}O_{14}$	1282.7325	1283.5800
E^3A–Am_**6**	$C_{102}H_{152}N_{18}O_{22}$	1981.1329	1982.4420
E^3A–Am_**8**	$C_{138}H_{206}N_{24}O_{30}$	2679.533	2681.304
E^3A–Am_**10**	$C_{174}H_{260}N_{30}O_{38}$	3377.934	3380.166
E^3A–Am_**12**	$C_{210}H_{314}N_{36}O_{46}$	4076.334	4079.028
E^3A–Am_**16**	$C_{282}H_{422}N_{48}O_{62}$	5473.134	5476.142

2.4.7 General Procedure for Self-assembly of Molecular Ladders of Length *n*

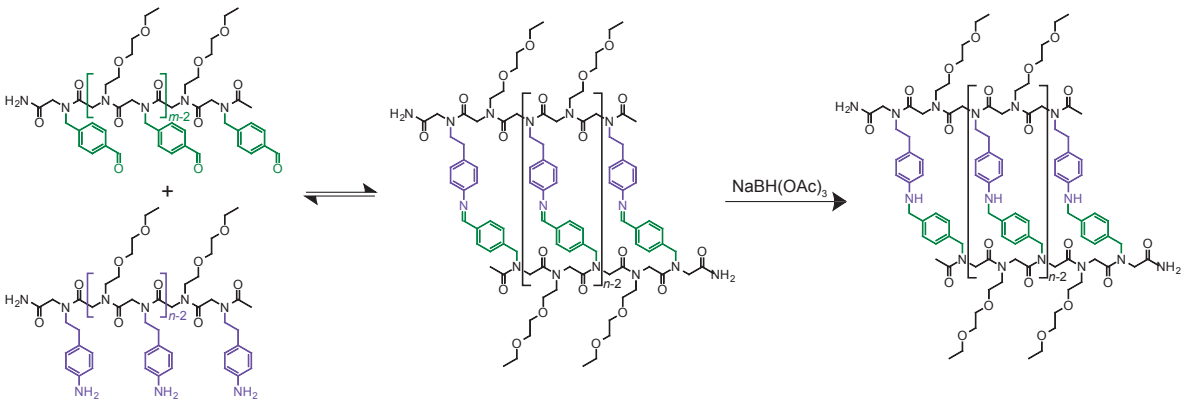

Scheme 2.4. Dimerization of peptoid-based molecular ladders (*m* = *n*).

The method to dimerize aldehyde- and amine-functionalized peptoid oligomers was adapted from a published approach.[5] 1 μmol of the peptoid oligomer E^3A–Al_***m*** was mixed with 1 μmol of its complementary strand E^3A–Am_***n***, where ***m*** = ***n***, in 2 mL $CHCl_3$. To the reaction mixture, $Sc(OTf)_3$ (0.04 eq. per imine bond, 10 mM stock solution dissolved in MeCN) was added and the mixture allowed to stir overnight. The reaction mixture was then directly analyzed by MALDI mass spectrometry and analytical GPC. Sodium triacetoxyborohydride ($NaBH(OAc)_3$, STAB) was subsequently added (10 equivalents per imine bond), the reaction mixture was stirred overnight to reduce the inter-strand imine groups to secondary amines, and the mixture was characterized by MALDI mass spectrometry.

2.5 Results and Discussion

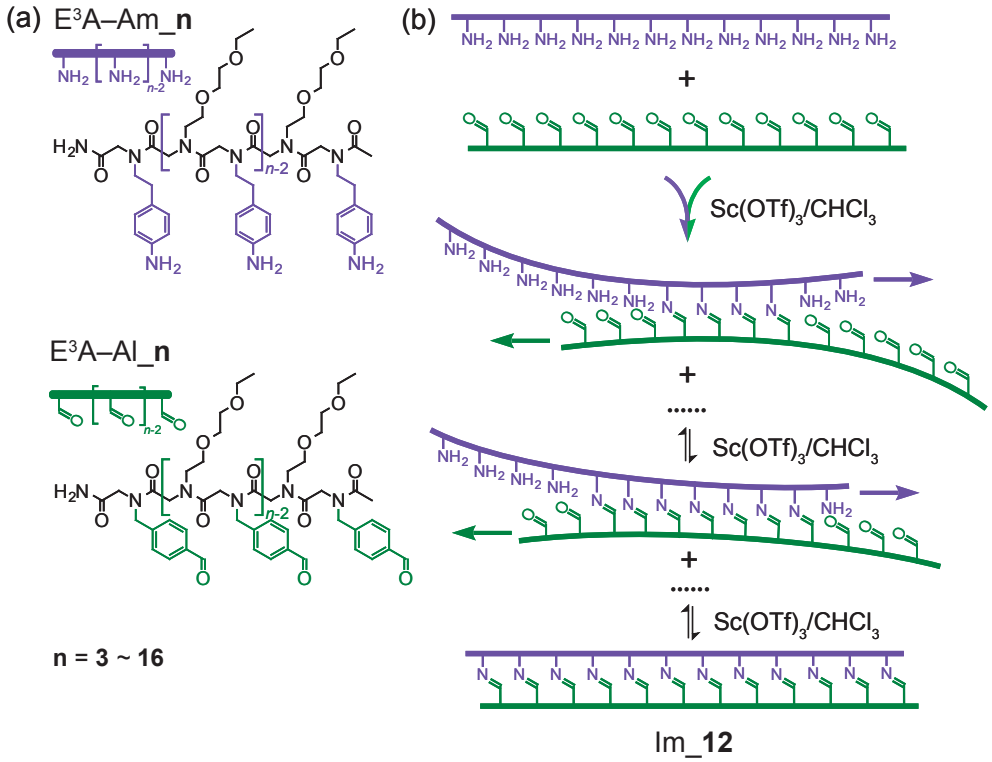

Scheme 2.5. Dynamic covalent assembly of *n*–rung peptoid-based molecular ladders initially by imine condensation reactions and followed by imine exchange reactions. (a) Structures of oligopeptoids bearing pendant amine functional groups (E^3A–Am_**n**) and aldehyde functional groups (E^3A–Al_**n**), respectively, where **n** refers to the number of amine- and aldehyde-bearing residues. (b) Dynamic covalent assembly of complementary dodecamine- and dodecaldehyde-peptoids into a 12–rung peptoid-based molecular ladder (Im_n, where Im denotes "imine linkages").

Oligomeric peptoid sequences incorporating pendant aldehyde and amine functional groups were prepared using the 'submonomer' solid-phase peptoid synthesis approach,[28] where a peptoid chain is grown *via* sequential addition reactions one unit at a time using an automated peptide synthesizer. These peptoid sequences were synthesized as alternating co-oligomers consisting of dynamic covalent monomer residues, utilizing monomers bearing benzaldehyde– and aniline–based functional groups protected with acid-labile groups to prevent unwanted side reactions during solid-phase synthesis,

interspersed with inert residues. Whereas the aldehyde and amine functional groups allow the hybridization of complementary peptoid chains through imine formation and exchange reactions, inert residues were incorporated to improve assembled ladder solubility. Moreover, these inert residues were employed to ensure that the dynamic covalent reactants remain on the same side of the chain owing to the Σ-strand structure adopted by peptoid where adjacent oligomer residues arrange into opposed rotational states.[39]

Upon cleavage from the solid support resin and protecting group deprotection by treatment with trifluoroacetic acid (TFA), the generated oligomeric peptoids were purified by preparative reverse-phase high performance liquid chromatography (RP-HPLC) and purity and molecular weights characterized by analytical HPLC, NMR, and electrospray ionization (ESI) as well as MALDI mass spectrometry, respectively (Figure 2.11~Figure 2.22). The dynamic covalent reactants incorporated on the synthesized peptoid oligomers were either exclusively aldehyde or amine functional groups to avoid potential premature aldehyde/amine condensation reactions that would preclude oligomer purification. Preliminary hybridization experiments of peptoids incorporating benzylamine or 2-methoxyethylamine as inert spacer residues resulted in rapid formation of a precipitate after complementary oligomer mixing, indicating poor solubility of the assembled structures. Fortunately, utilizing 2-(2-ethoxyethoxy)ethylamine (E^3A) as the spacer residue was found to afford solubility of both the unhybridized oligomers and the subsequent assembled molecular ladders in chloroform, and thus was employed as the alternating co-monomer for the peptoid sequences throughout this study. Structures of the synthesized peptoid co-oligomers E^3A–Al_**n** and E^3A–Am_**n**, where ***n*** refers to the

number of repeat units for the aldehyde- and amine-bearing oligomers, respectively, are shown in Scheme 2.5

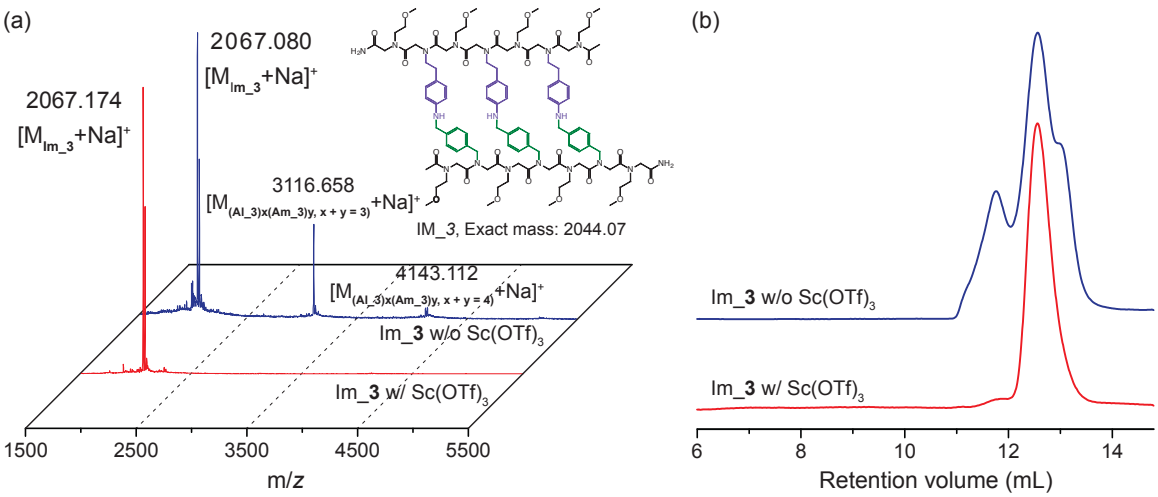

Figure 2.24. Influence of $Sc(OTf)_3$ on the rate of molecular ladder formation. (a) MALDI-TOF mass spectra and (b) GPC traces of the crude reaction mixtures.

Previously, scandium triflate was demonstrated to efficiently increase the transamination and imine methathesis reaction rates by up to 5 orders of magnitude, when compared with the uncatalyzed reactions.[24] Therefore, we initially examined the influence of Sc(III) on the rate of dynamic covalent assembly of peptoid based ladders. Here, peptoid sequences E^3A–Al_**3** and E^3A–Am_**3**, mixed in 1:1 stoichiometric ratios (1 mM) in chloroform, were allowed to react for 1 hour either with or without the addition of 4 mol% $Sc(OTf)_3$, followed by reduction with sodium triacetoxyborohydride (STAB). As shown by Figure 2.24, MALDI-TOF mass spectra of the crude reaction mixtures demonstrate the rapid and exclusive generation of the desired Im_**3** molecular ladder in the presence of $Sc(OTf)_3$, whereas the assembly reaction performed in the absence of the Sc(III) catalyst did not proceed to completion, yielding additional, out-of-registry species

composed of three and four peptoid strands. Similarly, GPC traces for the crude reaction mixtures (Figure 2.24) confirm the presence of high molecular weight, out-of-registry species for the assembly reaction performed in the absence of Sc(III). Thus, all the subsequent dynamic covalent assemblies of complementary oligomeric peptoid sequences into molecular ladders were performed in the presence of 4 mol% Sc(III).

Here, aldehyde- and amine-functionalized peptoid sequences E^3A-Al_**n** and E^3A-Am_**n**, where ***n*** = 3 ~ 16, were added in equal molar ratios (1 mM) into chloroform with 4 mol% scandium(III) triflate (Scheme 2.5) and the reaction mixture was stirred at room temperature. Aliquots of the reaction mixture were directly subjected to matrix-assisted laser desorption/ionization (MALDI) mass spectrometry, performed with 2-(4-hydroxyphenylazo)benzoic acid (HABA) as the matrix, and gel permeation chromatography (GPC) with chloroform/methanol /triethylamine (94/4/2, v/v/v) as the eluent.

2.5.1 Formation of Short Peptoid-based *n*-Rung Ladders (*n* = 3~6)

As for the formation of short *n*-rung ladders with length from 3 to 6, no precipitate or cloudiness was observed throughout the course of the reaction, indicating good solubility of both transient intermediates and the resultant molecular ladders, and an absence of particulate, cross-linked polymer.

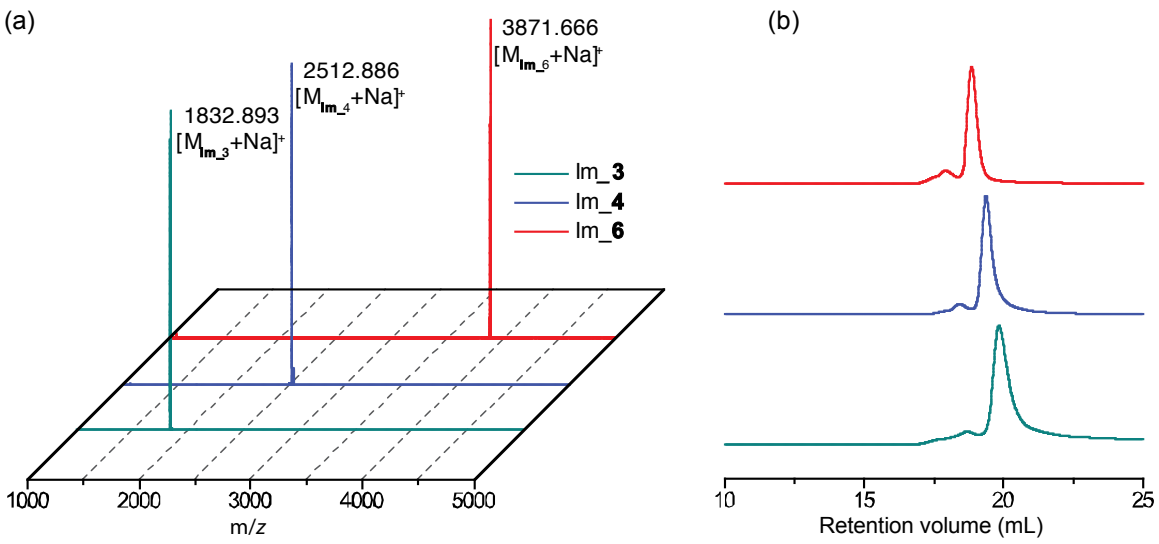

Figure 2.25. Characterization of peptoid-based molecular ladders (n = 3 ~ 6). *(a) MALDI mass spectra of the crude reaction mixtures. Expected exact mass: $[M_{Im\_3}+Na]^+$ = 1832.927; $[M_{Im\_4}+Na]^+$ = 2512.286; $[M_{Im\_6}+Na]^+$ = 3871.002. (b) GPC traces for crude reaction mixtures. The traces are normalized to the height of the largest peak. Im_**3**, V_r = 19.82 mL, M_n = 2270 g/mol, PDI = 1.01; Im_**4**, V_r = 19.37 mL, M_n = 2870 g/mol, PDI = 1.01; Im_**6**, V_r = 18.87 mL, M_n = 3770 g/mol, PDI = 1.01 (polystyrene standards).

MALDI mass spectra of the crude peptoid dimerization reaction mixtures are shown in Figure 2.25. These mass spectra indicate only a single product from each dimerization reaction, where the observed dominant peaks correspond to the desired molecular ladder structures Im_**3**, **4**, and **6**, demonstrative of the successful formation of the desired ladder structures which are the only reasonable products equivalent to the observed molecular weights. Although the $[M+Na]^+$ ion predominates in each of these mass spectra, minor peaks attributable to $[M+H]^+$ and $[M+K]^+$ ions are also observed. Peaks which could be assigned to misaligned or out-of-register products, anticipated to arise at m/z values of +18 (i.e., the molecular weight of the H_2O condensation product) for each unreacted amine/aldehyde pair, or to unreacted peptoid oligomers were not observed in any of these

mass spectra. Moreover, higher molecular weight species, potentially resulting from the co-reaction of more than two peptoid strands (i.e., $(E^3A\text{-}Al\_\boldsymbol{m})_x(E^3A\text{-}Am\_\boldsymbol{n})_y$, where $\boldsymbol{m} = \boldsymbol{n}$ and $x+y>2$), were not observed.

Near-exclusive formation of the desired ladder structures was further confirmed by GPC chromatograms showing one major peak preceded by very small peaks potentially attributable to low concentrations of higher molecular weight species (Figure 2.25). In each case, by comparing to low dispersity polystyrene standards, the elution volumes confirm the molecular weights corresponding to the resultant molecular ladders.

Furthermore, GPC traces of peptoid-based ladder oligomers were deconvoluted by fitting Gaussian functions to simulate the peaks using a script written in-house with Matlab R2012a (Mathworks Inc.). In each case, the baseline was subtracted and then 5-6 simulated peaks were utilized to fit the spectra. Deconvolution of the experimental GPC chromatograms revealed that the obtained molecular ladders were uniform with dispersities approaching 1 (see Figure 2.28 and Table 2.3). Interestingly, although the GPC chromatograms suggest the presence of small amounts of higher molecular weight, out-of-registry byproducts in the reaction mixtures, no corresponding evidence for these byproducts is apparent in the MALDI mass spectra.

Finally, STAB was added to the reaction mixture to reduce the interstrand imine groups to secondary amines, irreversibly fixing the assembled structures and MALDI mass spectrometry was again performed (Figure 2.26). Attempts to characterize the reduced molecular ladders by GPC proved unsuccessful owing to insufficient signal intensities from both UV and differential refractive index (DRI) detectors.

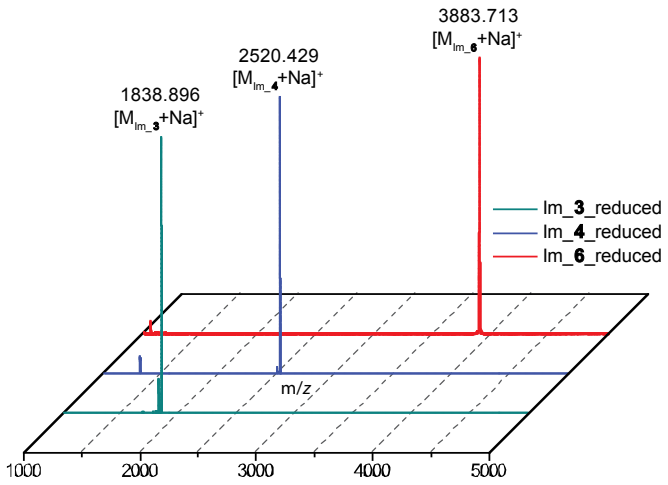

Figure 2.26. MALDI mass spectra of reduced molecular ladders (n = 3~6).
*Expected exact mass: $[M_{Im\_3}+Na]^+$ = 1838.974; $[M_{Im\_4}+Na]^+$ = 2520.348; $[M_{Im\_6}+Na]^+$ = 3883.09.

2.5.2 Formation of Long Peptoid-based *n*-Rung Ladders (*n* = 8~16)

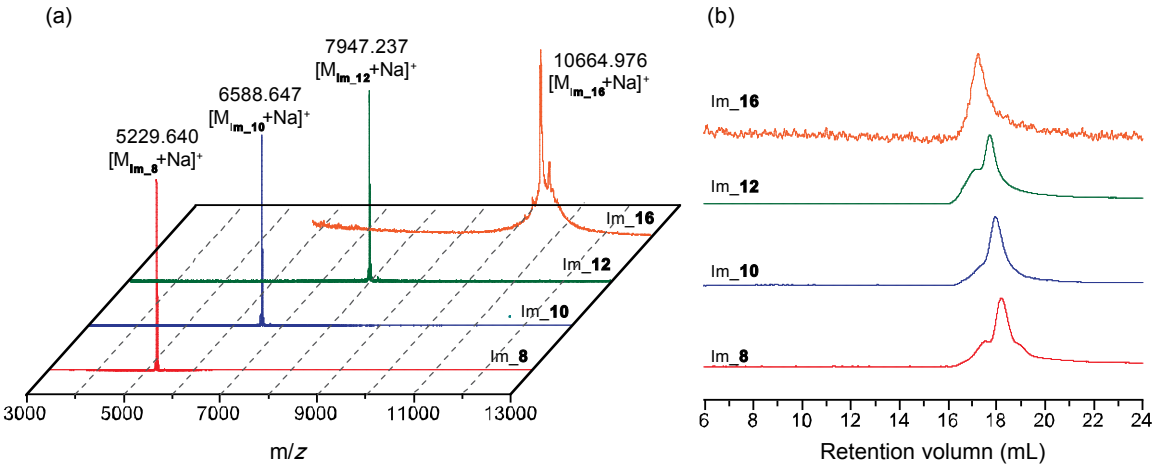

Figure 2.27. Characterizations of peptoid-based molecular ladders (n = 8 ~ 16).
*(a) MALDI mass spectra of the crude reaction mixtures. Expected exact mass: $[M_{Im\_8}+Na]^+$ = 5229.718 g/mol; $[M_{Im\_10}+Na]^+$ = 6588.647 g/mol; $[M_{Im\_12}+Na]^+$ = 7947.150 g/mol; $[M_{Im\_16}+Na]^+$ = 10664.583 g/mol. MALDI analyses including Im_**8** ~ Im_**12** were performed in reflectron positive ion mode whereas MALDI analysis of Im_**16** was performed in linear positive ion mode; (b) GPC traces for crude reaction mixtures. The traces are normalized to the height of the largest peak. Im_**8**, V_r = 18.23 mL, M_n = 5494 g/mol, PDI = 1.02; Im_**10**, V_r = 18.00 mL, M_n = 6332 g/mol, PDI = 1.03; Im_**12**, V_r = 17.75 mL, M_n = 7503 g/mol, PDI = 1.02; Im_**16**, V_r = 17.27 mL, M_n = 10570 g/mol. (polystyrene standards).

MALDI mass spectra of the crude reaction mixtures of longer peptoid ladder formations (n = 8~ 16) are illustrated in Figure 2.27. In these mass spectra, the observed molecular weights of each dominant peak correspond to the expected values of desired molecular ladder structures Im_**8**, **10**, **12**, and **16** respectively, indicating the successful formation of desired ladder structures which are the only reasonable products. $[M+Na]^+$ ions were detected as the dominant ion species, but minor peaks attributable to $[M+H]^+$ were also observed. Unreacted single peptoid strands were not observed in any of these MALDI mass spectra, indicating that the dimerization reaction reached completion. Moreover, higher molecular weight species, resulting from the co-reaction of more than two peptoid strands (i.e., $(Al\_\boldsymbol{n})_x(Am\_\boldsymbol{n})_y$, where $x + y > 2$), were not detected, suggesting that the assembly process is not dominated by a toehold displacement mechanism which would transiently give rise to such species. However, in addition to the desired *n*–rung molecular ladders, a small amount of out-of-registry molecular ladders with (*n*-1) rungs, anticipated to arise at m/*z* values of +18 (i.e., the molecular weight of the H_2O condensation product) for each unreacted amine/aldehyde pair, was also detected in the reaction mixtures of Im_**8**, **10**, and **12** (Figure 2.27), where the percentage of molecular ladders that are out-of-registry progressively increases as the number of reactive pendant groups *n* affixed to the precursor strands is raised. Moreover, for Im_**16**, a mixture of out-of-registry ladders with different numbers (i.e., *n*-1, *n*-2, *n*-3, *n*-4 etc.) of rungs was observed even after extending the reaction time to over 2 weeks.

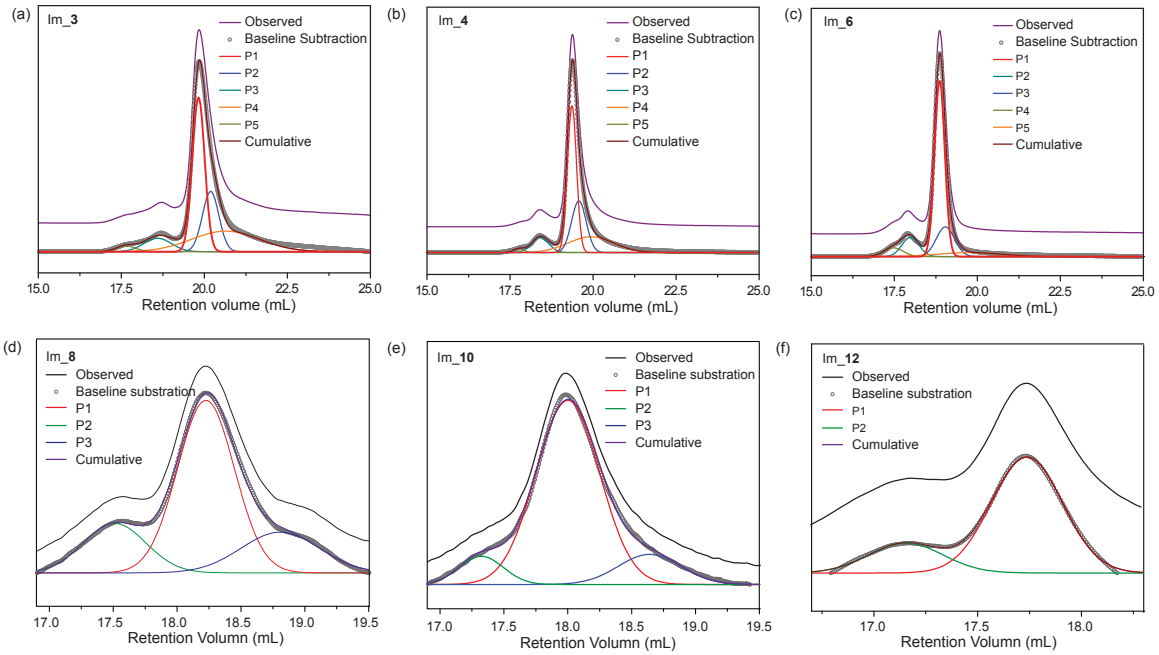

Figure 2.28. Deconvoluted GPC traces of peptoid-based ladders (n = 3 ~ 16). *(a) Im_**3**, (b) Im_**4,** (c) Im_**6,** (c) Im_**6,** (d) Im_**8,** (e) Im_**10,** (f) Im_**12** (straight reaction mixtures). The target product peak is labeled in red.

Table 2.3. GPC analysis of peptoid-based, dimerized molecular ladders

Code	M_n by GPC (g/mol)	Dispersity	Expected M_n (g/mol)	Area (%)
Im_**3**	2270	1.01	1810	60.6
Im_**4**	2870	1.01	2490	67.2
Im_**6**	3770	1.01	3850	75.8
Im_**8**	5494	1.02	5210	61%
Im_**10**	6332	1.03	6570	79%
Im_**12**	7503	1.02	7930	79%
Im_**16**	10570	-*	10649	-*

* Unable to be determined due to the low signal-to-noise ratio of GPC trace for Im_**16**

Further evidence of molecular ladder formation was obtained from analytical gel permeation chromatography (GPC) as performed on the crude reaction mixtures. In each case, the chromatogram showed one major peak preceded by small peaks (Figure 2.27), indicating that, although the prevailing species were the desired ladder structures,

material at concentrations too low and/or molecular weights too high for detection by reflectron mode MALDI mass spectrometry remained trapped as higher molecular weight species (i.e., misaligned or out-of-registry ladders). Nevertheless, the molecular weights of the major species as determined by GPC corresponded to the expected values of the desired ladder structures (Figure 2.27 and Table 2.3).

Previously, m-phenylene-ethynylene-based oligomers were utilized as precursors for the self-assembly of molecular ladders *via* imine metathesis; however, the resultant ladders became kinetically trapped at four or more rungs, severely limiting the synthetic yield for ladders composed of five or more rungs as misaligned, out-of-registry byproducts were unable to self-correct.[5, 26] In contrast, the utilization of peptoid-based precursor oligomers enabled the dynamic covalent assembly of molecular ladders in high yield and with over triple the number of inter-strand bonds as those previously described that employed a rigid backbone.[5, 26] This suggests that the number of inter-strand interactions does not necessarily determine the maximum molecular ladder length attainable; rather, the structure of the backbone significantly influences the ability of the oligomeric precursor strands to achieve registry. Indeed, the particular suitability of the oligomers used here to generate long molecular ladders is likely attributable to several factors, including the inherent flexibility of the peptoid backbone,[33, 36-38] the alternating zigzag, Σ-strand structure of the monomeric residues,[39] and the proximity of the dynamic covalent pendant groups to each other, providing cooperative binding and thus promoting hybridization selectivity and formation of the desired products.[14] Notably, some out-of-registry, intermediate structures were still detected for the peptoid-based molecular ladders assembled here. As the number of reactive pendant groups on the precursor

oligomers rises, the intermediate out-of-registry ladder structures must necessarily undergo increased numbers of inter-strand bond rearrangement reactions to form the ideal in-registry ladders. As a result, these intermediate structures become kinetically trapped for oligomers with sufficiently high numbers of reactive pendant groups such that the thermodynamically favoured products can no longer be formed on reasonable timeframes, irrespective of the precursor oligomer structures employed.

2.6 Conclusions

We have demonstrated the synthesis of amine/aldehyde functionalized dynamic covalent peptoid based oligomers and their assembly through Sc(III)-catalysed rearrangement into molecular ladders with up to 16 rungs, the longest generated to date. MALDI-TOF mass spectrometric analysis demonstrated their formation and was used to analyse molecular ladder formation dynamics for each system. The success of our peptoid-based ladder formation suggests that the flexibility of the peptoid backbone likely helps curtail kinetic trapping while the close spacing between dynamic covalent functional groups affords cooperative binding, improving hybridization selectivity and enabling formation of the desired product. Our ability to construct molecular ladders with up to 16 rungs opens up possibilities to design and fabricate robust, complex nanostructures based on the self-assembly of sequence-specific, dynamic covalent oligomers.

2.7 References

1. Whitesides, G. M.; Mathias, J. P.; Seto, C. T., Molecular Self-Assembly and Nanochemistry: A Chemical Strategy for the Synthesis of Nanostructures. *Science* **1991,** *254* (5036), 1312-1319.

2. Whitesides, G. M.; Boncheva, M., Beyond molecules: Self-assembly of mesoscopic and macroscopic components. *Proc. Natl. Acad. Sci. U. S. A.* **2002,** *99* (8), 4769-4774.

3. Lehn, J. M., Perspectives in Chemistry - Steps towards Complex Matter. *Angew. Chem. Int. Ed.* **2013,** *52* (10), 2836-2850.

4. Herrmann, A., Dynamic combinatorial/covalent chemistry: a tool to read, generate and modulate the bioactivity of compounds and compound mixtures. *Chem. Soc. Rev.* **2014,** *43* (6), 1899-1933.

5. Hartley, C. S.; Elliott, E. L.; Moore, J. S., Covalent assembly of molecular ladders. *J. Am. Chem. Soc.* **2007,** *129* (15), 4512-4513.

6. Lehn, J.-M., *Supramolecular chemistry*. Wiley-VCH, Weinheim: 1995; Vol. 1.

7. Steed, J. W.; Atwood, J. L., *Supramolecular chemistry, 2nd Edition*. John Wiley & Sons: 2009.

8. Philp, D.; Stoddart, J. F., Self-assembly in natural and unnatural systems. *Angew. Chem. Int. Ed.* **1996,** *35* (11), 1155-1196.

9. Mattia, E.; Otto, S., Supramolecular systems chemistry. *Nat. Nanotechnol.* **2015,** *10* (2), 111-119.

10. Rothemund, P. W. K., Folding DNA to create nanoscale shapes and patterns. *Nature* **2006,** *440* (7082), 297-302.

11. Andersen, E. S.; Dong, M.; Nielsen, M. M.; Jahn, K.; Subramani, R.; Mamdouh, W.; Golas, M. M.; Sander, B.; Stark, H.; Oliveira, C. L. P.; Pedersen, J. S.; Birkedal, V.; Besenbacher, F.; Gothelf, K. V.; Kjems, J., Self-assembly of a nanoscale DNA box with a controllable lid. *Nature* **2009,** *459* (7243), 73-76.

12. Wei, B.; Dai, M. J.; Yin, P., Complex shapes self-assembled from single-stranded DNA tiles. *Nature* **2012,** *485* (7400), 623-626.

13. Ke, Y. G.; Ong, L. L.; Shih, W. M.; Yin, P., Three-Dimensional Structures Self-Assembled from DNA Bricks. *Science* **2012,** *338* (6111), 1177-1183.

14. Wei, T.; Jung, J. H.; Scott, T. F., Dynamic Covalent Assembly of Peptoid-Based Ladder Oligomers by Vernier Templating. *J. Am. Chem. Soc.* **2015,** *137* (51), 16196-16202.

15. Wei, T.; Furgal, J. C.; Jung, J. H.; Scott, T. F., Long, self-assembled molecular ladders by cooperative dynamic covalent reactions. *Polymer Chemistry* **2017,** *8* (3), 520-527.

16. Rowan, S. J.; Cantrill, S. J.; Cousins, G. R. L.; Sanders, J. K. M.; Stoddart, J. F., Dynamic covalent chemistry. *Angew. Chem. Int. Ed.* **2002,** *41* (6), 898-952.

17. Jin, Y. H.; Yu, C.; Denman, R. J.; Zhang, W., Recent advances in dynamic covalent chemistry. *Chem. Soc. Rev.* **2013,** *42* (16), 6634-6654.

18. Hunt, R. A. R.; Otto, S., Dynamic combinatorial libraries: new opportunities in systems chemistry. *Chem. Commun.* **2011,** *47* (3), 847-858.

19. Jin, Y. H.; Wang, Q.; Taynton, P.; Zhang, W., Dynamic Covalent Chemistry Approaches Toward Macrocycles, Molecular Cages, and Polymers. *Acc. Chem. Res.* **2014,** *47* (5), 1575-1586.

20. Belowich, M. E.; Stoddart, J. F., Dynamic imine chemistry. *Chem. Soc. Rev.* **2012,** *41* (6), 2003-2024.

21. Belowich, M. E.; Valente, C.; Smaldone, R. A.; Friedman, D. C.; Thiel, J.; Cronin, L.; Stoddart, J. F., Positive Cooperativity in the Template-Directed Synthesis of Monodisperse Macromolecules. *J. Am. Chem. Soc.* **2012,** *134* (11), 5243-5261.

22. Bozdemir, O. A.; Barin, G.; Belowich, M. E.; Basuray, A. N.; Beuerle, F.; Stoddart, J. F., Dynamic covalent templated-synthesis of [c2] daisy chains. *Chem. Commun.* **2012,** *48* (84), 10401-10403.

23. Jin, Y. H.; Jin, A.; McCaffrey, R.; Long, H.; Zhang, W., Design Strategies for Shape-Persistent Covalent Organic Polyhedrons (COPs) through Imine Condensation/Metathesis. *J. Org. Chem.* **2012,** *77* (17), 7392-7400.

24. Giuseppone, N.; Schmitt, J. L.; Schwartz, E.; Lehn, J. M., Scandium(III) catalysis of transimination reactions. Independent and constitutionally coupled reversible processes. *J. Am. Chem. Soc.* **2005,** *127* (15), 5528-5539.

25. Avestro, A. J.; Belowich, M. E.; Stoddart, J. F., Cooperative self-assembly: producing synthetic polymers with precise and concise primary structures. *Chem. Soc. Rev.* **2012,** *41* (18), 5881-5895.

26. Elliott, E. L.; Hartley, C. S.; Moore, J. S., Covalent ladder formation becomes kinetically trapped beyond four rungs. *Chem. Commun.* **2011,** *47* (17), 5028-5030.

27. Simon, R. J.; Kania, R. S.; Zuckermann, R. N.; Huebner, V. D.; Jewell, D. A.; Banville, S.; Ng, S.; Wang, L.; Rosenberg, S.; Marlowe, C. K.; Spellmeyer, D. C.; Tan, R. Y.; Frankel, A. D.; Santi, D. V.; Cohen, F. E.; Bartlett, P. A., Peptoids: A modular approach to drug discovery. *Proc. Natl. Acad. Sci. U. S. A.* **1992,** *89* (20), 9367-9371.

28. Zuckermann, R. N.; Kerr, J. M.; Kent, S. B. H.; Moos, W. H., Efficient Method for the Preparation of Peptoids [Oligo(N-substituted glycines)] by Submonomer Solid-Phase Synthesis. *J. Am. Chem. Soc.* **1992,** *114* (26), 10646-10647.

29. Wu, C. W.; Sanborn, T. J.; Huang, K.; Zuckermann, R. N.; Barron, A. E., Peptoid oligomers with α-chiral, aromatic side chains: sequence requirements for the formation of stable peptoid helices. *J. Am. Chem. Soc.* **2001,** *123* (28), 6778-6784.

30. Burkoth, T. S.; Fafarman, A. T.; Charych, D. H.; Connolly, M. D.; Zuckermann, R. N., Incorporation of Unprotected Heterocyclic Side Chains into Peptoid Oligomers via Solid-Phase Submonomer Synthesis. *J. Am. Chem. Soc.* **2003,** *125* (29), 8841-8845.

31. Horn, T.; Lee, B.-C.; Dill, K. A.; Zuckermann, R. N., Incorporation of chemoselective functionalities into peptoids via solid-phase submonomer synthesis. *Bioconjug. Chem.* **2004,** *15* (2), 428-435.

32. Zuckermann, R. N., Peptoid Origins. *Biopolymers* **2011,** *96* (5), 545-555.

33. Sun, J.; Zuckermann, R. N., Peptoid Polymers: A Highly Designable Bioinspired Material. *Acs Nano* **2013,** *7* (6), 4715-4732.

34. Knight, A. S.; Zhou, E. Y.; Francis, M. B.; Zuckermann, R. N., Sequence Programmable Peptoid Polymers for Diverse Materials Applications. *Adv. Mater.* **2015,** *27* (38), 5665-5691.

35. Robertson, E. J.; Battigelli, A.; Proulx, C.; Mannige, R. V.; Haxton, T. K.; Yun, L. S.; Whitelam, S.; Zuckermann, R. N., Design, Synthesis, Assembly, and Engineering of Peptoid Nanosheets. *Acc. Chem. Res.* **2016,** *49* (3), 379-389.

36. Rosales, A. M.; Murnen, H. K.; Zuckermann, R. N.; Segalman, R. A., Control of Crystallization and Melting Behavior in Sequence Specific Polypeptoids. *Macromolecules* **2010,** *43* (13), 5627-5636.

37. Rosales, A. M.; Murnen, H. K.; Kline, S. R.; Zuckermann, R. N.; Segalman, R. A., Determination of the persistence length of helical and non-helical polypeptoids in solution. *Soft Matter* **2012,** *8* (13), 3673-3680.

38. Bradley, E. K.; Kerr, J. M.; Richter, L. S.; Figliozzi, G. M.; Goff, D. A.; Zuckermann, R. N.; Spellmeyer, D. C.; Blaney, J. M., NMR structural characterization of oligo-N-substituted glycine lead compounds from a combinatorial library. *Mol. Divers.* **1997,** *3* (1), 1-15.

39. Mannige, R. V.; Haxton, T. K.; Proulx, C.; Robertson, E. J.; Battigelli, A.; Butterfoss, G. L.; Zuckermann, R. N.; Whitelam, S., Peptoid nanosheets exhibit a new secondary-structure motif. *Nature* **2015,** *526* (7573), 415-420.

40. Perron, V.; Abbott, S.; Moreau, N.; Lee, D.; Penney, C.; Zacharie, B., A Method for the Selective Protection of Aromatic Amines in the Presence of Aliphatic Amines. *Synthesis-Stuttgart* **2009,** (2), 283-289.

41. Ouari, O.; Chalier, F.; Bonaly, R.; Pucci, B.; Tordo, P., Synthesis and spin-trapping behaviour of glycosylated nitrones. *J Chem Soc Perk T 2* **1998,** (10), 2299-2307.

42. Sun, J.; Stone, G. M.; Balsara, N. P.; Zuckermann, R. N., Structure-Conductivity Relationship for Peptoid-Based PEO-Mimetic Polymer Electrolytes. *Macromolecules* **2012,** *45* (12), 5151-5156.

43. Tran, H.; Gael, S. L.; Connolly, M. D.; Zuckermann, R. N., Solid-phase Submonomer Synthesis of Peptoid Polymers and their Self-Assembly into Highly-Ordered Nanosheets. *J. Vis. Exp.* **2011,** (57), e3373.

Chapter 3
Reaction Kinetics and Registry Mechanism of n-Rung Molecular Ladder Formation

3.1 Original Publication Information

Wei, T.; Furgal, J. C.; Jung, J. H.; Scott, T. F., Long, self-assembled molecular ladders by cooperative dynamic covalent reactions. *Polym. Chem.y* **2017,** *8* (3), 520-527.

Modifications have been made to the original document in order to adapt the content to the proper format.

3.2 Abstract

Three potential mechanisms for the self-assembly of peptoid-based molecular ladders *via* the dimerization of oligomeric precursors bearing dynamic covalent pendant groups were delineated here. These include a 'molecular zipper', whereby hybridization starts at one end followed by a series of imine condensation reactions to zip up complementary strands, or a 'molecular hand-shake line' or 'toehold displacement', whereby the molecular ladder formation would occur by shuffling or exchanging through bond rearrangement *via* cooperative transimination and imine metathesis reactions. MALDI mass spectrometry was used to determine the hybridization registry mechanism, with distance measurements using Förster resonance energy transfer (FRET) further confirming the registry mechanism, indicating that two complementary strands initially

interact and bind by rapidly 'zipping-up' at any point generating molecular ladders with an arbitrary number of rungs, followed by slowly shuffling through a 'molecular hand-shake line' until these ladders come into registry.

3.3 Introduction

The utilization of peptoids as nanoconstruction media in conjunction with dynamic covalent chemistry provides a promising route towards the fabrication of exquisite molecular architectures with exacting structural control and robustness. Previously, we reported the dynamic covalent assembly of complementary $n \times n$ oligopeptoids into molecular ladders with n rungs via scandium (III)-catalysed imine metathesis through dimerization.[1-2] The success of peptoid-based molecular ladder formation with up to 16 rungs demonstrates advantages of peptoids as precursor strands over more rigid precursors such as oligo(m-phenylene-ethynylene) where the ladder formation became kinetically trapped at four or more rungs.[3-4]

Despite the successful utilization of covalent interactions to effect the fabrication of peptoid-based molecular ladders, the registry mechanism remains ill defined. Based on our previous observations,[1] we propose three potential mechanisms that may govern the assembly of molecular ladders bearing covalent rungs. In the first of these hypothetical mechanisms, hybridization proceeds when two adjacent complementary strands come together at any point along their respective chains, initiating a series of amine/aldehyde condensation reactions through a 'zipper' mechanism, resulting in rapid ladder formation. Alternatively, molecular ladders could assemble *via* a 'hand-shake line' shuffling mechanism, whereby complementary strands bind at opposite ends and come into registry

through bond-rearrangement *via* transimination and imine metathesis reactions. Finally, the reaction could proceed whereby strands affixed to out-of-registry ladders would be replaced by a toehold-type displacement process,[5-6] again *via* transimination and imine metathesis reactions, to ultimately afford in-registry molecular ladders. Whereas the 'handshake line' mechanisms imply that a kinetic limit preventing registry will eventually be reached as the number of inter-strand interactions (i.e., ladder rungs) increases, a 'zipper' mechanism does not require dynamic inter-strand interactions such that the registry of significantly longer ladder species could be achieved. Notably, these two mechanisms are not necessarily mutually exclusive, and both could contribute significantly to the assembly of molecular ladders. Here, we investigate the dynamic covalent assembly of long precursor oligomeric peptoids and determine the limit of ladder formation when sufficiently long precursor oligomers result in the kinetic trapping of energetically disfavoured products. Moreover, we examine the hypothesized registry mechanisms by characterizing the hybridization kinetics of ladder formation by subjecting aliquots of the reaction mixture to mass spectrometry and Förster resonance energy transfer (FRET)-based distance measurements.

3.4 Experimental

3.4.1 General Experimental Procedures

All chemicals and reagents, unless specified, were purchased from commercial sources and used as received without any further purification. Matrix-assisted laser desorption/ionization (MALDI) mass spectra were recorded using a Bruker Autoflex mass spectrometer, whereas electrospray ionization (ESI) mass spectra were recorded

using an Agilent Q-TOF 1200 series spectrometer. All MALDI analyses were performed in reflectron positive ion mode using 2-(4-hydroxyphenylazo)benzoic acid (HABA) as the matrix, where 3 μL of a solution of the sample in chloroform (1.5 mM) was mixed with 10 μL of a mixture of 6 mg matrix in 300 μL acetonitrile, spotted on a MALDI sample plate (Bruker), and allowed to air dry. Reverse phase high performance liquid chromatography (RP-HPLC) was performed using a Shimadzu LC-6AD HPLC pump, equipped with a Shimadzu FRC 70A fraction collector, using analytical and preparative reversed phase Phenomenex Luna C18(2) columns with a linear gradient of water and acetonitrile as the eluent at 30°C, and monitored with a Shimadzu Prominence UV/vis detector at 214 nm. Analytical gel permeation chromatography (GPC) was similarly performed using a Shimadzu LC-6AD HPLC pump, equipped with a series of three Phenogel GPC/SEC columns (length 300 mm × diameter 7.8 mm, pore sizes of 500, 100, and 50 Å) with 94:4:2 (v/v/v) $CHCl_3$:MeOH:Et_3N as the eluent at 30°C, and monitored with a Shimadzu Prominence UV/vis detector at 313 nm. The analytical GPC was calibrated utilizing low dispersity polystyrene standards (low molecular weight Readycal Set, Fluka). UV-vis measurements were recorded on an Agilent Cary 60 spectrophotometer in anhydrous chloroform in quartz cuvettes with a 1 cm path length. Scans were taken over the range of 300 to 650 nm, and a background spectrum of pure solvent was subtracted from each scan. Sample concentrations were on the order of 100 μM for each of the peptoids studied. Spectra were then normalized for comparison. Circular dichroism (CD) spectra were collected on a Jasco-815 CD spectrometer. Peptoids were dissolved in acetonitrile at concentrations of 25 mM.

3.4.2 Experimental Procedures for Kinetics of Molecular Ladder Formation

Hybridization kinetics experiments were performed for peptoid-based molecular ladders with 4, 8, 10, and 12 rungs. The synthesis, purification and characterization of oligopeptoid sequences employed here are described in Chapter 2 Experimental section. An inert peptoid sequence comprised of E^3A spacer, denoted as E^3A_**21**, was used at a known concentration as an internal standard for this kinetics study. E^3A_**21** was synthesized by a submonomer approach to solid-phase synthesis as reported previously using an automated synthesizer,[1] further purified by preparative RP-HPLC, and characterized by MALDI mass spectrometry and analytical RP-HPLC (Figure 3.1). Samples were prepared by adding $Sc(OTf)_3$ (0.04 eq. per imine bond, 10 mM stock solution dissolved in MeCN) and between 4 and 20 nmol E^3A_**21** into anhydrous chloroform, followed by the addition of 1 μmol of the peptoid oligomer Al_**n** and 1 μmol of Am_**n** into the mixture, making a total reaction volume of 1 mL. Aliquots of the reaction mixture were taken at increasing time intervals, and examined by MALDI mass spectrometry with a Bruker Autoflex mass spectrometer. Multiple regions of interest were ionized in each sample to obtain an average ratio of target peak areas, and concentrations of target molecular ladders and out of registry molecular ladders were calculated by comparing to the peak area of the internal standard.

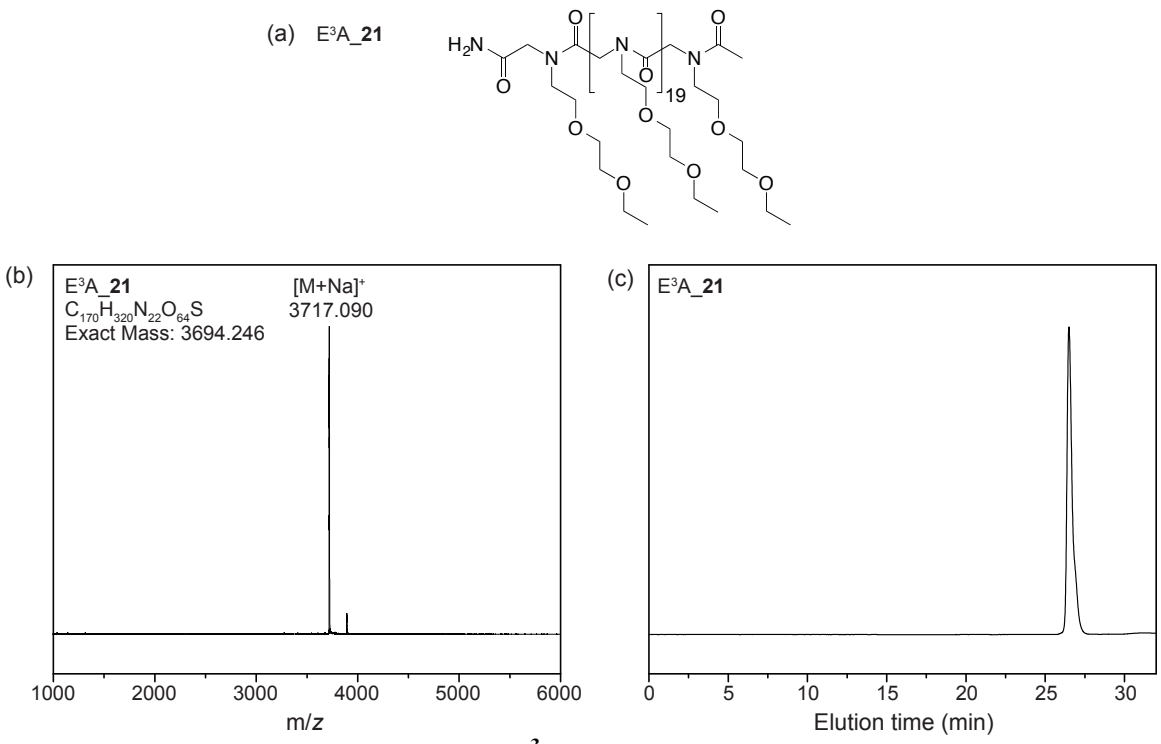

Figure 3.1. Characterizations of the E^{3}A_21 internal standard employed in kinetics experiments: (a) chemical structure, (b) MALDI mass spectrum and (c) analytical HPLC trace of E^{3}A_21 purified preparative RP-HPLC.

*Expected molecular weights: $[M+Na]^+$ = 3717.235; Purity: 98.8%. Analytical HPLC method: flow rate at 1 mL/min; A: H_2O, B: MeCN; 20% B 0 – 4 min, 20% – 80% B 4 – 28 min, 80% – 20% B 28 – 32 min.

3.4.3 Synthesis and Characterization of DABCYL-EN for Subsequent Solid-phase Peptoid Synthesis Scheme 4.3. Dynamic covalent assembly of peptoid-based ladders by Vernier-Templating. (a) Structures of linear oligopeptoids bearing pendant amine (E^{3}A-Am_*n*) and aldehyde (E^{3}A-Al_*m*) functional groups. (b) Vernier-templated assembly of

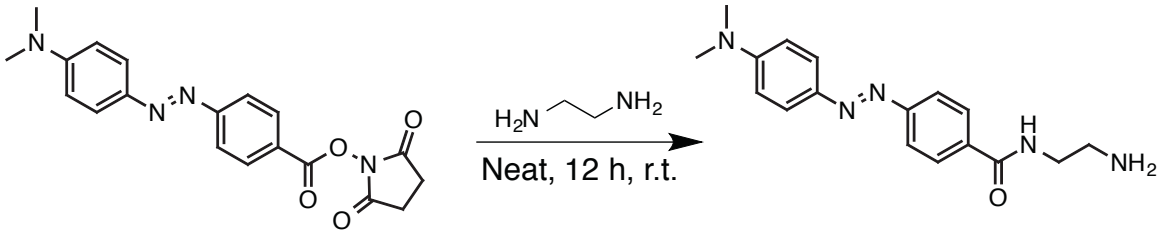

Scheme 3.1. Synthesis of DABCYL-EN for subsequent use as a primary amine-bearing submonomer in solid-phase peptoid synthesis.

To a 20 mL vial equipped with magnetic stirrer, 500 mg (1.36 mmol) of DABCYL succinimide ester and 10 mL (excess) of distilled ethylene diamine were added. The reaction was allowed to stir for 12 h and then excess ethylene diamine was removed by rotary evaporation. DCM (3 × 15 mL) was then added to the vial to extract the product and combined. The combined DCM solution was then washed with distilled water (2 × 10 mL) to remove excess amine and succinimide. The organic layer was dried over Na_2SO_4, filtered and solvent removed by rotary evaporation. The resulting red/orange solid was then dried for 3 h under high vacuum (398 mg, 91% yield).

^{1}H NMR (700 MHz, DMSO-d6) δ: 8.52 (s, 1H, -N*H*-), 7.99 (d, 2H, Ar), 7.82 (m, 4H, Ar), 6.84 (d, 2H, Ar), 3.29 (t, 2H, -NH-CH_2-), 2.70 (t, 2H, -CH_2-NH_2), 2.08 (s, 6H, -N(CH_3)$_2$)

^{13}C NMR (175 MHz, DMSO-d6) δ: 165.73, 153.88, 152.81, 142.62, 134.94, 128.32, 125.07, 121.50, 111.57, 43.11, 41.30, 30.70

ESI+: 312.1 m/z $[M+H]^+$

3.4.4 Synthesis and Characterization of Oligopeptoids for FRET Study

Six primary amine monomers, 4-(2-aminoethyl)-*N*-(*tert*-butixycarbonyl) phenylamine (Am), 4-(1,3-dioxacyclopent-2-yl)benzylamine (Al), 2-(2-ethoxyethoxy)ethylamine (E^3A), benzylamine (Bz), EDANS and DABCYL-EN were utilized for the synthesis of peptoids for FRET study (Figure 3.2). Peptoids containing EDANS and DABCYL were prepared according to the aforementioned submonomer approach to solid-phase synthesis (see 2.4 Experimental). However, 0.2 M EDANS in DMF/DBU (4:1, v/v) and 0.2 M DABCYL-EN in NMP were used for halide displacement instead. Additionally, halide displacement with EDANS was proceeded twice to ensure the reaction completion. Subsequently, the resultant peptoids were cleaved from the resin beads by treatment with a TFA cleavage cocktail and purified by preparative HPLC.

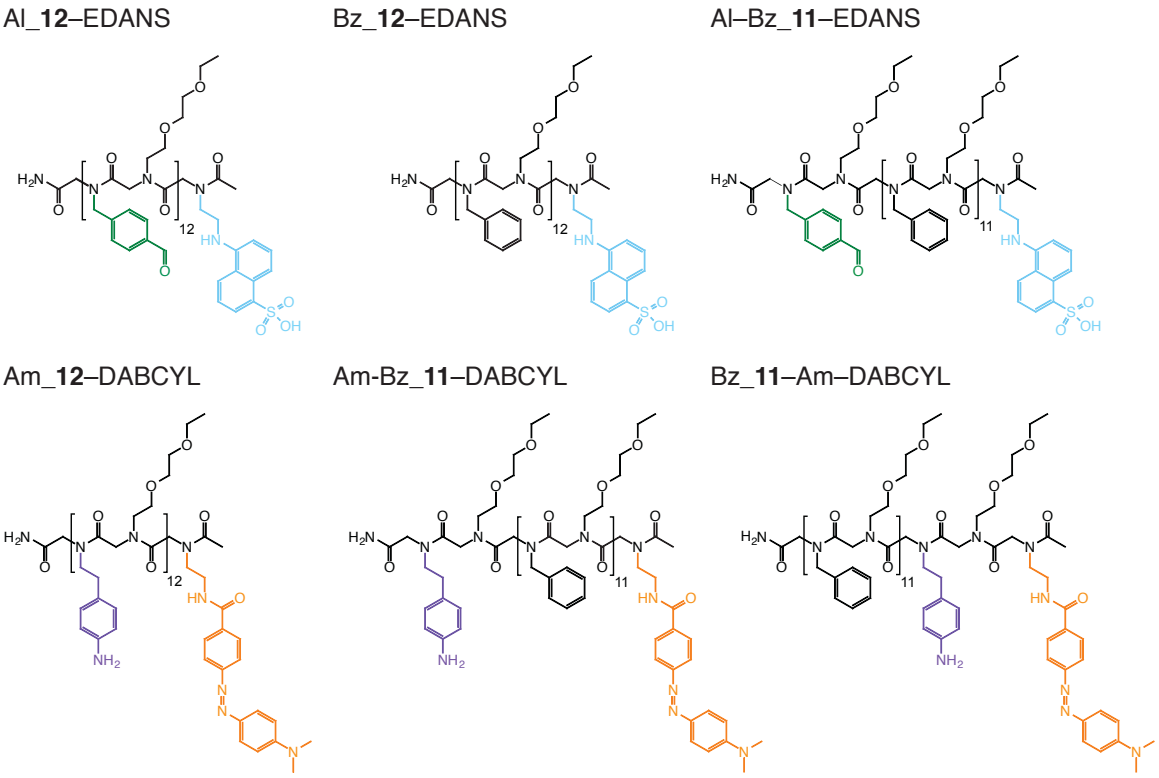

Figure 3.2. Chemical Structure of peptoid sequences subjected to FRET study.

Peptoids containing DABCYL were purified by preparative RP-HPLC using a linear gradient of H_2O (A) and MeCN (B) at a flow rate of 12 mL/min. The purified fractions were combined, concentrated, reconstituted in 50% MeCN/H_2O (v/v), frozen with liquid nitrogen and lyophilized to afford fluffy white powders. The purity of the collected peptoids with DABCYL was further examined by analytical RP-HPLC. Peptoids containing EDANS were purified using 0.1%TFA in both water (A) and MeCN (B) as eluent. The purified fractions were combined and evaporated to dryness. The resultant peptoids were dissolved in methanol and evaporated to dryness several times to remove the trace amount of TFA.

Preparative HPLC method:

(a) Al_**12**–EDANS: (1) 40% B, 0.1 – 4.1 min; (2) 40% – 70% B, 4.1 – 31.7 min; (3) 70% – 40% B, 31.7 – 33.7 min;

(b) Am_**12**–DABCYL: (1) 30% B, 0.1 – 4.1 min; (2) 30% – 75% B, 4.1 – 34.1 min; (3) 75% – 30% B, 34.1 – 36.1 min;

(c) Bz_**12**–EDANS: (1) 50% B, 0.1 – 4.1 min; (2) 50% – 85% B, 4.1 – 32.9 min; (3) 85% – 50% B, 32.9 – 34.9 min;

(d) Al-Bz_**11**–EDANS: (1) 50% B, 0.1 – 4.1 min; (2) 50% – 85% B, 4.1 – 36.1 min; (3) 85% – 50% B, 36.1 – 38.1 min;

(e) Am-Bz_**11–**DABCYL & Bz_**11**–Am-DABCYL (1) 55% B, 0.1 – 4.1 min; (2) 55% – 95% B, 4.1 – 32.7 min; (3) 95% – 55% B, 32.7 – 4.7 min.

Table 3.1. Structural information of peptoid sequences subjected to FRET study.

Code	Formula	Exact mass M (g/mol)	Molecular weight (g/mol)
Al_**12**–EDANS	$C_{232}H_{307}N_{27}O_{65}S$	4543.127	4546.192
Am_**12**–DABCYL	$C_{237}H_{350}N_{42}O_{51}$	4600.6085	4603.650
Bz_**12**–EDANS	$C_{220}H_{307}N_{27}O_{53}S$	4207.188	4210.072
Al–Bz_**11**–EDANS	$C_{221}H_{307}N_{27}O_{54}S$	4235.183	4238.082
Am–Bz_**11**–DABCYL	$C_{226}H_{317}N_{31}O_{51}$	4281.317	4284.188
Bz_**12**–Am–DABCYL	$C_{226}H_{317}N_{31}O_{51}$	4281.317	4284.188

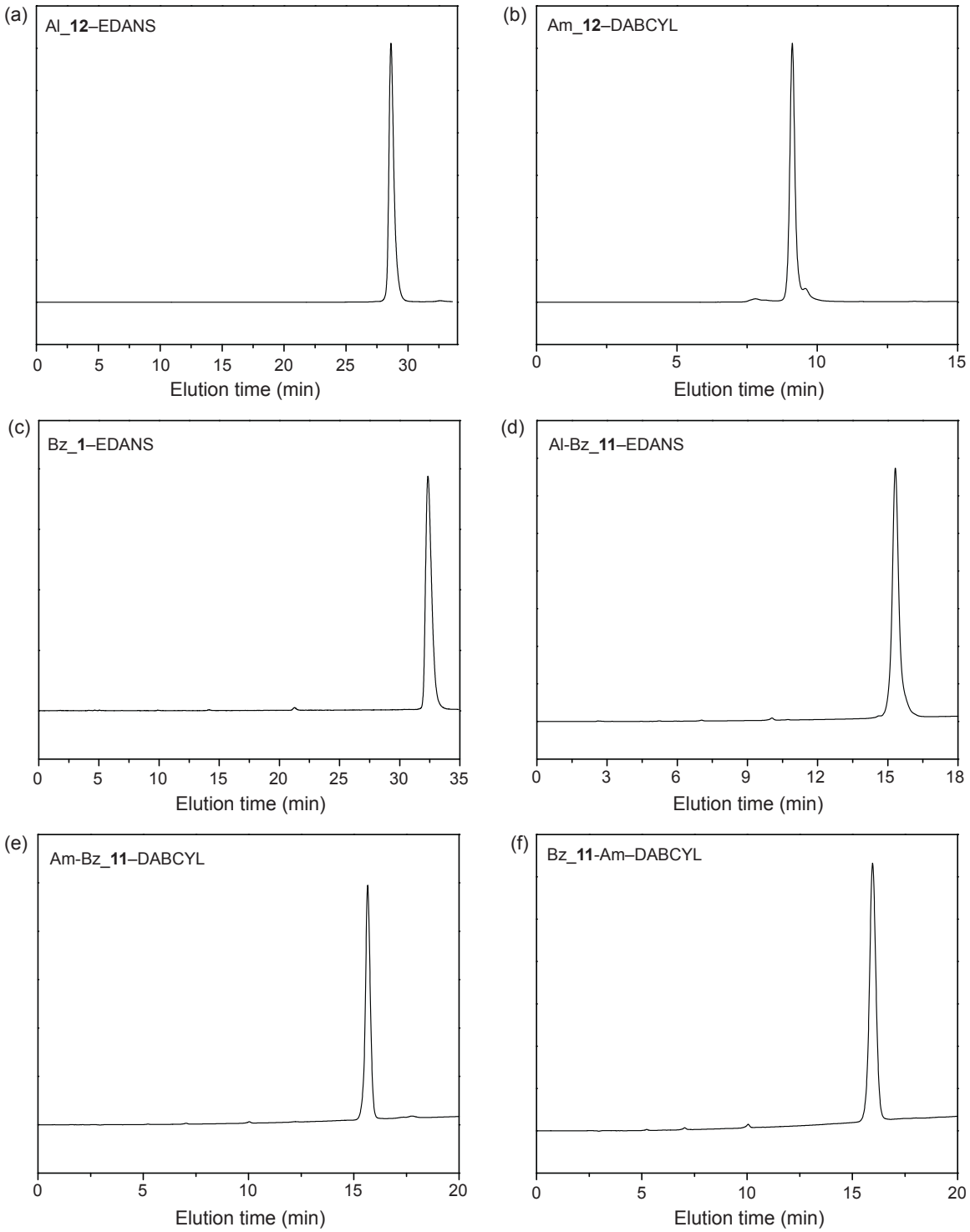

Figure 3.3. Analytical HPLC traces of oligopeptoids comprised of FRET pairs.
*Purity: Al_12-EDANS, 99.3%; Am_12-DABCYL, 95.8%; Bz_12-EDANS, 98.4%; Al-Bz-11-EDANS, 97.9%, Am-Bz-11-DABCYL, 96.1%; Bz-11-Am-DABCYL, 97.2%.

MS (ESI+): ESI-MS spectra were acquired and deconvoluted by the Agilent Qualitative Analysis Program.

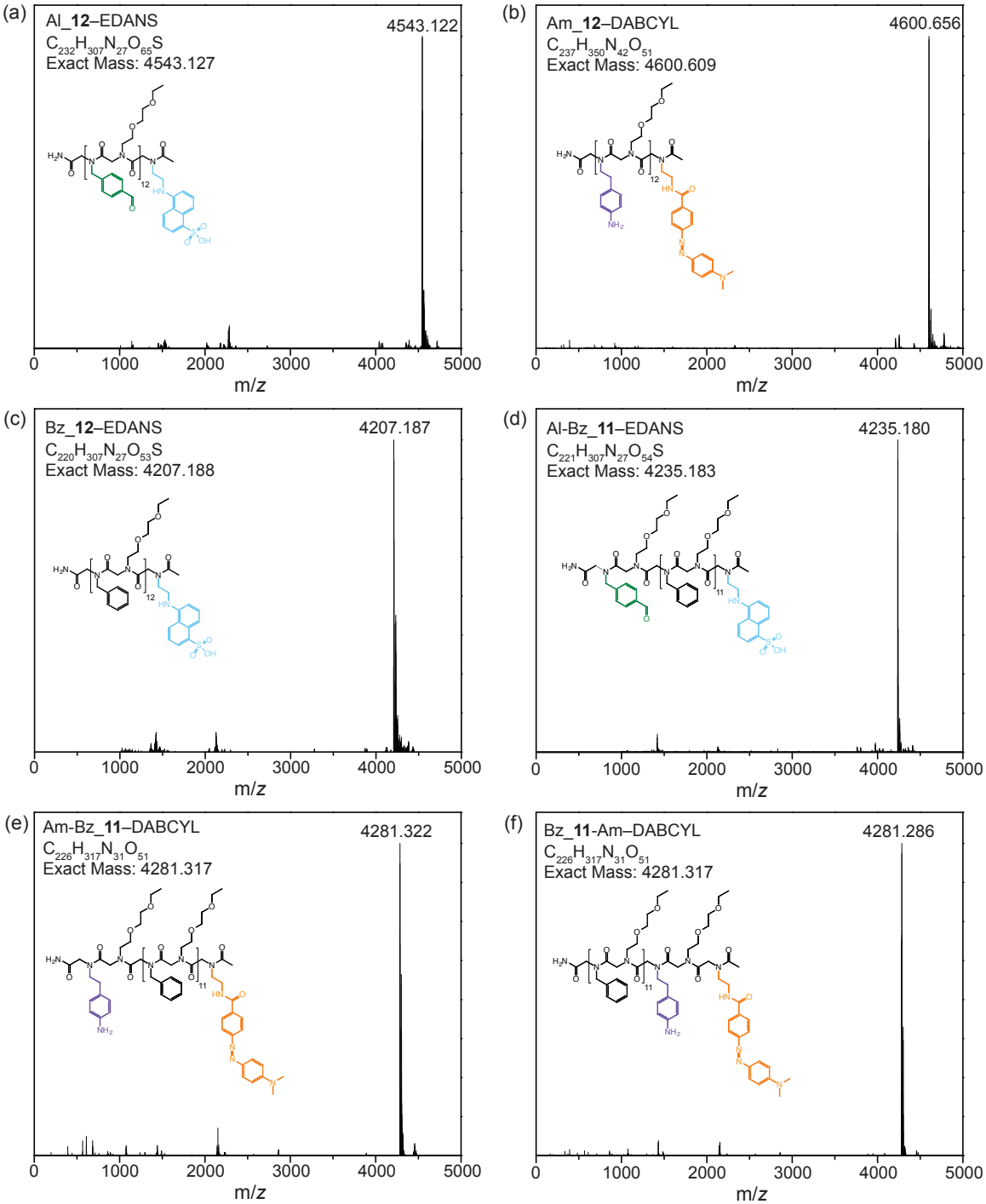

Figure 3.4. Deconvoluted ESI-MS spectra of oligopeptoids containing FRET pairs purified by preparative RP-HPLC: (a) Al_12–EDANS; (b) Am_12–DABCYL; (c) Bz_12–EDANS; (d) Al–Bz_11–EDANS; (e) Am–Bz_11–DABCYL; (f) Bz_11–Am–DABCYL.

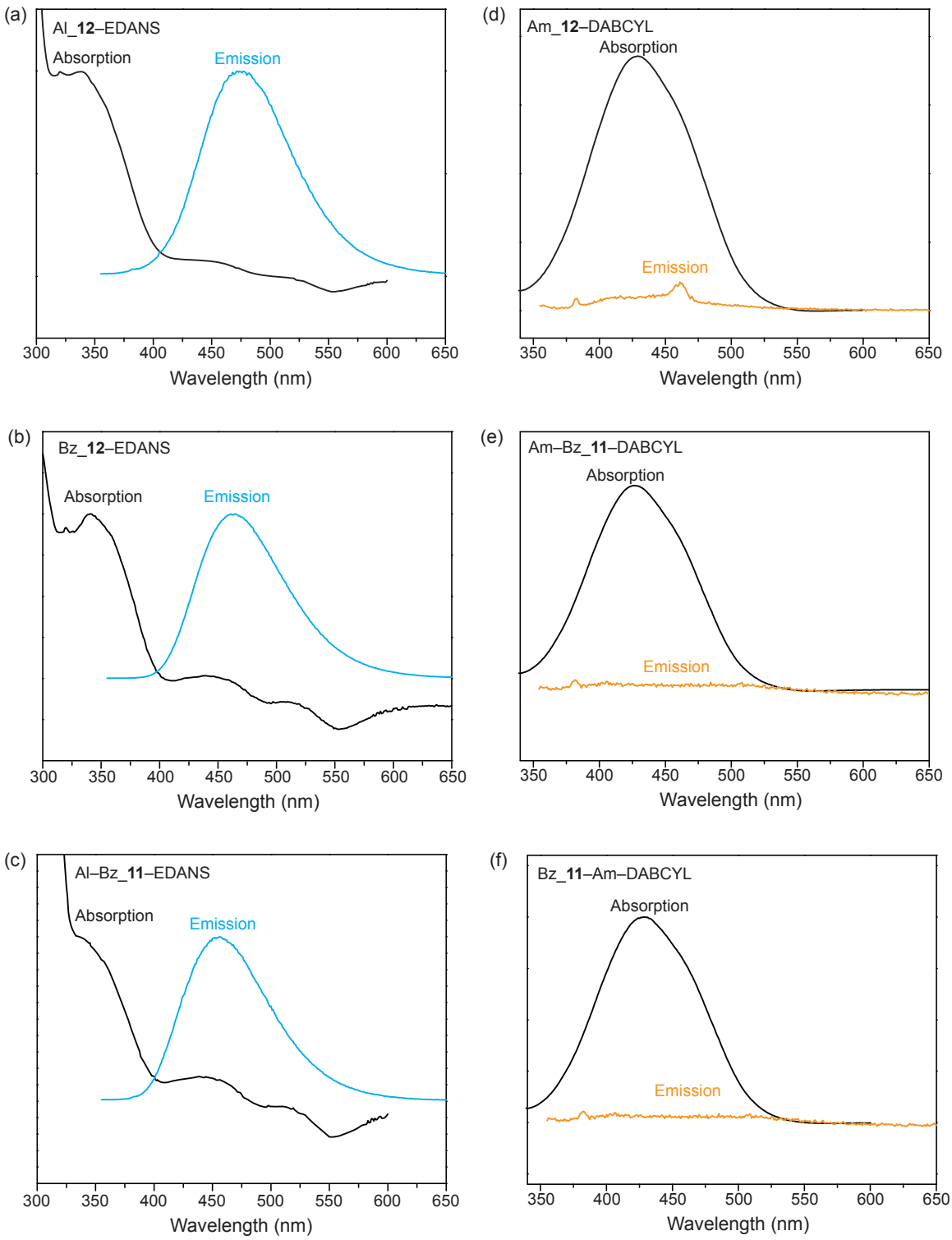

Figure 3.5. UV absorption and emission of peptoids containing either EDANS or DABCYL subjected to FRET study: (a) Al_12–EDANS, 99.3%; (b) Bz_12–EDANS; (c) Al–Bz_11–EDANS; (d) Am_12–DABCYL; (e) Am–Bz_11–DABCYL; (f) Bz_11–Am–DABCYL.

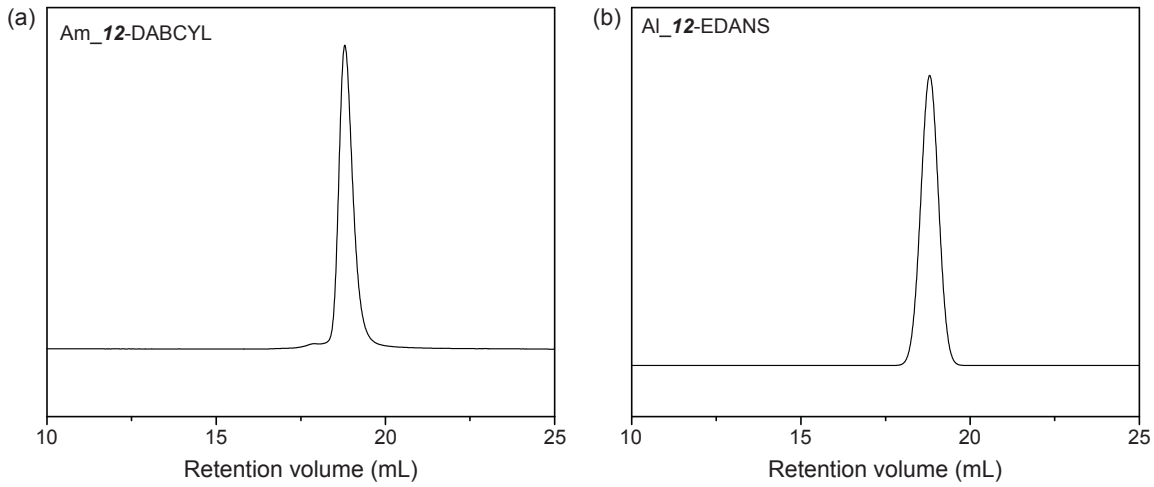

Figure 3.6.Analytical GPC of (a) Am_12-DABCYL and (b) Al_12-EDANS.
*Analytical GPC method: isocratic flow rate at 1 mL/min; eluent: $CHCl_3/CH_3OH/Et_3N$ (94/4/2, v/v/v). Am_**12**–DABCYL, V_r = 18.41 mL, M_n = 4932 g/mol; Al_**12**–EDANS, V_r = 18.70 mL, M_n = 4155 g/mol.

3.4.5 Photoluminescence Spectroscopy

Photoluminescence measurements were obtained on a Horiba Fluoromax-2 spectrofluorometer. Samples were prepared by adding 50 nmol EDANS peptoid solution and 2.4 μL of 10 mM $Sc(OTf)_3$ into 2 mL of solvent (chloroform) in a 4 mL quartz cuvette (1 cm path length) with magnetic stir bar. Basic fluorescence measurements were then taken, excited at 343 nm and collected over the range 355 – 650 nm with slits set at 2.5 nm, and temperature controlled at 25°C. Then 50 nmol DABCYL peptoid were then added to the system for FRET type kinetics measurements. Kinetics experiments were taken in single wavelength collection mode at 464 nm over a course of 16 hours at increasing intervals (i.e., every 30 sec for 5 min, every 15 min for 1 hours, every 30 min for 2 hours, and then hourly for the remaining time points).

3.5 Results and Discussion

3.5.1 Kinetics of Molecular Ladder Formation with *n* Rungs

Hybridization kinetics of molecular ladders with different numbers of rungs (i.e., 4, 8, 10, and 12) were examined by taking aliquots of the reaction mixture over time and characterizing them with MALDI mass spectrometry. The evolution of molecular ladder Im_**12** formation captured by MALDI mass spectrometry over the course of 13 days is presented in Figure 3.7.

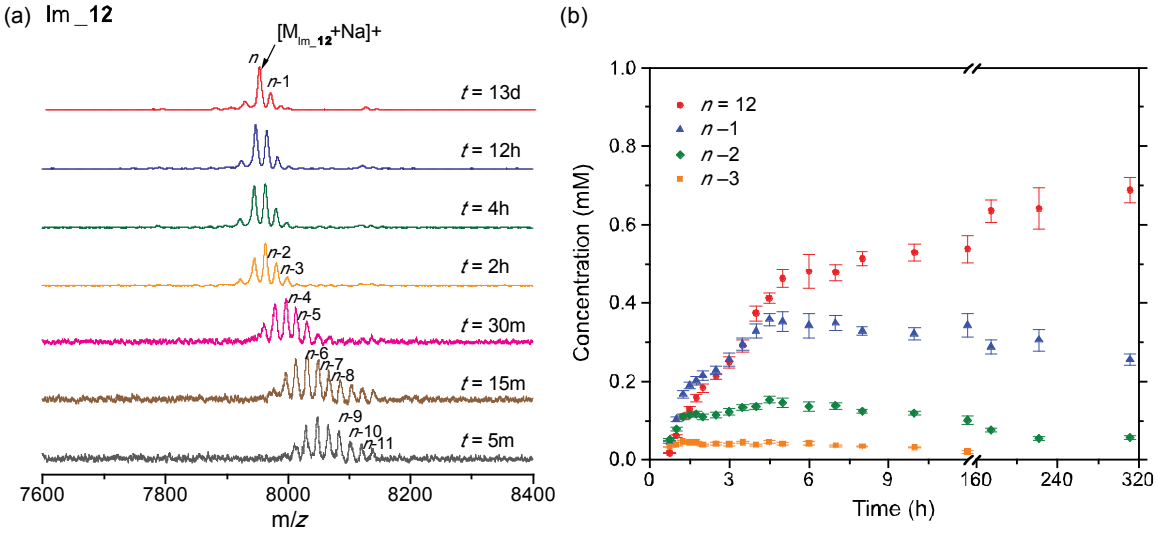

Figure 3.7. Kinetics of the formation of molecular ladder with *n* = 12 rungs (Im_12) over the course of 13 days. (a) MALDI-TOF mass spectra of the crude reaction mixture at increasing time intervals, and (b) concentration of the desired molecular ladder Im_12 and its out-of-registry intermediates versus time during the self-assembly process.

The desired ladder structure with 12 rungs was not initially observed in the mass spectra whereas a distribution of peaks corresponding to intermediate, out-of-registry ladders with different numbers of rungs (≤ 8) were present as soon as hybridization started. These peaks were evenly spaced with an interval of 18, corresponding to the

molecular weight of the H_2O condensation product for each unreacted amine/aldehyde pair. As the reaction proceeded, the distribution of these intermediate out-of-registry molecular ladders shifted towards lower molecular weight as more out-of-registry ladders with fewer rungs continuously underwent inter-strand bond rearrangement to generate more imine linkages. As a result, intermediate ladder structures with more rungs, approaching the desired ladder structure, progressively increased with the disappearance of transient, intermediate ladder species with fewer rungs. At t = 45 min, the desired, in-registry ladder with 12 rungs was detected; however, several out-of-registry ladders (n-1, n-2, and n-3) were still present.

Concentrations of the target ladder as well as its out-of-registry intermediates were calculated at various time points during the reaction (Figure 3.7b) by comparing to an inert internal standard (Figure 3.1) with a known concentration and, given their chemical and molecular weight similarities, assuming that the ionization efficiencies in MALDI of all in- and out-of-registry ladders for each set of precursor oligomers are essentially equal.[7-9] This assumption is supported by recognizing that, after complete consumption of the precursor oligomers (at ~5 h for n = 12), the summations of the calculated molecular ladder concentrations approximate the expected value of 1 mM (Figure 3.7b). For Im_**12**, an initially rapid increase in concentration of the desired ladder was observed after 45 min. The generation of the in-registry, 12–rung ladder slowed precipitously after 12 h and its concentration slowly reached a plateau of ~0.7 mM. The concentration of out-of-registry ladders gradually decreased and ladders with n-2 and n-3 rungs were near-absent after 2 days, although a small percentage of the out-of-registry ladder with n-1 rungs was still present even after 13 days reaction time.

Table 3.2. Molecular weight of the desired molecular ladder with *n* = 12 rungs and its out of registry ladders subjected to MALDI analysis.

Im_12	Expected Exact Mass M (g/mol)	Expected $[M+Na]^+$	Observed $[M+Na]^+$ by MALDI
n = 12	7924.161	7947.150	7946.661
n-1	7942.172	7965.161	7964.742
n-2	7960.182	7983.171	7982.973
n-3	7978.193	8001.182	8000.485
n-4	7996.204	8019.193	8018.546
n-5	8014.214	8037.203	8036.782
n-6	8032.225	8055.214	8054.671
n-7	8050.235	8073.224	8027.702
n-8	8068.246	8091.235	8090.625
n-9	8086.256	8109.245	8108.447
n-10	8104.267	8127.256	8126.153
n-11	8122.277	8145.266	8143.880

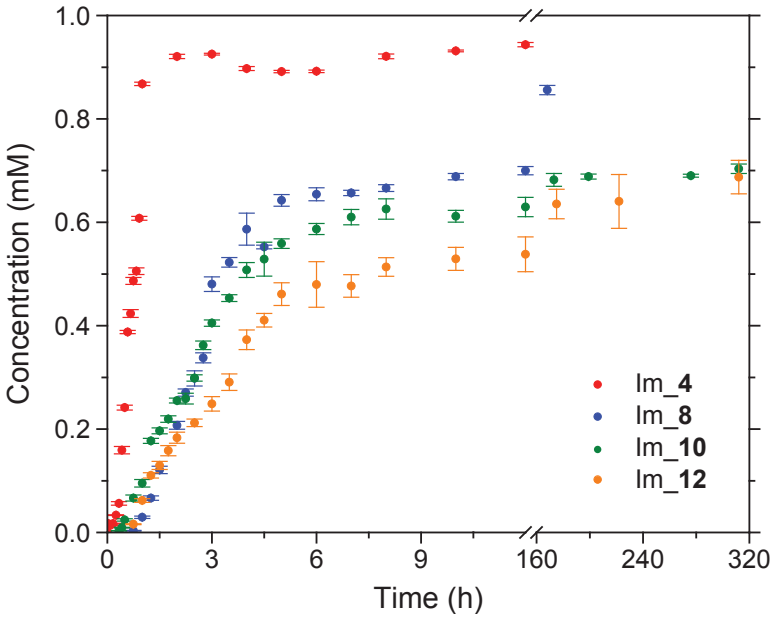

Figure 3.8. Concentration evolution of desired molecular ladders with *n* rungs (*n* =4, 8, 10, and 12).

The hybridization kinetics for the formation of molecular ladders Im_**8** and Im_**10** followed analogous trends but were relatively rapid compared with those for Im_**12**. For both Im_**8** and Im_**10**, a distribution of intermediate out-of-registry ladders with fewer rungs (≤ 6 or 8, respectively) was initially observed and which shifted towards lower molecular weights to yield more in-registry ladders as the hybridization reactions proceeded (Figure 3.8, Figure 3.9, and Figure 3.10).

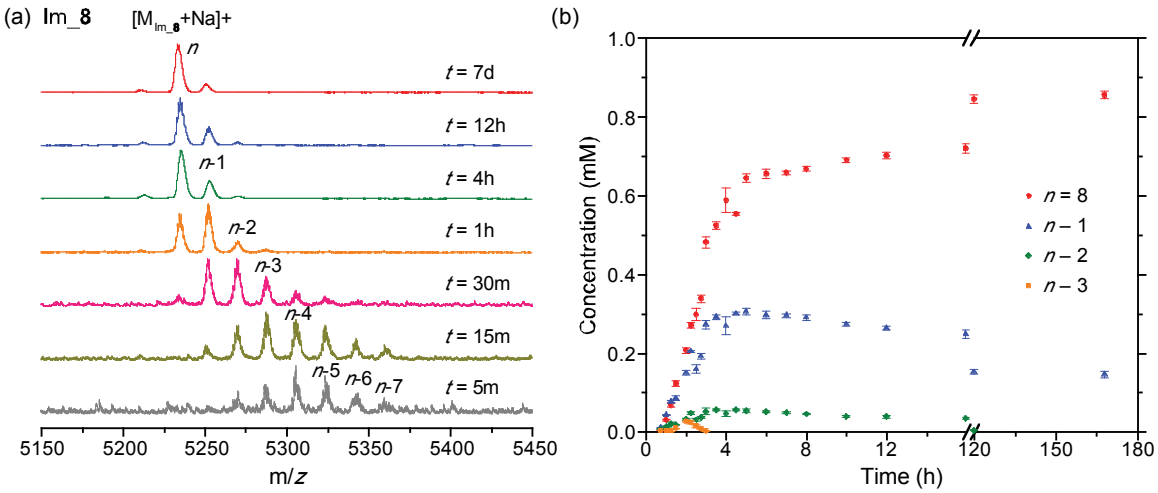

Figure 3.9. Kinetics of the formation of molecular ladder with *n* = 8 rungs over the course of 7 days. (a) MALDI-TOF mass spectra of the crude reaction mixture at increasing time intervals; (b) Concentration of the desired molecular ladder Im_8 and its out of registry molecular ladders versus time during the molecular ladder assembly process.

Detectable concentrations of the desired ladders with either 8 or 10 rungs, respectively, started to form after 30 min and the concentrations of these desired ladders increased until it plateaued after 16 h reaction time. The majority of out-of-registry ladders for both systems transitioned to the desired ladder within 12 h but a tiny fraction of out-of-registry ladders with *n*-1 rungs still remained after reacting for over a week.

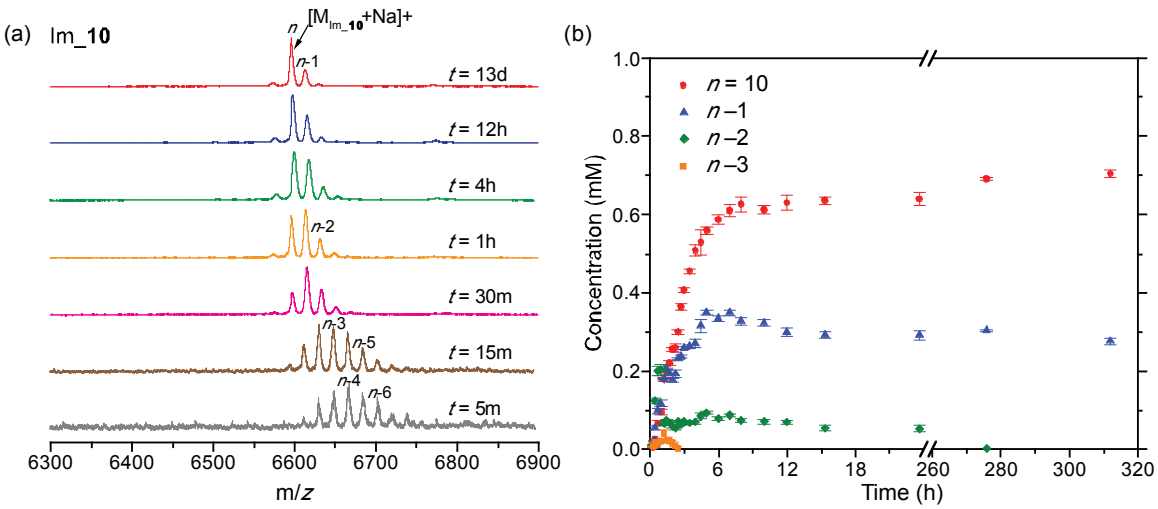

Figure 3.10. Kinetics of the formation of molecular ladder with *n* = 10 rungs over the course of 13 days. (a) MALDI-TOF mass spectra of the crude reaction mixture at increasing time intervals; (b) Concentration of the desired molecular ladder Im_10 and its out of registry molecular ladders versus time during the molecular ladder assembly process.

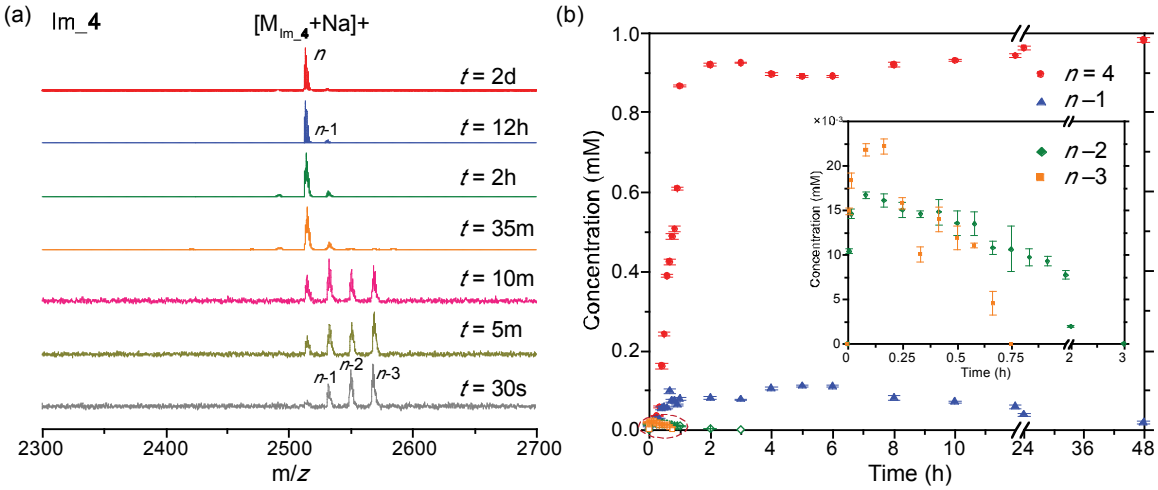

Figure 3.11. Kinetics of the formation of molecular ladder with *n* = 4 rungs over the course of 2 days. (a) MALDI-TOF mass spectra of the crude reaction mixture at increasing time intervals; (b) Concentration of the desired molecular ladder Im_4 and its out of registry molecular ladders versus time during the molecular ladder assembly process.

Much faster reactions kinetics were demonstrated for the formation of molecular ladder Im_**4** where the desired ladder structures formed and rapidly increased in concentration after 5 min reaction time (Figure 3.8 and Figure 3.11). Additionally, the

majority of the out-of-registry ladders (*n*-1, *n*-2 and *n*-3) disappeared after 35 min and near-exclusive generation of the desired ladder Im_**4** was achieved after 16 h. Importantly, the molecular weights of the Am_**4** and Al_**4** peptoids were sufficiently low such that higher molecular weight species composed of more than two of the precursor strands could potentially be detected by MALDI mass spectrometry in reflectron mode; however, whereas molecular species composed of two precursor oligomeric strands were observed throughout the assembly reaction, assemblies composed of three precursor strands were observed in low concentrations exclusively at the very beginning of the reaction (Figure 3.11) and those composed of four or more oligomers were not observed at all. Hybridization kinetics for Im_**16** were unable to be determined here owing to the poor resolution of the MALDI mass spectrometer in linear, rather than reflectron mode.

Table 3.3. Molecular weight of the desired molecular ladder with *n* = 4 rungs and its out of registry ladders subjected to MALDI analysis.

Im_4	Expected Exact Mass M (g/mol)	Expected $[M+Na]^+$	Observed $[M+Na]^+$ by MALDI
n = 4	2489.296	2512.285	2512.661
n-1	2507.307	2530.296	2530.625
n-2	2525.317	2548.306	2548.609
n-3	2543.328	2566.317	2566.586

Although the MALDI mass spectra indicate that the ladder assembly is not dominated by a strand displacement mechanism, discerning between the 'zipper' and 'handshake line' mechanisms is less apparent as either mechanism could lead to the steady increase in number of rungs formed as illustrated in Figure 3.7 and Figure 3.8; however, the rung-generation reactions for each of these mechanisms might be expected to proceed at very different rates. If the hybridization followed a 'zipper'-type mechanism, the rung-

generation rate should be self-accelerating as, once the reaction started, the amine and aldehyde functional groups would be progressively confined in close proximity to each other.

Table 3.4. Molecular weight of the desired molecular ladder with *n* = 8 rungs and its out of registry ladders subjected to MALDI analysis.

Im_8	Expected Exact Mass M (g/mol)	Expected $[M+Na]^+$	Observed $[M+Na]^+$ by MALDI
n = 8	5206.729	5229.718	5229.993
n-1	5224.739	5247.728	5248.767
n-2	5242.75	5265.739	5266.512
n-3	5260.76	5283.749	5284.495
n-4	5278.771	5301.760	5302.477
n-5	5296.782	5319.771	5320.580
n-6	5314.792	5337.781	5338.778
n-7	5332.803	5355.792	5356.677

Table 3.5. Molecular weight of the desired molecular ladder with *n* = 10 rungs and its out of registry ladders subjected to MALDI analysis.

Im_*10*	Expected Exact Mass M (g/mol)	Expected $[M+Na]^+$	Observed $[M+Na]^+$ by MALDI
n = 10	6565.445	6588.434	6588.421
n-1	6583.456	6606.445	6606.459
n-2	6601.466	6624.455	6624.260
n-3	6619.477	6642.466	6642.578
n-4	6637.487	6660.476	6660.633
n-5	6655.45	6678.487	6679.984
n-6	6673.508	6696.500	6696.167
n-7	6691.519	6714.508	6715.235
n-8	6709.53	6732.519	6733.553

Conversely, the rate of hybridization via a 'handshake line' mechanism would slow as the number of generated rungs increased resulting in a raised number of bond rearranging transimination and imine metathesis reactions having to occur in concert until the oligomeric strands come into registry. A comparison of the results presented in Figure 3.7~Figure 3.11 reveals that, although a distribution of transient, out-of-registry intermediate ladders are rapidly generated immediately after starting the hybridization reaction starts for all molecular ladder lengths examined, both the number of rungs observed at the assembly onset and the time required to achieve registry increase for longer precursor oligomers. These results suggest that the assembly of the desired molecular ladders proceeds by a hybrid mechanism where out-of-registry, intermediate ladders are initially generated by a zipper-type series of rapid imine condensation reactions,[10] where the increased number of rungs upon assembly for longer oligomers is attributable to the greater probability of complementary strands initially interacting mid-chain rather than exclusively at their termini. Subsequently, the error correction originating from the imine bond reversibility enables these out-of-registry intermediate ladders to undergo inter-strand, 'handshake line'-type dynamic shuffling and achieve a thermodynamic minimum, thereby affording in-registry ladders with n rungs. This bond exchange via transamination and imine metathesis reactions, albeit catalysed by Sc(III), is the rate limiting step and depends on the number of imine linkages.[1] As the length of molecular ladders increases, there are more imine linkages for intermediate ladders to break and reform in order to form in-registry ladders. Although in-registry ladders are the most thermodynamically-favoured reaction products, kinetic trapping impedes the formation of much longer molecular ladders, explaining why the formation of a

molecular ladder with 4 rungs proceeds much more rapidly than its counterpart with 16 rungs.

3.5.2 Registry Mechanism of *n* × *n* Molecular Ladder Formation by Förster Resonance Energy Transfer (FRET)

To further investigate the registry mechanism of molecular ladder formation, Förster resonance energy transfer (FRET), a spectroscopic approach to determine the distance between fluorescence donor and quenching acceptor functional groups,[11-14] was utilized. As the efficiency of fluorescence quenching is inversely proportional to the sixth power of the distance between the donor and acceptor moieties, FRET is particularly sensitive to small distance changes and thus is a powerful technique for exploring many phenomena that involve changes in molecular proximity.[11-20] Upon hybridization between complementary peptoid sequences, the resultant molecular ladder formation should lead to a reduction in the physical distance between the donor and acceptor moieties, thereby enhancing fluorophore/quencher energy transfer. Hence, by recording the decrease in fluorescence intensity with time, hybridization progress can be continuously monitored to elucidate the registry mechanism.

We covalently affixed a fluorescent donor moiety, 5-[(2-aminoethyl)amino] naphthalene-1-sulfonic acid (EDANS), to the *N*-terminus of a dodecaldehyde peptoid sequence and similarly tethered a quencher moiety, 4-(4-dimethylaminophenylazo) benzoic acid (DABCYL) to the *N*-terminus of a complementary dodecamine peptoid strand (Figure 3.12a). An additional E^3A spacer was inserted between the chromophore (either the fluorescence donor or acceptor) and the final amine- or aldehyde-based

dynamic covalent functionality (as shown in Figure 3.12a) to avoid potential steric effects by the bulkychromophores hindering oligomer hybridization.

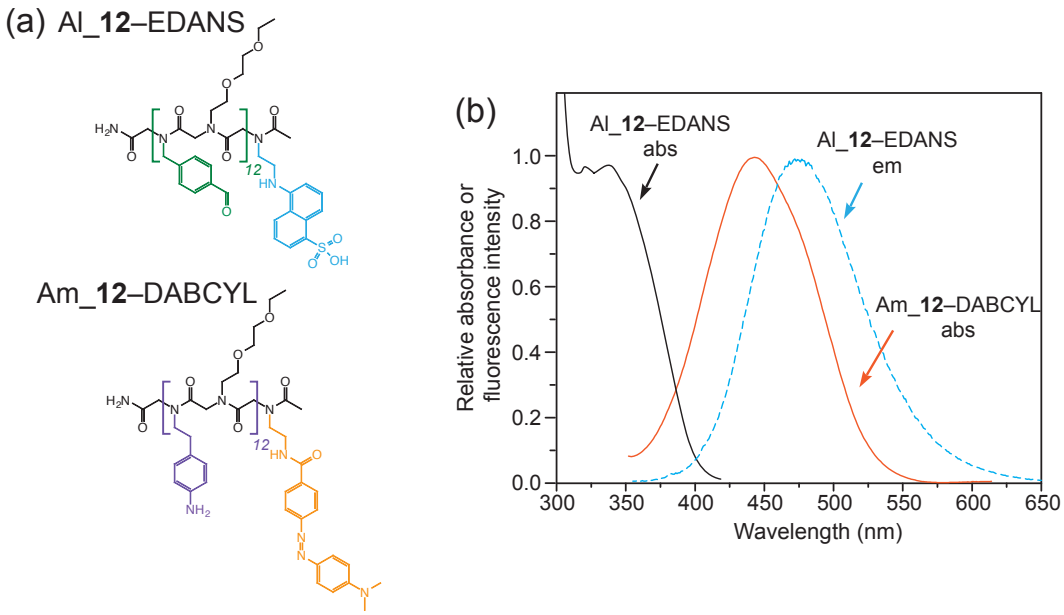

Figure 3.12. (a) Structures of chromophore-labeled peptoid sequences. A dodecaldehyde strand was affixed with a fluorescence donor EDANS (Al_12–EDANS) whereas its complementary dodecamine sequence was affixed with a quencher DABCYL (Am_12–DABCYL). As the fluorescence donor and quencher come in close proximity once the molecular ladder forms, radiationless energy transfer between the moieties quenches the donor fluorescence. (b) The absorption and fluorescence spectra of Al_12–EDANS, and the absorption spectrum of Am_12–DABCYL.

EDANS and DABCYL were chosen as a donor/acceptor pair as these moieties are readily incorporated into peptoids with slight or no modifications, the fluorescent emission of EDANS exhibits good spectral overlap with the strong visible absorption band of DABCYL (Figure 3.12b), and efficient energy transfer between these moieties has been demonstrated previously.[15-17, 19] A primary amine derivative of DABCYL was synthesized from DABCYL succinimide ester, enabling its facile utilization as a submonomer during solid-phase peptoid synthesis in order to incorporate the quencher

moiety into the peptoid. In contrast, although EDANS is commercially available bearing a primary amine functional group capable of direct incorporated into the peptoid as a submonomer during solid-phase peptoid synthesis, its poor solubility in DMF necessitated the addition of 20 vol% 1,8-diazabicycloundec-7-ene (DBU) for effective solvation. Notably, although DBU has traditionally been considered non- nucleophilic,[21] we determined that a fraction of the peptoid strands were terminated by a DBU moiety, a side product generated during the EDANS addition step; however, this impurity was able to be removed by HPLC.

Peptoid sequences containing either a fluorescence donor or a quencher were designed as control systems to validate the use of EDANS and DABCYL as an appropriate FRET pair in our studies (Figure 3.13). Benzyl groups were incorporated as inert, structural analogue residues in the peptoid control sequences to substitute for dynamic covalent functionalities (i.e., aniline and benzaldehyde pendant groups). Two non-reactive peptoid sequences, BZ_**12**–EDANS and BZ_**11**–Am–DABCYL, were employed as a negative control, non-quenching system (control I, see Figure 3.13). Upon equimolar mixing in $CHCl_3$, the residual fluorescence intensity for control I equilibrated at over 90% of its original value, indicating poor energy transfer between the unbound FRET pair. Given that the Förster distance, $\boldsymbol{R}_0$, the inter-chromophore distance at which half of the excited donor fluorescence is quenched, for this FRET pair is estimated to be 33 Å,[15] two additional control experiments were performed to ensure the ability of this pair to monitor dodecamer assembly throughout the hybridization of the Im_**12** molecular ladder.

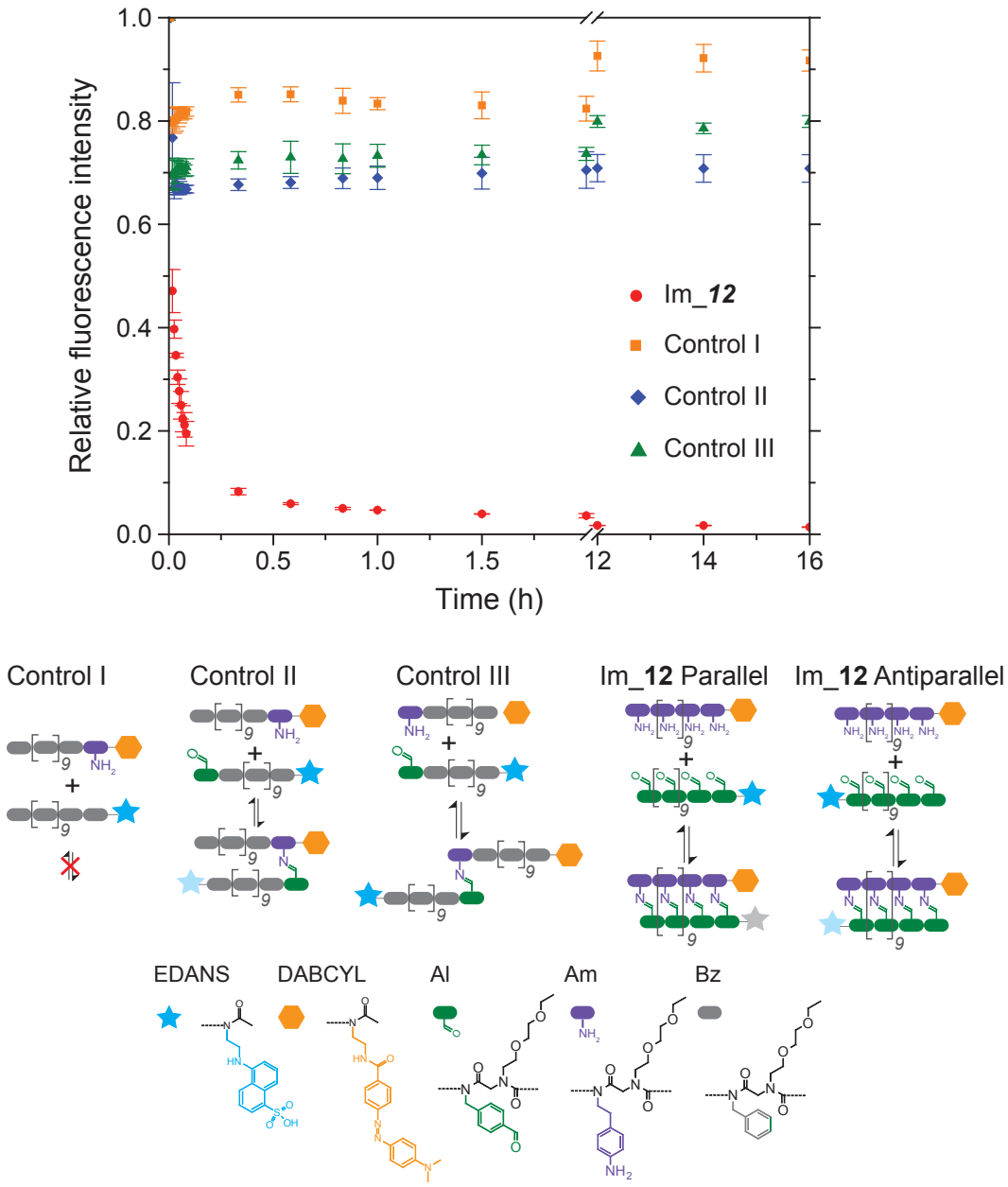

Figure 3.13. Examining dynamic covalent peptoid hybridization by Förster resonance energy transfer (FRET). The relative fluorescence intensity of chloroform solutions containing 25 μM donor- and acceptor-functionalized peptoids.

*Control I is a negative control incorporating a mono-amine and aldehyde-free peptoids. Control II contains mono-amine and mono-aldehyde peptoids where the reactive groups are positioned adjacent to the chromophore and at the opposite end of the strand from the chromophore, respectively, whereas Control III contains mono-amine and mono-aldehyde peptoids where the reactive groups are both positioned at the opposite ends of their respective strands from the chromophore. Im_**12** incorporates dodeca-amine and dodeca-aldehyde peptoids able to participate in parallel or anti-parallel hybridization such that the chromophores are positioned either adjacent to each other or at opposite ends of the resultant molecular ladder.

These two control experiments, Control II and Control III, both examined the influence of chromophore pair spacing on FRET efficiency using mono-amine and mono-aldehyde peptoids to afford species that are analogous to dodeca-amine and dodeca-aldehyde peptoids that have only reacted once at their respective termini. Control II, where the amine- and aldehyde-based reactive pendant groups are affixed adjacent to the chromophore and at the opposite end of the strand from the chromophore, respectively, positions the fluorophore and fluorescence donor 27 monomer residues apart.

Conversely, Control III, where amine and aldehyde pendant groups are both affixed at the opposite ends of their respective strands from the chromophore, positions the FRET pair 49 residues apart. Importantly, the residual fluorescence intensities for Control II and Control III equilibrated at 71% and 80%, respectively (Figure 3.13), indicating that this FRET pair should be well-suited to monitoring the Im_**12** molecular ladder hybridization. Thus, after confirming its suitability, the EDANS/DABCYL FRET pair was used to examine the assembly of the dodecameric Im_**12** molecular ladder. As shown in Figure 3.13, the fluorescence intensity rapidly decreased to 47% residual fluorescence within a minute upon commencement of hybridization and continued decreasing until it reached 5% at an hour. After one hour, the fluorescence intensity slightly decreased overtime and plateaued at 1% residual fluorescence after 16 h. The large initial fluorescence intensity decrease indicates that the distance between the fluorescence donor and quencher moieties rapidly decreased, attributable to the hybridization between complementary sequences initially following a rapid 'zipper' mechanism to immediately generate intermediate, out-of-registry ladders. Subsequently, the small decrease in the fluorescence intensity that occurs over several hours indicates that the hybridization proceeds *via* a

much slower mechanism, anticipated by slow, 'handshake line'-type shuffling of the intermediate, out-of-registry ladders until the fully-aligned ladders are achieved. This FRET study thus corroborates the previous observations based on MALDI spectra that the dynamic covalent assembly of these complementary peptoid sequences occurs by a hybrid mechanism whereby amine- and aldehyde-bearing strands initially zip up to form intermediate, out-of-registry ladders which subsequently convert to fully-condensed ladders via 'handshake line' shuffling. Notably, as complementary peptoid strands in the molecular ladders assembled here do not exhibit any ordered secondary structure (Figure 3.14), they could potentially align either parallel or anti-parallel to each other, polarity that is analogous to the antiparallel, 5′→3′ polarity exhibited by strands in the DNA double helix,[22] affording significantly different inter-chromophore distances.

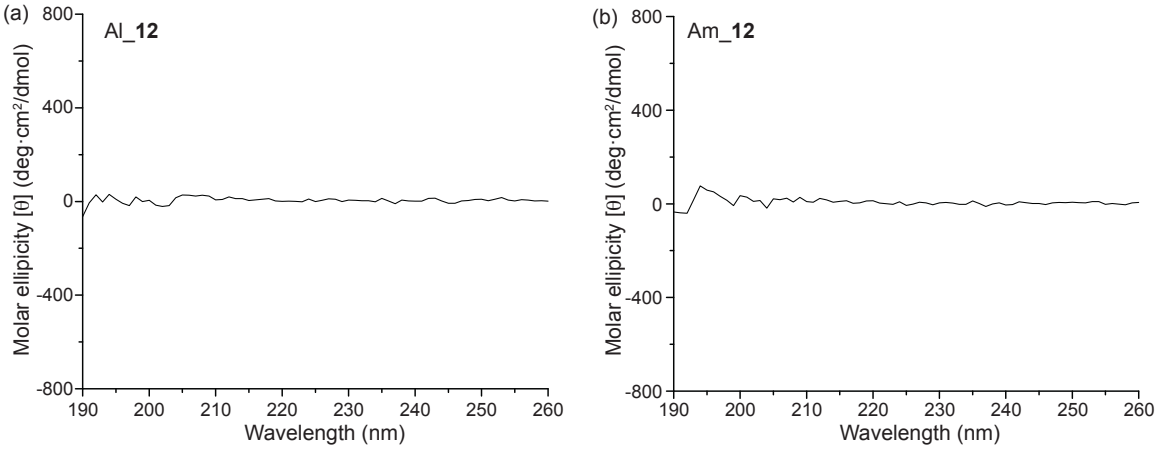

Figure 3.14. Circular dichroism (CD) spectra of Al_12 and Am_12.
*CD spectra were collected on a Jasco-815 CD spectrometer. Peptoids were dissolved in acetonitrile at concentrations of 25 mM. Blank scans containing only acetonitrile were collected and subtracted as background. Al_12 and Am_12 both exhibit spectra typical of random coil conformations, confirming non-ordered secondary structures for achiral peptoids.[23]

As the residual fluorescence intensity equilibrated at 71% when the donor and quencher are positioned at opposite ends of a dodecameric molecular ladder (see Control II), non-selective strand alignment would yield a residual fluorescence intensity of 36%, assuming that the FRET efficiency approaches unity when the donor and quencher are immediately adjacent to each other, as would be the case for parallel strand alignment. However, the observed fluorescence intensity for the assembly of Im_**12** after 16 h reaction time decreased to 1% residual fluorescence, suggesting that the strands in the assembled molecular ladders are predominantly oriented parallel to each other.

3.6 Conclusions

We have demonstrated the synthesis of amine/aldehyde functionalized dynamic covalent peptoid based oligomers and their assembly through Sc(III)-catalysed rearrangement into molecular ladders with up to 16 rungs, the longest generated to date. MALDI-TOF mass spectrometric analysis demonstrated their formation and was used to analyse molecular ladder formation dynamics for each system. The hybridization kinetics of molecular ladder formation showed that, as anticipated, the hybridization rate and degree of registry completion decrease as the ladder length increases. Hybridization kinetics also gave insight into the potential mechanisms at play in ladder formation, with the most likely mechanism being a combination of the primary mechanism of initial binding and 'zipping up' through adjacent imine/aldehyde condensation reactions at any point along the backbone to form out of registry molecular ladders. The secondary mechanism proceeds via transamination and imine metathesis reactions to shuffle the imine bonds until the molecular ladders come into registry through a molecular

handshake line, with the latter being the rate-limiting step. This is further confirmed by FRET analysis techniques that reinforced the MALDI-TOF kinetic analysis and was used to determine that the hybridization is almost entirely parallel in nature, due to the final fluorescence quenched state of the fully hybridized ladder system. Our ability to fabricate molecular ladders with up to 16 rungs and the understanding of their hybridization kinetics open up possibilities to design and construct robust, complex nanostructures based on the self-assembly of sequence-specific, dynamic covalent oligomers.

3.7 References

1. Wei, T.; Jung, J. H.; Scott, T. F., Dynamic Covalent Assembly of Peptoid-Based Ladder Oligomers by Vernier Templating. *J. Am. Chem. Soc.* **2015,** *137* (51), 16196-16202.

2. Wei, T.; Furgal, J. C.; Jung, J. H.; Scott, T. F., Long, self-assembled molecular ladders by cooperative dynamic covalent reactions. *Polymer Chemistry* **2017,** *8* (3), 520-527.

3. Hartley, C. S.; Elliott, E. L.; Moore, J. S., Covalent assembly of molecular ladders. *J. Am. Chem. Soc.* **2007,** *129* (15), 4512-4513.

4. Elliott, E. L.; Hartley, C. S.; Moore, J. S., Covalent ladder formation becomes kinetically trapped beyond four rungs. *Chem. Commun.* **2011,** *47* (17), 5028-5030.

5. Zhang, D. Y.; Seelig, G., Dynamic DNA nanotechnology using strand-displacement reactions. *Nat. Chem.* **2011,** *3* (2), 103-113.

6. Zhang, D. Y.; Winfree, E., Control of DNA Strand Displacement Kinetics Using Toehold Exchange. *J. Am. Chem. Soc.* **2009,** *131* (47), 17303-17314.

7. Meng, W.; Muscat, R. A.; McKee, M. L.; Milnes, P. J.; El-Sagheer, A. H.; Bath, J.; Davis, B. G.; Brown, T.; O'Reilly, R. K.; Turberfield, A. J., An autonomous molecular assembler for programmable chemical synthesis. *Nat. Chem.* **2016,** *8* (6), 542-548.

8. He, Y.; Liu, D. R., Autonomous multistep organic synthesis in a single isothermal solution mediated by a DNA walker. *Nat. Nanotechnol.* **2010,** *5* (11), 778-782.

9. Furgal, J. C.; Goodson III, T.; Laine, R. M., D 5h [PhSiO 1.5] 10 synthesis via F− catalyzed rearrangement of [PhSiO 1.5] n. An experimental/computational analysis of likely reaction pathways. *Dalton Trans.* **2016,** *45* (3), 1025-1039.

10. Layer, R. W., The Chemistry of Imines. *Chem. Rev.* **1963,** *63* (5), 489-510.

11. Stryer, L.; Haugland, R. P., Energy transfer: a spectroscopic ruler. *Proc. Natl. Acad. Sci. U. S. A.* **1967,** *58* (2), 719-726.

12. Schuler, B.; Lipman, E. A.; Steinbach, P. J.; Kumke, M.; Eaton, W. A., Polyproline and the "spectroscopic ruler" revisited with single-molecule fluorescence. *Proc. Natl. Acad. Sci. U. S. A.* **2005,** *102* (8), 2754-2759.

13. Lee, B. C.; Zuckermann, R. N.; Dill, K. A., Folding a nonbiological polymer into a compact multihelical structure. *J. Am. Chem. Soc.* **2005,** *127* (31), 10999-11009.

14. Lee, B. C.; Chu, T. K.; Dill, K. A.; Zuckermann, R. N., Biomimetic nanostructures: Creating a high-affinity zinc-binding site in a folded nonbiological polymer. *J. Am. Chem. Soc.* **2008,** *130* (27), 8847-8855.

15. Matayoshi, E. D.; Wang, G. T.; Krafft, G. A.; Erickson, J., Novel Fluorogenic Substrates for Assaying Retroviral Proteases by Resonance Energy-Transfer. *Science* **1990,** *247* (4945), 954-958.

16. Wang, G. T.; Matayoshi, E.; Huffaker, H. J.; Krafft, G. A., Design and Synthesis of New Fluorogenic Hiv Protease Substrates Based on Resonance Energy-Transfer. *Tetrahedron Lett.* **1990,** *31* (45), 6493-6496.

17. Sokol, D. L.; Zhang, X.; Lu, P.; Gewirtz, A. M., Real time detection of DNA·RNA hybridization in living cells. *Proc. Natl. Acad. Sci. U. S. A.* **1998,** *95* (20), 11538-11543.

18. Zhang, J.; Tamilarasu, N.; Hwang, S. W.; Garber, M. E.; Huq, I.; Jones, K. A.; Rana, T. M., HIV-1 TAR RNA enhances the interaction between Tat and cyclin T1. *J. Biol. Chem.* **2000,** *275* (44), 34314-34319.

19. Guo, J. B.; Xu, C.; Li, X. C.; Chen, S., A Simple, Rapid and Sensitive FRET Assay for Botulinum Neurotoxin Serotype B Detection. *PLoS One* **2014,** *9* (12).

20. Wang, S. Z.; Vafabakhsh, R.; Borschell, W. F.; Ha, T.; Nichols, C. G., Structural dynamics of potassium-channel gating revealed by single-molecule FRET. *Nat. Struct. Mol. Biol.* **2016,** *23* (1), 31-36.

21. Taylor, J. E.; Bull, S. D.; Williams, J. M. J., Amidines, isothioureas, and guanidines as nucleophilic catalysts. *Chem. Soc. Rev.* **2012,** *41* (6), 2109-2121.

22. Lu, X. J.; Olson, W. K., 3DNA: a software package for the analysis, rebuilding and visualization of three-dimensional nucleic acid structures. *Nucleic Acids Res.* **2003,** *31* (17), 5108-5121.

23. Shin, H.-M.; Kang, C.-M.; Yoon, M.-H.; Seo, J., Peptoid helicity modulation: precise control of peptoid secondary structures via position-specific placement of chiral monomers. *Chem. Commun.* **2014,** *50* (34), 4465-4468.

Chapter 4

Long, Self-assembled Molecular Ladders by Vernier Templating

4.1 Original Publication Information

Wei, T.; Jung, J. H.; Scott, T. F., Dynamic Covalent Assembly of Peptoid-Based Ladder Oligomers by Vernier Templating. *J. Am. Chem. Soc.* **2015,** *137* (51), 16196-16202.

Modifications have been made to the original document in order to adapt the content to the proper format.

4.2 Abstract

Dynamic covalent chemistry, in conjunction with template-directed assembly, enables the fabrication of extended nanostructures that are both precise and tough. Here, we demonstrate the dynamic covalent assembly of peptoid-based molecular ladders with up to 12 rungs *via* scandium(III)-catalyzed imine metathesis by employing the principle of Vernier templating, where small precursor units with mismatched numbers of complementary functional groups are co-reacted to yield larger structures with sizes determined by the respective precursor functionalities. Owing to their monomer diversity and synthetic accessibility, sequence-specific oligopeptoids bearing dynamic covalent pendant groups were employed as precursors for molecular ladder fabrication. The generated structures were characterized using matrix-assisted laser desorption/ionization

(MALDI) mass spectrometry and gel permeation chromatography (GPC), confirming successful molecular ladder fabrication.

4.3 Introduction

Despite the recent advances in self-assembly for 'bottom-up' construction techniques, approaches to achieve hybridization registry between large, complementary oligomers and polymers have long been challenging owing to kinetic trapping, even for those employing non-covalent interactions. Moreover, the fabrication of large structures typically requires templates of equivalent sizes, which themselves are difficult to synthesize[1-2] owing to the intractability of sequence-specific polymer synthesis.[3] A recently-described self-assembly approach to address the limitations of conventional template assembly employs the co-reaction of oligomeric precursors with unequal numbers of complementary functional groups.[1-9] This process, known as Vernier Templating, results in assembled structures where each component precursor only participates in as many interactions as its number of reactive functional groups allows, whereas the total number of interaction sites on the Vernier complex is equal to the lowest common multiple of the functionality on the respective precursors (see Scheme 4.1). Thus, this templated molecular fabrication approach curtails the kinetic trapping that would otherwise impede the selective assembly of long precursor strands and affords a facile route to the generation of large constructs from relatively small, oligomeric precursors.[1-9] Implementations of Vernier templating have utilized several different mechanisms. For example, metal-ligand interactions between transition metals and porphyrin-based oligomers have been employed to assemble a variety of structures, including triple-stranded Vernier complexes,[6] and macrocycles that, upon subsequent

ligation, yielded large structures containing different numbers of porphyrin units.[1, 7-8] Additionally, several groups[3, 9] have demonstrated the Vernier-templated assembly of length-programmed DNA nanostructures. Notably, these Vernier templating self-assembly approaches reported to date have relied upon relatively weak intermolecular interactions. In contrast, the alternative approach of DCC-mediated Vernier templating provides an avenue for the construction of large and tough assemblies with well-defined sizes.

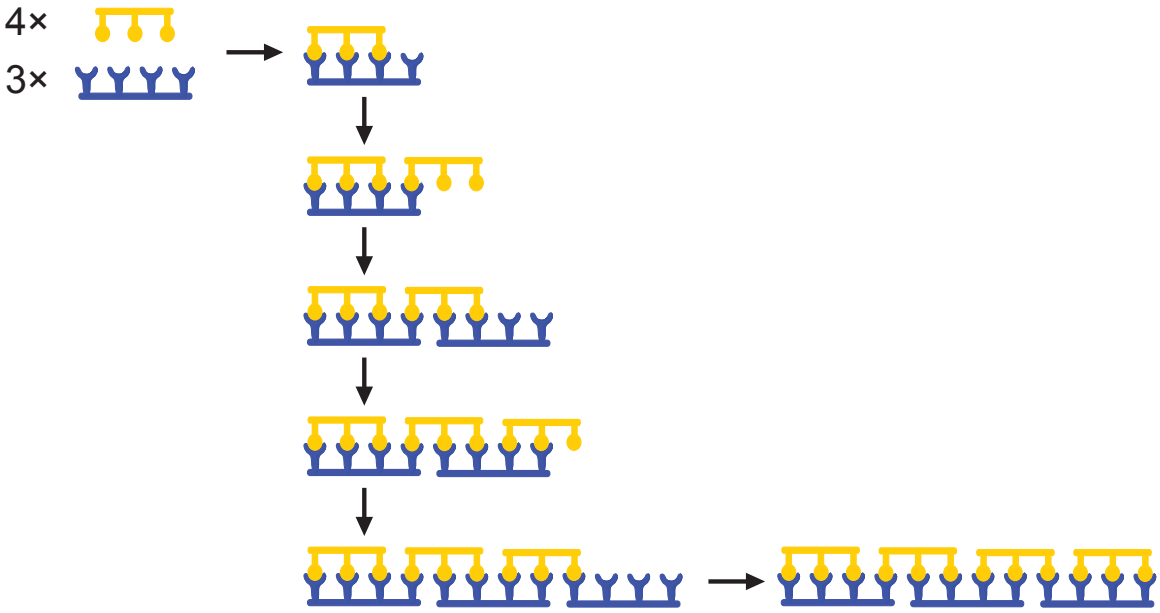

Scheme 4.1. Vernier templates for macromolecular synthesis.
*Vernier assemblies form from precursor molecules of mismatched numbers of complementary reactive sites (here, yellow circles bind to blue hooks). After the formation of an initial complex, these mismatched precursor molecules continue binding to each other until all reactive sites are occupied.

We employ scandium(III)-catalyzed imine metathesis to mediate the dynamic covalent assembly of peptoid-based molecular ladders through Vernier templating by co-reacting oligomeric precursors of non-commensurate lengths. To the best of our

knowledge, this work represents the first demonstration of Vernier-templated self-assembly *via* dynamic covalent chemistry.

4.4 Experimental

4.4.1 General Experimental Procedure

All chemicals and reagents, unless specified, were purchased from commercial sources and used as received without any further purification. ^{1}H and ^{13}C NMR spectra were collected using Varian MR400 and Varian VNMRS 700 spectrometers. Chemical shifts were measured in δ (ppm) relative to residual solvent signals as internal standards ($CDCl_3$: 7.24 for ^{1}H, 77.23 for ^{13}C; CD_3OD: 4.78 and 3.31 for ^{1}H, 49.15 for ^{13}C). Matrix-assisted laser desorption/ionization (MALDI) mass spectra were recorded using a Bruker Autoflex mass spectrometer, whereas electrospray ionization (ESI) mass spectra were recorded using an Agilent Q-TOF 1200 series spectrometer. All MALDI analyses, were performed in reflectron positive ion mode using 2-(4-hydroxyphenylazo)benzoic acid (HABA) as the matrix, where 3 μL of a solution of the sample in chloroform (1.5 mM) was mixed with 10 μL of a mixture of 6 mg matrix in 300 μL acetonitrile, spotted on a MALDI sample plate (Bruker), and allowed to air dry. Reverse phase high performance liquid chromatography (RP-HPLC) was performed using a Shimadzu LC-6AD HPLC pump, equipped with a Shimadzu FRC 70A fraction collector, using analytical and preparative reversed phase Phenomenex Luna C18(2) columns with a linear gradient of water and acetonitrile as the eluent at 30°C, and monitored with a Shimadzu Prominence UV/vis detector at 214 nm. Analytical gel permeation chromatography (GPC) was similarly performed using a Shimadzu LC-6AD HPLC pump, equipped with a series of

three Phenogel GPC/SEC columns (length 300 mm × diameter 7.8 mm, pore sizes of 500, 100, and 50 Å) with 94:4:2 (v/v/v) $CHCl_3$:MeOH:Et_3N as the eluent at 30°C, and monitored with a Shimadzu Prominence UV/vis detector at 313 nm. The analytical GPC was calibrated utilizing low dispersity polystyrene standards (Polystyrene Standard (Low Molecular) Readycal Set, Fluka).

4.4.2 Monomer Synthesis

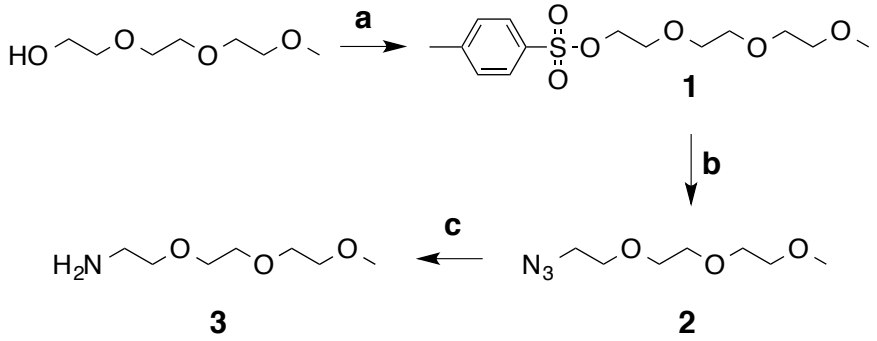

Scheme 4.2. 2-(2-(2-Methoxyethoxy)ethoxy)ethylamine (ME^3A) (3). Reagents and conditions: (a) tosyl chloride, THF, 0°C, (b) NaN_3, DMF, 60°C, 36 h, and (c) TPP, water.[10]

2-(2-(2-Methoxyethoxy)ethoxy)ethyl tosylate (**1**). Triethylene glycol monomethyl ether (24.6 g, 0.15 mol) and 50 mL of THF were charged to a 500 mL round bottom flask with a magnetic stirrer. This reaction mixture was cooled to 0°C and 50 ml of 6 M NaOH was added, followed by dropwise addition of tosyl chloride (54 g, 0.28 mol) in 80 ml THF under N_2. After stirring for 1 h at 0°C, the reaction mixture was allowed to reach room temperature and stirred for another 1 h. The resulting mixture was extracted with Et_2O (400 ml) and the organic layer was washed with 1 M NaOH and water. After drying over

$MgSO_4$, the solution was evaporated under vacuum to yield 47g of **1** as a colorless liquid (yield 98%).

^{1}H NMR (400 MHz, $CDCl_3$) δ: 7.77 (d, J = 8.0, 2H, -S-C=CH-C*H*), 7.32 (d, J = 8.0, 2H, -S-C=CH-C*H*), 4.13 (t, J = 5.0, 2H, -CH_2-C*H*$_2$-O-Ts), 3.66 (t, J = 4.0, 2H, C*H*$_2$-CH_2-O-Ts), 3.57 (m, 6H, O-C*H*$_2$-C*H*$_2$-O-C*H*$_2$-CH_2-O-CH_3), 3.50 (m, 2H, O-CH_2-C*H*$_2$-O-CH_3), 3.35 (s, 3H, O-C*H*$_3$), 2.44 (s, 3H, C-C*H*$_3$).

^{13}C NMR (100 MHz, $CDCl_3$) δ: 144.78 (1C, -S-C_q-Ar), 132.95 (1C, C_p-Ar), 130.26 (1C, C_m-Ar), 129.80 (1C, C_m-Ar), 127.88 (1C, C_o-Ar), 126.93 (1C, C_o-Ar), 71.83 (1C, O-CH_2-*C*H_2-O-CH_3), 70.64 (1C, O-*C*H_2-CH_2-O-CH_3), 70.45 (2C, O-*C*H_2-*C*H_2-O-CH_2-CH_2-O-CH_3), 69.28 (1C, -*C*H_2-CH_2-O-Ts), 68.56 (1C, -CH_2-*C*H_2-O-Ts), 58.90 (1C, O-*C*H_3), 21.56 (1C, C-*C*H_3).

2-(2-(2-Methoxyethoxy)ethoxy)ethyl azide (**2**). A 500 mL round bottom flask was charged with compound **1** (44.6 g, 0.14 mol) and DMF (250 ml) under N_2. To this mixture, NaN_3 (31.5 g, 3.5 eq, 0.49 mol) was added. The reaction mixture was heated at 60°C for 36 h and then cooled to room temperature. The reaction mixture was diluted with a large amount of water and extracted with Et_2O. The organic layer was washed with water and dried over $MgSO_4$, and evaporated under vacuum to afford compound **2** as a yellow liquid 22 g (83%).

^{1}H NMR (400 MHz, $CDCl_3$) δ: 3.63 (m, 8H, O-C*H*$_2$-C*H*$_2$-O-C*H*$_2$-C*H*$_2$-O-CH_3), 3.52 (m, 2H, N_3-CH_2-C*H*$_2$-O), 3.35 (m, 5H, O-C*H*$_3$ and N_3-C*H*$_2$-CH_2-O).

^{13}C NMR (100 MHz, $CDCl_3$) δ: 71.83 (1C, O-CH_2-*C*H_2-O-CH_3), 70.57 (2C, O-*C*H_2-*C*H_2-O-CH_2-CH_2-O-CH_3), 70.49 (1C, O-*C*H_2-CH_2-O-CH_3), 69.93 (1C, N_3-CH_2-*C*H_2-O), 58.87 (1C, O-*C*H_3), 50.58 (1C, N_3-*C*H_2-CH_2-O).

2-(2-(2-Methoxyethoxy)ethoxy)ethylamine (ME^{3}A) (**9**). A 250 mL three necked round bottom flask equipped with magnetic stirrer was charged with compound **2** (20 g, 0.13 mmol) and THF (160 ml). Triphenylphosphine (TPP) (40 g, 0.15 mol, 1.1 eq) was then added and stirred overnight at room temperature under N_2. The reaction mixture was quenched with water (220 mL), and allowed to stir for another day. The resulting solution was washed with toluene and DCM, and evaporated under vacuum to yield compound **3** as a yellow liquid (13 g, 61%).

^{1}H NMR (400 MHz, $CDCl_3$) δ: 3.52-3.32 (m, 10H, NH_2-CH_2-C*H*$_2$-O-C*H*$_2$-C*H*$_2$-O-C*H*$_2$-C*H*$_2$-O-CH_3), 3.24 (s, 3H, O-C*H*$_3$), 2.73 (m, 2H, NH_2-C*H*$_2$-CH_2-O).

^{13}C NMR (100 MHz, $CDCl_3$) δ: 73.72 (1C, NH_2-CH_2-*C*H_2-O), 71.77 (1C, O-CH_2-*C*H_2-O-CH_3), 70.42 (1C, O-*C*H_2-CH_2-O-CH_2-CH_2-O-CH_3), 70.35 (1C, O-CH_2-*C*H_2-O-CH_2-CH_2-O-CH_3), 70.10 (1C, O-*C*H_2-CH_2-O-CH_3), 58.82 (1C, O-*C*H_3), 41.60 (1C, NH_2-*C*H_2-CH_2-O).

MS (ESI+) (m/z): calcd for $C_7H_{18}NO_3^+$: $[M+H]^+$ = 164.1281, found: *m*/*z* = 164.1285 $[M+H]^+$.

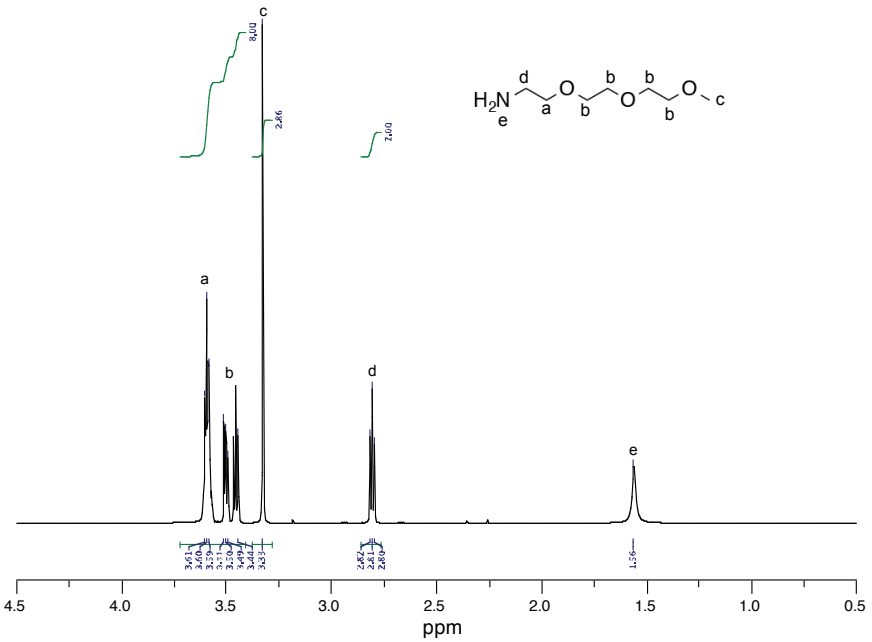

Figure 4.1. 1H NMR spectrum of 2-(2-(2-Methoxyethoxy)ethoxy)ethylamine (ME^{3}A).

4.4.3 Synthesis and Characterization of Peptoids for Vernier Templating and Molecular Ladder Scrambling

Four primary amine monomers, 4-(2-aminoethyl)-*N*-(*tert*-butixycarbonyl) phenylamine (Am), 4-(1,3-dioxacyclopent-2-yl)benzylamine (Al), 2-(2-ethoxyethoxy) ethylamine (E^{3}A), 2-(2-(2-Methoxyethoxy)ethoxy) ethylamine (ME^{3}A) were utilized to prepare peptoids for the study here. Peptoids were synthesized according to the aforementioned submonomer approach to solid-phase synthesis (see Chapter 2). Subsequently, the resultant peptoids were cleaved from the resin beads by treatment with a TFA cleavage cocktail and purified by preparative HPLC. Characterization of purified peptoids containing E^{3}A inert spacer is shown in Chapter 2.

4.4.3.1 ESI Mass Spectra of Purified, Aldehyde- and Amine-Functionalized Peptoids Incorporating ME^{3}A Spacer

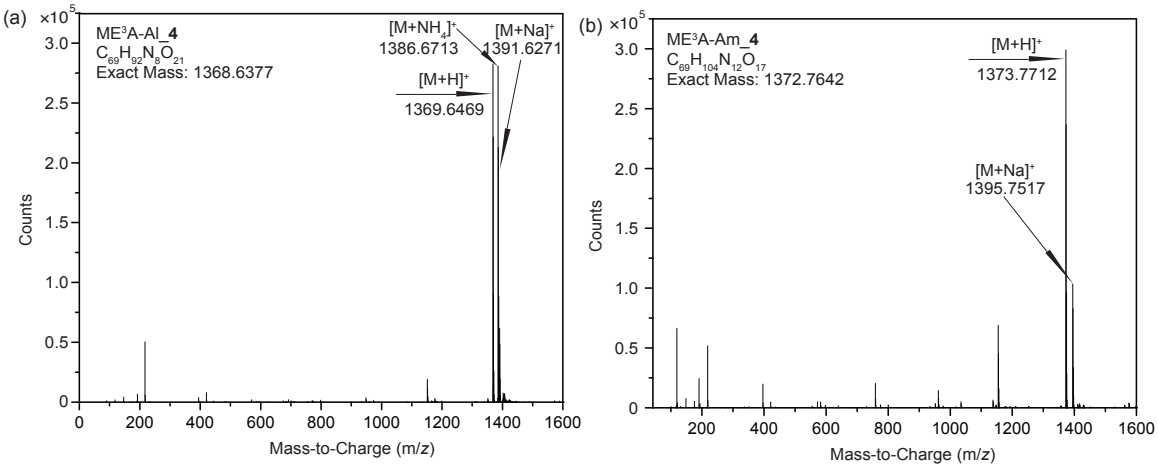

Figure 4.2. ESI mass spectra of aldehyde- and amine-functionalized oligopeptoids incorporating ME^{3}A spacer purified by preparative RP-HPLC: (a) ME^{3}A-Al_4 & (b) ME^{3}A-Am_4.

ME^{3}A-Al_**4**: calcd for $C_{69}H_{92}N_8O_{21}$: $[M+H]^+$ = 1369.6450, $[M+NH_4]^+$ = 1386.6716, $[M+Na]^+$ = 1391.6270, found: *m*/*z* = 1369.6469 $[M+H]^+$, *m*/*z* = $[M+NH_4]^+$ = 1386.6713, *m*/*z* = 1391.6271 $[M+Na]^+$

ME^{3}A-Am_**4**: calcd for $C_{69}H_{104}N_{12}O_{17}$: $[M+H]^+$ = 1373.7715, $[M+Na]^+$ = 1395.7534, found: *m*/*z* = 1373.7712 $[M+H]^+$, *m*/*z* = 1395.7517 $[M+Na]^+$

4.4.3.2 NMR Spectra of Purified, Aldehyde- and Amine-Functionalized Peptoids Incorporating ME^{3}A Spacer

ME^{3}A-Al_**4**

^{1}H NMR (700 MHz, $CDCl_3$) δ: 9.89-9.99 (m, Ar-C*H*O), 7.75-7.89 (m, Ar), 7.31-7.50 (m, Ar), 4.56-4.76 (m, Ar-CH_2-N-), 4.16-4.36 (m, -N-CH_2-CO-), 3.86-4.04 (m, -N-CH$_2$-CH_2-O-), 3.39-3.60 (m, -O-CH_2-CH_2-O-), 3.26-3.30 (m, -O-CH_3, -N-CH_2-CH$_2$-O-), 2.02-2.12 (m, -CO-CH_3).

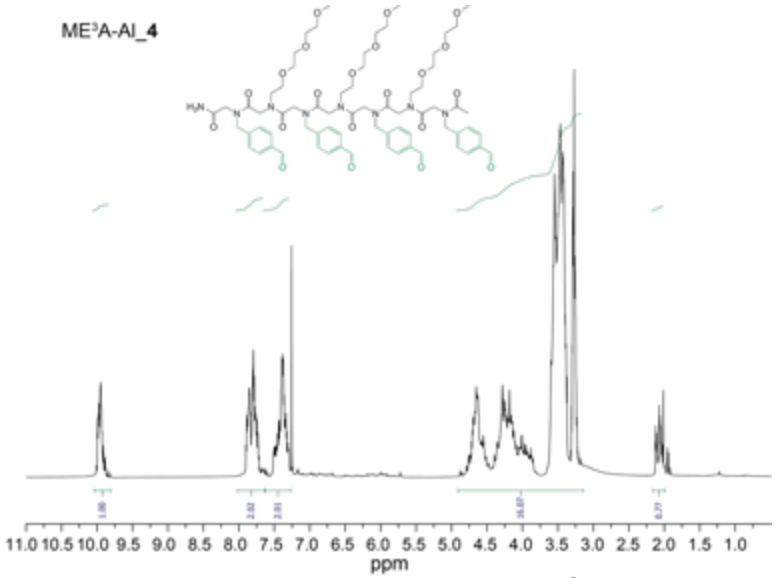

Figure 4.3.**[1]H NMR spectrum (700 MHz, $CDCl_3$) of ME[3]A-Al_4.**

ME[3]A-Am_**4**

[1]H NMR (700 MHz, $CDCl_3$) δ: 6.84-6.96 (m, Ar), 6.55-6.59 (m, Ar), 3.73-4.31 (br, -N-CH_2-CO-), 3.49-3.61 (m, -O-CH_2-CH_2-O-, Ar-CH_2-CH_2-N-, -N-CH_2-CH_2-O-), 3.32-3.34 (m, -O-CH_3, -N-CH_2-CH_2-O-), 2.58-2.69 (br, Ar-CH_2-CH_2-N-), 1.84-1.96 (m, -CO-CH_3).

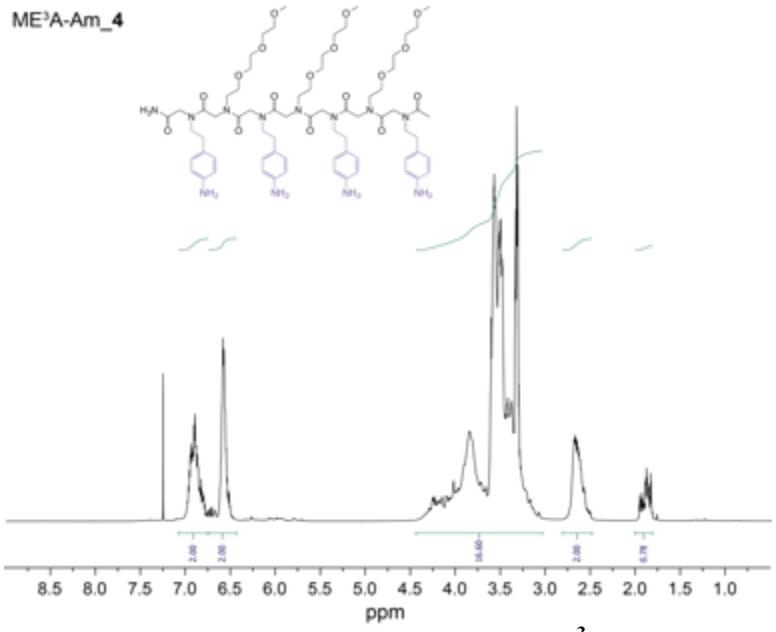

Figure 4.4. [1]H NMR spectrum (700 MHz, $CDCl_3$) of ME[3]A-Am_4.

4.4.3.3 Analytical HPLC Traces of Purified, Aldehyde- and Amine-Functionalized Oligopeptoids Incorporating ME^{3}A Spacer

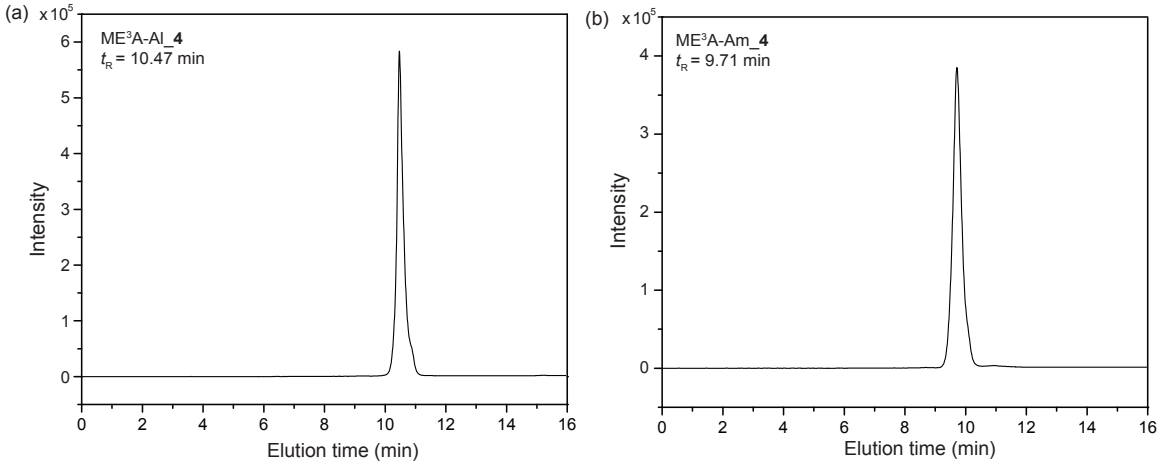

Figure 4.5. Analytical HPLC traces of aldehyde- and amine-functionalized oligopeptoids incorporating ME^{3}A spacer: (a) ME^{3}A-Al_4 (purity 98%) & (b) ME^{3}A-Am_4 (purity 97%).
*Analytical HPLC method: flow rate at 1 mL/min; A: H_2O, B: MeCN; 20% – 80% B 0 – 13 min, 80% – 20% B 13 – 16 min.

4.4.4 General Procedure for Vernier-templated Self-assembly of Molecular Ladders of Length $m \times n$

A 1 μmol self-assembly scale was performed by mixing E^{3}A-Al_***m*** with its complementary strand E^{3}A-Am_***n***, where $m \neq n$ but in a 1:1 aldehyde:amine stoichiometric ratio, in 2 mL $CHCl_3$. To the reaction mixture, $Sc(OTf)_3$ (0.04 eq. per imine bond, 10 mM stock solution dissolved in MeCN) was added and the mixture allowed to stir for 7 days. The reaction mixture was again directly characterized by MALDI mass spectrometry and analytical GPC, after which $NaBH(OAc)_3$ was added to reduce the inter-strand imine groups and the mixture was again characterized by MALDI mass spectrometry.

4.4.5 Procedure for Dynamic Covalent Assembly of Ladder ME^{3}A-Im_4

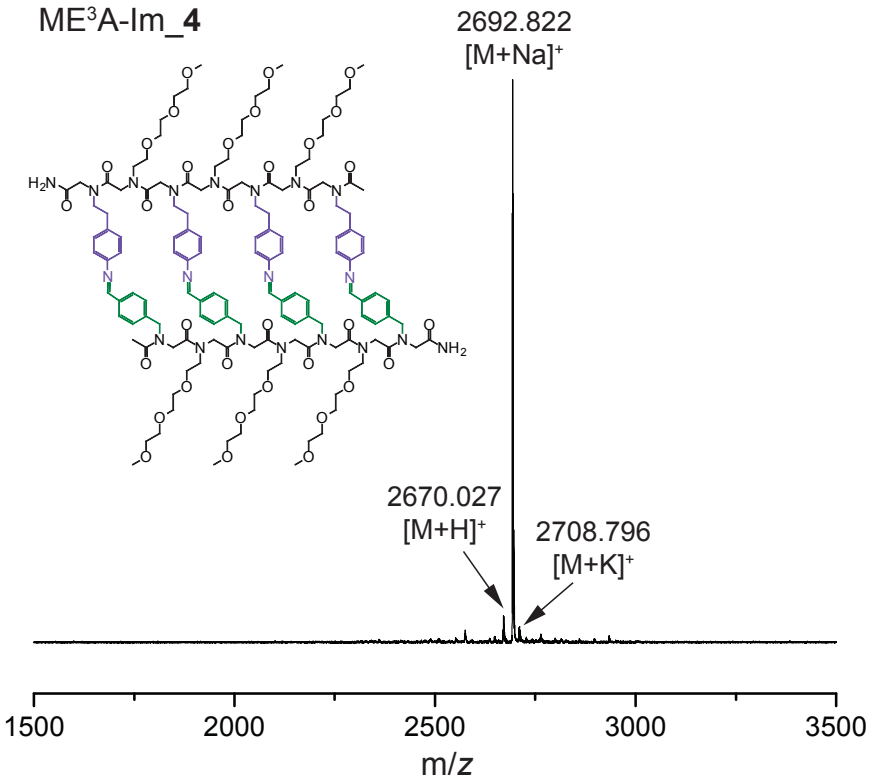

Figure 4.6. MALDI mass spectrum of molecular ladder formed by dynamic covalent dimerization of oligopeptoids incorporating ME^{3}A spacer.
*Expected exact mass: $[M_{ME^3A\text{-}Im\_4}+H]^+$ = 2670.367, $[M_{ME^3A\text{-}Im\_4}+Na]^+$ = 2692.349, $[M_{ME^3A\text{-}Im\_4}+K]^+$ = 2708.323.

1 μmol of the peptoid oligomer ME^{3}A-Al_**4** was mixed with 1 μmol of its complementary strand ME^{3}A-Am_**4** in 2 mL $CHCl_3$. To the reaction mixture, $Sc(OTf)_3$ (0.04 eq. per imine bond, 10 mM stock solution dissolved in MeCN) was added and the mixture allowed to stir overnight. The reaction mixture was then directly analyzed by MALDI mass spectrometry. MALDI mass spectrum of the crude peptoid dimerization reaction mixture is illustrated in Figure 4.6. The mass spectrum indicates the presence of only a single product, where the observed dominant peak corresponded to the desired molecular ladder structure ME^{3}A-Im_4, demonstrating the successful formation of the

desired ladder structure that is the only reasonable product equivalent to the observed molecular weight. This reaction mixture is used further for the molecular ladder scrambling experiment.

4.4.6 Procedure for Molecular Ladder Scrambling by Strand Exchange

Scrambling between single peptoid strands and molecular ladders were examined by combining 100 μL of 10 mM E^3A-Am_**4** in MeCN with 16 μL of 10 mM $Sc(TOf)_3$ in MeCN, diluting with $CHCl_3$ to a total volume of 1 mL, and mixing with 1 mL of a 1 mM solution of the peptoid-based, 4-rung ladder ME^3A-Im_**4**, described above, such that the peptoid strand and molecular ladder were present in a 1:1 stoichiometric ratio and the final $Sc(OTf)_3$ concentration was 0.08 mM. Scrambling between different molecular ladders was similarly examined by mixing 1 mL of 1 mM Im_**4** (the peptoid-based, 4-rung molecular ladder incorporating E^3A as the spacer residue) in $CHCl_3$ with 1 mL of 1 mM ME^3A-Im_**4**, both described previously, such that the molecular ladders were present in a 1:1 stoichiometric ratio, again with 0.08 mM $Sc(OTf)_3$. Aliquots of the reaction mixture were examined by MALDI mass spectrometry over the course of 9 days to determine the extent of ladder scrambling. Multiple regions of interest were ionized in each sample to obtain an average ratio of target peak intensities, and concentrations of scrambled molecular ladders were estimated by comparing MALDI mass spectrometry signal intensities of the scrambled products with those of the parent molecular ladders.

4.5 Results and Discussion

4.5.1 Vernier-templated Assembly of Complementary *m*×*n* Oligopeptoids

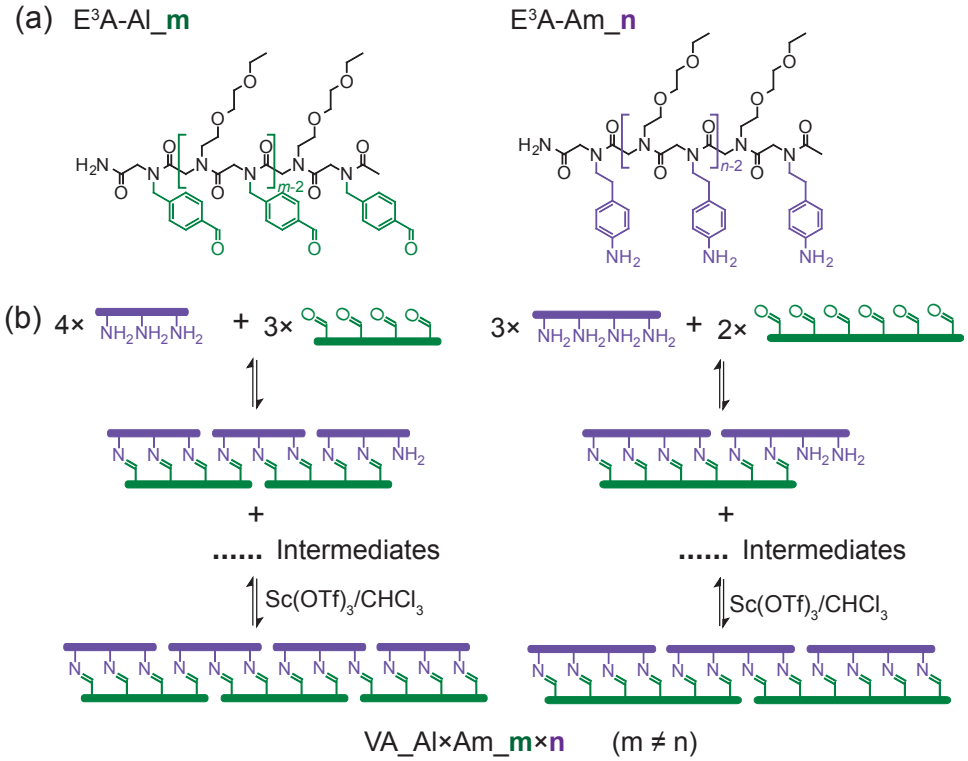

Scheme 4.3. Dynamic covalent assembly of peptoid-based ladders by Vernier-Templating. (a) Structures of linear oligopeptoids bearing pendant amine (E³A-Am_*n*) and aldehyde (E³A-Al_*m*) functional groups. (b) Vernier-templated assembly of complementary oligopeptoids with non-commensurate functionalities into molecular ladders with *m* × *n* rungs (VA_Al×Am_*m*×*n*, where VA is 'Vernier assembly').

The Vernier template-directed assembly of molecular ladders was investigated *via* application of Sc(III)-catalyzed metathesis of inter-strand imine bonds. Aldehyde- and amine-functionalized peptoid oligomers were added to chloroform such that the stoichiometric ratio of dynamic covalent reactants was 1:1; however, the functionalities of the peptoids E³A-Al_***m*** and E³A-Am_***n*** in the reaction mixture were not commensurate (i.e., ***m*** ≠ ***n***) (Scheme 4.3). In the presence of a catalytic amount of

scandium(III) triflate, the reaction mixture was stirred at room temperature for one week and analyzed by both MALDI mass spectrometry and GPC. The self-assembly of four different oligomer combinations were examined: VA_Al×Am_**3**×**4** (i.e., trialdehyde/tetraamine), VA_Al×Am _**4**×**3** (tetraaldehyde/ triamine), VA_Al×Am_**4**×**6** (tetraaldehyde/hexaamine), and VA_Al×Am_**6**×**4** (hexaaldehyde/tetraamine). These combinations were selected as each reaction was anticipated to yield 12-rung molecular ladder products, based on the lowest common multiple of both 3×4 and 4×6.

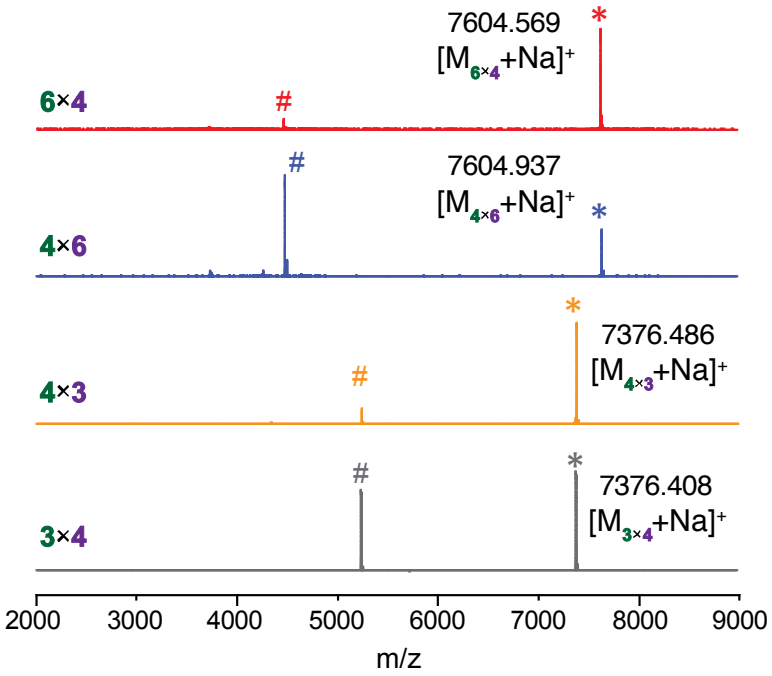

Figure 4.7. MALDI Mass spectra of Vernier-templated 12-rung molecular ladders. The target ladder structures are labeled with * symbols and the intermediates are labeled with #. Expected molecular weights for the target ladders: $[M_{3\times4}+Na]^+ = [M_{4\times3}+Na]^+ =$ 7376.810 g/mol; $[M_{4\times6}+Na]^+ = [M_{6\times4}+Na]^+ =$ 7604.946 g/mol. Intermediates are identified as $(E^3A\text{-Al\_}\mathbf{3})_3(E^3A\text{-Am\_}\mathbf{4})_2$; $(E^3A\text{-Al\_}\mathbf{4})_2(E^3A\text{-Am\_}\mathbf{3})_3$, $(E^3A\text{-Al\_}\mathbf{4})_2(E^3A\text{-Am\_}\mathbf{3})_2$; $(E^3A\text{-Al\_}\mathbf{4})_2(E^3A\text{-Am\_}\mathbf{6})_1$; $(E^3A\text{-Al\_}\mathbf{6})_1(E^3A\text{-Am\_}\mathbf{4})_2$.

Notably, although the ladders VA_Al×Am_**3**×**4** and VA_Al×Am_**4**×**3** share the same molecular weight, and the ladders VA_Al×Am_**4**×**6** and VA_Al×Am_**6**×**4** similarly

share the same molecular weight, the different numbers of E^3A solubilizing groups incorporated into the constituent peptoid strands results in different molecular weights between the Vernier-templated trimer/tetramer and tetramer/hexamer systems despite both yielding 12-rung molecular ladders.

MALDI mass spectra of the crude and reduced hybridization reaction mixtures utilizing non-commensurate length precursor strands shown in **Figure 4.7** and **Figure 4.8**, respectively, demonstrate major peaks assignable to the desired 12-rung ladder structures with observed molecular weights equivalent to the expected values, demonstrating the success of this dynamic covalent approach to Vernier-templated self-assembly.

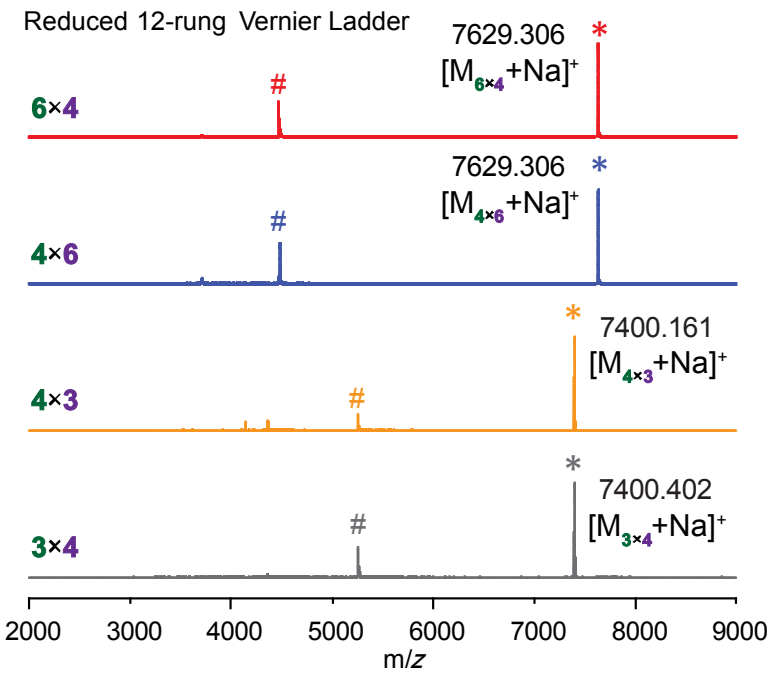

Figure 4.8. MALDI mass spectra of reduced, Vernier-templated 12-rung ladders. The target ladder structures are labeled with * symbols and the intermediates are labeled with #. Expected molecular weights for the target ladders: $[M_{3\times4}+Na]^+ = [M_{4\times3}+Na]^+ = 7400.997$; $[M_{4\times6}+Na]^+ = [M_{6\times4}+Na]^+ = 7629.134$. Intermediates are identified as $(E^3A\text{-}Al\_\mathbf{3})_3(E^3A\text{-}Am\_\mathbf{4})_2$; $(E^3A\text{-}Al\_\mathbf{4})_2(E^3A\text{-}Am\_\mathbf{3})_3$, $(E^3A\text{-}Al\_\mathbf{4})_2(E^3A\text{-}Am\_\mathbf{3})_2$; $(E^3A\text{-}Al\_\mathbf{4})_2(E^3A\text{-}Am\_\mathbf{6})_1$; $(E^3A\text{-}Al\_\mathbf{6})_1(E^3A\text{-}Am\_\mathbf{4})_2$.

Notably, in addition to the desired product, the mass spectra also indicate the presence of partially assembled intermediates. For example, mass spectra of the trimer and tetramer peptoid co-reactions revealed peaks corresponding to partially-assembled intermediates of $(E^3A\text{-}Al\_\mathbf{3})_3(E^3A\text{-}Am\_\mathbf{4})_2$ for the trialdehyde/tetraamine system, and $(E^3A\text{-}Al\_\mathbf{4})_2(E^3A\text{-}Am\_\mathbf{3})_3$ and $(E^3A\text{-}Al\_\mathbf{4})_2(E^3A\text{-}Am\_\mathbf{3})_2$ for the tetraaldehyde/triamine system. Similarly, for the tetramer and hexamer peptoid co-reactions, additional peaks in the mass spectra are assignable to the intermediate $(E^3A\text{-}Al\_\mathbf{4})_2(E^3A\text{-}Am\_\mathbf{6})_1$ for the tetraaldehyde/hexamine system, and $(E^3A\text{-}Al\_\mathbf{6})_1(E^3A\text{-}Am\_\mathbf{4})_2$ for the hexaaldehyde/ tetraamine system.

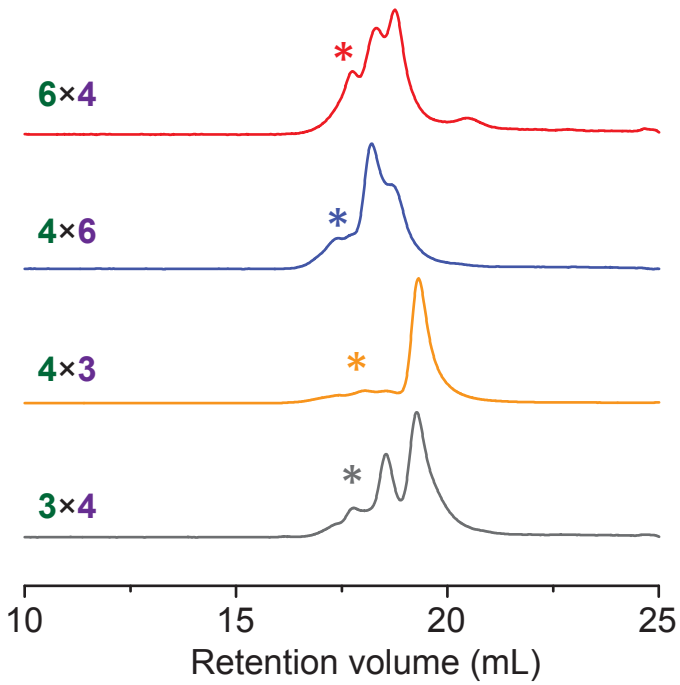

Figure 4.9. GPC traces of Vernier-templated 12-rung molecular ladders.
The traces are normalized to the height of the largest peak. The target ladder structures are labeled with * symbol. VA_Al×Am_**3**×**4**, V_r = 17.78 mL, M_n = 7270 g/mol, PDI = 1.04; VA_Al×Am_**4**×**3**, V_r = 17.81 mL, M_n = 7120 g/mol, PDI = 1.05; VA_Al×Am_**4**×**6**,

V_r = 17.72 mL, M_n = 7700 g/mol, PDI = 1.06; VA_Al×Am_**6**×**4**, V_r = 17.73 mL, M_n = 7650 g/mol, PDI = 1.01.

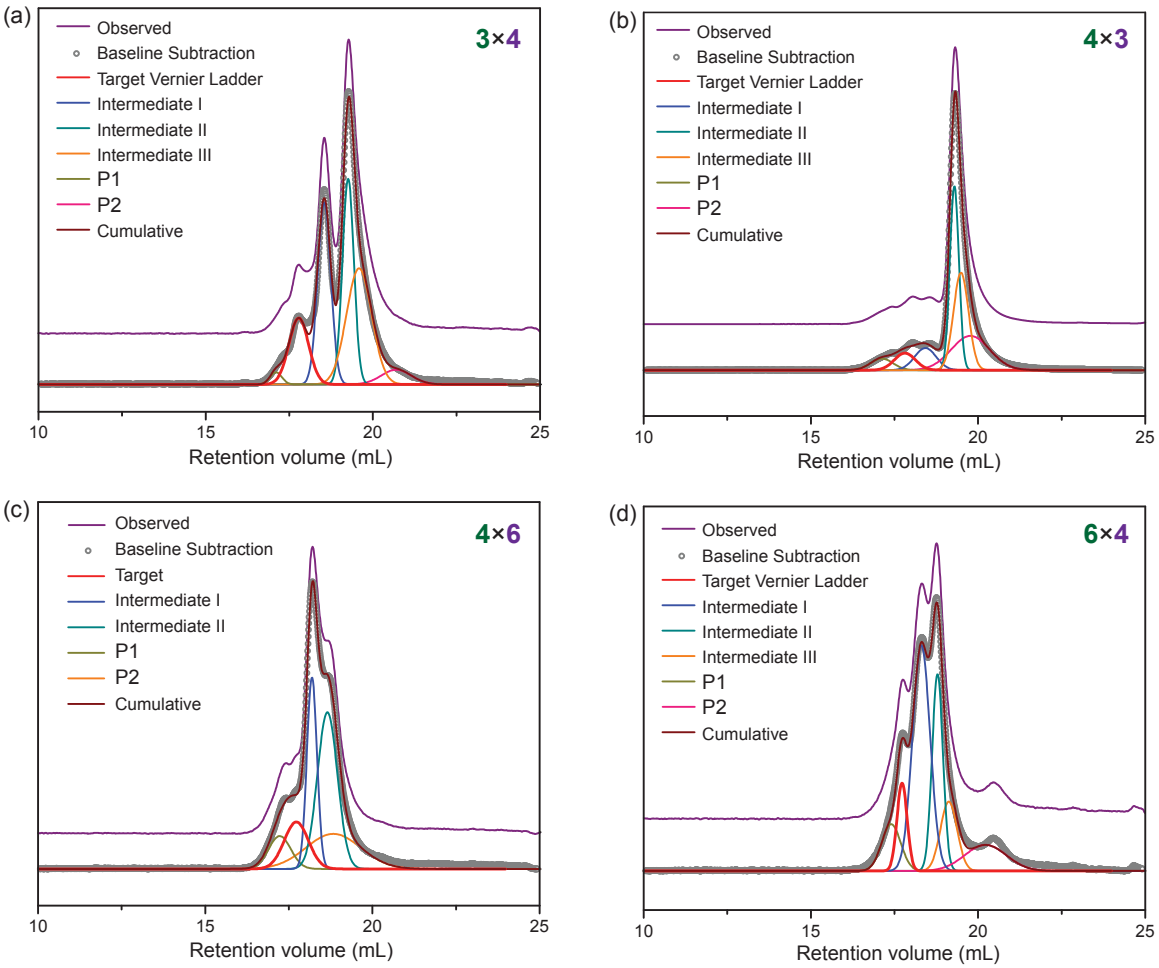

Figure 4.10. Deconvoluted GPC traces of peptoid-based, Vernier-templated 12-rung molecular ladders (a) VA_Al×Am_3×4, (b) VA_Al×Am_4×3, (c) VA_Al×Am_4×6, and (d) VA_Al×Am_6×4 (straight reaction mixtures).
*The target product peak is labeled in red.

Further evidence of Vernier assembly was obtained from GPC as performed on the crude reaction mixtures (**Figure 4.9**). Here, the multiple observed peaks correspond both to the desired 12-rung molecular ladders and to the partially-assembled intermediates. These reaction mixture chromatograms were deconvoluted by automated peak fitting (see Figure 4.10), enabling peaks attributable to the multiple species in the mixtures to be

resolved. By determining the potential structures that could be formed during the assembly process, we assigned the resolved peaks to the desired Vernier ladders and specific intermediate structures (see Table 4.1~Table 4.4).

The area percentages of the desired ladder structures as determined from GPC peak deconvolution were relatively low (~6.5 – 14.7%, Table 4.1~Table 4.4) and no correlation was observed between the precursor oligomer lengths and the 12-rung molecular ladder yield. The resolved peaks assigned to the desired Vernier ladder structures exhibit uniformity with molecular weights closely corresponding to the expected values. However, as the partially-assembled intermediates as determined by GPC peak deconvolution are not wholly consistent with those present in the MALDI mass spectra, we could not rule out the presence of additional, out-of-registry ladder complexes. Despite the extended reaction times and excellent registry observed for the dimerization of complementary $n \times n$ oligopeptoids, the attained mixtures, composed of the desired Vernier ladders and partially-assembled intermediates, may result from sluggish strand exchange amongst the generated molecular ladders. To further examine the origin of this slow elimination of out-of-registry intermediates, we monitored the scrambling of molecular ladders by mass spectrometry.

Table 4.1. Deconvoluted peak analysis of VA_Al×Am_3×4.

Product	Schematic structure	M_n by GPC (g/mol)	Dispersity	Area (%)	Expected M_n (g/mol)
Target	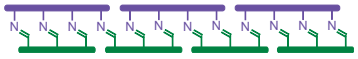	7270	1.04	13.7	7360
Intermediate I	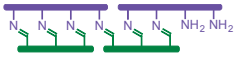	4530	1.01	24.9	4320
Intermediate II	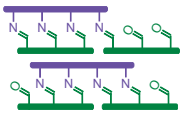	3030	1.01	24.8	3070

Intermediate III	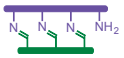	2530	1.04	30.6	2160

Table 4.2. Deconvoluted peak analysis of VA_Al×Am_4×3.

Product	Schematic structure	M_n by GPC (g/mol)	Dispersity	Area (%)	Expected M_n (g/mol)
Target	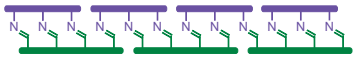	7120	1.05	6.5	7360
Intermediate I	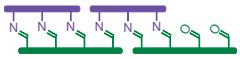	4830	1.04	8.6	4320
Intermediate II	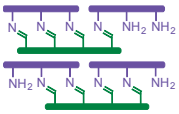	2980	1.01	30.1	3080
Intermediate III	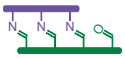	2680	1.01	26.4	2160

Table 4.3. Deconvoluted peak analysis of VA_Al×Am_4×6.

Product	Schematic structure	M_n by GPC (g/mol)	Dispersity	Area (%)	Expected M_n (g/mol)
Target	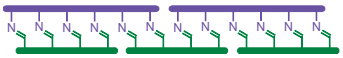	7700	1.06	12.8	7590
Intermediate I	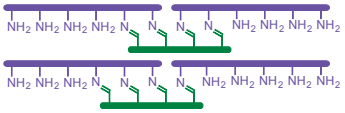	5640	1.01	21.8	5170
Intermediate II	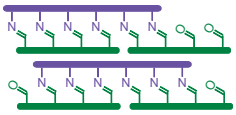	4220	1.03	35.4	4430

Table 4.4. Deconvoluted peak analysis of VA_Al×Am_6×4.

Product	Schematic structure	M_n by GPC (g/mol)	Dispersity	Area (%)	Expected M_n (g/mol)
Target	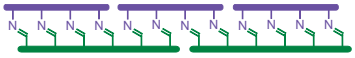	7650	1.01	8.8	7590
Intermediate I	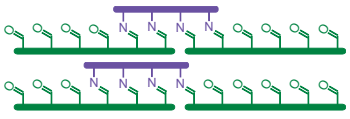	5220	1.03	39.2	5160
Intermediate II	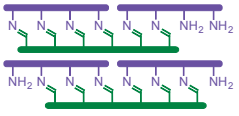	3940	1.01	21.0	4440

Intermediate III	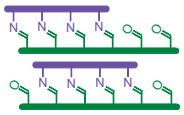	3250	1.02	11.4	3190

4.5.2 Molecular Ladder Scrambling by Strand Exchange

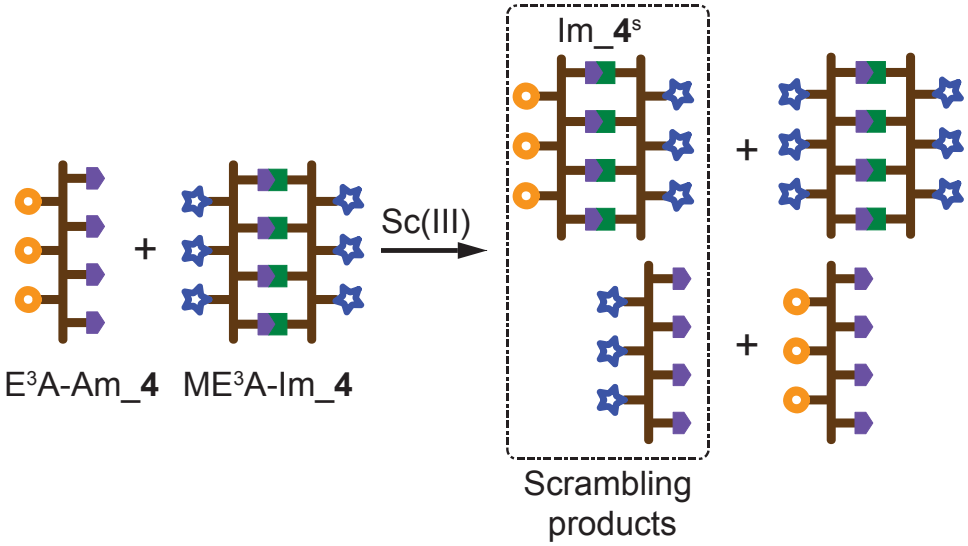

Scheme 4.4. Scrambling between a tetra-amine peptoid strand and a peptoid-based, 4-rung molecular ladder.
*Upon mixing of a tetra-functional single strand and a 4-rung molecular ladder, strand exchange proceeds until an equilibrium mixture of single strands and molecular ladder is afforded.

The Vernier-templated assembly described here involves multiple, simultaneous reactions, including transimination and imine metathesis, to facilitate bond rearrangements and yield the most thermodynamically favored products. As indicated above, in addition to the desired Vernier ladders, we observed the continued presence of intermediate species in the reaction mixtures even after extended reaction times. To determine if the existence of intermediate species is a result of the respective reactions having not reached equilibrium, we performed kinetic studies of peptoid-based molecular ladder scrambling through two different approaches: transimination between a

tetraamine-bearing peptoid and a 4-rung molecular ladder (**Scheme 4.4**), and imine metathesis between two different 4-rung molecular ladders (Scheme 4.5). These tetrafunctional oligomeric species were selected because there are at most four interactions amongst individual strands in the Vernier assemblies. Here, we employed precursor peptoid oligomers bearing different spacer residues such that, upon molecular ladder scrambling, molecular weights of the generated scrambled products differs from their parent molecular ladders, enabling facile detection by MALDI mass spectrometry.[11]

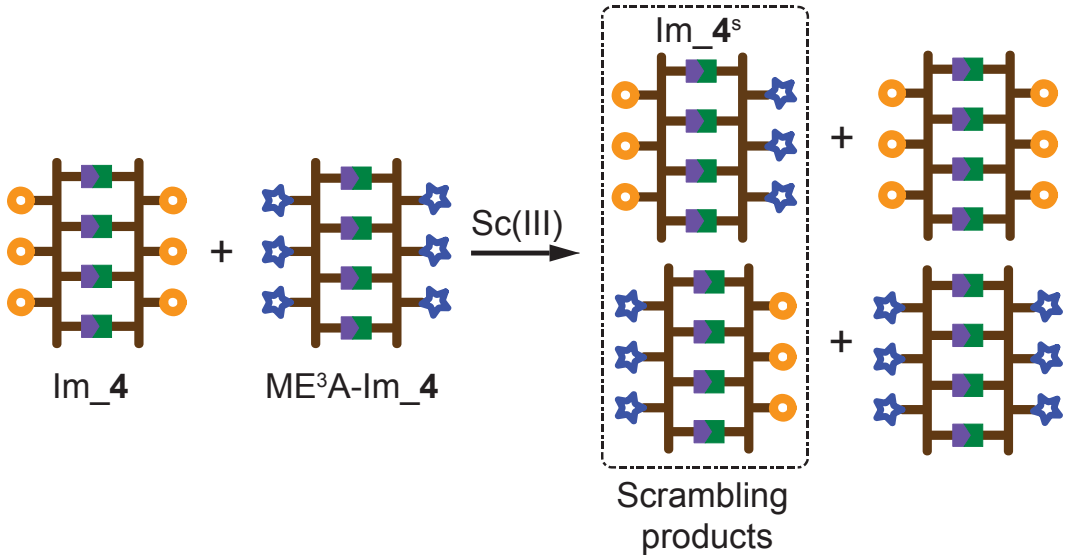

Scheme 4.5. Scrambling between two different 4-rung peptoid-based ladders.
* Upon mixing of the different 4-rung molecular ladders, strand exchange proceeds until an equilibrium mixture of molecular ladders is afforded.

Strand exchange by transimination was examined by utilizing a single-stranded tetraamine peptoid E^3A-Am_**4** in conjunction with ME^3A-Im_**4**, a peptoid-based, 4-rung molecular ladder incorporating 2-(2-(2-methoxyethoxy)ethoxy)ethylamine (ME^3A) as the spacer residue (see Scheme 4.2). E^3A-Am_**4** and ME^3A-Im_**4** were added in a 1:1 stoichiometric ratio to chloroform with a catalytic amount of scandium (III) triflate and

mixed at room temperature. Aliquots of the reaction mixture were examined directly by MALDI mass spectrometry over the course of 9 days to determine the rate and extent of ladder scrambling.

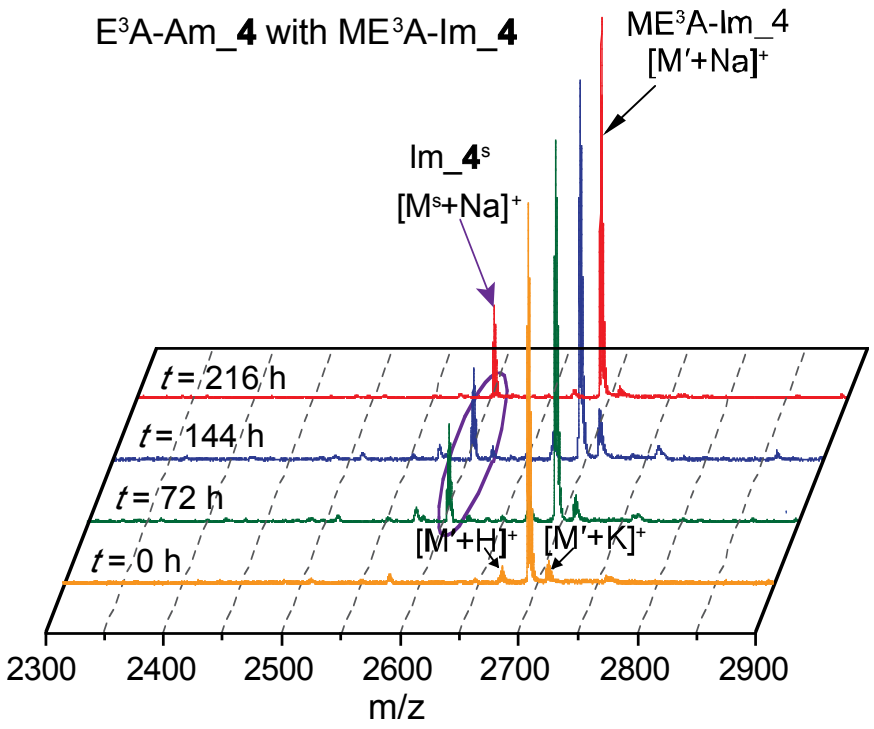

Figure 4.11. MALDI mass spectra of scrambling *via* transimination between E^{3}A-Am_4 and ME^{3}A-HB_4 at different time points.
***** Im_**4**^{s} denotes a scrambled molecular ladder composed of E^{3}A-Am_**4** and ME^{3}A-Al_**4** strands.

MALDI mass spectra of the tetraamine/4-rung molecular ladder reaction mixture (Figure 4.11) demonstrate peaks attributable to both the parent molecular ladder ME^{3}A-Im_**4** and its scrambled product Im_4^{s}, generated by the transimination reaction between ME^{3}A-Im_**4** and E^{3}A-Am_**4**. As shown in Figure 4.13, this transimination-mediated strand exchange proceeds rapidly and scrambling products were observed after 12 hours; indeed, the concentration of the scrambled ladder product plateaus after approximately 72

hours, indicating that equilibrium is reached well within the extended reaction timeframe of the Vernier-templated syntheses.

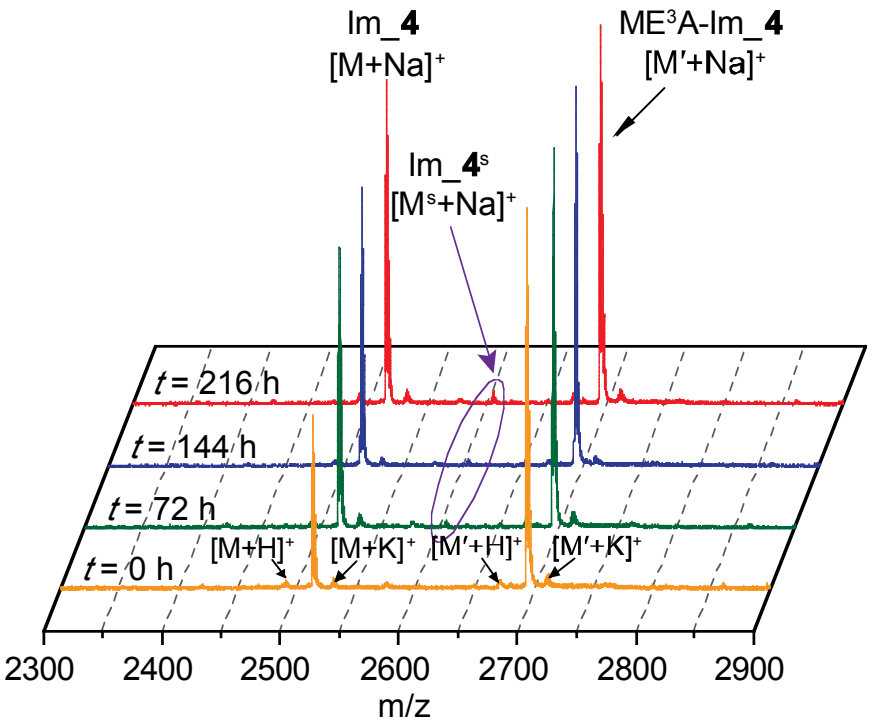

Figure 4.12. MALDI mass spectra of scrambling *via* imine metathesis between Im_4 and ME^{3}A-Im_4 at different time points.
* Im_**4**^{s} denotes scrambled molecular ladders composed either of E^{3}A-Am_**4** and ME^{3}A-Al_**4** or ME^{3}A-Am_**4** and E^{3}A-Al_**4** strands

Strand exchange *via* imine metathesis was also investigated between 4-rung molecular ladders bearing different spacer residues (see Scheme 4.5). Using an experimental approach similar to that employed for molecular ladder scrambling by transimination, the molecular ladder Im_**4**, composed of peptoid oligomers bearing E^{3}A spacer residues, was mixed with ME^{3}A-Im_**4** in a 1:1 stoichiometric ratio in chloroform with a catalytic amount of scandium (III) triflate at room temperature, and aliquots of the reaction mixture were examined by MALDI mass spectrometry. Although peaks

attributable to the parent molecular ladders and the scrambled product are observable in the MALDI mass spectra of the two 4-rung molecular ladder imine metathesis reaction mixture (Figure 4.12), the product concentration is low. Indeed, as shown in Figure 4.13, strand exchange between molecular ladders *via* imine metathesis is particularly sluggish as the concentration of the scrambled product continues to increase even after reaction for over a week, indicating that elimination of the out-of-registry intermediates generated during the Vernier assembly reaction proceeds very slowly. Thus, the strand exchange between molecular ladders *via* imine metathesis likely acts as the rate-determining reaction for this approach to Vernier-templated assembly.

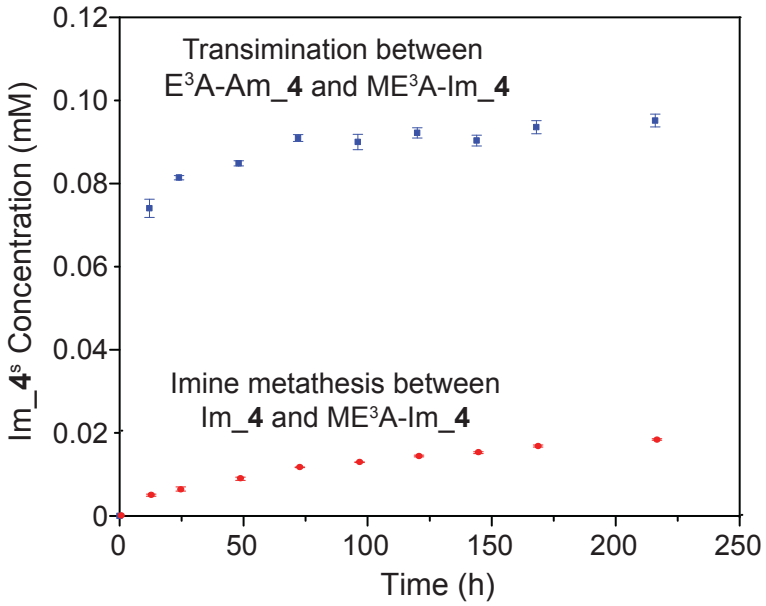

Figure 4.13. Concentration of scrambled molecular ladders versus time during strand exchange *via* transimination or imine metathesis.

4.6 Conclusion

We demonstrated previously molecular ladders containing up to sixteen rungs were successfully and selectively assembled by the Sc(III)-catalyzed dimerization of complementary, amine- and aldehyde-bearing oligopeptoids with commensurate lengths. Nevertheless, to curtail the kinetic trapping of thermodynamically disfavored products inevitably resulting from the hybridization of sufficiently long precursor oligomers, we utilized the Vernier-template directed, dynamic covalent self-assembly of oligomeric peptoids to create large, molecular ladder structures, the lengths of which were pre-determined by the functionalities of the precursor strands. MALDI mass spectrometry and GPC, performed on the reaction mixture after one week reaction time, confirmed the formation of the desired ideal molecular ladder structures in addition to the presence of partially-assembled intermediates. Scrambling experiments indicated that, whereas transimination between an amine-bearing peptoid and a molecular ladder proceeded rapidly, imine metathesis between two different molecular ladders had not reached equilibrium after nine days reaction time; thus, despite the extended reaction time, the continued presence of partially-assembled intermediates in the Vernier assembly mixture was attributed to the slow inter-ladder imine metathesis.

By utilizing dynamic covalent interactions to mediate the self-assembly of complementary sequences, we believe this approach will prove particularly suitable for the fabrication of multi-dimensional nanostructures with unparalleled thermal, chemical and mechanical stability. Additionally, the structural diversity and sequence-specific nature of peptoids make them excellent candidates as construction media for complex nanostructures.

4.7 References

1. O'Sullivan, M. C.; Sprafke, J. K.; Kondratuk, D. V.; Rinfray, C.; Claridge, T. D. W.; Saywell, A.; Blunt, M. O.; O'Shea, J. N.; Beton, P. H.; Malfois, M.; Anderson, H. L., Vernier templating and synthesis of a 12-porphyrin nano-ring. *Nature* **2011,** *469* (7328), 72-75.

2. Hunter, C., Supramolecular Chemistry Bigger and Better Synthesis. *Nature* **2011,** *469* (7328), 39-41.

3. Greschner, A. A.; Bujold, K. E.; Sleiman, H. F., Controlled Growth of DNA Structures From Repeating Units Using the Vernier Mechanism. *Biomacromolecules* **2014,** *15* (8), 3002-3008.

4. Lindsey, J. S., Self-assembly in synthetic routes to molecular devices. Biological principles and chemical perspectives: a review. *New J. Chem.* **1991,** (15), 153-180.

5. Kelly, T. R.; Xie, R. L.; Weinreb, C. K.; Bregant, T., A molecular vernier. *Tetrahedron Lett.* **1998,** *39* (22), 3675-3678.

6. Hunter, C. A.; Tomas, S., Accurate length control of supramolecular oligomerization: Vernier assemblies. *J. Am. Chem. Soc.* **2006,** *128* (27), 8975-8979.

7. Kondratuk, D. V.; Perdigao, L. M. A.; Sullivan, M. C. O.; Svatek, S.; Smith, G.; Shea, J. N. O.; Beton, P. H.; Anderson, H. L., Two Vernier-Templated Routes to a 24-Porphyrin Nanoring. *Angew. Chem. Int. Ed.* **2012,** *51* (27), 6696-6699.

8. Kondratuk, D. V.; Perdigão, L. M. A.; Esmail, A. M. S.; O'Shea, J. N.; Beton, P. H.; Anderson, H. L., Supramolecular nesting of cyclic polymers. *Nature Chemistry* **2015,** *7* (4), 317-322.

9. Li, X.; Hao, C. H.; Tian, C.; Wang, P. F.; Mao, C. D., Vernier assembly: controlling DNA polymerization via length mismatching. *Chem. Commun.* **2014,** *50* (48), 6361-6363.

10. Sun, J.; Stone, G. M.; Balsara, N. P.; Zuckermann, R. N., Structure-Conductivity Relationship for Peptoid-Based PEO-Mimetic Polymer Electrolytes. *Macromolecules* **2012,** *45* (12), 5151-5156.

11. Elliott, E. L.; Hartley, C. S.; Moore, J. S., Covalent ladder formation becomes kinetically trapped beyond four rungs. *Chem. Commun.* **2011,** *47* (17), 5028-5030.

Chapter 5

In Situ Deprotection and Dynamic Covalent Assembly Using a Dual Role Catalyst

5.1 Original Publication Information

Abstract, introduction, experimental and the first three sections of results and discussion are published in the following paper. Modifications have been made to the original document in order to adapt the content to the proper format.

Wei, T.; Furgal J. C.; Scott, T. F., In Situ Deprotection and Dyanmic Covalent Assembly Using a Dual Role Catalyst. *Chem. Commun.* **2017,** *53*, 3874–3877.

5.2 Abstract

Utilization of constituent molecular precursors bearing multiple, coreactive functional groups would significantly increase the structural complexity attainable by dynamic covalent self-assembling systems. However, the synthesis of molecular precursors bearing multiple, covalently coreactive functional group types requires the use of orthogonal protecting groups to eliminate side reactions which result in the formation of cross-linked, intractable materials and impede synthetic and purification efforts. To prevent premature amine-aldehyde condensation for oligomers bearing both groups, we employed a dual-role Lewis acid catalyst scandium(III) triflate for both *in situ* acetal deprotection and subsequent imine exchange, effecting oligomer assembly. We also

optimized the reaction conditions to successfully realize *in situ* deprotection and self-assembly of different oligopeptoid sequences into *n*-rung molecular ladders.

5.3 Introduction

Dynamic covalent chemistry (DCC) refers to covalent bond-forming reactions that are readily reversible or rearrangeable such that the reaction products are under thermodynamic control.[1] Although DCC-based approaches have emerged as useful mechanisms to mediate molecular self-assembly, yielding robust, nanostructured materials,[2-5] the utilization of constituent molecular precursors bearing multiple, coreactive functional groups would significantly increase the structural complexity attainable by dynamic covalent self-assembling systems. Indeed, the utility of employing molecules bearing multiple functional group types that could potentially interact with each other is evident in the exquisite nanostructures capable of being generated by biomacromolecular self-assembly.[6] Unfortunately, the synthesis of molecular precursors bearing multiple, covalently coreactive functional group types requires the utilization of protecting groups to eliminate side reactions owing to premature reaction of the dynamic covalent reactive groups. Moreover, the premature deprotection of these functionalities would result in the generation of cross-linked, intractable material, impeding both purification and, if kinetically-trapped, subsequent self-assembly of the precursor molecules. Thus, utilization of molecular species bearing multiple coreactive functional groups necessitates performing deprotection of at least one of the protecting groups *in situ*.[7-8]

The condensation reaction between amines and aldehydes has proven to be particularly useful for the generation of robust, self-assembled structures[2-4, 9-10] owing to

their synthetic accessibility and the participation of the generated imines in transimination and imine metathesis, molecular rearrangement reactions that are readily catalyzed by rare earth metal (III) triflates with scandium triflate being particularly active.[11] Aldehydes are commonly protected with acid-labile acetal groups,[12] although a limited number of other carbonyl protecting groups are sometimes used.[13] In contrast, a wide variety of functionalities that are labile under diverse reaction conditions have been developed to protect amine groups.[14]

To examine the dynamic covalent assembly of molecules functionalized with coreactive groups, we utilized sequence-specific oligo(peptoid)s (i.e., oligomeric, *N*-substituted glycines)[15] bearing protected aldehyde and amine pendant groups. These peptoid oligomers were generated using Zuckerman's submonomer method which consists of alternating acylation and displacement reactions using a haloacetic acid and a primary amine,[16] necessitating the use of protecting groups able to be compatible with alkaline reaction conditions. For this system, three potential orders of operation could be applied to reveal the reactive functional groups and effect self-assembly, whereby either the aldehyde, the amine, or both protecting groups would be deprotected *in situ*. Importantly, use of oligomers bearing multiple protected dynamic covalent pendant groups necessitates the *in situ* deprotection proceeding to near-completion as any remaining protecting groups would be defects that impede the subsequent self-assembly process.

5.4 Experimental

5.4.1 General Experimental Procedure

All chemicals and reagents, unless specified, were purchased from commercial sources and used as received without any further purification. ^{1}H and ^{13}C NMR spectra were collected using Varian MR400, MR500 and Varian VNMRS 500 spectrometers. Chemical shifts were measured in δ (ppm) relative to residual solvent signals as internal standards (CD_3OD: 4.87 for ^{1}H, 49.15 for ^{13}C; CD_3CN: 1.94 for ^{1}H; DMSO: 2.50 for ^{1}H). Matrix-assisted laser desorption/ionization (MALDI) mass spectra were recorded using a Bruker Autoflex mass spectrometer, whereas electrospray ionization (ESI) mass spectra were recorded using an Agilent Q-TOF 1200 series spectrometer. All MALDI analyses were performed in reflectron positive ion mode using 2-(4-hydroxyphenylazo)benzoic acid (HABA) as the matrix, where 2 μL of a solution of the sample (1 mM) was mixed with 6 μL of a mixture of 6 mg matrix in 300 μL acetonitrile, spotted on a MALDI sample plate (Bruker), and allowed to air dry. Reverse phase high performance liquid chromatography (RP-HPLC) was performed using a Shimadzu LC-6AD HPLC pump, equipped with a Shimadzu FRC 70A fraction collector, using analytical and preparative reversed phase Phenomenex Luna C18(2) columns with a linear gradient of water and acetonitrile as the eluent at 30°C, and monitored with a Shimadzu Prominence UV/vis detector at 214 nm.

5.4.2 Monomer Synthesis

Synthesis of 4-(2-aminoethyl)-*N*-(2-(2-nitrophenyl)propylcarbonyloxy)phenylamine

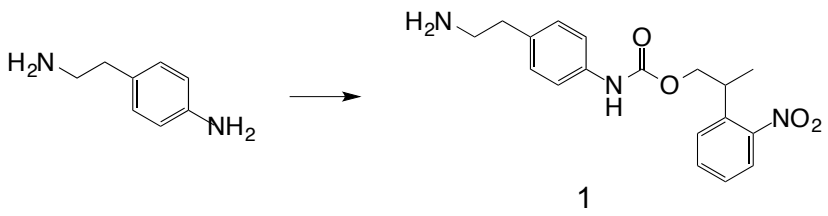

1

Scheme 5.1. Synthesis of 4-(2-aminoethyl)-N-(2-(2-nitrophenyl) propylcarbonyloxy) phenylamine (1). Reagents and conditions: 2-(2-nitrophenyl)propyl chloroformate (NPPOC chloride), 10% aq. acetic acid, 1,4-dioxane, r.t. overnight.

NPPOC chloride (0.58 g, 2.4 mmol) in 20 mL 1, 4-dioxane was added dropwise to a stirred solution of 4-(2-aminoethyl)aniline (0.3 g, 2 mmol) in 20 mL 10% aq. acetic acid at 0°C. The reaction mixture was stirred at room temperature overnight. The reaction mixture was diluted with a large amount of deionized (DI) water and washed with Et_2O three times. The aqueous phase was adjusted to pH 14 by 2 M NaOH (aq) and was extracted with Et_2O three times. The combined organic layer was washed with DI water three times, dried over Na_2SO_4, filtered, and evaporated to dryness to yield **1** as a yellow oil (0.48 g, 70%).

^{1}H NMR (400 MHz, CD_3OD) δ: 7.78 (d, 1H), 7.64-7.70 (m, 2H), 7.43-7.48 (m, 1H), 7.32 (d, 2H), 7.12 (2H), 4.30-4.40 (m, 2H), 3.63-3.70 (m, 1H), 2.85 (t, 2H), 2.71 (t, 2H), 1.41 (d, 3H).

^{13}C NMR (100 MHz, CD_3OD) δ: 155.72, 152.03, 138.42, 135.67, 133.77, 130.08, 129.57, 128.67, 124.97, 120.29, 69.46, 44.21, 39.45, 35.01, 18.36.

MS (ESI+): calcd for $C_{18}H_{21}N_3O_4$: $[M+H]^+$ = 344.1605 $[M+Na]^+$ = 366.1424, found: m/z = 344.1624, $[M+H]^+$, m/z = 366.1422 $[M+Na]^+$.

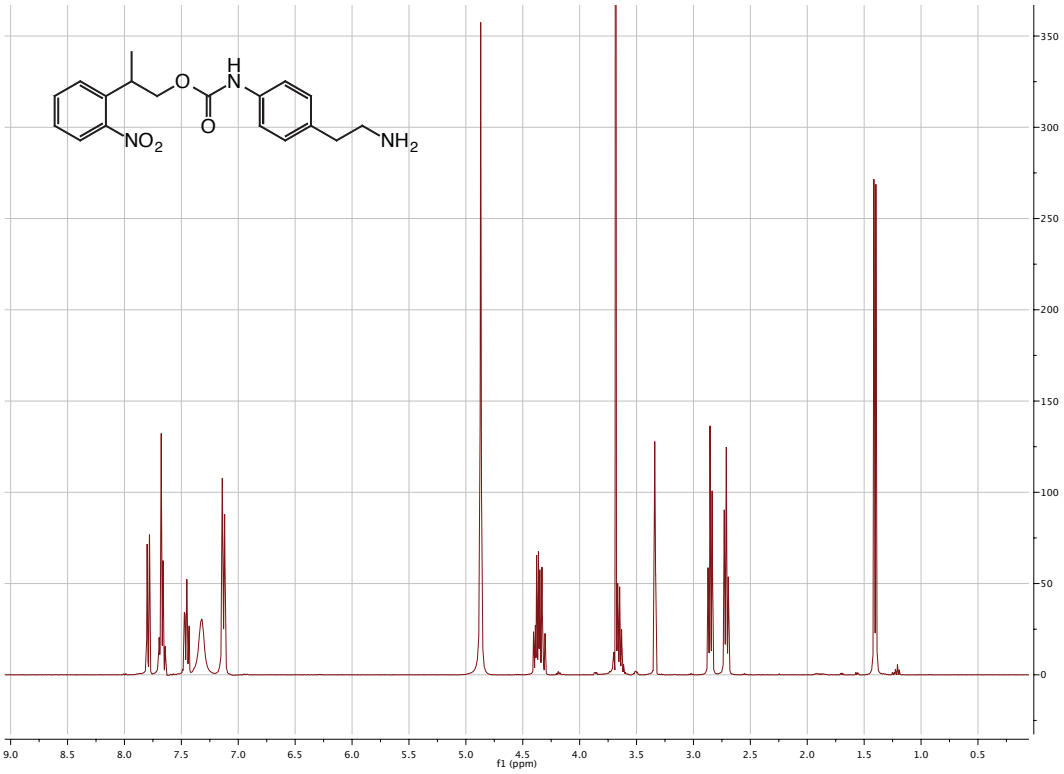

Figure 5.1. ^{1}H NMR spectrum of compound 1.

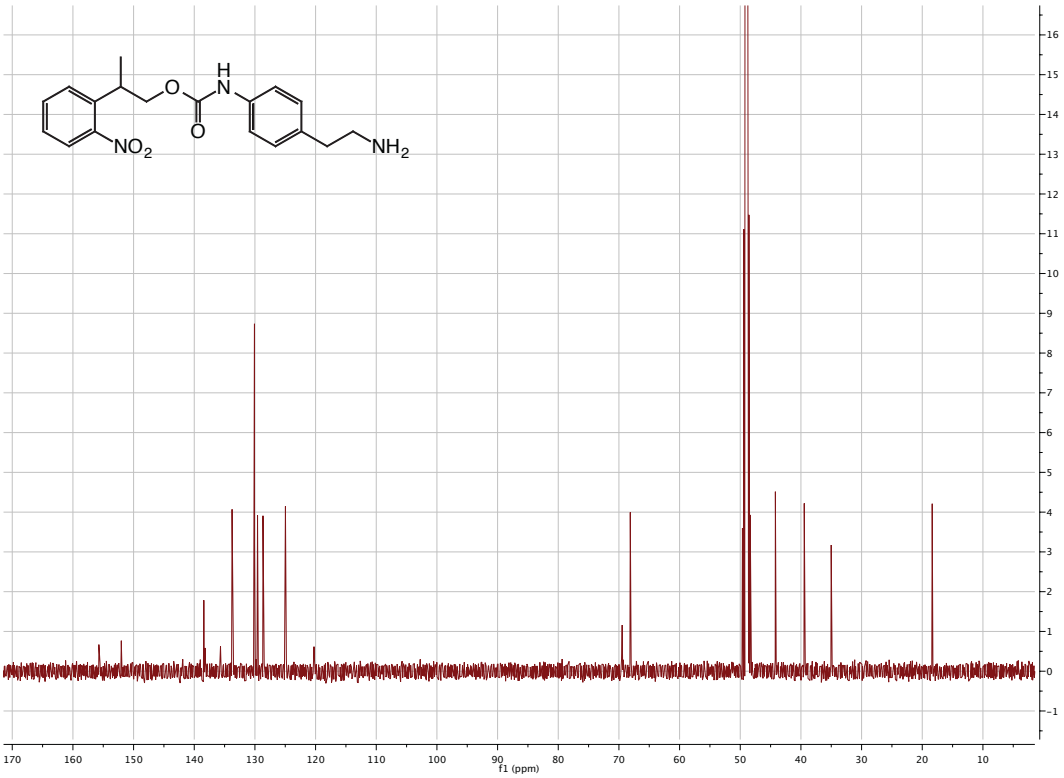

Figure 5.2. ^{13}C NMR spectrum of compound 1.

Synthesis of 4-(2-aminoethyl)-N-(2-(trimethylsilyl)ethoxycarbonyloxy)phenylamine

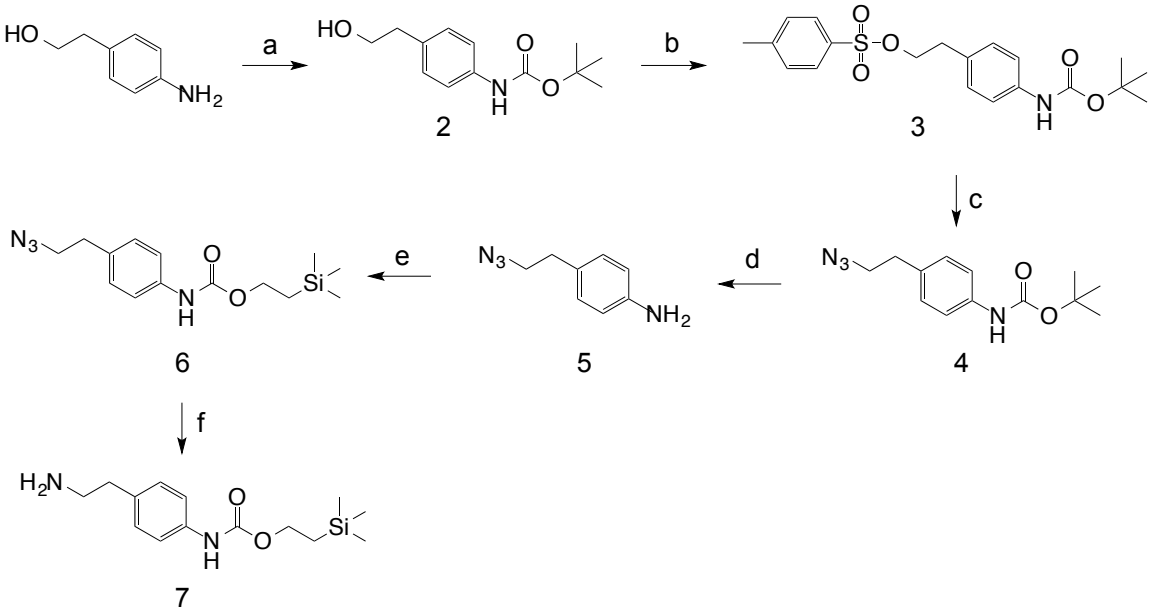

Scheme 5.2. **Synthesis of 4-(2-aminoethyl)-N-(2-(trimethyl)ethoxycarbonyloxy) phenylamine (7).** Reagents and conditions: (a) di-tert-butyl dicarbonate, THF, r.t., overnight; (b) tosyl chloride, THF, 6 M NaOH, 0°C; (c) NaN_3, DMF, 60°C; (d) TFA, DCM, r.t., 30 min; (e) N-[2-(trimethylsilyl) ethoxycarbonyloxy] succinimide, DMF, 60°C, overnight; (f) TPP, THF, DI water.

***tert*-butyl (4-(2-hydroxyethyl)phenyl)carbamate (2).** Di-*tert*-butyl dicarbonate (g, mmol) was added into a solution of 2-(4-aminophenyl)ethanol (2g, 14.6 mmol) in 50 mL THF. The reaction mixture was stirred at room temperature overnight, concentrated by reduced vacuum, and then precipitated in hexanes. The precipitate was filtered and dried under high vacuum to yield white powder (3.24 g, 94%).

^{1}H NMR (500 MHz, CD_3OD) δ: 7.29 (d, 2H, Ar), 7.13 (d, 2H, Ar), 3.71 (t, 2H, -CH_2-OH), 2.75 (t, 2H, -CH_2-Ar), 1.51 (s, 9H, (-CH_3)$_3$).

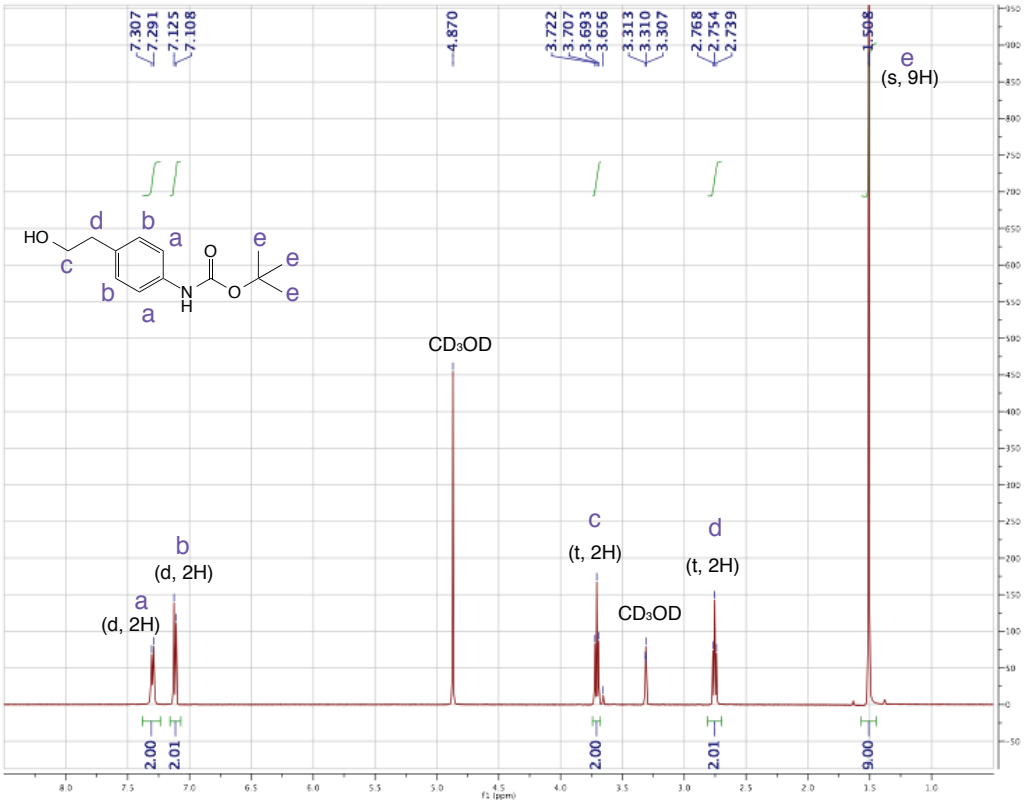

Figure 5.3. ^{1}H NMR spectrum of compound 2.

4-((*tert*-butoxycarbonyl)amino)phenethyl 4-methylbenzenesulfonate (3). Compound **2** (1.68 g, 7.07 mmol) and 10 mL of THF were charged to a 100 mL round bottom flask with a magnetic stirrer. This mixture was cooled to 0°C and 10 mL of 6 M NaOH aq. was added, followed by dropwise addition of tosyl chloride (2.7g, 14.14 mmol) in 20 mL THF under N_2. After stirring for 1 h at 0°C, the reaction mixture was allowed to reach room temperature and stirred overnight. The resulting mixture was extracted with EtOAc and the organic layer was washed with 1 M NaOH and DI water. The solution was evaporated under vacuum and the resultant solids were recrystallized in hexanes with a trace of THF to yield **3** as a white crystalline solid (2.71 g, 98 %).

^{1}H NMR (500 MHz, DMSO) δ: 9.26 (s, 1H, -N*H*-COO-), 7.64 (d, 2H, -S-C=C*H*-CH), 7.30 (d, 2H, -S-C=CH-C*H*), 7.30 (d, 2H, -CH_2-C=CH-C*H*), 7.01 (d, 2H, -CH_2-C=C*H*-CH), 4.17 (t, 2H, -SO_2-O-CH_2-), 2.79 (t, 2H, -CH_2-CH_2-Ar), 2.40 (s, 3H, -Ar-CH_3), 1.47 (s, 9H, $(-CH_3)_3$).

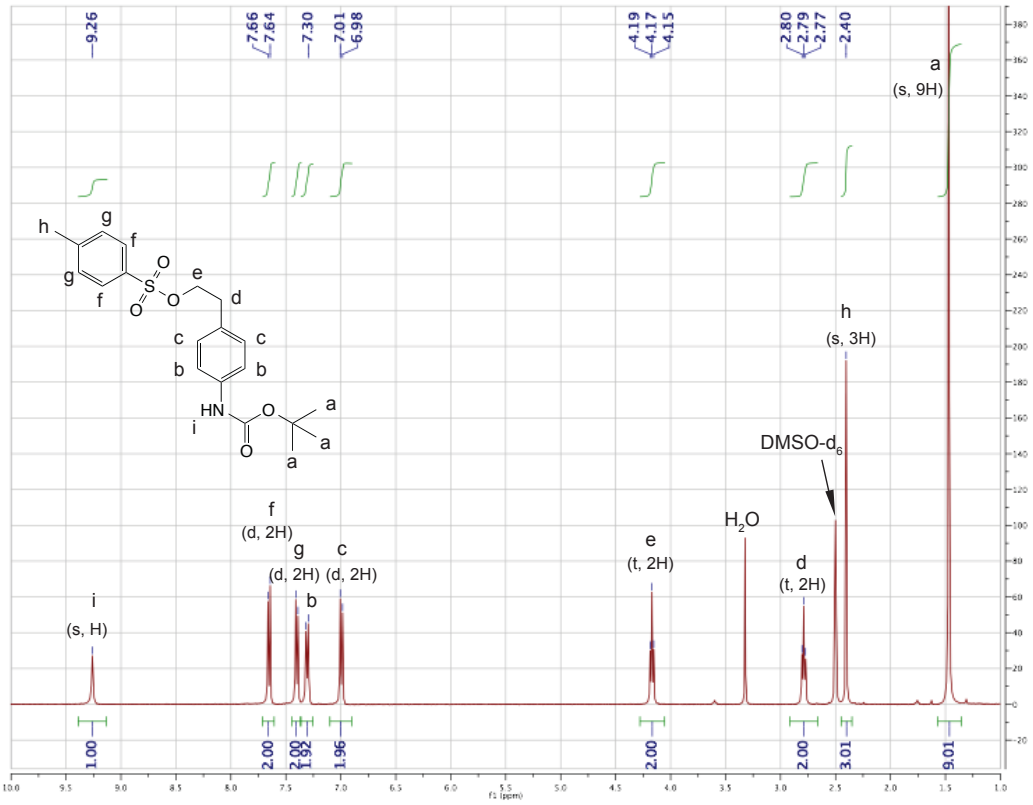

Figure 5.4. ^{1}H NMR spectrum of compound 3.

***tert*-butyl (4-(2-azidoethyl)phenyl)carbamate (4).** NaN_3 (0.6 g, 8.2 mmol) was added into a solution of compound **3** (1.5 g, 3.83 mmol**)** in 20 mL of DMF. The reaction mixture was purged with N_2, stirred at 60°C for 36 h, and then cooled to room temperature. The reaction mixture with diluted with a large amount of water and

extracted with extracted with EtOAc. The organic layer was washed with water, dried over $NaSO_4$, and evaporated under vacuum to afford **4** as an off-white solid (0.90 g, 90%).

^{1}H NMR (500 MHz, CD_3OD) δ: 7.33 (d, 2H, -CH_2-C=CH-C*H*), 7.16 (d, 2H, -CH_2-C=C*H*-CH), 3.47 (t, 2H, -CH_2-CH_2-Ar), 2.82 (t, 2H, N_3-CH_2-CH_2-Ar), 1.52 (s, 9H, (-CH_3)$_3$).

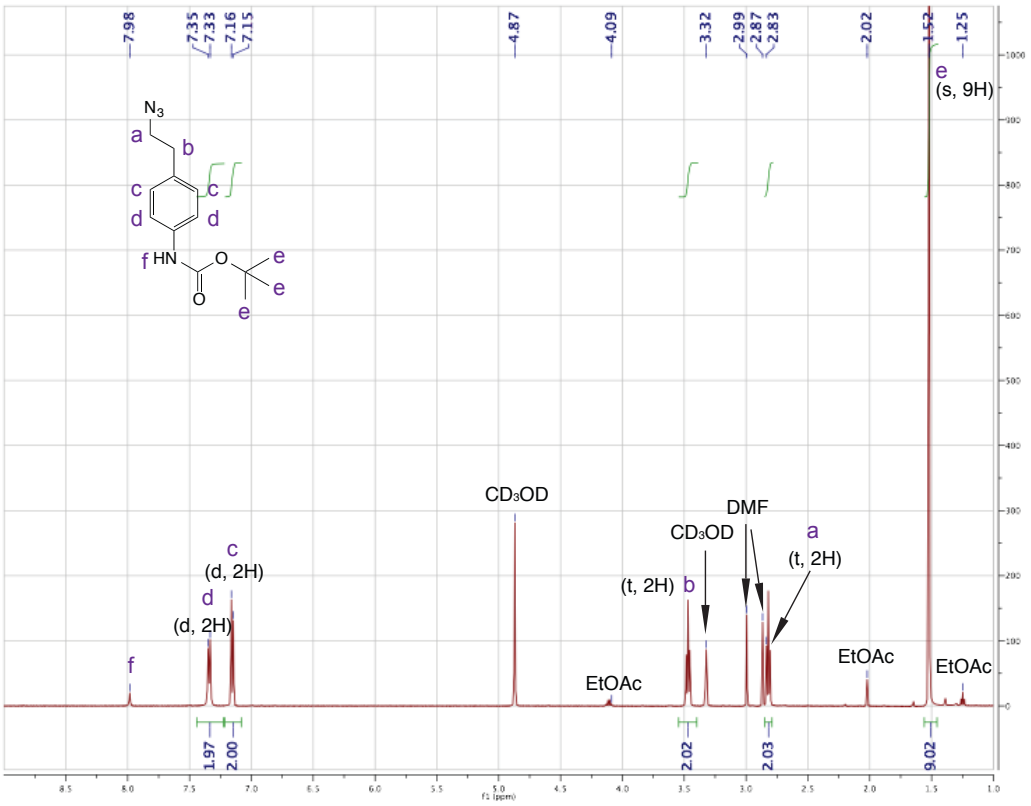

Figure 5.5. ^{1}H NMR spectrum of compound 4.

4-(2-azidoethyl)aniline (5). Compound **4** (0.9 g, 3.50 mmol) was subjected to 20% of TFA in DCM (v/v, 20 mL) at room temperature for 30 min. After concentrated under reduced vacuum, the mixture was dissolved in water, treated with saturated $NaHCO_3$ to

adjust pH to 8, subsequently extracted with EtOAc three times. The organic layers were combined, washed with DI water three times, dried over Na_2SO_4, filtered, and evaporated to dryness to yield **5** as a yellow oil (0.45 g, 79%).

^{1}H NMR (500 MHz, CD_3OD) δ: 6.99 (d, 2H, -CH_2-C=C*H*-CH), 6.70 (d, 2H, -CH_2-C=CH-C*H*), 3.47 (t, 2H, -CH_2-CH_2-Ar), 2.82 (t, 2H, N_3-CH_2-CH_2-Ar).

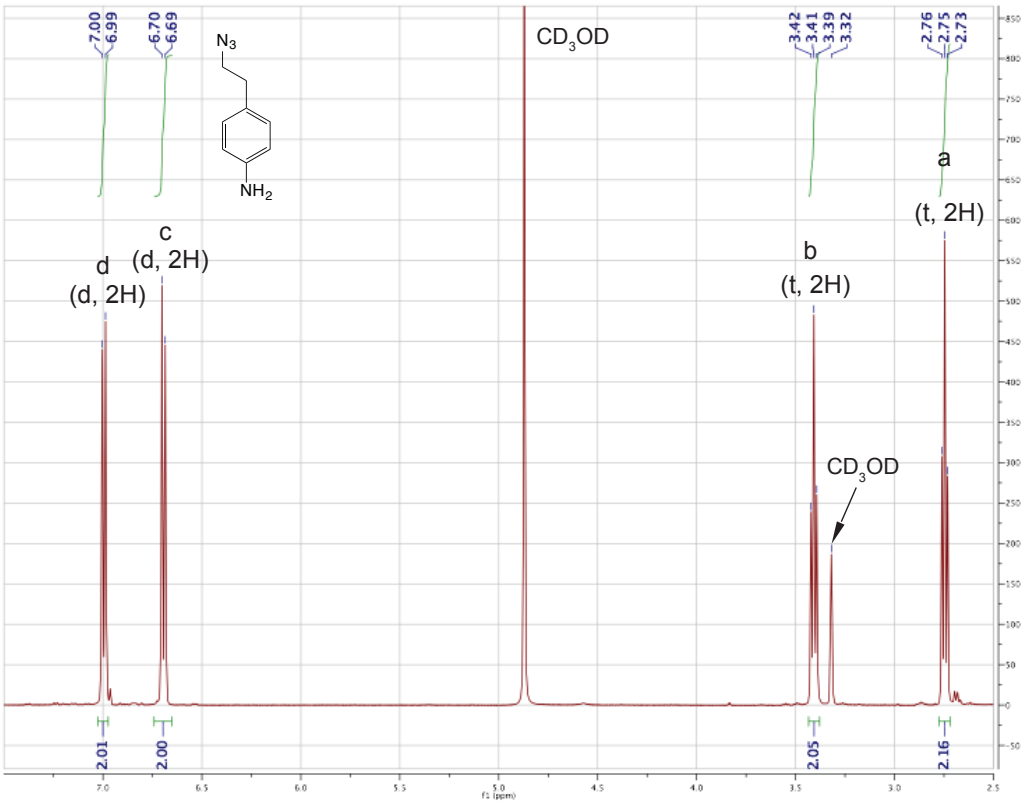

Figure 5.6. ^{1}H NMR spectrum of compound 5.

2-(trimethylsilyl)ethyl (4-(2-azidoethyl)phenyl)carbamate (6). *N*-[2-(trimethylsilyl) ethoxycarbonyloxy] succinimide (0.84 g, 3.24 mmol) was added into a solution of compound **5** (0.50 g, 3.08 mmol) in 30 mL DMF. The reaction mixture was stirred at 60°C overnight, then cooled to room temperature and concentrated by reduced vacuum.

The crude product was purified by silica gel column chromatography using 3:1 HEX/EtOAc (v/v) to yield **6** as a white crystalline solid (0.95 g, 96%).

^{1}H NMR (500 MHz, CD_3CN) δ: 7.61 (s, 1H, -N*H*-COO-), 7.37 (d, 2H, -CH_2-C=CH-C*H*), 7.17 (d, 2H, -CH_2-C=C*H*-CH), 4.21 (t, 2H, -O-CH_2-CH_2-Si-), 3.48 (t, 2H, -CH_2-CH_2-Ar), 2.82 (t, 2H, N_3-CH_2-CH_2-Ar), 1.03 (t, 2H, -O-CH_2-CH_2-Si-), 0.05 (s, 9H, -Si-(CH_3)$_3$).

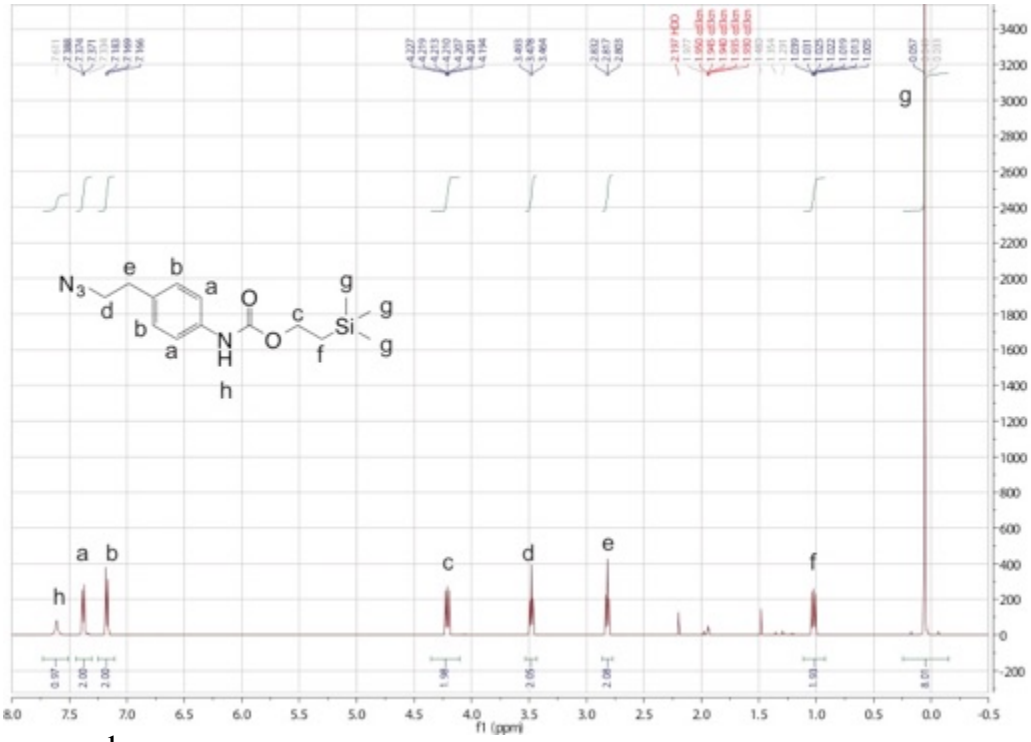

Figure 5.7. ^{1}H NMR spectrum of compound 6.

4-(2-aminoethyl)-N-(2-(trimethylsilyl)ethoxycarbonyloxy)phenylamine (7).

Triphenylphosphine (0.89 g, 3.42 mmol) was added into a solution of compound **6** (0.95 g, 3.11 mmol) in 20 mL THF. The reaction mixture was stirred at room temperature overnight under N_2.The reaction mixture was quenched with 28 mL water, allowed to stir for another day, and concentrated to yield viscous oil. The oil was further purified on a

silica gel column, initially flushed with EtOAc and subsequently eluted with a 9/1 to 8/2 chloroform/methanol (v/v) gradient. The fractions were combined and evaporated to yield **7** as an off-white solid (0.62, 71%).

^{1}H NMR (500 MHz, CD_3CN) δ: 7.94 (s, 1H, -N*H*-COO-), 7.33 (d, 2H, -CH_2-C=CH-C*H*), 7.09 (d, 2H, -CH_2-C=C*H*-CH), 4.17 (t, 2H, -O-C*H*$_2$-CH_2-Si-), 2.78 (t, 2H, NH_2-C*H*$_2$-CH_2-Ar), 2.61 (t, 2H, NH_2-CH_2-C*H*$_2$-Ar), 1.00 (t, 2H, -O-CH_2-C*H*$_2$-Si-), 0.01 (s, 9H, -Si-(CH_3)$_3$).

MS (ESI+): calcd for $C_{14}H_{24}N_2O_2Si$: $[M+H]^+$ = 281.1680 $[M+Na]^+$ = 303.1499, found: *m*/*z* = 281.1728, $[M+H]^+$, *m*/*z* = 303.1510 $[M+Na]^+$.

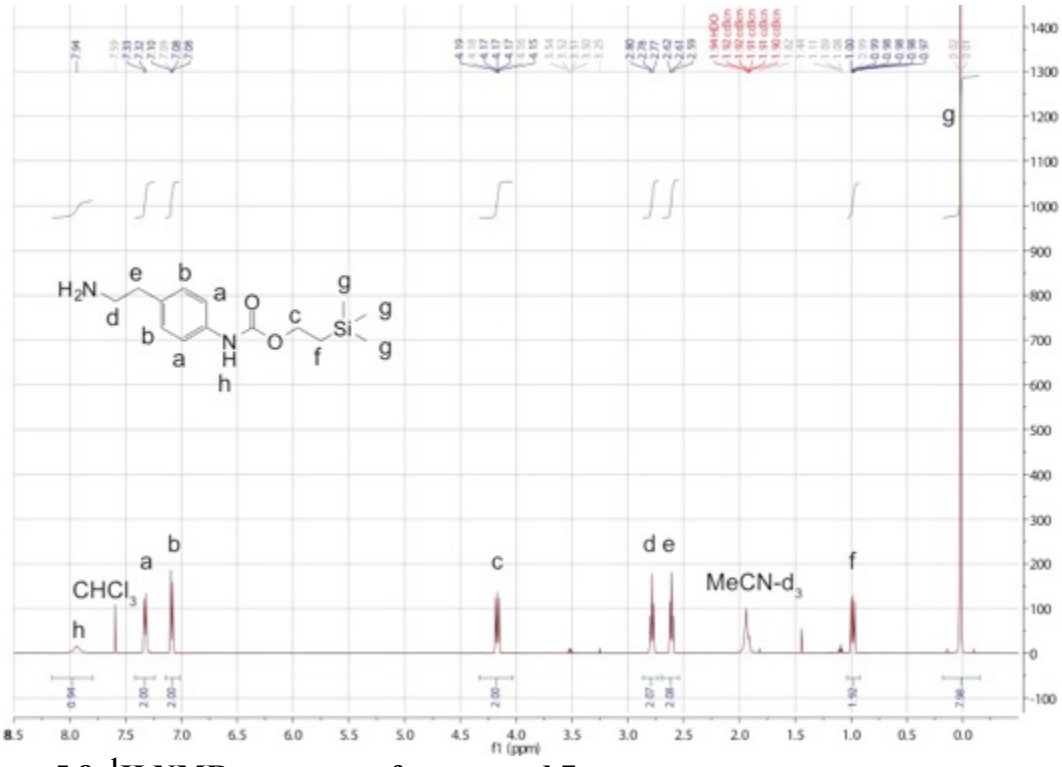

Figure 5.8. ^{1}H NMR spectrum of compound 7.

Synthesis of 4-(2-aminoethyl)-N-(allylcarbonyloxy)phenylamine

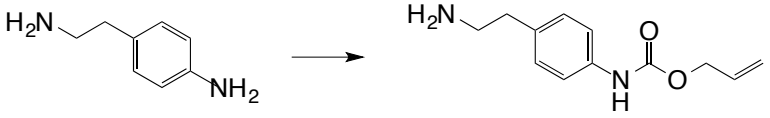

8

Scheme 5.3. Synthesis of 4-(2-aminoethyl)-N-(allylcarbonyloxy)phenylamine. Conditions: allyl chloroformate, 10% aq. acetic acid, 1,4-dioxane, r.t. overnight.

Allyl chloroformate (4.9 g, 40.4 mmol) in 150 mL 1,4-dioxane was added into to a solution of 4-(2-aminoethyl)aniline (5 g, 36.7 mmol) in 150 mL 10% aq. acetic acid. The reaction mixture was stirred at room temperature overnight and then diluted with 500 mL deionized (DI) water and washed with Et_2O (300 mL) three times. The aqueous phase was adjusted to pH 14 by addition of 2 M NaOH (aq) and was extracted with Et_2O (150 mL) three times. The combined organic layer was washed with DI water three times, dried over Na_2SO_4, filtered, and evaporated to dryness to yield **1** as a light yellow solid (5.6 g, 69%).

^{1}H NMR (500 MHz, CD_3OD) δ: 7.36 (d, 2H, Ar), 7.15 (d, 2H, Ar), 5.95-6.04 (m, 1H, -C*H*=CH_2), 5.39 (d, 1H, -CH=C*H*H), 5.34 (d, 1H, -CH=CH*H*), 4.63 (d, 2H, -CH_2-CH=CH_2), 2.82-2.86 (m, 2H, -CH_2-NH_2), 2.70 (t, 2H, -CH_2-Ar).

^{13}C NMR (125 MHz, CD_3OD) δ: 154.85, 137.00, 134.98, 133.51, 129.36, 119.41, 116.92, 65.62, 59.89,

43.47, 38.72.

MS (ESI+): calcd for $C_{12}H_{16}N_2O_2$: $[M+H]^+$ = 221.1285 $[M+Na]^+$ = 243.1104, found: *m*/*z* = 221.1286, $[M+H]^+$, *m*/*z* = 243.1101 $[M+Na]^+$.

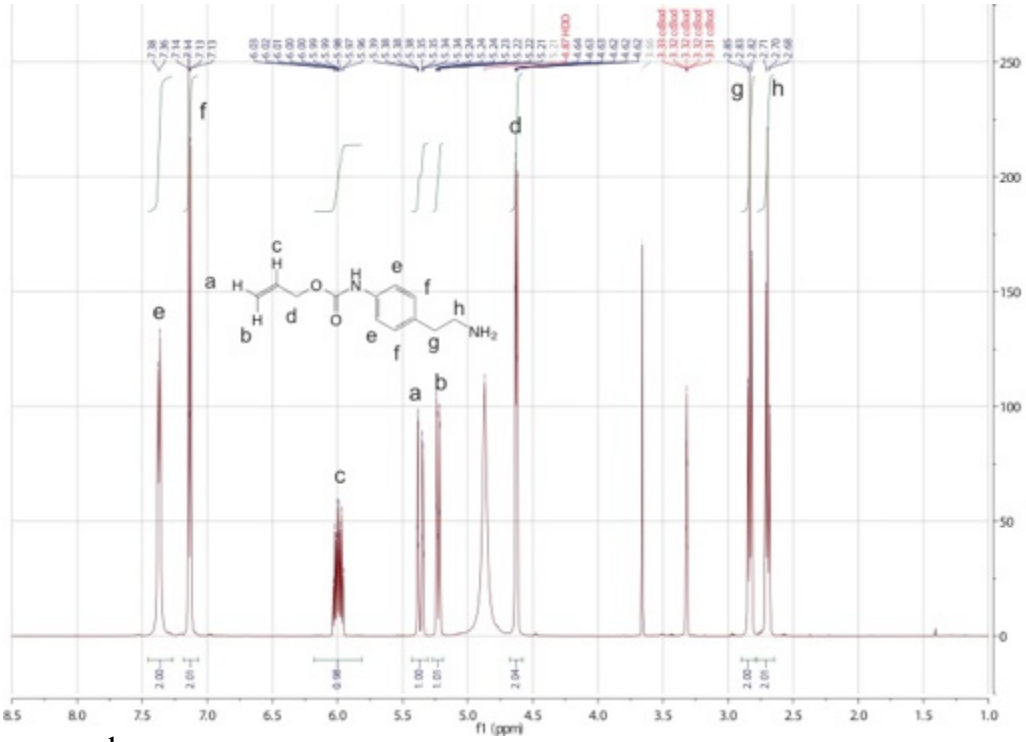

Figure 5.9. ^{1}H NMR spectrum of compound 8.

5.4.3. Solid-phase Synthesis of Oligo(peptoid)s

The synthesis of oligo(peptoid) NPPOC-Am_**3** was performed on 222 mg of Rink amide resin (0.1 mmol scale, 100-200 mesh, 1% DVB, ChemPrep Inc.), whereas oligo(peptoid)s Teoc-Am_**4**, ActAl_**4**, ActAl_**2**-Am_**2** and ActAl_**4**-Am_**4** were synthesized on Fmoc-Photolabile SS (0.1 mmol scale, 100-200 mesh, 1% DVB, Advanced ChemTech). All solid-phase peptoid syntheses were performed using an automated microwave peptide synthesizer (Liberty Blue, CEM Corporation). Three primary amine monomers, 4-(1,3-dioxacyclopent-2-yl)benzylamine, 2-(2-ethoxyethoxy) ethylamine (E^3A), and 2-(2-(2-methoxyethoxy)ethoxy)ethyl amine (ME^3A) were synthesized according to a published approach.[17] 4-(2-aminoethyl)-N-(2-(2-nitrophenyl) propylcarbonyloxy)phenylamine (**1**), 4-(2-aminoethyl)-N-(2-(trimethylsilyl) ethoxy-

carbonyloxy) phenylamine (**7**), and 4-(2-aminoethyl)-N-(allylcarbonyloxy) phenylamine (**8**) were synthesized as described above. All other monomers, reagents, and solvents were purchased from commercial sources and directly used without further purification. Oligo(peptoid)s were synthesized according to a published submonomer approach to solid-phase peptoid synthesis.[17] The resin was swelled for 5 min at room temperature and subsequently deprotected with 20% 4-methylpiperidine in DMF (v/v) for 30 s at 75°C and 90 s at 90°C, followed by bromoacetylation for 5 min at 75°C with simultaneous addition of 1.5 mL of 1.0 M bromoacetic acid in DMF and 1.5 mL of 1.0 M DIC in DMF. Halide displacement was then carried out by adding 2.5 mL of 0.5 M primary amine monomer in NMP followed by an incubation of 5 min at 75°C. These bromoacetylation and displacement reactions were alternated until the desired peptoid sequence was achieved. All synthesized oligo(peptoid)s were acetylated by treatment with acetic anhydride to cap the secondary amine end groups.

TFA cleavage from the resin

TFA cleavage procedure was followed by a published approach.[10] The resultant Rink amide resin containing oligopeptoid NPPOC-Am_**3** was transferred to a 25 mL solid-phase peptide synthesis vessel (CG-1866, Chemglass), rinsed with DCM three times, and further treated with 4 mL of TFA cleavage cocktail (95% TFA in DCM) for 10 min while bubbling with nitrogen at room temperature. The TFA cleavage solution was collected by filtering through the fritted glass into a 25 mL round bottom flask. The remaining resin was further rinsed twice with 2 mL of fresh TFA cleavage cocktail to collect any residual

oligo(peptoid). The cleavage solution was combined and evaporated by blowing a gentle stream of nitrogen to yield crude oligo(peptoid) NPPOC-Am_**3**, the structure of which is shown in Figure 5.10. The crude product was reconstituted in HPLC grade 50% MeCN/water (v/v) and further purified by preparative HPLC.

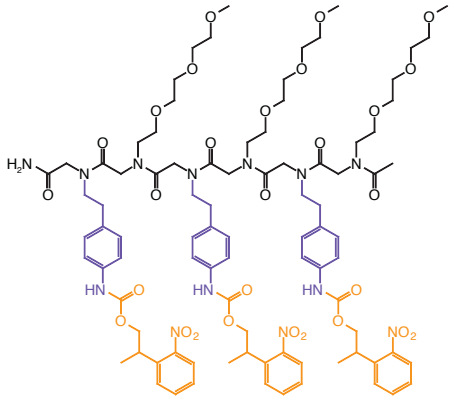

Figure 5.10. Chemical structure of oligopeptoid NPPOC-Am_3.

Photo-cleavage from the resin

The resultant Fmoc-photolabile resins were suspended in 10 mL DMF in 20 mL glass vial respectively and, after purging with nitrogen for 1 min, the vial capped and the suspension stirred while under irradiation at approximately 25 $mW.cm^{-2}$ with 405 nm for 36 h. The DMF cleavage solution was collected by filtering the suspension through a glass frit and were pooled and evaporated to dryness under vacuum to yield crude oligo(peptoid)s ActAl_**2**–Boc-Am_**2**, Teoc-Am_**4**, and ActAl_**4** as light yellow oils (shown in Figure 5.11). Each crude product was reconstituted in 50% HPLC grade MeCN/H_2O and further purified by preparative RP-HPLC.

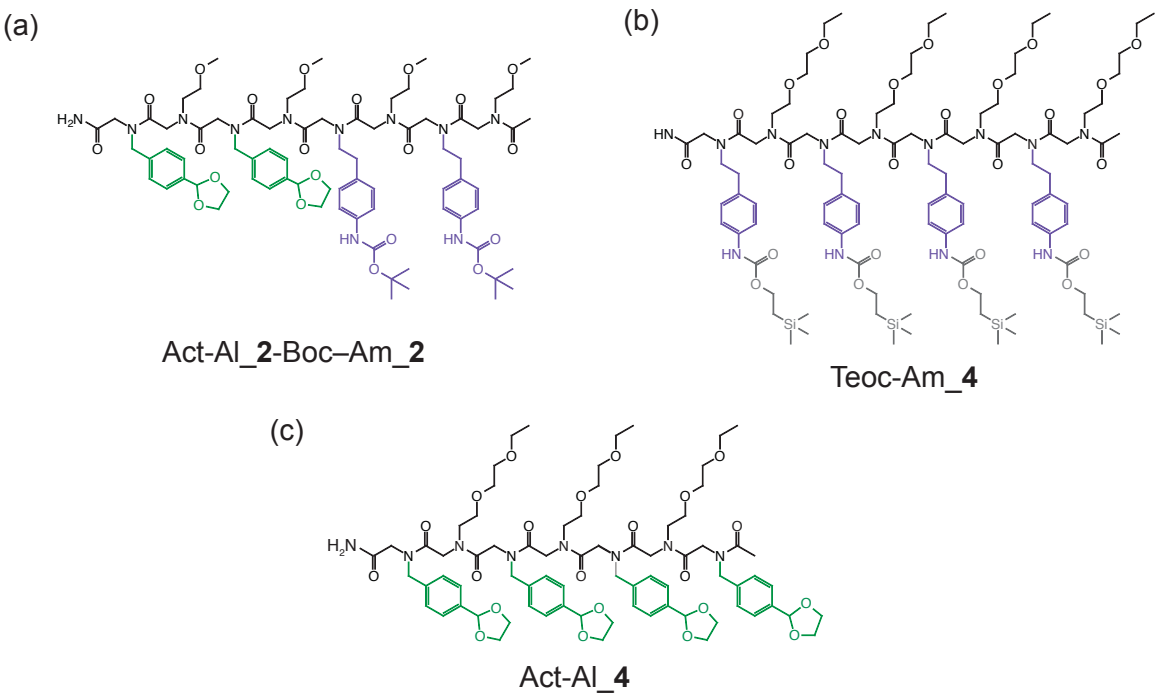

Figure 5.11. Chemical structures of oligopeptoids (a) Act-Al_2-Boc-Am_2, (b) Teoc-Am_4 and (c) Act-Al_4.

The method to remove Alloc protecting groups was adapted from a published approach.[18] Resin (0.1 mmol, 0.75 mmol/g) was suspended in dry DCM (0.4 mL) and subjected to Alloc deprotection by treatment with phenylsilane ($PhSiH_3$, 0.62mL, 5 mmol, 25 eq. per Alloc group) and tetrakis(triphenylphosphine) palladium(0) [$Pd(PPH_3)_4$, 23.1 mg, 0.02 mmol, 0.1 eq. per Alloc group] at room temperature for 1 h. Reagents and solvent were removed by filtration under reduced pressure, the resin was washed with dry DCM, and the deprotection procedure was repeated twice. The resin was finally washed with DCM and MeOH, dried and further subjected to photo-cleavage *via* the aforementioned approach to yield oligo(peptoid) Act-Al_**2**–Am_**2**. Oligo(peptoid) Act-Al_**4**–Am_**4** was prepared using the same approach. The crude product was reconstituted in 20% ~ 30% HPLC grade MeCN/H_2O and further purified by preparative RP-HPLC.

Alloc deprotection and photo-cleavage

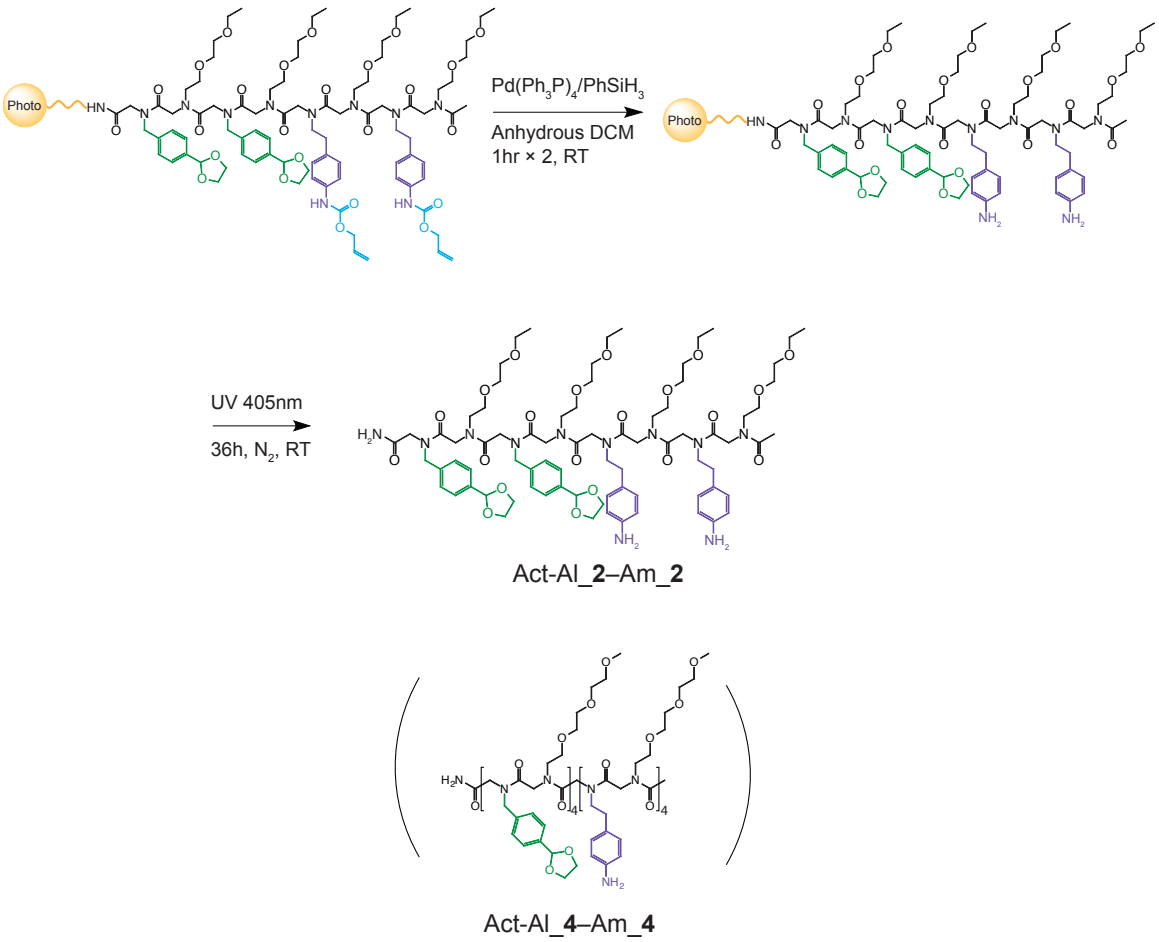

Scheme 5.4. Synthetic procedure for oligo(peptoid)s Act-Al_2–Am_2 and Act-Al_4–Am_4.

Purification of Oligo(peptoid)s by Preparative RP-HPLC

All oligo(peptoid)s were purified by preparative RP-HPLC using a linear gradient of H_2O (A) and MeCN (B) at a flow rate of 10 mL/min. The purified fractions were combined, concentrated, reconstituted in 50% MeCN/H_2O (v/v), frozen with liquid

nitrogen, and lyophilized to afford fluffy white powder. The purity of the collected oligo(peptoid)s was examined by analytical RP-HPLC.

Preparative HPLC method:

(1) Act-Al_**2**–Boc-Am_**2**: (a) 30%, 0.1 – 4.1 min; (b) 30% – 85%, 4.1 min – 22.5 min; (c) 85% – 30%, 22.5 min – 24.5 min.

(2) NPPOC-Am_**3**: (a) 50%, 0.1 – 4.1 min; (b) 50% – 90%, 4.1 – 30.1 min; (c) 90% – 50%, 30.1 – 32.1 min.

(3) Teoc-Am_**4**: (a) 75%, 0.1 – 2.1 min; (b) 75% – 95%, 2.1 min – 18.1 min: (c) 95%, 18.1 min – 26.1 min; (d) 95% – 75%, 26.1 min – 28.1 min.

(4) Act-Al_**4**: (a) 30% B, 0.1 – 4.1 min; (b) 30% – 75% B, 4.1 – 26.1 min; (c) 75% – 30% B, 26.1 – 28.1 min.

(5) ActAl_**2**–Am_**2**: (a) 30% B, 0.1 – 4.1 min; (b) 30% – 70% B, 4.1 – 24.1 min; (c) 70% – 30% B, 24.1 – 26.1 min.

(6) ActAl_**4**–Am_**4**: (a) 30%, 0.1 – 4.1 min; (b) 30% – 80%, 4.1 min – 33.1 min; (c) 80% – 30%, 33.1 min – 35.1 min.

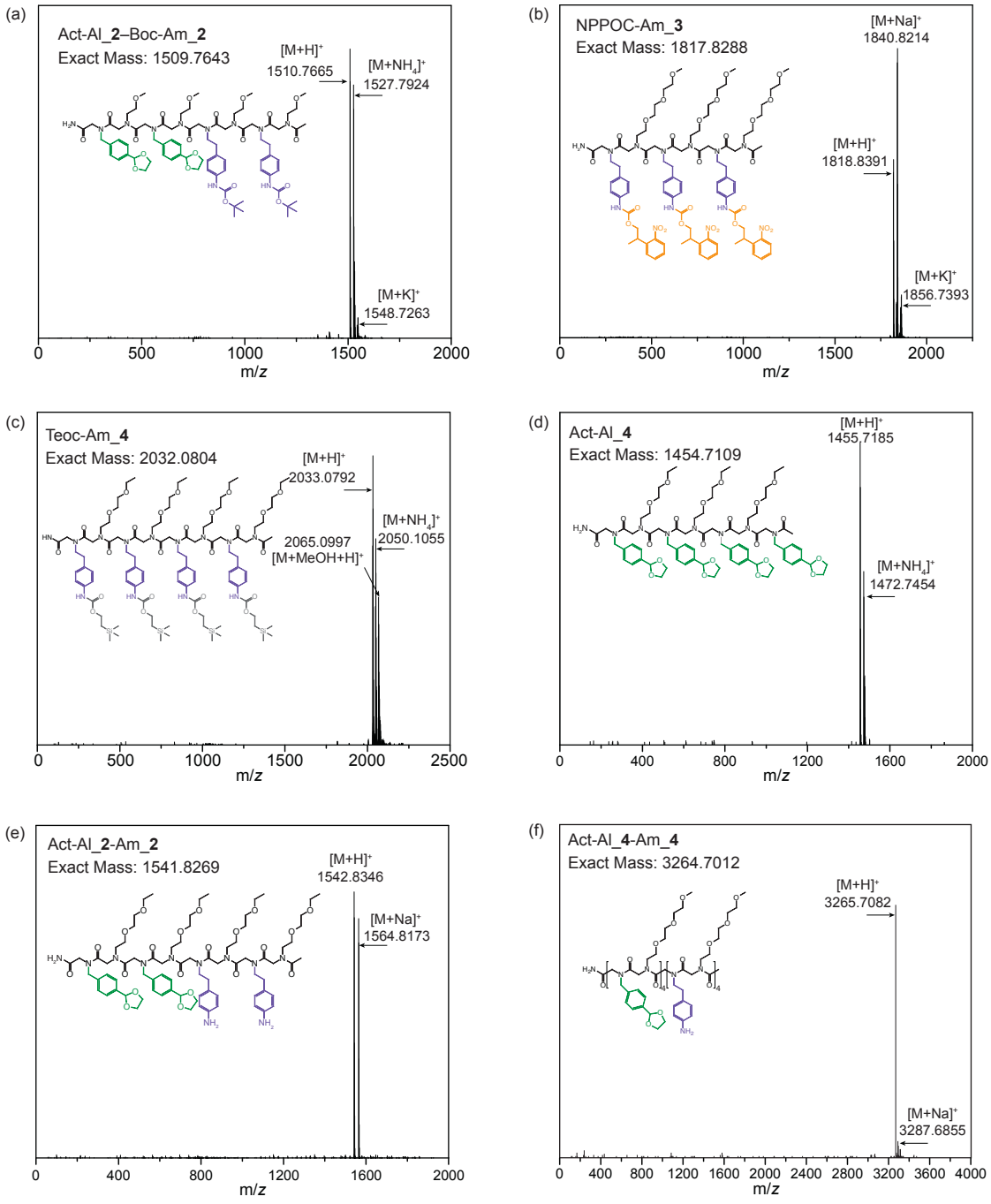

Figure 5.12. ESI spectra of oligo(peptoid)s purified by preparative HPLC. (a) Act-Al_**2**–Boc-Am_**2**: expected $[M+H]^+$ = 1510.7716, $[M+NH_4]^+$ = 1527.7981, $[M+K]^+$ = 1548.7274, purity: 99.2%; (b) NPPOC-Am_**3**: expected $[M+H]^+$ = 1818.8361, $[M+Na]^+$ = 1840.8180, $[M+K]^+$ = 1856.7920, purity: 99.0%; (c) Teoc-Am_**4**: expected $[M+H]^+$ = 2033.0877, $[M+NH_4]^+$ = 2050.1142, $[M+MeOH+H]^+$ = 2065.1139, purity: 99.3%; (d) Act-Al_**4**: expected $[M+H]^+$ = 1455.7182, $[M+NH_4]^+$ = 1472.7447, purity: 98.5%; (e) Act-Al_**2**–Am_**2**: expected $[M+H]^+$ = 1542.8342, $[M+Na]^+$ = 1564.8161, purity: 99.0%; (f) Act-Al_**4**–Am_**4**: expected $[M+H]^+$ = 3265.7085, $[M+Na]^+$ = 3287.6904, purity: 98.9%.

5.4.4 Amine Protecting Groups and Deprotection

5.4.4.1 NPPOC Protecting Group

1 μmol of the oligo(peptoid) NPPOC-Am_**3** (10 mM stock solution in MeCN) was mixed in a solution of 10 mM pyrene (a photosensitizer) in DMAC/EtOH/dioxane (v/v/v: 1:1:1) and purged with nitrogen. This reaction mixture was stirred under 365 nm UV irradiation at 10.8 $mW.cm^{-2}$ for 5 hours. Aliquots were taken and subjected to LCMS analysis. As indicated by ESI spectra, deprotection of the NPPOC-Am_**3** oligomer by UV irradiation did not proceed to completion, even after extended periods and in the presence of photosensitizers, as partially- and fully-protected oligomers were still observed in mass spectra of the reaction mixtures.

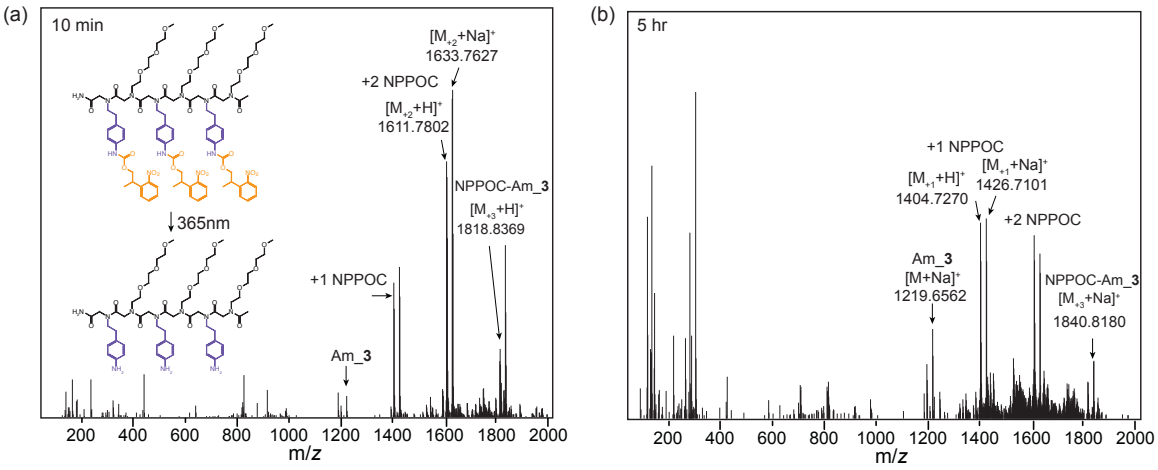

Figure 5.13. Photodeprotection of NPPOC.
* ESI spectra of NPPOC-Am_**3** irradiated at 365 nm in the presence of pyrene for (a) 10 min and (b) 5 hour. Am_**3** denotes the fully-deprotected oligo(peptoid), whereas +1 and +2 NPPOC indicate partially-deprotected oligo(peptoid)s with one or two NPPOC protecting groups remaining. Expected exact mass: Am_**3** $[M_{Am\_3}+Na]^+$ = 1219.6585; +1 NPPOC: $[M_{+1}+H]^+$ = 1404.7297, $[M_{+1}+Na]^+$ = 1426.7116; +2 NPPOC: $[M_{+2}+H]^+$ = 1611.7829, $[M_{+2}+Na]^+$ = 1633.7648.

5.4.4.2 Teoc Protecting Group

(a) Er(III)-mediated Deprotection

0.2 μmol of oligo(peptoid) Teoc-Am_**4** (10 mM stock solution in MeCN) was treated with 5 equivalents of erbium (III) triflate in chloroform saturated with water at room temperature overnight and the reaction mixture was directly subjected to ESI analysis. As suggested by ESI, deprotection of Teoc-Am_**4** by Er(III) did not approach completion as partially-deprotected oligomers were detected in mass spectra of the reaction mixtures.

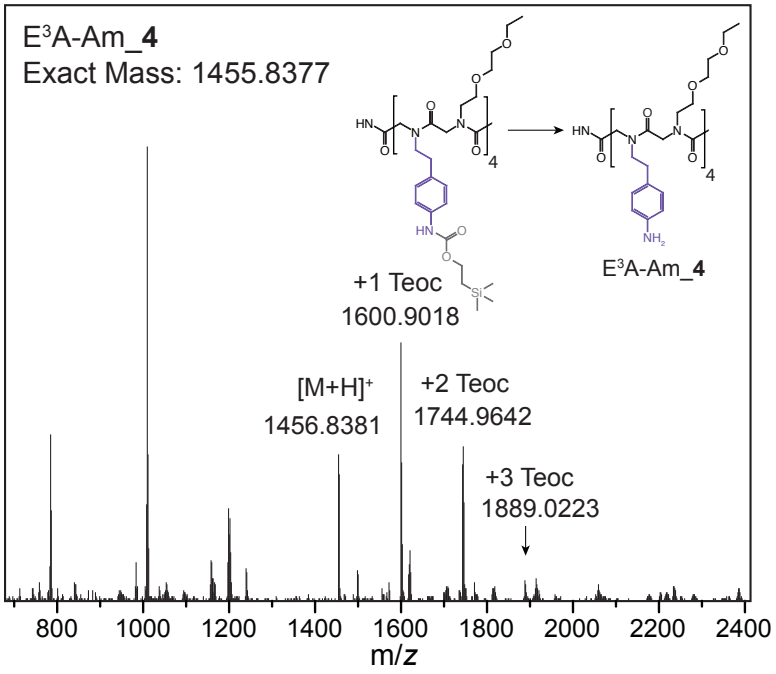

Figure 5.14. **Erbium(III)-mediated deprotection of Teoc.**
*E^3A-Am_**4** denotes the fully-deprotected oligo(peptoid), whereas +1, +2 and +3 Teoc indicate partially-deprotected oligo(peptoid)s with one, two and three Teoc protecting groups remaining. Expected exact mass: E^3A-Am_**4** $[M_{E3A\text{-}Am\_4}+H]^+$ = 1455.8387; +1 Teoc $[M_{+1}+H]^+$ = 1600.9057; +2 Teoc $[M_{+2}+H]^+$ = 1744.9664; +3 Teoc $[M_{+3}+Na]^+$ = 1889.0270.

(b) TBAF Deprotection

0.5 μmol of the oligo(peptoid) Teoc-Am_**4** (10 mM stock solution in MeCN) was treated with 7 eq. of 1M TBAF in THF overnight and the reaction mixture was further subjected to both ESI and analytical HPLC analysis.

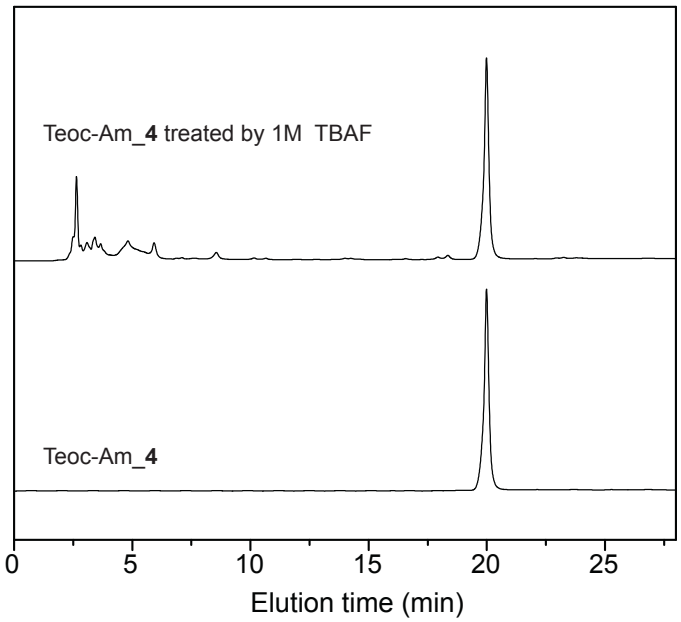

Figure 5.15. **Analytical HPLC traces of oligo(peptoid) Teoc-Am_4 before and after treatment with 1 M TBAF.**
*The elution time of both traces is 19.846 min, suggesting that F^--mediated Teoc deprotection did not proceed under the applied reaction conditions.

5.4.4.3 Alloc Protecting Group

The deprotection of Alloc groups was carried out by the aforementioned procedure using oligo(peptoid) Alloc-Am_**4**. After removal of Alloc protecting groups, the crude peptoids were analyzed by ESI+ mass spectrometry. As shown by Figure 5.16, a complete deprotection of Alloc groups was achieved by Pd(0).

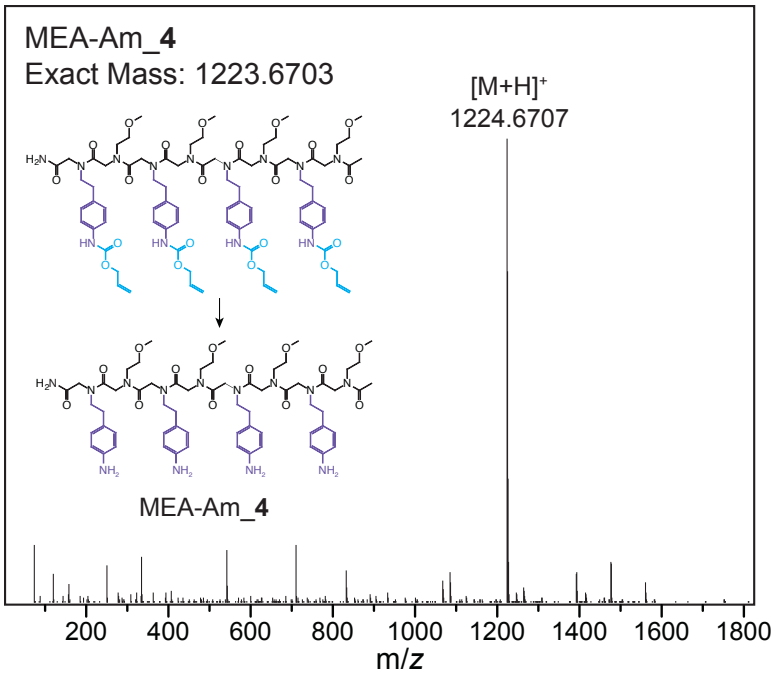

Figure 5.16. **Deprotection of Alloc by Pd(0) in the presence of phenylsilane.**
* MEA-Am_**4** denotes the fully-deprotected oligo(peptoid). Expected exact mass: MEA-Am_**4** $[M_{Am\_4}+H]^+$ = 1455.8387; +1 Teoc $[M_{+1}+H]^+$ = 1600.9057; +2 Teoc $[M_{+2}+H]^+$ = 1744.9664; +3 Teoc $[M_{+3}+Na]^+$ = 1889.0270.

5.4.5 Deprotection of Acetal Group by Lewis Acids

We initially examined the deprotection of acetal-protected aldehyde bearing peptoids by using Lewis acids such as erbium triflate and scandium triflate. 0.2 μmol of oligo(peptoid) Act-Al_**4** (10 mM in MeCN) was treated with 5 equivalents of either $Er(OTf)_3$ or $Sc(OTf)_3$ in chloroform saturated with water at room temperature overnight and the reaction mixture was directly subjected to MALDI analysis (Figure 5.17).

5.5 Results and Discussion

5.5.1 Orthogonal Protecting Groups for Amines and Aldehydes

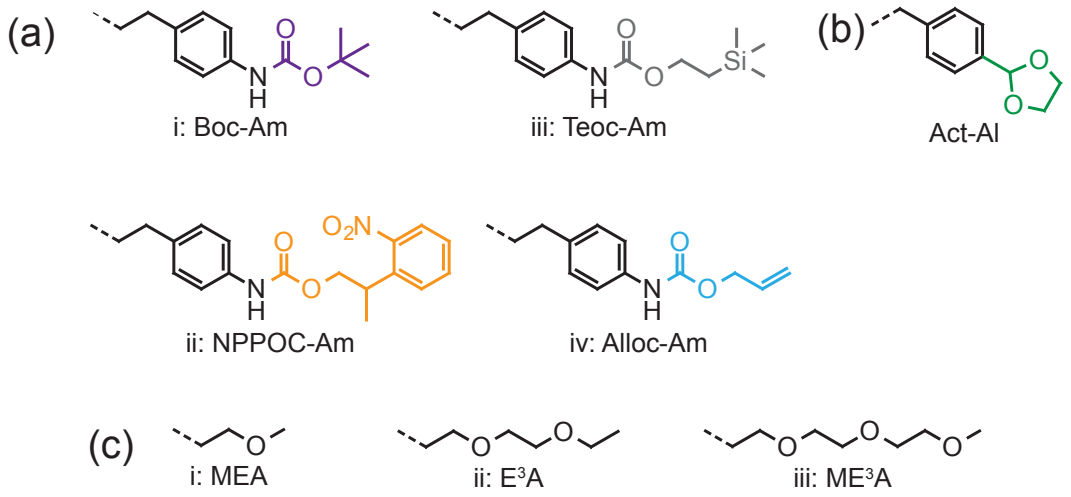

Scheme 5.5. Structures of the oligo(peptoid) pendant groups used in this study. (a) Protecting groups for the aromatic amine pendant group included i) *tert*-butyloxycarbonyl (Boc-Am), ii) 2-(2-nitrophenyl)propoxycarbonyl (NPPOC-Am), iii) trimethylsilylethoxycarbonyl (Teoc-Am), and iv) allyloxycarbonyl (Alloc-Am). (b) The aromatic aldehyde pendant group was protected by an ethylene acetal. (c) Reactive pendant groups were separated by spacer residues bearing inert pendant groups, including i) methoxyethyl, ii) ethoxyethoxyethyl, and iii) methoxyethoxyethoxyethyl, incorporated to maintain solubility of the resultant structures upon self-assembly.

Our initial attempt to implement *in situ* deprotection employed treatment of peptoids bearing both ethylene acetal (i.e., 1,3-dioxolane) and *tert*-butyloxycarbonyl (Boc)-protected amine groups (see Scheme 5.5 (a)), acid-labile protecting groups,[12, 14] with trifluoroacetic acid (TFA) and subsequently neutralization of the reaction mixture to both prevent oligomer degradation[19] and allow the amine-aldehyde condensation to proceed (Scheme 5.6). This approach proved unsuccessful as the oligomeric precursors

immediately precipitated upon neutralization, preventing assembly of the desired product. Subsequently, owing the facile acetal deprotection by acid treatment, we envisaged an approach whereby oligomers functionalized with acetals and orthogonal, acid-insensitive protecting groups would first be treated with TFA to reveal the aldehyde pendant groups, purified, then subjected to neutral deprotection conditions *in situ* to reveal the amine groups, again leading to oligomer self-assembly.

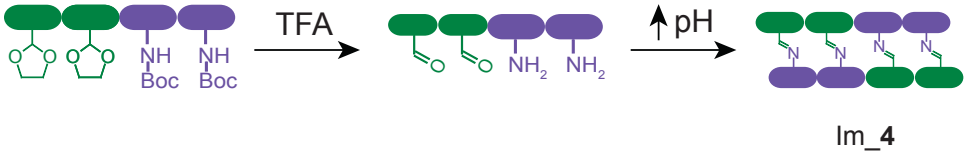

Im_**4**

Scheme 5.6. Acetal-aldehyde and Boc-amine bearing peptoid oligomers are treated with TFA to effect *in situ* acetal and Boc deprotection and oligomer self-assembly.

A common technique to achieve *in situ* deprotection is the photolysis of photocaged groups, a particularly attractive approach as no reagent need be added to the system to cleave the protecting group.[20] For this reason, photocaged species have found extensive use as *in situ* cleavable protecting groups in many applications, from peptide self-assembly and gelation[21] to the release of amines for Michael addition catalysis;[22] indeed, the irradiation conditions employed for photocleavage have proven so innocuous that cleavage of photodegradable hydrogels has been performed even in the presence of live cells.[23-24] We consequently employed 2-(2-nitrophenyl)propoxycarbonyl (NPPOC, Scheme 5.5(a)), a photolabile amine protecting group that is stable under the TFA treatment used for acetal deprotection[25] while being readily cleavable under ultraviolet (UV) light,[22] and examined its deprotection extent upon irradiation. Unfortunately, deprotection of an peptoid bearing multiple NPPOC-protected amine groups by UV

irradiation did not proceed to completion, even after extended periods and in the presence of photosensitizers, apparent by the observed occurrence of partially and fully protected oligomers in mass spectra of the reaction mixtures (see Figure 5.13).

These unsuccessful attempts prompted a wholly different approach to *in situ* deprotection. A previous study reported that erbium(III) triflate can rapidly deprotect acetal-protected aldehydes,[26] while zinc bromide can deprotect the amine protecting group trimethylsilylethoxycarbonyl (i.e., Teoc, Scheme 5.5),[27] suggesting the potential for a single Lewis acid to serve in three catalytic roles for this system, yielding the *in situ* deprotection of both amine and aldehyde groups while concurrently catalyzing the rearrangement of the imine product generated upon aldehyde/amine condensation.

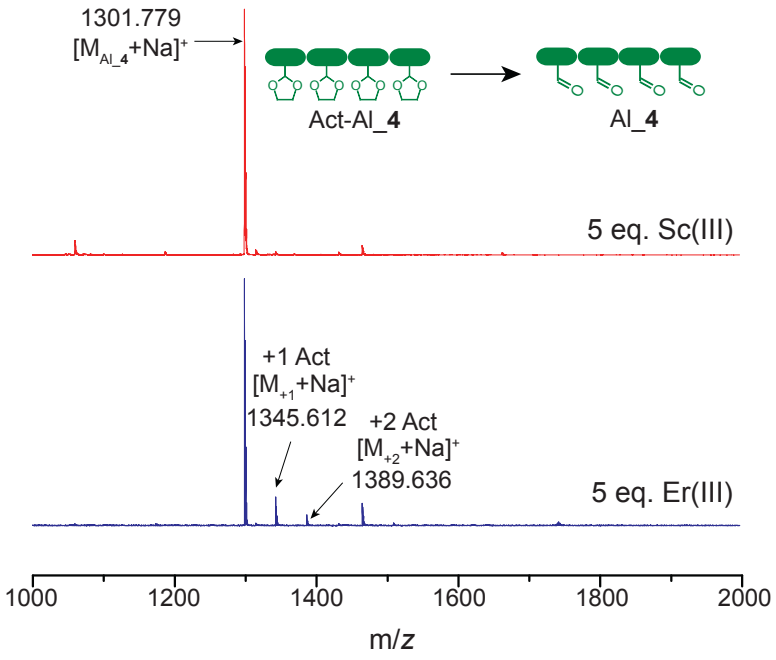

Figure 5.17. **Deprotection of acetal group by Lewis acids.**
* Oligo(peptoid) Act-Al_**4** bearing ethylene acetal-protected aldehydes was treated with 5 eq. $Er(OTf)_3$ or 5 eq. $Sc(OTf)_3$ to yield Al_**4**. +1 and +2 Act denote partially-deprotected oligo(peptoid)s with one or two acetal groups remaining. Expected exact mass: Al_**4** $[M_{Act\text{-}Al\_4}+Na]^+$ = 1301.441 g/mol; +1 Act $[M_{+1}+Na]^+$ = 1345.621 g/mol; +2 Act $[M_{+2}+Na]^+$ = 1389.648 g/mol.

We found that, although treatment of peptoid oligomers bearing either ethylene acetal or amine-protected Teoc pendant groups with $Er(OTf)_3$ did indeed result in deprotection, the deprotection extents did not approach completion, even at very high loadings of this Lewis acid (see Figure 5.14 and Figure 5.17). Attempts to improve the deprotection yields were performed by treatment of the protected oligomers with $Sc(OTf)_3$, a significantly stronger Lewis acid than its erbium-based counterpart.[28] However, although $Sc(OTf)_3$ exhibited high activity towards ethylene acetal deprotection (as detailed below), it proved ineffective for Teoc deprotection.

Given the successful and near-quantitative acetal deprotection by $Sc(OTf)_3$ (see Figure 5.17) and its aforementioned catalytic activity in imine exchange reactions, we opted to still examine amine protecting groups that are labile under neutral conditions but switch the deprotection order such that oligomers with ethylene acetal and protected amine pendant groups could be deprotected to reveal free amine groups, then purified and subjected to Sc(III)-mediated acetal deprotection *in situ*. Although cleavage of the silyl-based Teoc protecting group did not proceed quantitatively upon treatment with either of the metal triflate Lewis acids examined, this group is commonly cleaved by treatment with a F^- source such as tetrabutylammonium fluoride (TBAF).[29] We treated a peptoid bearing multiple Teoc-protected amine groups with TBAF, anticipating rapid deprotection; however, attempts to characterize the resultant material by either ESI or MALDI mass spectrometry were unsuccessful. Nevertheless, we noted that the HPLC elution volume for the Teoc-bearing peptoid did not change after TBAF treatment (see

Figure 5.15), suggesting that the F^--mediated Teoc deprotection did not proceed as expected.

The allyloxycarbonyl (Alloc, Scheme 5.5) protecting group, known to be readily cleavable under neutral conditions by treatment with Pd(0) in the presence of a hydrogen donor,[14] was finally examined to provide deprotection orthogonal to that of the acetal groups. Here, the deprotection of a peptoid bearing multiple Alloc-protected amines by treatment with Pd(0) in the presence of phenylsilane afforded quantitative deprotection (Figure 5.16), whereas an ethylene acetal-bearing peptoid subject to the same reaction conditions remained intact. Thus, ethylene acetals in combination with Alloc-protected amines offered a viable and elegant system for orthogonal deprotection and self-assembly whereby, after the Alloc groups were selectively deprotected, the acetals could be cleaved in situ using Sc(III) which would also serve to catalyze exchange of the imine groups resulting from the subsequent condensation reactions between the amine and revealed aldehyde groups (see Scheme 5.7).

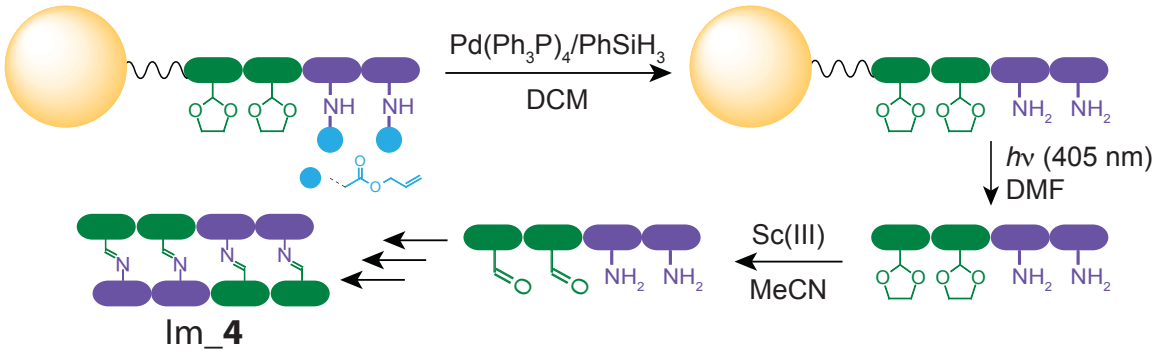

Scheme 5.7. Upon Pd(0)-catalyzed Alloc deprotection, amine- and acetal-bearing oligomers generated by solid phase peptoid synthesis are photocleaved from resin, purified, and treated with $Sc(OTf)_3$ to effect *in situ* acetal deprotection and oligomer self-assembly.

5.5.2 Optimization of Acetal Deprotection by Sc(III)

The acetal deprotection efficiency, reaction rate and equilibrium of amine-aldehyde condensation reaction, and imine exchange reaction rates strongly depend on solvent used and its water content, molar equivalents (with respect to the number of acetal groups) of catalyst (i.e., $Sc(OTf)_3$) in solution, as well as on the temperature. Given the necessity to achieve complete deprotection *in situ* prior to self-assembly, the acetal deprotection reaction conditions were first determined. Initially, the influence of solvent on deprotection conversion was examined by treatment of the tetra(ethylene acetal)-bearing peptoid Act-Al_**4** with Sc(III) at 50°C in a range of organic solvents (see Figure 5.18).

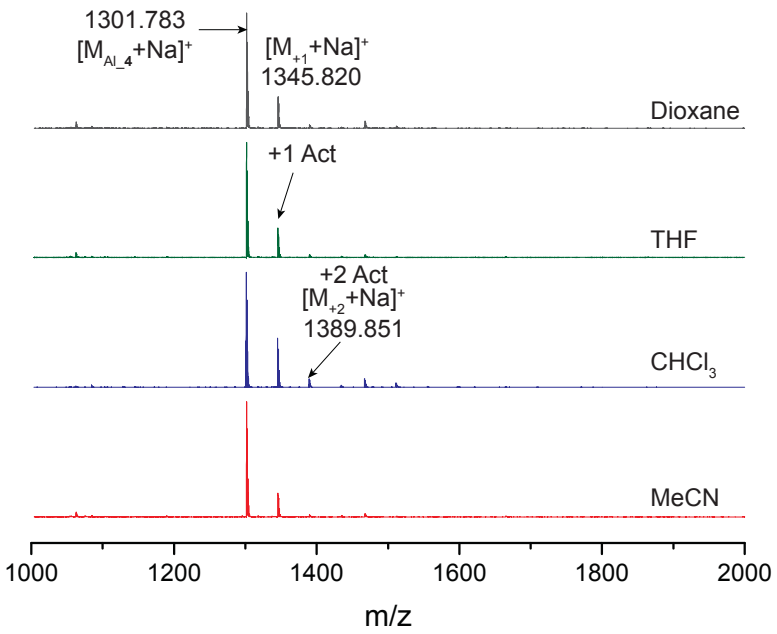

Figure 5.18. Influence of solvent on acetal deprotection by Sc(III).
* Oligo(peptoid) Act-Al_**4** bearing ethylene acetal-protected aldehydes was treated with 0.2 eq. Sc(III) at 50°C in different solvents overnight and the reaction mixture was directly subjected to MALDI analysis.

Table 5.1. Yields of acetal deprotection by 0.2 eq. Sc(III) at 50°C in different solvents.

Solvent	MeCN	$CHCl_3$	THF	Dioxane
Yield of fully-deprotected oligomer (%)	81.4	64.6	75.1	75.6

Although we previously used chloroform as solvent for the dynamic covalent assembly of peptoids,[4, 10] when employed for the Sc(III)-mediated acetal deprotection, it afforded the lowest yield of the fully deprotected, tetraaldehyde-bearing peptoid Al_**4** of the solvents examined, whereas acetonitrile afforded the highest yield and was thus utilized for further study (Table 5.1).

Subsequently, the water content was investigated and the deprotection yield improved significantly at even relatively low amounts of added water, increasing from 81.4% for neat acetonitrile to 97.3% for 1 v/v% water in acetonitrile. The deprotection yield further increased to 99.2% at 5 v/v% water in acetonitrile; however, raising the water content beyond this concentration afforded little to no yield improvement (see Figure 5.19).

Table 5.2. Yields of acetal deprotection by 0.2 eq. Sc(III) at 50°C with different water contents.

Amount of H_2O in MeCN (v/v%)	0	1	5	10	20
Yield of fully-deprotected oligomer (%)	81.4	97.3	99.2	99.5	99.3

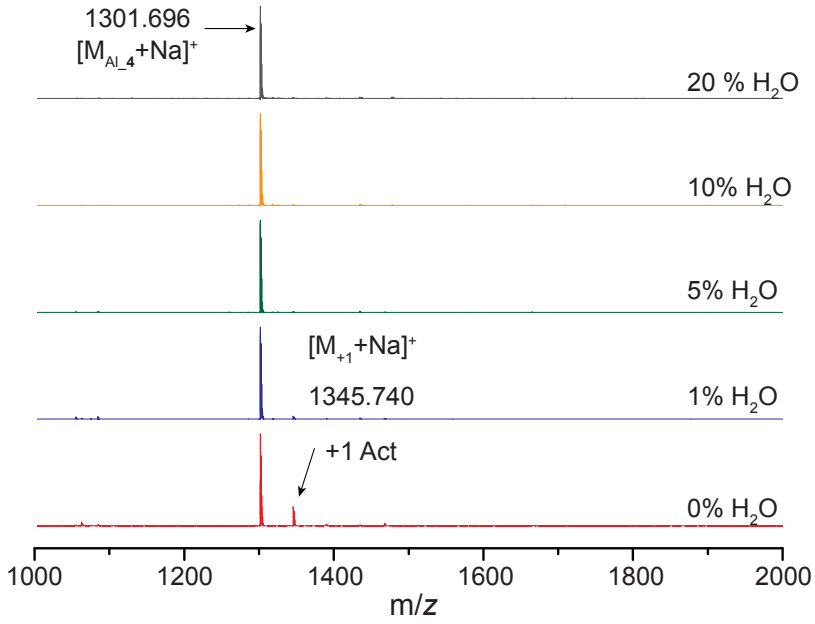

Figure 5.19. Influence of water content on acetal deprotection at 50°C.
* Oligo(peptoid) Act-Al_**4** bearing ethylene acetal-protected aldehydes was treated with 0.2 eq. Sc(III) at 50°C overnight in a mixture of water/MeCN. The volume percentage of water in MeCN was varied from 0% to 20%. The reaction mixture was directly subjected to MALDI analysis.

A previous study found that, when compared with the uncatalyzed reactions, 0.04 molar equivalents of Sc(III) increased imine exchange reaction rates by up to 5 orders of magnitude; however, at higher catalyst loadings (>0.20 eq.), the catalyst itself shifted the system thermodynamic equilibrium.[11] To understand how Sc(III) concentration would affect the equilibrium of imine-metathesis based peptoid ladder formation, we varied Sc(III) concentrations from 0.04 to 0.5 equivalent per imine bond to catalyze 8-rung ladder formation and the reaction mixtures were directly analyzed by MALDI mass spectrometry as shown in Figure 5.20. In all cases, we detected the desired 8-rung molecular ladders. However, the amount of out-of-registry ladders increases with Sc(III) concentration. At 0.5 eq. Sc(III), higher molecular weight species, resulting from the co-reaction of more than two peptoid strands (i.e., (Al_**8**)$_1$(Am_**8**)$_2$) were detected, which is

undesirable. This suggests higher amount of Sc(III) (i.e., 0.5 eq.) would significantly slow down the bond rearrangement process through imine exchange reactions to generate desired ladder products and would likely shift the equilibrium towards amine/aldehyde instead of imine, preventing the formation of in-registry ladders. Therefore, the amount of Sc(III) applied should yield a complete aldehyde deprotection while not affect the equilibrium of ladder formation.

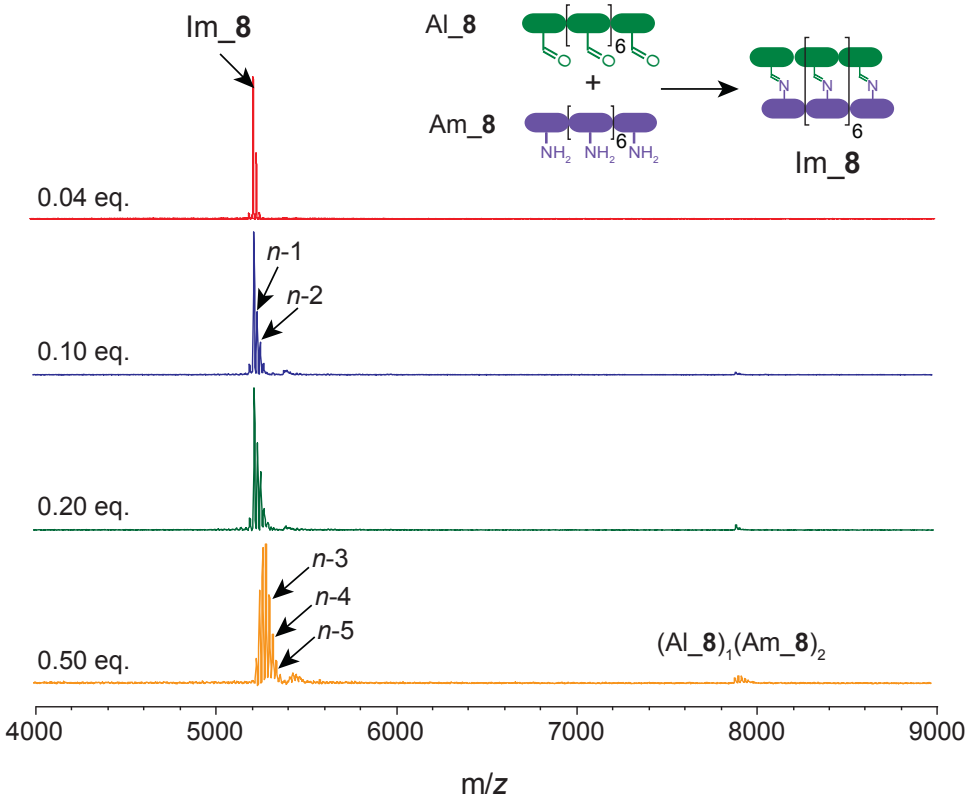

Figure 5.20. Influence of Sc(III) concentration on the equilibrium of peptoid-based 8-rung ladder (Im_8) formation.

Our preliminary examination of Sc(III)-mediated ethylene acetal deprotection revealed that raised Sc(III) loadings (>0.15 eq.) were necessary to approach quantitative aldehyde yields (see Figure 5.21). Notably, whereas the inclusion of water and raised

Sc(III) loading enhanced acetal deprotection conversion, their presence would interfere with the thermodynamic equilibrium of the amine-aldehyde condensation reaction. Thus, to minimize the water and Sc(III) concentrations necessary to reach quantitative deprotection, the reaction temperature was further raised to 70°C to facilitate the acetal deprotection as well as increase imine exchange rates.

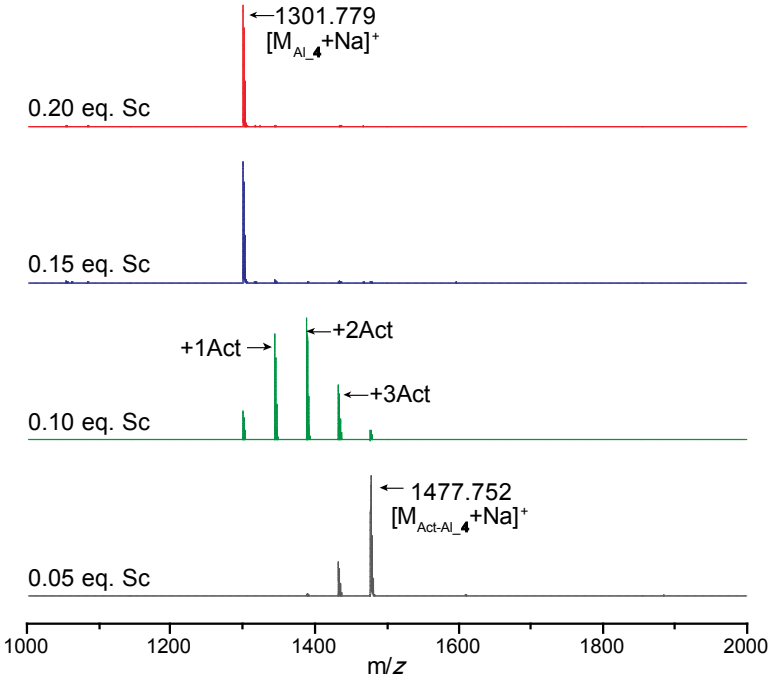

Figure 5.21. Influence of Sc(III) concentration on acetal deprotection characterized by MALDI mass spectrometry.
* $Sc(OTf)_3$ treatment is performed in 95% acetonitrile/water (v/v) overnight at 50°C on Act-Al_**4** (expected exact mass: $[M_{Act\text{-}Al\_4}+Na]^+$ = 1477.700 g/mol), a peptoid bearing four pendant ethylene acetal groups. Al_**4** (expected exact mass: $[M_{Al\_4}+Na]^+$ = 1301.441 g/mol) is the fully deprotected oligomer, whereas +1Act, +2Act, and +3Act are partially deprotected oligomers bearing one, two, and three ethylene acetal groups, respectively.

Table 5.3. Yields of acetal deprotection in 2 v/v% water/MeCN at 50°C with different equivalents of Sc(III).

Sc(III) equivalents	0.05	0.10	0.15	0.20
Yield of fully-deprotected oligomer (%)	–	8.1	98.0	99.2

Initially, decreasing the water content to 2 v/v% while maintaining 0.20 eq. of Sc(III) afforded a near complete deprotection with 99% yield however, further reducing the water content to 1 v/v% resulted in a lower yield of 97.4% fully deprotected oligomer (see Figure 5.22).

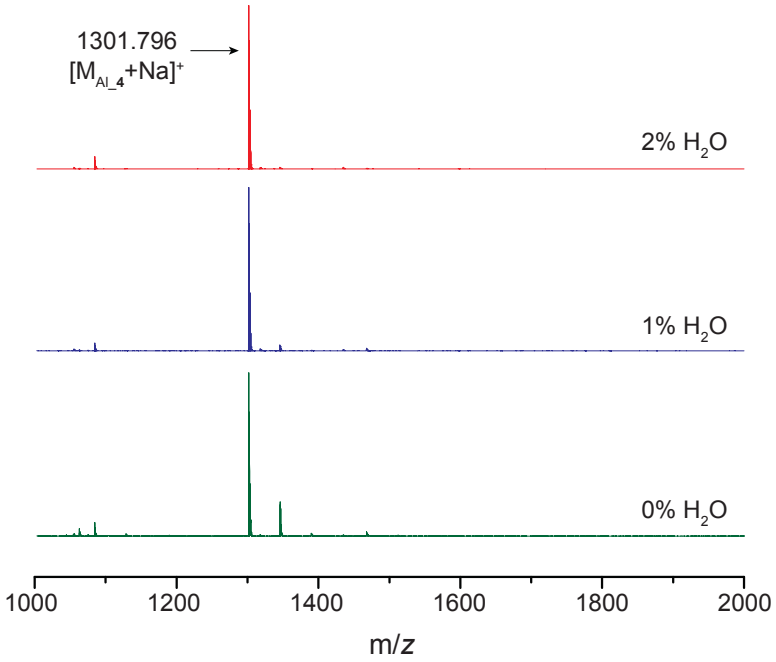

Figure 5.22. Influence of water content on acetal deprotection at 70°C.
* Oligo(peptoid) Act-Al_**4** bearing ethylene acetal-protected aldehydes was treated with 0.2 eq. Sc(III) at 70°C overnight in a mixture of water/MeCN. The volume percentage of water in MeCN was varied from 0% to 20%. The reaction mixture was directly subjected to MALDI analysis.

Table 5.4. Yields of acetal deprotection by 0.2 eq. Sc(III) at 70°C with different water contents.

Amount of H_2O (v/v%)	0	1	2
Yield of fully-deprotected oligomer (%)	81.0	97.4	99.0

Although the influence of water on conversion was minimally impacted by temperature, the conversion drastically improved to 98.1% for 0.10 eq. of Sc(III) at 70°C,

compared with only 8.1% at 50°C. Both 0.15 and 0.20 eq. of Sc(III) yielded near complete deprotection at 70°C, affording 98.4% and 99.0% of the fully deprotected oligomer, respectively (see Figure 5.23). Thus, utilizing 0.10 – 0.20 eq. of Sc(III) in the presence of 2 – 5 vol% of water in acetonitrile at 70°C would afford near complete oligomer deprotection.

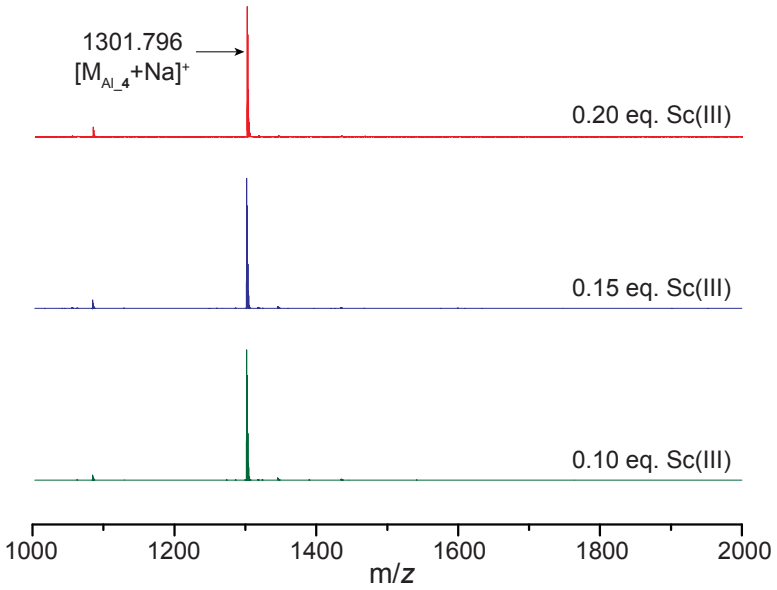

Figure 5.23. Effect of Sc(III) on acetal deprotection at 70°C.
* Oligo(peptoid) Act-Al_**4** bearing acetal-protected aldehydes was treated with 0.10 – 0.20 equivalents Sc(III) in 2 v/v% water/MeCN at 70°C overnight. The reaction mixture was directly subjected to MALDI analysis.

Table 5.5. Yields of acetal deprotection in 2 v/v% water/MeCN at 70°C with different equivalents of Sc(III).

Sc(III) equivalents	0.10	0.15	0.20
Yield of fully-deprotected oligomer (%)	98.1	98.4	99.0

5.5.3 Sc(III) as a Dual Role Catalyst

To assess the feasibility of using Sc(III) as a dual role catalyst, both deprotecting the acetal *in situ* while simultaneously catalyzing the subsequent oligomer self-assembly, a model peptoid sequence composed of two acetal-protected aldehyde and two free amines (i.e., Act-Al_**2**–Am-**2**) was synthesized and utilized. Upon *in situ* deprotection, the self-assembly of this oligomeric sequence should result in anti-parallel self-hybridization, generating a 4-rung molecular ladder, denoted here as Im_**4** (see Scheme 5.7).

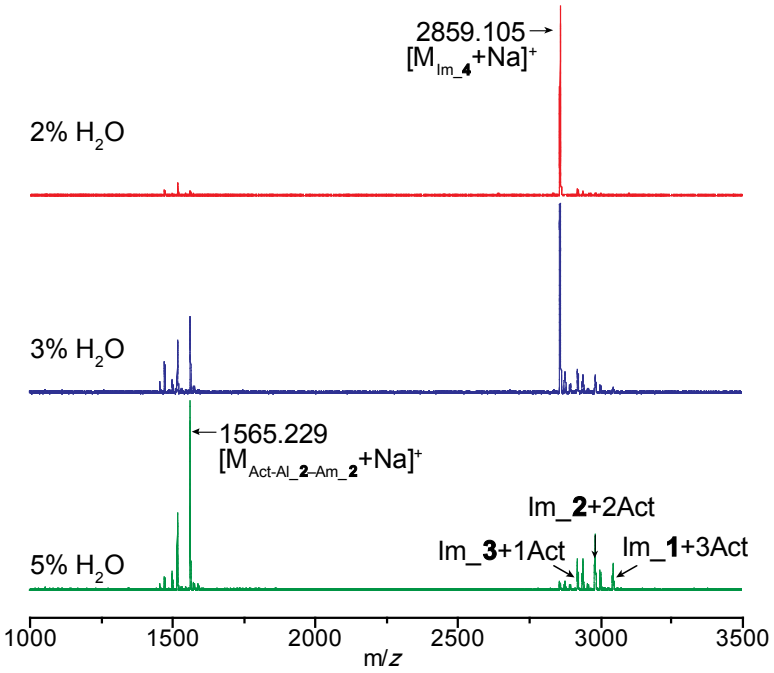

Figure 5.24. Influence of water content on acetal deprotection and subsequent self-assembly of 4-rung peptoid ladders characterized by MALDI mass spectrometry.
* Act-Al_**2**–Am_**2** (expected exact mass: $[M_{Act\text{-}Al\_2\text{–}Am\_2}+Na]^+$ = 1564.816 g/mol) treated with 0.2 eq. $Sc(OTf)_3$ in acetonitrile/water overnight at 70°C. Im_**4** (expected exact mass: $[M_{Im\_4}+Na]^+$ = 2858.496 g/mol) is the desired in-registry molecular ladder, whereas Im_**3**+1Act, Im_**2**+2Act, and Im_**1**+3Act are out-of-registry, partially deprotected ladders bearing three imine/one acetal, two imine/two acetal, and one imine/three ethylene acetal groups, respectively.

Initially, the impact of water content on *in situ* deprotection and hybridization was evaluated by subjecting Act-Al_**2**–Am-**2** to 0.2 eq. Sc(III) at 70°C while varying the fraction of water in acetonitrile from 2 to 5 v/v%. Mass spectrometry of the crude reaction mixture containing 0.2 eq. Sc(III) and 2 v/v% water revealed the near exclusive assembly of the desired Im_**4** structure, with negligible amounts of acetal-protected single peptoid strands and out-of-registry species observed (see Figure 5.24). In contrast, the occurrence of acetal-protected single peptoids and corresponding out-of-registry ladders became more pronounced as the water content was raised; indeed, at 5 v/v% water, the desired Im_**4** structure was a negligible component of the reaction mixture.

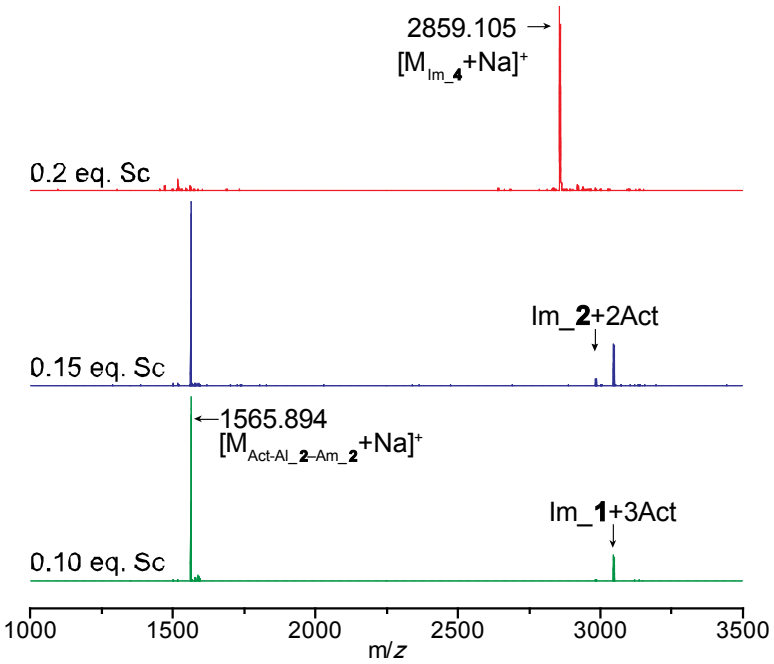

Figure 5.25. Influence of Sc(III) concentration on acetal deprotection and subsequent self-assembly of 4-rung peptoid ladders (Im_4) characterized by MALDI mass spectrometry.
* Act-Al_**2**–Am_**2** treated with $Sc(OTf)_3$ in 2 v/v% water in acetonitrile overnight at 70°C.

Subsequently, the effect of Sc(III) concentration on *in situ* deprotection and oligomer self-assembly was further evaluated based on 2 v/v% of water by varying the equivalents of Sc(III) from 0.1 to 0.2 eq. Despite the near-exclusive generation of the desired structure at 0.2 eq. Sc(III), reducing the amount of Sc(III) in solution dramatically reduced the acetal deprotection yield such that the primary components of the reaction mixtures at 0.1 and 0.15 eq. Sc(III), as indicated by mass spectra of the crude reaction mixtures, were the fully protected oligomer (i.e., starting material) and small amounts of dimerized oligomers still bearing unprotected acetal groups (see Figure 5.25).

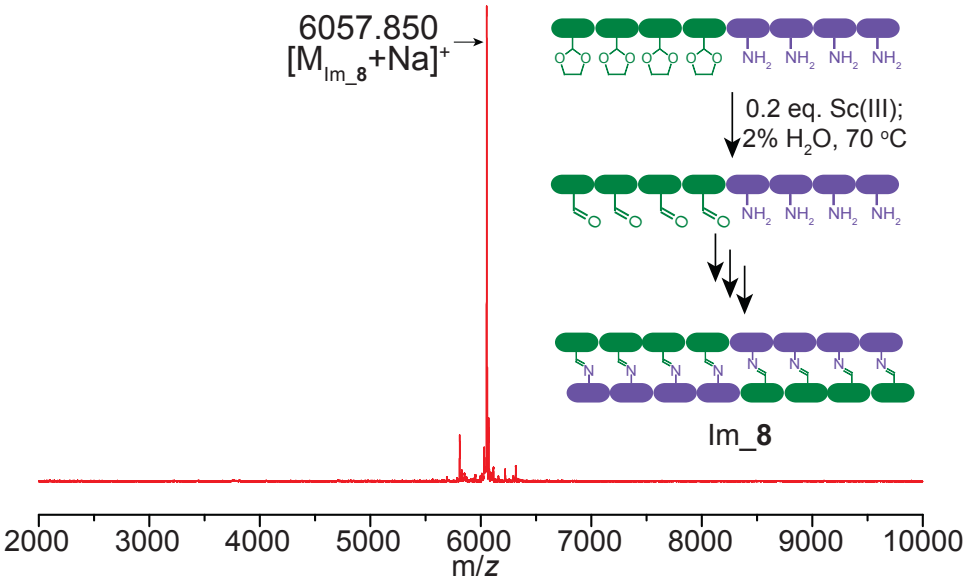

Figure 5.26. *In situ* deprotection and self-assembly of a 8-rung peptoid ladder (Im_8) by using Sc(III) as a dual role catalyst.
* Act-Al_**4**–Am_**4** (expected exact mass: $[M_{\text{Act-Al\_4–Am\_4}}+Na]^+$ = 3287.609 g/mol) treated with 0.2 eq. $Sc(OTf)_3$ in 2 v/v% water in acetonitrile overnight at 70°C. Im_**8** (expected exact mass: $[M_{\text{Im\_8}}+Na]^+$ = 6056.097 g/mol) is the desired in-registry molecular ladder.

The reaction conditions of 0.2 eq. Sc(III) with 2 v/v% water in acetonitrile at 70°C that successfully realized *in situ* deprotection and self-assembly of the short model oligomer were validated by applying them to an octafunctional peptoid sequence bearing

a block of four ethylene acetal and a block of four amine groups (i.e., Act-Al_**4**–Am-**4**). This sequence again successfully underwent anti-parallel self-hybridization to afford an 8-rung molecular ladder (Im_**8**, see Figure 5.26).

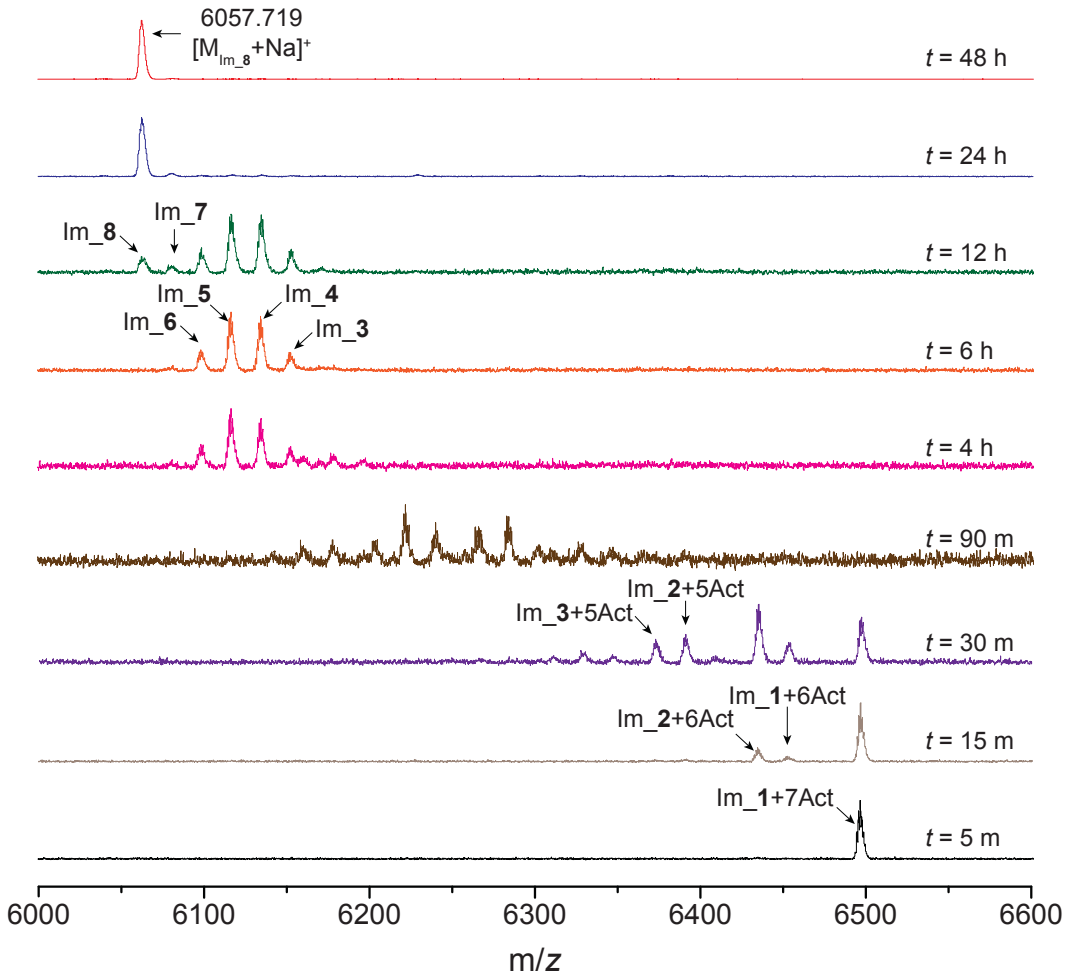

Figure 5.27. Kinetics of *in situ* deprotection and molecular ladder formation for Act-Al_4–Am-4, treated with 0.20 equivalents Sc(III) in 2 v/v% water/MeCN at 70°C. MALDI mass spectra of the crude reaction mixture are shown at increasing time intervals.

* Im_**8** (expected exact mass: [M$_{Im_8}$+Na]$^+$ = 6056.097 g/mol) is the desired in-registry molecular ladder. Im_**7**, Im_**6**, Im_**5**, Im_**4**, and Im_**3** are out-of-registry, fully deprotected ladders bearing seven, six, five, four, and three imine groups, respectively. Im_**3**+5Act, Im_**2**+5Act, Im_**2**+6Act, Im_**1**+6Act, and Im_**1**+7Act are out-of-registry, partially deprotected ladders bearing three imine/five acetal, two imine/five acetal, two imine/six acetal, one imine/six acetal, and one imine/seven ethylene acetal groups, respectively.

Moreover, characterization of this reaction mixture over time by MALDI mass spectrometry (Figure 5.27) revealed after 5 minutes the formation of an oligomeric dimer joined by a single imine bond and bearing seven ethylene acetal protecting groups. Subsequently, a mixture of intermediate molecular ladders with varying numbers of imine linkages and degrees of deprotection emerged until complete ethylene acetal deprotection was achieved at 6 hours, after which dynamic imine exchange reactions continued until Im_**8** was generated.

5.5.4 Information-bearing Peptoids and Self-assembly of Complex Structures

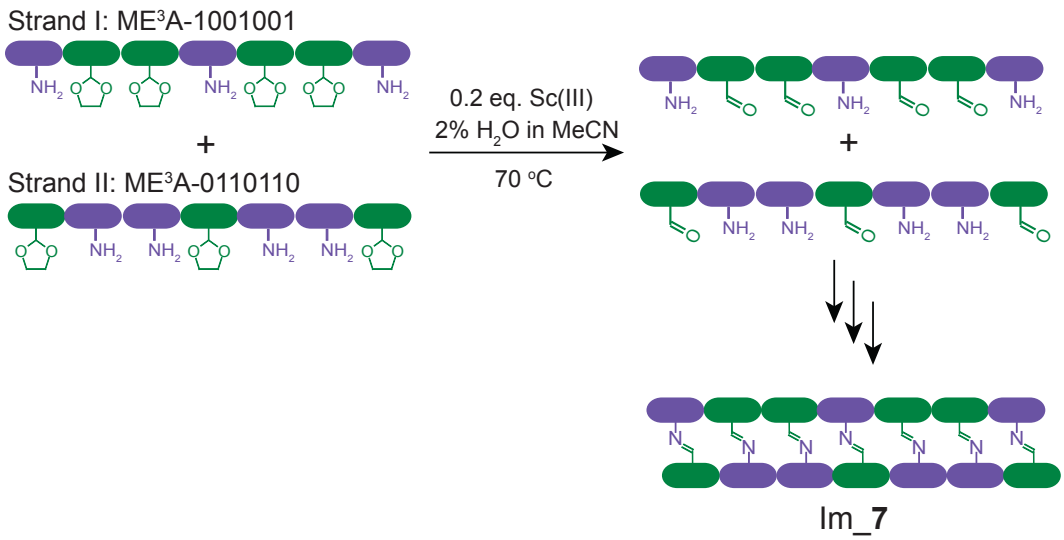

Scheme 5.8. Incorporation of sequence information into peptoid strands and subsequent self-assembly of complementary strands into peptoid-based ladders.
* Here, 1 denotes amine and 2 denotes aldehyde.

We successfully demonstrated Sc(III) could be applied as a dual role catalyst for both *in situ* deprotection and subsequent self-assembly of peptoid sequences bearing a block of acetal protected aldehydes and a block of amines into *n*–rung molecular ladders (see

Figure 5.25 and Figure 5.26). However, all peptoid strands utilized previously for the self-assembly of ladders contain relatively simple chain structures and sequences.

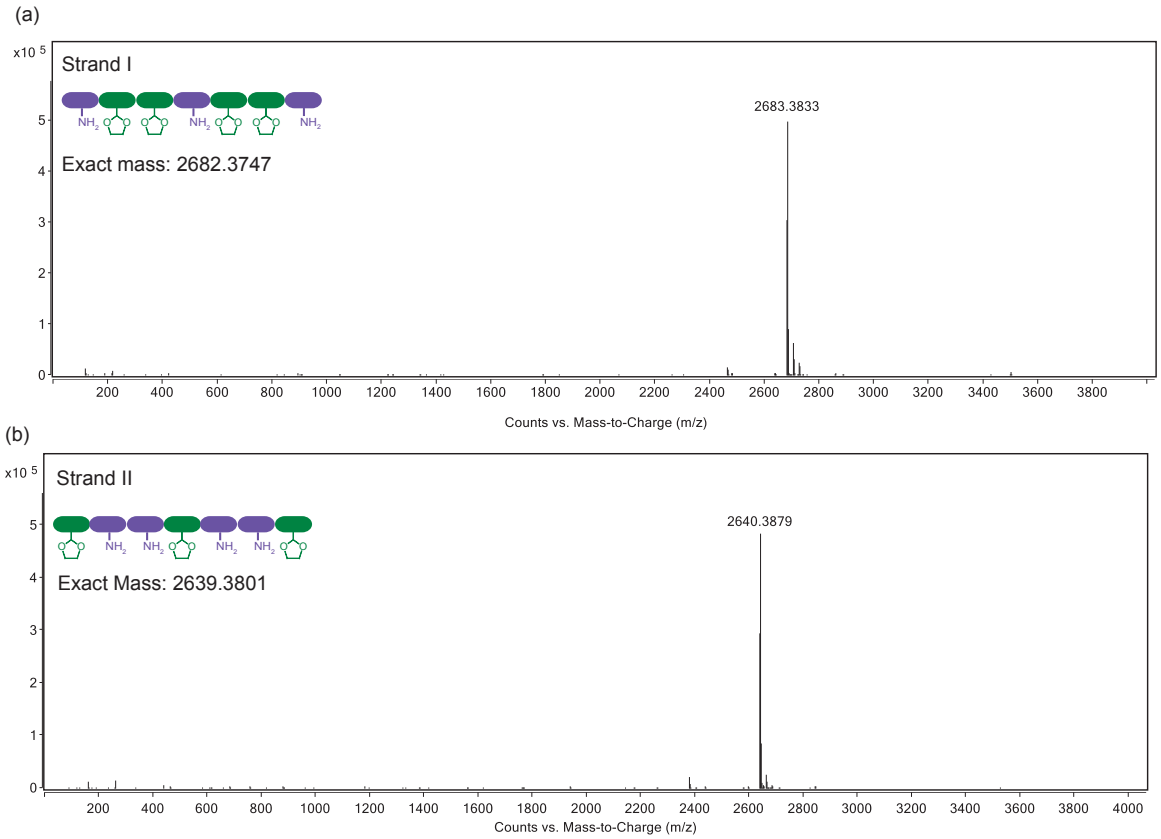

Figure 5.28. ESI spectra of information-bearing complementary peptoid strands (a) ME3A-1001001 and (b) ME3A-0110110 purified by preparative HPLC.
* Strand I: expected [M+H]+ = 2683.3820, purity: 99.0%; strand II: expected [M+H]+ = 2640.3874, purity: 99.2%; Preparative HPLC method: flow rate at 10 mL/min; A: H_2O, B: MeCN; (a) strand I: 30% B 0 – 4 min, 30% – 65% B 4 – 27.33 min, 65% – 30% B 27.33 – 29.33 min; (b) strand II: 35% B 0 – 4 min, 35% – 65% B 4 – 28 min, 65% – 35% B 28 – 30 min.

Therefore, this section discusses the incorporation of sequence information into peptoid strands and the utilization of these strands for the self-assembly of complex nanostructures. We designed complementary peptoid sequences such as ME^3A-1001001 (strand I) and ME^3A-0110110 (strand II) for this study, where "1" denotes amine and "2" denotes aldehyde as shown in Scheme 5.8. Both peptoid strands are deliberately designed

to have palindrome sequences that read the same backward as forward. Thus, either parallel or antiparallel strand alignment would not affect the formation of in-registry 7–rung peptoid ladder.

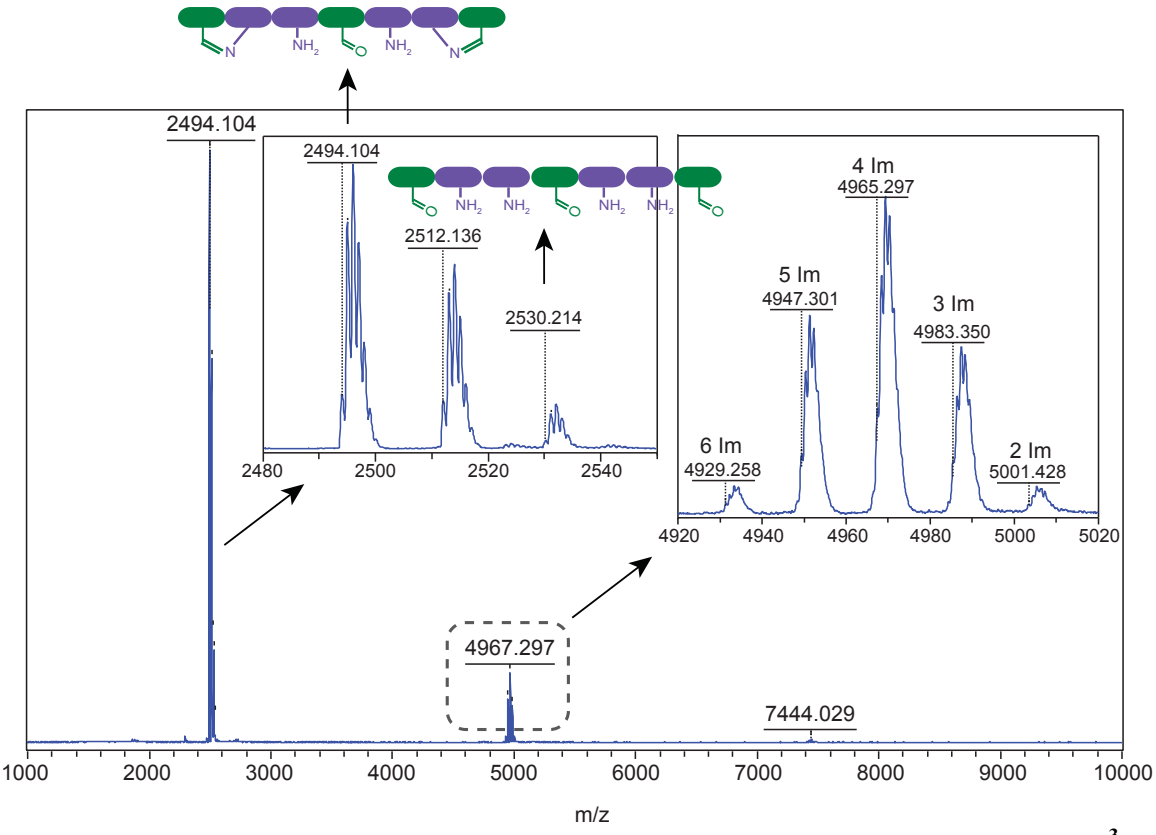

Figure 5.29. Self-assembly of information-bearing complementary peptoids ME^{3}A-1001001 (strand I) and ME^{3}A-0110110 (strand II) into a 7-rung ladder (Im_7) characterized by MALDI mass spectrometry.

* Strand I and Strand II were treated with 0.2 eq. $Sc(OTF)_3$ in 2 v/v% water in acetonitrile at 70°C for 1 day. Im_**7** (expected exact mass: $[M_{Im\_7}+Na]^+$ = 4910.487 g/mol) is the desired in-registry ladder, whereas 6 Im, 5 Im, 4 Im, 3 Im and 2 Im denote the out-of-registry ladders bearing 6, 5, 4, 3, and 2 imine linkages respectively. Expected exact mass of out-of-registry ladders: $[M_{6\ Im}+Na]^+$ = 4928.499 g/mol, $[M_{5\ Im}+Na]^+$ = 4946.5094 g/mol, $[M_{4\ Im}+Na]^+$ = 4964.519 g/mol, $[M_{3\ Im}+Na]^+$ = 4982.529 g/mol, $[M_{2\ Im}+Na]^+$ = 5000.539 g/mol. The peak of molecular weight 2530.214 g/mol detected by MALDI belongs to completely deprotected strand II, whereas the peak of M_w = 2512.136 g/mol corresponds to completely deprotected strand II reacting with itself to form one imine linkage. Similarly, the peak of M_w = 2494.104 g/mol corresponds to completely deprotected strand II reacting with itself to form two imine linkages.

Peptoid sequences 1001001 (strand I) and 0110110 (strand II) incorporating ME^3A inert spacer units were prepared following the same approach described by Scheme 5.4. The resultant peptoids were purified by preparative reverse-phase HPLC and purity and molecular weights characterized by analytical HPLC and ESI mass spectrometry, respectively (see Figure 5.28). The optimized reaction conditions of 0.2 eq. Sc(III) with 2 v/v% water in acetonitrile at 70°C were applied here to afford *in situ* deprotection of aldehydes while simultaneously catalyze the subsequent 7–rung ladder formation through imine metathesis. As indicated by MALDI spectrum of crude reaction mixture (Figure 5.29), the desired 7–rung in-registry ladders were not detected whereas several out-of-registry ladders with different number of rungs (n = 2~6) were present. These peaks were evenly spaced with an interval of 18, corresponding to the molecular weight of the water condensation product for each unreacted amine/aldehyde pair. Even after an extended reaction time such as 7 days, the formation of ideal 7–rung ladders was still not observed, indicating the system might be kinetically trapped. As discussed in Chapter 3, peptoid ladder formation initially adopts a "zipper" mechanism where two complementary strands bind through adjacent imine/aldehyde condensation at any point along the backbone to form out-of-registry ladders. Then, these out-of-registry ladders shuffle through imine bonds by transimination and imine metathesis until the ladders come into registry through a molecular handshake line, which is the rate-limiting step for ladder formation. However, the incorporation of information–the sequential order of amines and aldehydes–into peptoid single strands might disrupt the cooperative binding and the handshake line mechanism, inhibiting the self-correction of out-of-registry intermediates through handshake line shuffling to form desired in-registry products.

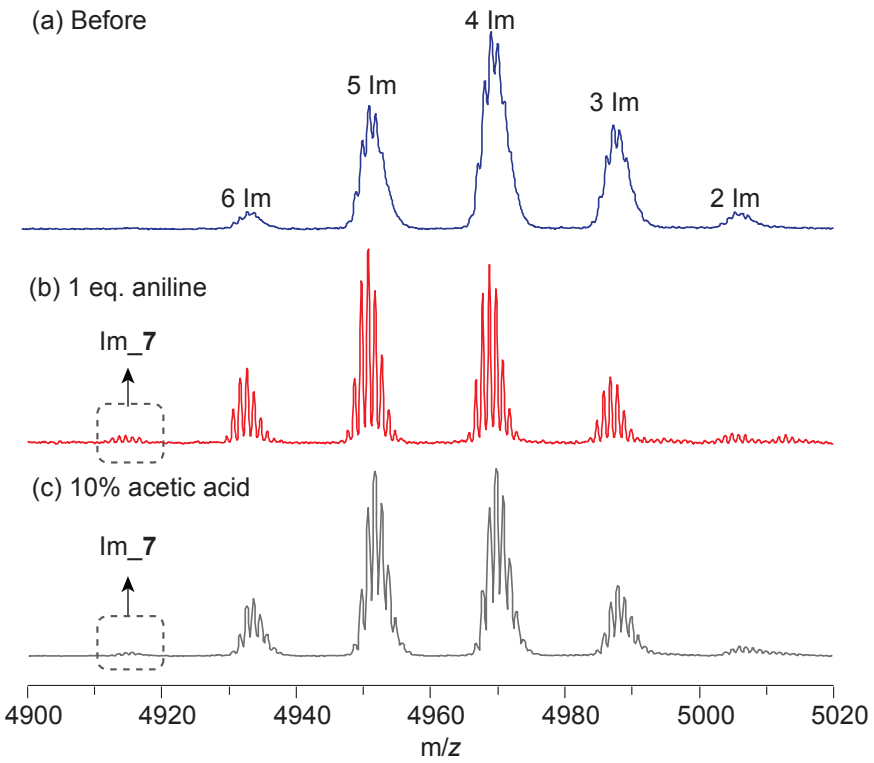

Figure 5.30. Facilitating handshake line shuffling to achieve in-registry molecular ladders with the addition of aniline or acetic acid.

To circumvent this, 1 equivalent of aniline was initially added to the reaction mixture to bridge the gap of cooperative binding and promote the handshake line shuffling (shown in Figure 5.30 (b)). After 1 day, we detected the formation of desired in-registry 7-rung peptoid ladders (Im_**7**). However the dominant species in the reaction mixture were still out-of-registry ladders and the formation of ideal ladder products was rather slow. Furthermore, 10% acetic acid was also added into the reaction mixture to examine if the addition of acid would shift the equilibrium of imine exchange reactions, therefore promoting ladder formation. As indicated by Figure 5.30 (c), the presence of a small amount of desired 7-rung ladders was observed however the addition of acetic acid did not significantly improve the ladder formation.

In addition to out-of-registry ladders, we also noticed the presence of "back-biting" species as a result of completely deprotected single strand self-reacting through condensation by amines/aldehydes on the same strand to form imine linkages. This "back-biting" is likely caused by the inherent flexibility of peptoid backbone. To stiffen the backbone, we used peptoid-peptide hybrids as backbone as α-amino acids would introduce chirality to the backbone (Figure 5.31). Peptide-peptoid hybrids comprise both α-amino acids and (N-alkyl) glycine monomers[30-31] and they could also be synthesized through a "sub-monomer" process consisting of two steps: an acylation step using bromoacetic acid and N, N'-diisopropyl carbodiimide (DIC) followed by reaction with a primary amine via nucleophilic displacement of the bromide.[32] Peptomer Leu-Am_**2**-Act-Al-**2**, as illustrated in Figure 5.31 (a), was prepared at 0.1 mmol scale using the CEM Liberty Blue automated microwave peptide synthesizer on Fmoc-photolabile resin (100-200 mesh, 1% DVB, Advanced ChemTech). Acylation was performed with bromoacetic acid and DIC in a 1:1.1 ratio for 5 min at 75 °C. Nucleophilic displacement was performed with various amines such as 4-(1,3-dioxacyclopent-2-yl) benzylamine, and 4-(2-aminoethyl)-N-(allylcarbonyloxy) phenylamine for 5 min at 75 °C. For non-peptoid residues (Leu), deprotection with 20% piperidine in DMF was performed in a single step of 1 min at 90 °C, and coupling reactions was performed with a five-fold excess of Fmoc-Leu-OH with 1:1:2 amino acid/HCTU/DIPEA for 5 min at 75 °C. The procedure to remove Alloc protecting groups for amines and to photo-cleave the hybrids from the resin was described previously. The resultant peptoid-peptide hybrids were purified by reverse-phase preparative HPLC and characterized by ESI mass spectrometry (Figure 5.31(b)).

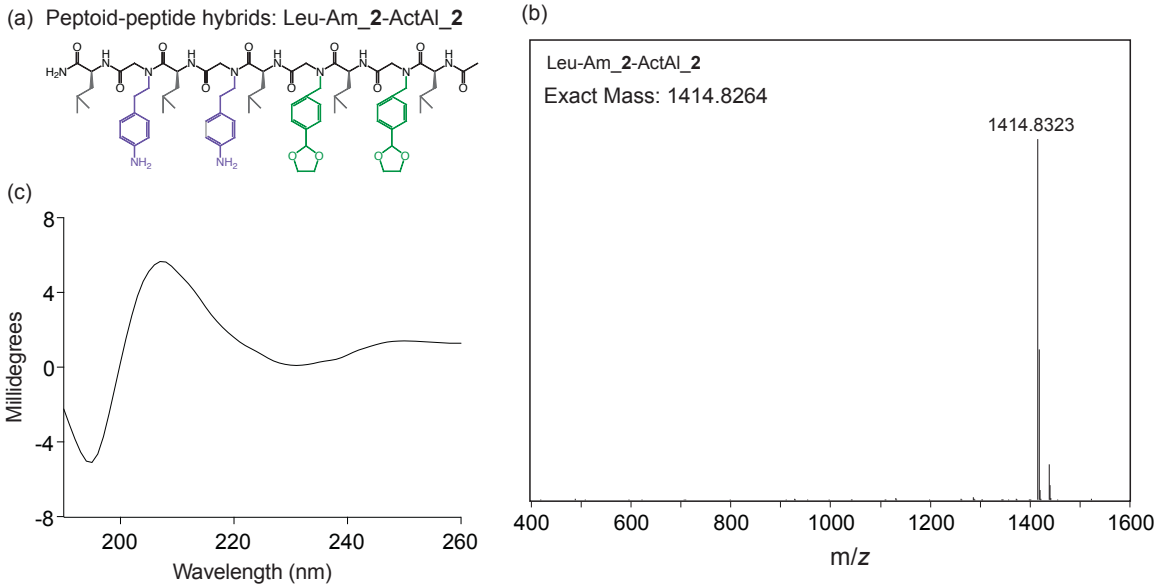

Figure 5.31. Characterization of peptomer Leu-Am_2-ActAl_2: (a) chemical structures; (b) ESI spectra of purified peptoids; (c) circular dichroism (CD) spectrum.

* CD spectrum was collected on a Jasco-815 CD spectrometer. Peptomer was dissolved in acetonitrile at concentration of 25 mM. Blank scans containing only acetonitrile was collected and subtracted as background.

Similarly, the reaction conditions of 0.2 eq. Sc(III) with 2 v/v% water in acetonitrile at 70°C were applied here to remove acetal protecting groups on the peptomer strands and catalyze the subsequent self-assembly of these strands into molecular ladders. Even though the 'back-biting' problem was alleviated with the utilization of peptoid-peptide hybrid backbone, the desired 4–rung in-registry ladders were not detected whereas several out-of-registry ladders with different number of rungs (n = 1~3) were present (Figure 5.32). These peaks were evenly spaced with an interval of 18, corresponding to the molecular weight of the water condensation product for each unreacted amine/aldehyde pair. Unfortunately even after an extended reaction time such as 7 days, the formation of ideal 4–rung ladders was still not observed.

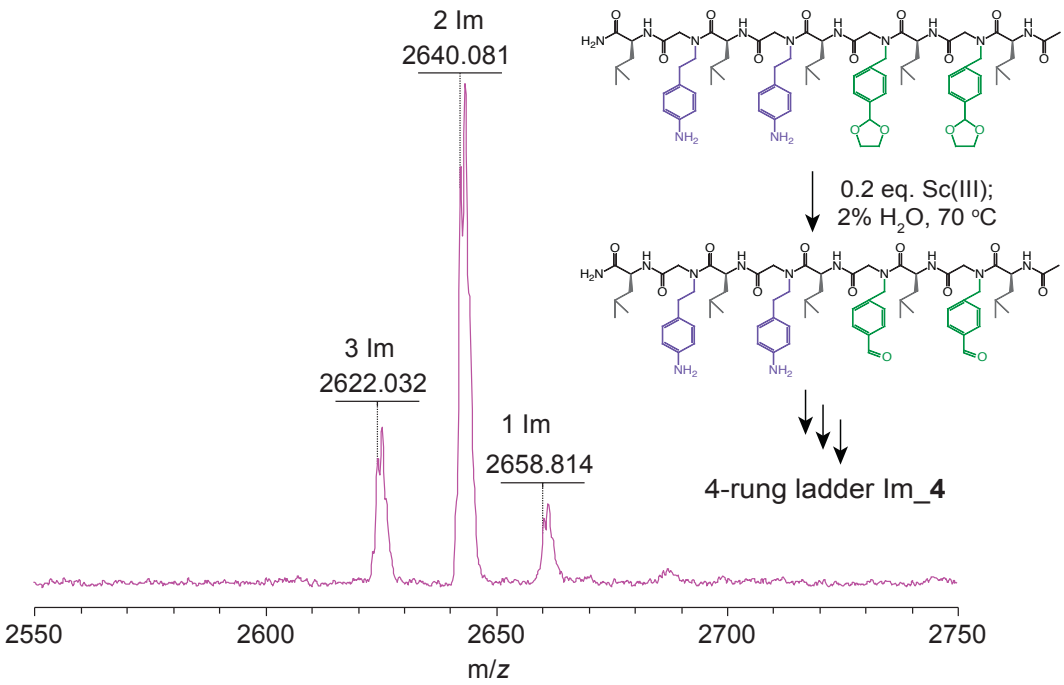

Figure 5.32. *In situ* deprotection and self-assembly of peptoid-peptide hybrids Leu-Am_2-ActAl_2 into a 4-rung molecular ladder (Im_4).
* Im_**4** (expected exact mass: $[M_{Im\_4}+Na]^+$ = 2604.495 g/mol) is the desired in-registry ladder, whereas 3 Im, 2 Im, and1 Im denote the out-of-registry ladders bearing 3, 2 and 1 imine linkages respectively. Expected exact mass of out-of-registry ladders: $[M_{3\ Im}+Na]^+$ = 2622.506 g/mol, $[M_{2\ Im}+Na]^+$ = 2640.516 g/mol, $[M_{1\ Im}+Na]^+$ = 2658.527 g/mol.

As discussed in Chapter 3, the ability of precursor strands to realize registry is significantly impacted by the backbone structure of oligomeric strands. Peptoid-based precursor oligomers are demonstrated to be advantageous as building blocks due to several reasons. First, the lack of inter- and intra-chain hydrogen bonding in the backbone and the main-chain chirality makes peptoid inherently flexible.[10, 15, 33-34] Moreover, adjacent backbone monomeric residues adopts opposed rotational states, resulting in an alternating zigzag, Σ('sigma')-strand structure, thereby enabling the peptoid backbone to remain linear and untwisted (see Figure 5.33).[35] Lastly, dynamic covalent pendant groups are close to each other, providing cooperative binding and therefore facilitating

hybridization selectivity and formation of the desired in-registry products.[10] As for peptoid-peptide hybrids, the incorporation of α-amino acids introduces inter- and intra-strand hydrogen bonding as well as chirality into peptoid-peptide hybrid (Figure 5.31 (c)). This also changes the distance between adjacent pendant groups. All these differences would potentially disrupt the Σ('sigma')-strand structure, twist the backbone and prohibit the cooperative binding, thus preventing the formation of desired in-registry ladder products. And this likely explains the absence of desired 4-rung ladders made of peptomers even after extended reaction times as described above.

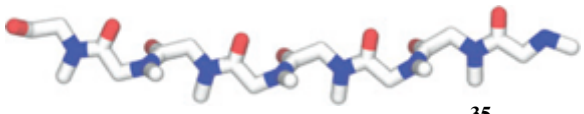

Figure 5.33. Illustration of Σ('sigma')-strand structure.[35]

5.6 Conclusion

We have demonstrated an approach for the dynamic covalent assembly of oligomeric species bearing both amine and aldehyde functional groups by employing $Sc(OTf)_3$ as a dual role catalyst, effecting both *in situ* ethylene acetal deprotection and imine exchange reactions. Given the utility of the amine-aldehyde condensation as a dynamic covalent self-rearranging system, we anticipate that this approach will find broad applicability for enabling the on-demand self-assembly of complex, robust structures.

5.7 References

1. Rowan, S. J.; Cantrill, S. J.; Cousins, G. R. L.; Sanders, J. K. M.; Stoddart, J. F., Dynamic covalent chemistry. *Angew. Chem. Int. Ed.* **2002,** *41* (6), 898-952.

2. Uribe-Romo, F. J.; Hunt, J. R.; Furukawa, H.; Klock, C.; O'Keeffe, M.; Yaghi, O. M., A Crystalline Imine-Linked 3-D Porous Covalent Organic Framework. *J. Am. Chem. Soc.* **2009,** *131* (13), 4570-4571.

3. Hartley, C. S.; Elliott, E. L.; Moore, J. S., Covalent assembly of molecular ladders. *J. Am. Chem. Soc.* **2007,** *129* (15), 4512-4513.

4. Wei, T.; Jung, J. H.; Scott, T. F., Dynamic Covalent Assembly of Peptoid-Based Ladder Oligomers by Vernier Templating. *J. Am. Chem. Soc.* **2015,** *137* (51), 16196-16202.

5. Wang, Q.; Yu, C.; Zhang, C. X.; Long, H.; Azarnoush, S.; Jin, Y. H.; Zhang, W., Dynamic covalent synthesis of aryleneethynylene cages through alkyne metathesis: dimer, tetramer, or interlocked complex? *Chemical Science* **2016,** *7* (5), 3370-3376.

6. Jones, M. R.; Seeman, N. C.; Mirkin, C. A., Programmable materials and the nature of the DNA bond. *Science* **2015,** *347* (6224), 12.

7. Lam, R. T. S.; Belenguer, A.; Roberts, S. L.; Naumann, C.; Jarrosson, T.; Otto, S.; Sanders, J. K. M., Amplification of acetylcholine-binding catenanes from dynamic combinatorial libraries. *Science* **2005,** *308* (5722), 667-669.

8. Wang, L.; Wang, G. T.; Zhao, X.; Jiang, X. K.; Li, Z. T., Hydrogen Bonding-Directed Quantitative Self-Assembly of Cyclotriveratrylene Capsules and Their Encapsulation of C-60 and C-70. *J. Org. Chem.* **2011,** *76* (9), 3531-3535.

9. Belowich, M. E.; Stoddart, J. F., Dynamic imine chemistry. *Chem. Soc. Rev.* **2012,** *41* (6), 2003-2024.

10. Wei, T.; Furgal, J. C.; Jung, J. H.; Scott, T. F., Long, self-assembled molecular ladders by cooperative dynamic covalent reactions. *Polymer Chemistry* **2017,** *8* (3), 520-527.

11. Giuseppone, N.; Schmitt, J. L.; Schwartz, E.; Lehn, J. M., Scandium(III) catalysis of transimination reactions. Independent and constitutionally coupled reversible processes. *J. Am. Chem. Soc.* **2005,** *127* (15), 5528-5539.

12. Li, W.; Li, J. C.; Wu, Y.; Fuller, N.; Markus, M. A., Mechanistic Pathways in CF3COOH-Mediated Deacetalization Reactions. *J. Org. Chem.* **2010,** *75* (4), 1077-1086.

13. Wuts, P. G. M.; Greene, T. W., Protection for the Carbonyl Group. In *Greene's Protective Groups in Organic Synthesis*, John Wiley & Sons, Inc.: 2006; pp 431-532.

14. Isidro-Llobet, A.; Alvarez, M.; Albericio, F., Amino Acid-Protecting Groups. *Chem. Rev.* **2009,** *109* (6), 2455-2504.

15. Sun, J.; Zuckermann, R. N., Peptoid Polymers: A Highly Designable Bioinspired Material. *Acs Nano* **2013,** *7* (6), 4715-4732.

16. Zuckermann, R. N.; Kerr, J. M.; Kent, S. B. H.; Moos, W. H., Efficient Method for the Preparation of Peptoids [Oligo(N-substituted glycines)] by Submonomer Solid-Phase Synthesis. *J. Am. Chem. Soc.* **1992,** *114* (26), 10646-10647.

17. Wei, T.; Jung, J. H.; Scott, T. F., Dynamic Covalent Assembly of Peptoid-Based Ladder Oligomers by Vernier Templating. *J. Am. Chem. Soc.* **2015,** *137* (51), 16196-16202.

18. Verzele, D.; Figaroli, S.; Madder, A., Shortcut Access to Peptidosteroid Conjugates: Building Blocks for Solid-Phase Bile Acid Scaffold Decoration by Convergent Ligation. *Molecules* **2011,** *16* (12), 10168-10186.

19. Kim, S.; Biswas, G.; Park, S.; Kim, A.; Park, H.; Park, E.; Kim, J.; Kwon, Y. U., Unusual truncation of N-acylated peptoids under acidic conditions. *Org. Biomol. Chem.* **2014,** *12* (28), 5222-5226.

20. Hansen, M. J.; Velema, W. A.; Lerch, M. M.; Szymanski, W.; Feringa, B. L., Wavelength-selective cleavage of photoprotecting groups: strategies and applications in dynamic systems. *Chem. Soc. Rev.* **2015,** *44* (11), 3358-3377.

21. Haines, L. A.; Rajagopal, K.; Ozbas, B.; Salick, D. A.; Pochan, D. J.; Schneider, J. P., Light-activated hydrogel formation via the triggered folding and self-assembly of a designed peptide. *J. Am. Chem. Soc.* **2005,** *127* (48), 17025-17029.

22. Xi, W. X.; Krieger, M.; Kloxin, C. J.; Bowman, C. N., A new photoclick reaction strategy: photo-induced catalysis of the thiol-Michael addition via a caged primary amine. *Chem. Commun.* **2013,** *49* (40), 4504-4506.

23. Kloxin, A. M.; Kasko, A. M.; Salinas, C. N.; Anseth, K. S., Photodegradable Hydrogels for Dynamic Tuning of Physical and Chemical Properties. *Science* **2009,** *324* (5923), 59-63.

24. Griffin, D. R.; Kasko, A. M., Photodegradable Macromers and Hydrogels for Live Cell Encapsulation and Release. *J. Am. Chem. Soc.* **2012,** *134* (31), 13103-13107.

25. DeForest, C. A.; Tirrell, D. A., A photoreversible protein-patterning approach for guiding stem cell fate in three-dimensional gels. *Nat Mater* **2015,** *14* (5), 523-531.

26. Dalpozzo, R.; De Nino, A.; Maiuolo, L.; Nardi, M.; Procopio, A.; Tagarelli, A., Er(OTf)(3) as a mild cleaving agents for acetals and ketals. *Synthesis-Stuttgart* **2004,** (4), 496-498.

27. Ferreira, F.; Vasseur, J. J.; Morvan, F., Lewis acid deprotection of silyl-protected oligonucleotides and base-sensitive oligonucleotide analogues. *Tetrahedron Lett.* **2004,** *45* (33), 6287-6290.

28. Tsuruta, H.; Yamaguchi, K.; Imamoto, T., Tandem mass spectrometric analysis of rare earth(III) complexes: evaluation of the relative strength of their Lewis acidity. *Tetrahedron* **2003,** *59* (52), 10419-10438.

29. Jarowicki, K.; Kocienski, P., Protecting groups. *J Chem Soc Perk T 1* **2001,** (18), 2109-2135.

30. Butterfoss, G. L.; Drew, K.; Renfrew, P. D.; Kirshenbaum, K.; Bonneau, R., Conformational Preferences of Peptide-Peptoid Hybrid Oligomers. *Biopolymers* **2014,** *102* (5), 369-378.

31. Olsen, C. A., Peptoid-Peptide Hybrid Backbone Architectures. *Chembiochem* **2010,** *11* (2), 152-160.

32. Olivos, H. J.; Alluri, P. G.; Reddy, M. M.; Salony, D.; Kodadek, T., Microwave-assisted solid-phase synthesis of peptoids. *Org Lett* **2002,** *4* (23), 4057-4059.

33. Rosales, A. M.; Murnen, H. K.; Zuckermann, R. N.; Segalman, R. A., Control of Crystallization and Melting Behavior in Sequence Specific Polypeptoids. *Macromolecules* **2010,** *43* (13), 5627-5636.

34. Rosales, A. M.; Murnen, H. K.; Kline, S. R.; Zuckermann, R. N.; Segalman, R. A., Determination of the persistence length of helical and non-helical polypeptoids in solution. *Soft Matter* **2012,** *8* (13), 3673-3680.

35. Mannige, R. V.; Haxton, T. K.; Proulx, C.; Robertson, E. J.; Battigelli, A.; Butterfoss, G. L.; Zuckermann, R. N.; Whitelam, S., Peptoid nanosheets exhibit a new secondary-structure motif. *Nature* **2015,** *526* (7573), 415-420.

Chapter 6
Concluding Remarks and Future Directions

6.1 Summary of Research

In this dissertation, we identified the key challenge in the field of molecular self-assembly is creating sophisticated nanoscale objects and devices that could achieve the same degree of structural and functional complexity commonly observed by biological supramolecular structures in nature.[1-2] Unfortunately, these naturally occurring supermolecules are rather fragile as a result of weak intermolecular interactions including hydrogen bonding, π-stacking, and van der waals interactions, etc.[3-4] Therefore, we proposed that dynamic covalent self-assembly provides new avenues to integrate the complex, information-driven assembly based on nucleic acids with the strength of covalent interactions. Among numerous dynamic covalent reactions, the imine formation between an amine and an aldehyde is of special interests owing to its fast and efficient reversibility and unique exchange reactions which can be significantly accelerated in the presence of a scandium (III) catalyst, thereby making it an outstanding candidate to mediate dynamic covalent assembly. Thus, we demonstrated the scandium-catalyzed imine metathesis based dynamic covalent assembly of complementary, sequence-specific peptoid oligomers for the fabrication of robust multi-dimensional nanostructures.

The success of constructing exquisite nanoscale architectures typically relies on the use of absolutely mono-disperse polymer chains of a precisely defined monomer

sequence.[5-6] But in synthetic polymers, efforts towards regulating the monomer sequence are still in their infancy. Whereas the modular and step-wise synthesis of peptoid polymers developed by Zuckermann[7] allows for precise control over the monomer sequences, thus providing great opportunities for the construction of well-defined nanostructures. Hence, in Chapter 2, we designed and prepared sequence-specific peptoids *via* a previously reported solid-phase synthesis approach.[7] The resultant peptoid sequences consisted of alternating repeat units between dynamic covalent residues bearing amine- or aldehyde-based pendant groups, and spacer residues bearing inert, ethylene oxide-based side groups.[1-2] Whereas the aldehyde and amine functional groups enable the hybridization of complementary peptoid strands through imine formation and exchange reactions, inert residues were introduced to improve the solubility of the assembled ladders and ensure that the dynamic covalent reactants remain on the same side of the chain.[1-2] Subsequently, the complementary aldehyde- and amine- bearing peptoids of the same length (n = 3~16) were mixed in an equimolar ratio by adding 0.04 equivalent scandium(III) triflate in chloroform, resulting in the formation of n-rung peptoid-based molecular ladders. Matrix-assisted laser desorption/ionization (MALDI) mass spectrometry and gel-permeated chromatography (GPC) were utilized to confirm the successful formation of peptoid-based ladders with up to 16 rungs. Here, a 16-rung peptoid-based molecular ladder is the longest ladder assembled by dynamic covalent chemistry to date. The success of peptoid-based molecular ladder formation demonstrates advantages of peptoids as precursor strands over more rigid precursors such as oligo(*m*-phenylene-ethynylene) where the ladder formation became kinetically trapped and unable to self-correct at four or more rungs.[8]

Despite the successful utilization of imine to effect the fabrication of peptoid-based molecular ladders, the registry mechanism was unclear. Thus, in Chapter 3, we proposed three potential mechanisms that may govern the assembly of molecular ladders. In the first hypothetical mechanism, hybridization proceeds when two adjacent complementary strands bind at any point along the chains, initiating a series of amine/aldehyde condensation reactions through a 'zipper' mechanism, resulting a rapid ladder formation. Alternatively, molecular ladders could assemble *via* a 'hand-shake' line shuffling mechanism, whereby complementary strands bind at opposite sides and come into registry through bond-rearrangement by imine exchange reactions. Lastly, the reaction could proceed whereby strands affixed to out-of-registry ladders would be replaced by toehold-type displacement process, again *via* imine exchange reactions to afford in-registry ladders. Whereas the 'handshake line' mechanism implies that a kinetic limit preventing registry will eventually be reached as the number of ladder rungs increases, a 'zipper' mechanism affords the registry of significantly longer ladders. However, those two mechanisms are not mutually exclusive, both of them contribute significantly to the ladder formation. Therefore, we examined the hypothetical mechanisms by monitoring the kinetics of ladder formation with MALDI–TOF mass spectrometry and Förster resonance energy transfer (FRET)–based distance measurements. The hybridization kinetics of ladder formation based on these two studies concluded that the actual mechanism is a combination of initial zipping up followed by handshake line shuffling. The hybridization kinetics also indicated the rate-limiting step for ladder formation was handshake line shuffling mechanism.

Chapter 4 addresses the limitation of conventional 'bottom-up' self-assembly technique that the construction of large nanostructures often relies on templates of equivalent sizes, which are synthetically challenging and difficult to purify. Thus, a unique approach–Vernier-templated assembly–that employs small templates to direct the assembly of relatively large structures was utilized here to tackle this limitation. In Vernier-templated assembly, two different precursors bearing with mismatched number of complementary binding sites will interact to form complexes that grow until all binding are occupied.[9-12] The length of Vernier assembly is precisely predetermined. Generally, if one precursor has *n* reactive sites and the other has m binding sites, the resulting Vernier assembly will yield a total of $n \times m$ interactions, providing *m* is not a multiple of *n*. However, previously reported implementations of Vernier templating have utilized relatively weak interactions such as metal-ligand interactions or hydrogen bonding. Therefore, dynamic imine chemistry, in conjunction with Vernier-templated assembly was demonstrated to afford extended nanostructures that are both precise and tough. Here, complementary sequence-specific peptoids bearing *n* number of amines and *m* number of aldehydes ($n \neq m$) on the respective strands were employed to assemble into ($n \times m$)–rung Vernier ladders. Again, MALDI-TOF and GPC were used to confirm the successful formation of desired ($n \times m$)–rung Vernier ladders. In addition to the desired Vernier ladders, partially assembled intermediate ladders were also noticed even after an extended reaction time. Thus, scrambling experiments that rely on the dynamic strand exchanges *via* transimination and/or imine metathesis were designed to understand the rate-limiting step of imine-directed Vernier assembly. Strand exchange *via* transimination utilizes a tetra-amine peptoid and a 4-rung peptoid ladder with a different inert spacer,

whereas strand exchange *via* imine metathesis involves two 4-rung peptoid ladders with two different inert spacer units. In both cases, scrambling ladder products were generated as the scrambling experiments proceeded. The kinetics of scrambling product formation was monitored by MALDI mass spectrometry, indicating the formation of scrambling products through transimination was much faster than imine metathesis. Thus, imine metathesis is the rate-limiting step for imine-directed Vernier assembly and this likely explains the continued presence of partially assembled intermediates was attributed to the slow inter-ladder imine metathesis.

In previous chapters, all peptoid sequences employed for the dynamic covalent assembly of molecular ladders consist of only one type of functional groups on the respective strands, and thus these strands represent the simplest combination of information that can be potentially stored in these sequences, such as '1111' and '0000' (amine and aldehyde are denoted as '1' and '0' respectively). A binary information coding system requires the incorporation of both amines and aldehydes on the same strand. However, this is very challenging, as unprotected amines and aldehydes on the same strand would prematurely react with each other intra- or inter-strand even before they hybridize with corresponding complementary strands, yielding kinetically trapped species and complicating the purification. In Chapter 5, we addressed this challenge by employing orthogonal protecting groups (PG) for both dynamic functional groups such as alloc-PG for amines and acetal-PG for aldehydes. Alloc-PG could be easily removed in the presence of palladium (0) under mild reaction conditions, whereas acetal-PG can be deprotected by scandium (III) triflate, which is newly discovered by us.[13] Up to this point, scandium (III) had only been investigated as a catalyst for imine exchange

reactions but was never reported before to remove acetal-PG. Thus, we developed a strategy that employs scandium(III) as a dual role catalyst to yield *in situ* deprotection of aldehyde and subsequently catalyze the imine exchange reactions to effect oligomer assembly. A few factors could potentially influence the efficiency of Sc(III) as a dual role catalyst including solvent, water, Sc(III) loading, and temperature. Thus we performed a systematic study to optimize the reaction conditions of using Sc(III) to effect both *in situ* deprotection and dynamic covalent assembly. We found that the utilization of acetonitrile as a solvent with 2% addition of water in presence of 0.2 equivalent Sc(III) at 70 °C would maximized Sc(III)'s efficiency as a dual role catalyst. Thus these conditions were applied to effect the *in situ* deprotection and dynamic covalent assembly of a tetra-peptoid (1100) bearing two amines and two acetal-protected aldehydes and similarly an octamer peptoid (11110000) consisted of four amines and four acetal-protected aldehydes. Those two peptoid sequences would yield a 4-rung ladder and an 8-rung ladder respectively. The reaction mixtures were directly analyzed by MALDI mass spectrometry and the formation of both 4- and 8-rung peptoid ladders were observed, indicating the success of Sc(III) as a dual role catalyst.

To conclude, we developed and synthesized complementary sequence-specific peptoids that contain dynamic functional amine and aldehyde groups and utilized these peptoid sequences for the self-assembly of robust molecular ladder structures. Given the utility of imine as a dynamic covalent self-rearranging system, we anticipate that the described approach will find broad applications for enabling the on-demand self-assembly of complex, robust nanostructures.

6.2 Future Work

The work in this thesis opens the door to several new avenues of research. This section briefly discusses potential future directions.

Chapter 5 describes the utilization of Sc(III) as a dual role catalyst to afford *in situ* deprotection of aldehyde while simultaneously catalyze imine exchange reactions to effect the subsequent dynamic covalent assembly of oligomers. This elegant approach could be applied to construct complex and robust nanostructures. One such example includes the dynamic covalent assembly of peptoid-based grids (Figure 6.1).

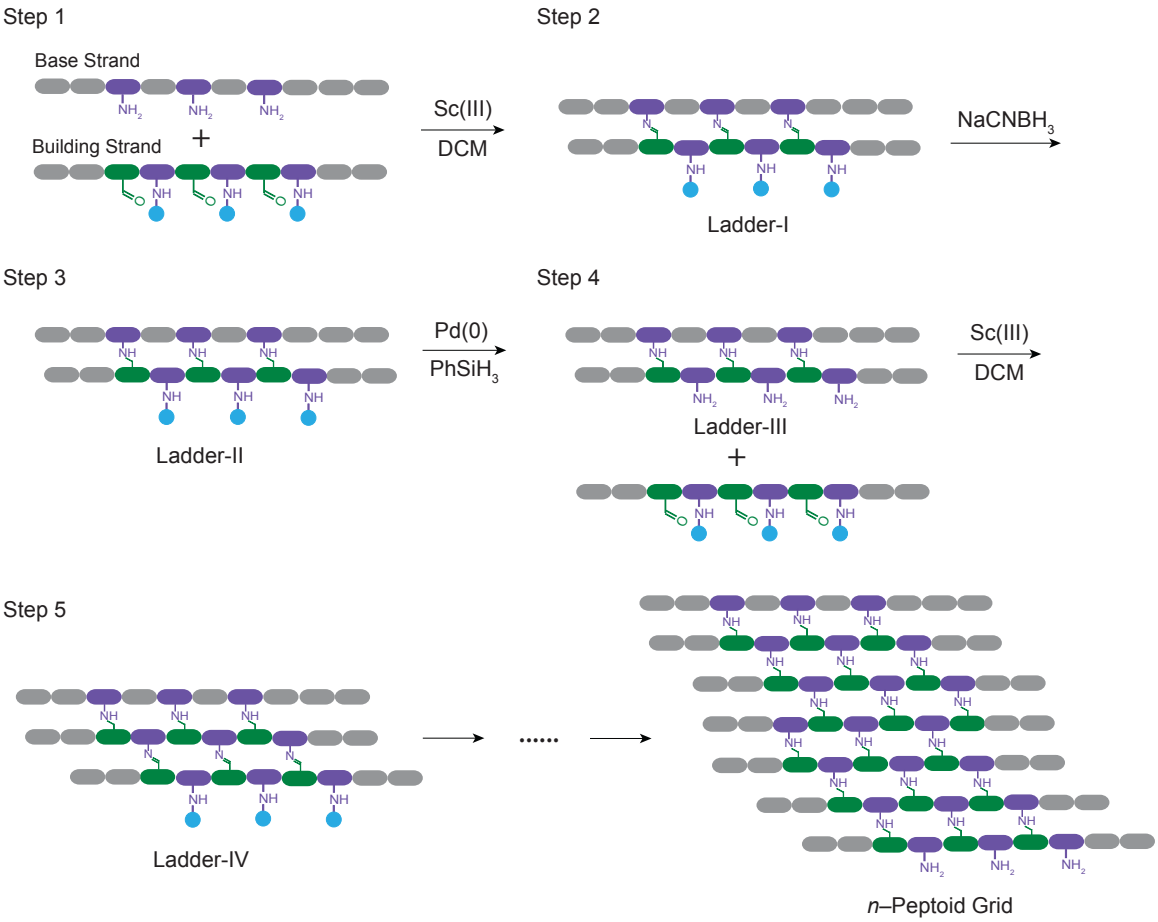

Figure 6.1. Dynamic covalent assembly of peptoid-based grids.

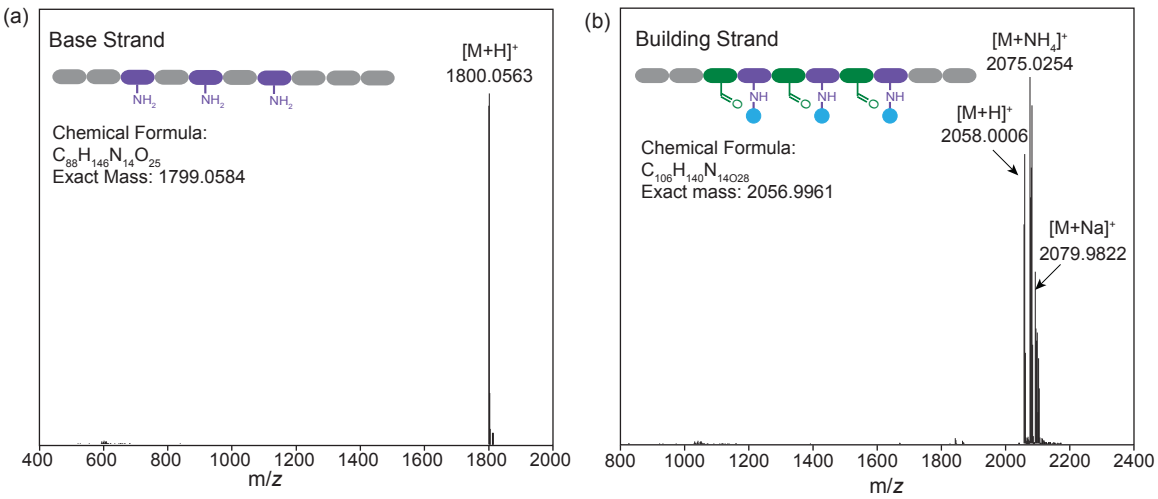

Figure 6.2. ESI mass spectra of base strand (a) and building strand (b) purified by preparative HPLC.
***** Base strand: expected $[M+H]^+$ = 1800.0657 g/mol; building strand: expected $[M+H]^+$ = 2058.0033 g/mol, $[M+NH_4]^+$ = 2075.0299 g/mol, $[M+Na]^+$ = 2079.9853 g/mol. Preparative HPLC method: flow rate at 10 mL/min; A: H_2O, B: MeCN; 40% B 0 – 4 min, 40% – 80% B 4 – 29 min, 80% – 40% B 29 – 31 min.

The dynamic covalent assembly of peptoid-based grids involves two peptoid sequences (a) a base peptoid sequence comprised of exclusively amines, and (b) a building strand bearing alternating dynamic covalent functional groups between an aldehyde and an alloc-protected amine. Those two peptoid sequences were prepared *via* a 'submonomer' approach to solid-phase synthesis described in Chapter 5, purified by preparative RP-HPLC and the resultant peptoids were characterized by ESI+ mass spectrometry as shown in Figure 6.2. Initially, an equimolar mixing of the base strand and building strand results in the formation of Ladder-I, and the ladder structure is confirmed by MALDI-TOF, which is illustrated by Figure 6.3 (a). To avoid potential strand exchange reactions in subsequent steps, imine linkages in Ladder-I are permanently fixed *via* reductive amination by treating with sodium cyanoborohydride overnight to yield Ladder-II (the reduced ladder was confirmed by MALDI as shown in

Figure 6.3 (b)). The subsequent removal of alloc protecting groups on Ladder-II by treatment with Pd(0) and the addition of another building strand allows for the formation of a triple ladder (Ladder-IV). Thus, by repeating these steps, the dynamic covalent assembly of *n*-peptoid grids could be achieved, which can be potentially used as high-precision nano-filtration membrane or smart matrix grids for energy harvesting.

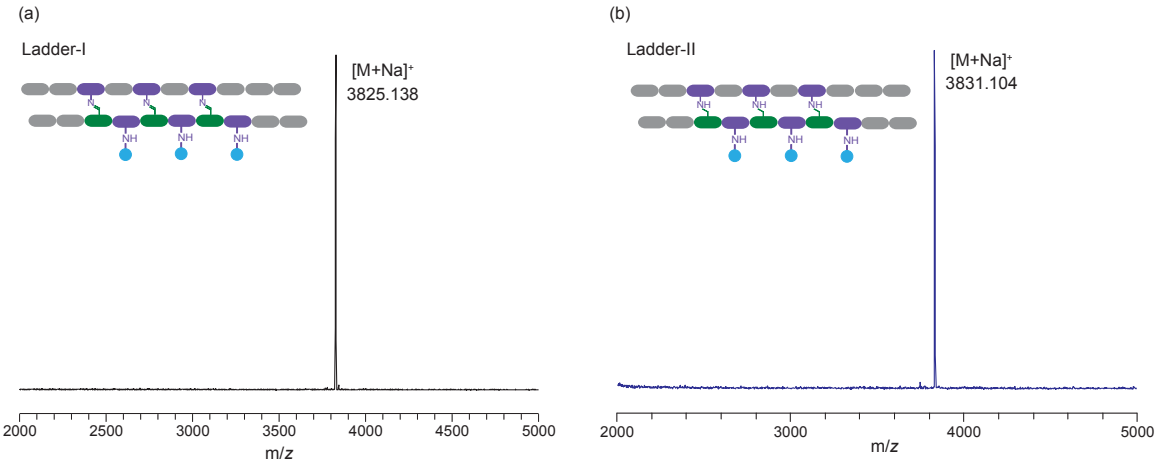

Figure 6.3. MALDI mass spectra of Ladder-I and Ladder-II.
* Expected exact mass of Ladder-I $[M_I+Na]^+$ = 3825.012 g/mol; expected exact mass of Ladder-II $[M_{II}+Na]^+$ = 3831.059 g/mol.

At the end of Chapter 5, we descried encoding sequence information into peptoid strands and utilize these peptoids for the subsequent self-assembly of information-bearing peptoid ladders, however, the ladder formation became kinetically trapped. This is possibly because the incorporation of information–the sequential order of amines and aldehydes–into peptoid single strands disrupt the cooperative binding and the handshake line mechanism, inhibiting the self-correction of out-of-registry intermediates through handshake line shuffling to form desired in-registry products. Thus, aniline was added to the reaction mixture hopefully to assist the cooperative binding and promote the

handshake line shuffling. Furthermore, acetic acid was also added into the reaction mixture to examine if the addition of acid would affect the equilibrium. Indeed, the addition of aniline or acetic acid into the reaction mixtures slightly promoted the desired in-registry ladder formation but it did not significantly improve the hybridization registry. To move forward, information-bearing dynamic covalent assembly necessitates a detailed investigation on the thermodynamic equilibrium of the ladder formation. Also, dynamic covalent residues of certain steric or electronic recognition features can be selected so as to favor the formation of a particular product. For example, in this study, the dynamic covalent pairs are based on aromatic amines and aldehydes, and the corresponding condensation product–aromatic imine–is more stable than its aliphatic counterpart. Thus, the utilization of aliphatic amine/aldehyde as dynamic covalent base pairs could potentially accelerate the dynamic imine exchange reactions, therefore improving the hybridization registry of information-bearing assembly. In addition, it's also worth looking into the modification of primary peptoid backbone structures to effect the information-bearing assembly. As described in Chapter 5, our initial attempt to use peptoid-peptide hybrids as backbone was proven to be unsuccessful, given that the introduction of chiral centers would potentially twist the backbone structure and disrupt the 'Σ'-strand structure observed in α-peptoids. β-peptoids are very promising as building blocks for dynamic covalent assembly due to the extra methylene unit in the backbone.

Another area of interest is the replication of sequence information in peptoids. This could be realized by employing a parent peptoid containing certain sequence information as a template. Vinyl monomers that comprised of either amine or aldehyde groups could thus pair up with the parent peptoid template by imine condensation. A subsequent *in situ*

living polymerization of vinyl groups could zip-up the polymer chain. Once this replicate strand is formed, it can be cleaved from the parent strand with the addition of acid.

6.3 References

1. Wei, T.; Jung, J. H.; Scott, T. F., Dynamic Covalent Assembly of Peptoid-Based Ladder Oligomers by Vernier Templating. *J. Am. Chem. Soc.* **2015,** *137* (51), 16196-16202.

2. Wei, T.; Furgal, J. C.; Jung, J. H.; Scott, T. F., Long, self-assembled molecular ladders by cooperative dynamic covalent reactions. *Polymer Chemistry* **2017,** *8* (3), 520-527.

3. Philp, D.; Stoddart, J. F., Self-assembly in natural and unnatural systems. *Angew. Chem. Int. Ed.* **1996,** *35* (11), 1155-1196.

4. Mattia, E.; Otto, S., Supramolecular systems chemistry. *Nat. Nanotechnol.* **2015,** *10* (2), 111-119.

5. Knight, A. S.; Zhou, E. Y.; Francis, M. B.; Zuckermann, R. N., Sequence Programmable Peptoid Polymers for Diverse Materials Applications. *Adv. Mater.* **2015,** *27* (38), 5665-5691.

6. Lutz, J. F.; Ouchi, M.; Liu, D. R.; Sawamoto, M., Sequence-Controlled Polymers. *Science* **2013,** *341* (6146), 628-636.

7. Zuckermann, R. N.; Kerr, J. M.; Kent, S. B. H.; Moos, W. H., Efficient Method for the Preparation of Peptoids [Oligo(N-substituted glycines)] by Submonomer Solid-Phase Synthesis. *J. Am. Chem. Soc.* **1992,** *114* (26), 10646-10647.

8. Hartley, C. S.; Elliott, E. L.; Moore, J. S., Covalent assembly of molecular ladders. *J. Am. Chem. Soc.* **2007,** *129* (15), 4512-4513.

9. O'Sullivan, M. C.; Sprafke, J. K.; Kondratuk, D. V.; Rinfray, C.; Claridge, T. D. W.; Saywell, A.; Blunt, M. O.; O'Shea, J. N.; Beton, P. H.; Malfois, M.; Anderson, H. L., Vernier templating and synthesis of a 12-porphyrin nano-ring. *Nature* **2011,** *469* (7328), 72-75.

10. Kondratuk, D. V.; Perdigao, L. M. A.; Sullivan, M. C. O.; Svatek, S.; Smith, G.; Shea, J. N. O.; Beton, P. H.; Anderson, H. L., Two Vernier-Templated Routes to a 24-Porphyrin Nanoring. *Angew. Chem. Int. Ed.* **2012,** *51* (27), 6696-6699.

11. Li, X.; Hao, C. H.; Tian, C.; Wang, P. F.; Mao, C. D., Vernier assembly: controlling DNA polymerization via length mismatching. *Chem. Commun.* **2014,** *50* (48), 6361-6363.

12. Hunter, C., Supramolecular Chemistry Bigger and Better Synthesis. *Nature* **2011,** *469* (7328), 39-41.

13. Wei, T.; Furgal, J. C.; Scott, T. F., In situ deprotection and dynamic covalent assembly using a dual role catalyst. *Chem. Commun.* **2017,** *53* (27), 3874-3877.